Mitochondrial translation in *Toxoplasma gondii*: Establishing tools, and characterizing essential mitoribosomal components

By

Alice Lacombe
B.Sc., M. Res. (Hons)

Submitted in fulfilment of the requirements for the
Degree of Doctor of Philosophy

July 2020

School of Life Sciences
College of Medical, Veterinary & Life Science
Institute of Infection, Immunity & Inflammation
University of Glasgow

1. Abstract

Apicomplexan parasites cause diseases such as malaria and toxoplasmosis. These parasites are obligate intracellular pathogen and divergent organisms whose cellular machineries often composed of unique structures of functions compared to model organisms. Studying fundamental mitochondrial biology in these organisms means defining the ancestral core of eukaryotic pathways while simultaneously identifying organism specific traits, that may also inspire drug discovery. Organellar translation has been a focus for the latter in recent years.

Due to extreme gene transfer to the nuclear genome, the apicomplexan mitochondrial genome encodes only three proteins: COXI, COXIII and COB, and a series of indirect evidence suggest active mitochondrial translation of these proteins. Evidence also point to several divergent features in this pathway compared to model organism, primarily the reliance on the import of the full set of tRNAs from the cytosol, and the unusual ribosome composition. Progress has been hampered by the lack of functional assays to detect apicomplexan mitochondrial translation, a shortage of knowledge of proteins involved in this process and the incapacity to detect mitoribosomes. We investigate the molecular detail of translation in apicomplexan organisms using *Toxoplasma gondii* as a model.

tRNA affinity pull down identified 7 candidate proteins with potential role in mitochondrial tRNA import. Using a bioinformatics screen based on mRNA expression patterns, 279 candidate mitochondrial housekeeping components were identified in *Toxoplasma*. 11 were validated, including the mitoribosomal small subunit protein 35 (*Tg*mS35). The small subunit of the mitoribosome was detected for the first time in apicomplexans through TgmS35 triple HA tagging. A new analytical pipeline detected defects in mitochondrial translation upon *Tg*mS35 depletion, while other mitochondrial functions remain unaffected.

Our findings provide further support for the divergent nature of apicomplexan mitochondrial translation and lay a foundation for the study of apicomplexan mitochondrial translation.

2. Contents

3. Publications arising from this work

Alice Lacombe[1], Andrew E. Maclean[1], Jana Ovciarikova[1], Julie Tottey[1,2], Alexander Mühleip[3], Paula Fernandes[1] and Lilach Sheiner[1]*. 2019. **Identification of the** *Toxoplasma gondii* **mitochondrial ribosome, and characterization of a protein essential for mitochondrial translation.** Molecular Microbiology. https://doi.org/10.1111/mmi.14357

[1] Wellcome Centre for Integrative Parasitology, University of Glasgow, 120 University Place, Glasgow, G12 8TA, UK.

[2] UMR 1282 ISP, INRA-Université François Rabelais de Tours, Nouzilly, France.

[3] Department of Biochemistry and Biophysics, Stockholm University, Stockholm, Sweden.

4. Author's declaration & Acknowledgment

4.1. Declaration

I, Alice Lacombe, hereby declare that I am the sole author of this thesis and performed all of the work presented, with the following exceptions highlighted below. No part of this thesis has been previously submitted for a degree at this or another university.

Alice Lacombe

Section 8:

- Bioinformatic screen by my supervisor Dr. Lilach Sheiner, University of Glasgow, UK.
- Western blot of crude mitochondria from nitrogen cavitation followed by differential centrifugation by Dr. Andrew MacLean from Dr. Lilach Sheiner's laboratory, University of Glasgow, UK.

Section 9:

- Split-CAS9 expressing cell line generated by Johannes Stortz from Prof. Markus Meissner's laboratory, University of Glasgow, UK.
- Vacuoles counting of the transient expression of Cas9, and of TGME240270 conditional knock down were performed by Jana Ovciarikova and Dr. Lilach Sheiner, University of Glasgow, UK, in order to keep the counting blind (unbiased).

Section 10:

- Alignments of LSUE ribosomal RNA gene sequences from published mitochondrial genome sequences were performed by Dr. Andrew MacLean from Dr. Lilach Sheiner's laboratory, University of Glasgow, UK.

- Complex IV activity assay for TgmS35-3HA cell line (before conditional knockdown generation) was performed by Dr. Andrew MacLean from Dr. Lilach Sheiner's laboratory, University of Glasgow, UK.

4.2. Acknowledgment

Henri, who instilled in my sister and I the value of hard work and ambition – no doubt I would have not even considered going as far as a PhD if it had not been for his education. And thank you to my grand-parents, Madeleine and Claude, who believed in me and who are so proud of my sister and I for becoming the first doctors in the family. Finally, I am so grateful for my beloved boyfriend Neil whose love and support throughout my PhD never failed. He held me tight in difficult times and celebrated with me when making progress and scientific breakthroughs. He brought sunshine to my life and I thank him with all my heart.

5. Nomenclature

°C	Degree Celsius	dNTP	Deoxynucleotide 5'-triphosphate
Δψ	Membrane potential	DTT	1,4-dithio-DL-threitol
µg	Microgram	EDTA	Ethylene diamine tetraacetic acid
µl	Microliter	EF	Elongation factor
µm	Micrometre	EM	Electron microscopy
µM	Micromolar	ER	Endoplasmic reticulum
AAC	ADP/ATP carrier	EtOH	Ethanol
ADP	Adenosine diphosphate	ETC	Electron transfer chain
AID	Auxin-inducible degron	FAD	Flavin adenine dinucleotide
aaRS	aminoacyl tRNA synthetase	FADH2	Flavin adenine dinucleotide + 2 hydrogen
Amp	Ampicillin	FBS	Fetal bovine serum
APS	Ammonium persulfate	Fe-S	Iron-sulfur
ATP	Adenosine triphosphate	fw	Forward
BLAST	Basic Local Alignment Search Tool	g	Gram or Gravity (context dependent)
BN PAGE	Blue Native Polyacrylamide Gel Electrophoresis	gDNA	Genomic deoxyribonucleic acid
bp	Base pair	GFP	Green fluorescent protein
BSA	Bovine serum albumin	GOI	Gene of interest
Ca^{2+}	Calcium	GSH	Glutathione
Cas9	CRISPR associated protein 9	GTP	Guanosine triphosphate
CAT	Chloramphenicol acetyltransferase	h	Hour
cDNA	Complementary deoxyribonucleic acid	H_2O	Water
CIP	Calf intestinal phosphatase	HEPES	4-(2-Hydroxyethyl)-piperazineethanesulphonic acid
cKD	Conditional Knock-down	HFF	Human foreskin fibroblast
Cox	Cytochrome c oxidase subunit	hrCN PAGE	High resolution clear native polyacrylamide gel electrophoresis
CRISPR	Clustered Regularly Interspaced Short Palindromic Repeats	HSP	Heat shock protein
C-terminal	Carboxyl terminal	Hx or hxgprt	Hypoxanthine-xanthine-guanine phosphoribosyl transferase
Cytb	Cytochrome b subunit	ICAP	Indispensable conserved apicomplexan protein
Da	Dalton	IF	Initiation factor
DD	Destabilisation domain	IFA	Immunofluorescence analysis
DDM	n-dodecylmaltoside	IMC	Inner membrane complex
DHFR	Dihydrofolate reductase	IMM	Inner mitochondrial membrane
DHODH	Dihydroorotate dehydrogenase	IMS	Inter membrane space
DiCre	Dimerisable Cre	IPTG	Isopropyl-O-D-thiogalactopyranoside
DMEM	Dulbecco's Modified Eagle's Medium	ISC	Iron-sulfur cluster
DMSO	Dimethyl sulfoxide	kbp	Kilo base pair
DNA	Deoxyribonucleic acid	kDa	Kilo Dalton
LB	Luria-Bertani	RF	Release factor
LoxP	Locus crossover in P1	RNA	Ribonucleic acid
M	Molar	RON	Rhoptry neck protein

MCF	Mitochondrial carrier family	ROP	Rhoptry protein
MDa	Mega Dalton	RRF	Ribosome Recycling Factor
mg	Milligram	rRNA	Ribosomal RNA
MIA	Mitochondrial Intermembrane space import and Assembly	RT	Room temperature
min	Minute	SAM	Sorting and Assembly Machinery
MITI	Mitochondrial tRNA import	SAG1	Surface antigen 1
ml	Millilitre	SD	Standard deviation
MLO	Mitochondria-like organelle	SDS-PAGE	Sodium dodecyl sulfate polyacrylamide gel electrophoresis
mM	Millimolar	sec	Second
mRNA	Messenger ribonucleic acid	SEM	Standard of the mean
MS	Mass scpectrometry	*spp.*	Species
mS35	Mitochondrial small subunit 35	*T. gondii* or *Tg*	*Toxoplasma gondii*
mt	Mitochondrial	TAE	Tris-acetate-EDTA
MW	Molecular weight	TEMED	N,N,N',N'-tetramethylethylenediamine
Myo	Myosin	TIM	Translocase of the Inner Membrane
NAD	Nicotinamide adenine dinucleotide	TJ	Tight junction
NADH	Nicotinamide adenine dinucleotide (NAD) + hydrogen (H).	TM	Transmembrane
NCBI	National Center for Biotechnology Information	TOM	Transporter of the Outer Membrane
NDH2	NADH dehydrogenases type 2	TCA cycle	Tricarboxylic acid cycle
ng	Nanogram	Tris	Tris [hydroxymethyl] aminomethane
nm	Nanometre	tRNA	transfer Ribonucleic acid
N-terminal	Amino terminal	U	Unit
OMM	Outer Mitochondrial Membrane	uS15m	Universal small subunit 15 mitochondrial
ORF	Open reading frame	UTR	Untranslated region
OXPHOS	Oxidative phosphorylation	UV	Ultraviolet
PAM	Presequence translocase-Associated import Motor	V	Volts
PBS	Phosphate buffered saline	VDAC	Voltage-dependent anion channel
PCR	Polymerase chain reaction	v/v	Volume/volume percentage
PFA	Paraformaldehyde	w/v	Weight/volume percentage
PH	Pleckstrin homology	WB	Western blot
P_i	Inorganic phosphate	WHO	World health organisation
POI	Protein of interest	WT	Wild-type
PV	Parasitophorous vacuole		
PVM	Parasitophorous vacuole membrane		
r	Repressible		
rev	Reverse		

6. Introduction

6.1. The phylum Apicomplexa

The Apicomplexa is a large phylum of protozoan parasites which gathers 4 highly diverse groups: *Gregarina, Cryptosporidia, Hematozoa*, and *Coccidia* (Woo *et al.*, 2015). Within this phylum, about 10 million species are estimated to exist, yet only 6000 have been identified (Adl *et al.*, 2007).

Except for gregarines which live in the extracellular environment of their host, all species are single-cell intracellular obligate parasites known to infect both vertebrates and invertebrates. They are disease causing agents responsible for an extensive economic burden worldwide from both a human and animal perspective (Levine, 1988). Plasmodium falciparum, one of the malaria causing agent in humans, disseminates through the bite of infected female Anopheles mosquitos and has caused over 400000 deaths in 2016, according to the World Health Organization report in 2017. By increasing control and prevention programmes, the incidence of malaria decreased by 41% between 2000 and 2015 (WHO, 2016).

Cryptosporidium spp. is another parasite that causes great harm to humans, especially amongst young children, immunocompromised or malnourished people, as it can lead to cryptosporidiosis – a severe gastrointestinal illness. This parasite disseminates through food and water worldwide, but has a higher prevalence in developing countries where it is associated with high morbidity and mortality amongst the population at risk (Checkley *et al.*, 2015).

Similarly, *Toxoplasma gondii* affects livestock and humans. However, while most apicomplexan parasites have limited host range or cell types, *T. gondii* can infect any warm-blooded animal and any cell with a nucleus within the host (Carruthers, 2002). This has led to a remarkable dissemination globally with a prevalence of one third of the human population worldwide, making it the world's most successful parasite. Mostly asymptomatic (Hill, Chirukandoth and Dubey, 2005; Pappas, Roussos and Falagas, 2009), *T. gondii* remains dormant in the brain and muscle tissue of healthy people in the form of cysts (Montoya and Liesenfeld, 2004). However, this parasite is also associated with severe conditions in

immunocompromised patients with the loss of sight and life-threatening complications, and congenital malformations and abortion in pregnant women (Hohlfeld *et al.*, 1989; Hill, Chirukandoth and Dubey, 2005; Weiss and Dubey, 2009).

6.2. Pathogenesis and clinical features

As mentioned above, *T. gondii* is associated with some severe clinical features in immunocomprised patients and unborn babies being the most at risk. Yet, these cases of severe toxoplasmosis represent less than 20% of all cases (Remington, 1974; Hill, Chirukandoth and Dubey, 2005; Flegr *et al.*, 2014). Indeed, in healthy individuals, toxoplasmosis is generally asymptomatic, or with only mild flu-like symptoms. In adults with a weakened immune system, a multitude of symptoms such as ocular toxoplasmosis, myocarditis, encephalitis, hydrocephalus can occur and be fatal (Maenz *et al.*, 2014). If a woman gets infected during pregnancy by tachyzoites, the fast replicating parasite form, these can go through the placenta, infect the foetus, and cause congenital toxoplasmosis (Figure 6.1). In most severe instances, it can result in miscarriages or stillbirth (Dunn *et al.*, 1999). However, if the baby survives, serious disabilities may result from this infection such as blindness, loss of hearing, severe cognitive defect, seizures, and organ enlargement (Garweg, de Groot-Mijnes and Montoya, 2011; Kamerkar and Davis, 2012; Maenz *et al.*, 2014). Furthermore, recent reports have insinuated a connection between *Toxoplasma* infection and neurological illnesses such as behavioural changes or schizophrenia (Elsheikha, Büsselberg and Zhu, 2016). This is in contradiction with other studies suggesting there is no correlation (Pappas, Roussos and Falagas, 2009). However, this line of study demands further research.

The variety of symptoms with the different degree of severity is also the reflection of infection with different strains of *T. gondii* found around the globe. Three types are the most studied: Type I, Type II and Type III, with Type I being the most virulent, and Type II and III much less virulent (Sibley *et al.*, 2009). They are primarily found in Europe, North America and Africa. These virulence differences can be explained by the different immune response pathways they trigger (Sibley *et al.*, 2009; Behnke *et al.*, 2011, 2015) according to their specific genetic background (Ajioka and Boothroyd, 2009; Behnke *et al.*, 2015). However, allelic

recombination can occur, creating new strains which do not fall under any of these previous categories. These "atypical" strains are mostly found in South America and Africa (Sibley *et al.*, 2009; Yang *et al.*, 2013).

6.3. Lifecycle of *Toxoplasma gondii*

T. gondii has a complex lifecycle as it can infect any warm-blooded animal and any nucleated cell within its host. However, two key lifecycles stand out (Dubey, Miller and Frenkel, 1970a; Frenkel, Dubey and Miller, 1970). (1) The sexual lifecycle, which is carried out inside felids only as their definitive host, allows sexual reproduction between two gametes with the possibility genetic recombination. (2) The asexual lifecycle, which is the fast multiplying cycle of the parasites, occurs inside any other warm-blooded animal as their intermediate hosts, and consists asexual replication with daughter cells being genetically identical to the parents (Weiss and Dubey, 2009; Robert-Gangneux and Dardé, 2012). In contrast to other apicomplexans, *T. gondii* can be transmitted at any stage of its lifecycle, whether it is by horizontal transmission (i.e., by ingestion of oocysts or bradyzoite cysts) or vertical transmission (by transplacental transmission of tachyzoites) (Su *et al.*, 2003).
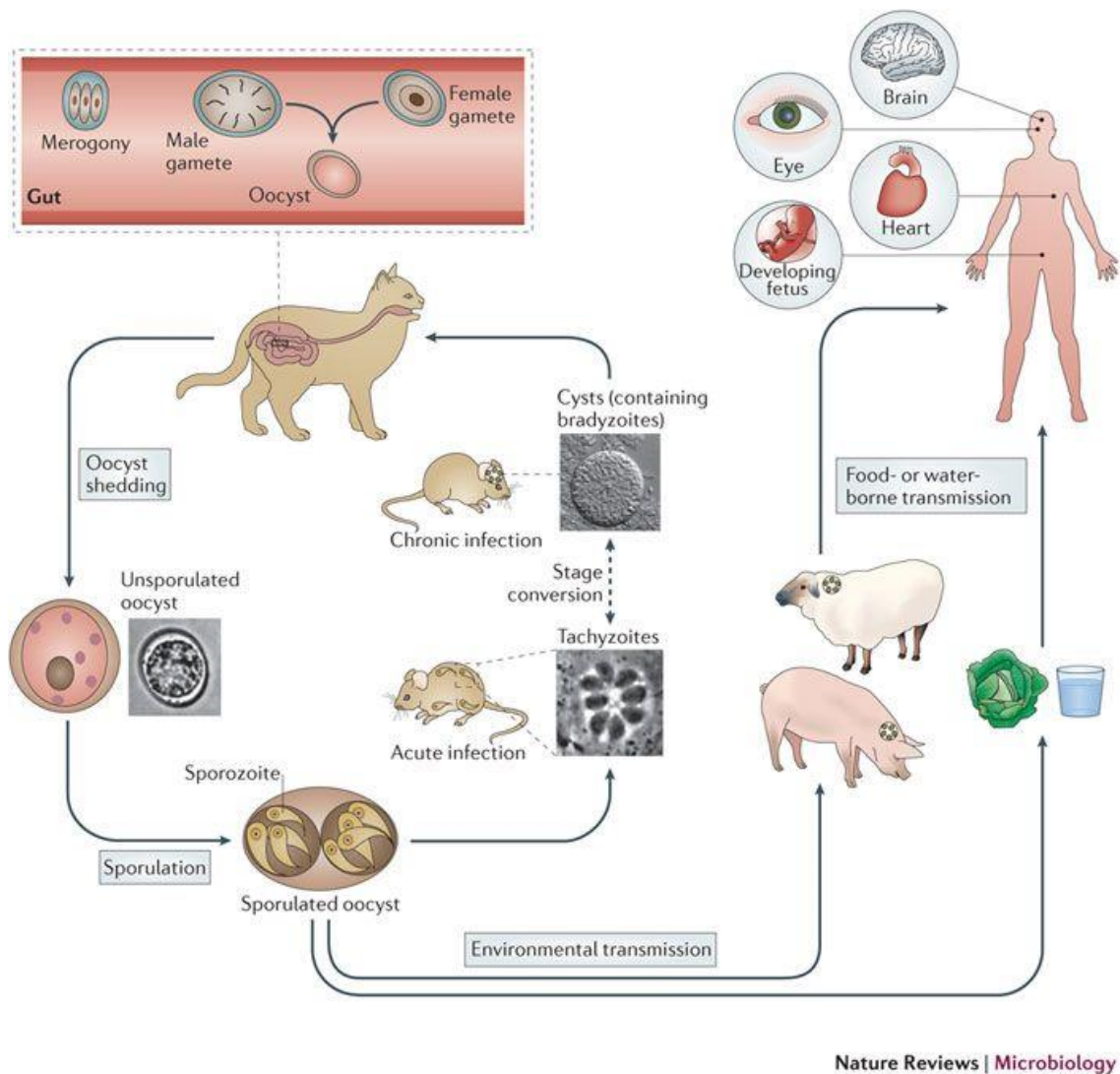
Figure 6.1 Lifecycle of *Toxoplasma gondii*.
The lifecycle of *T. gondii* is divided between a sexual stage in felid and an asexual stage in intermediate and incidental hosts. Reprinted from Hunter & Sibley, 2012; Licence 4867110244049.

6.3.1. Lifecycle in the definitive host

The sexual lifecycle, taking place strictly in felids, is the stage where sexual reproduction is possible. Definitive hosts become infected after ingesting food or other intermediate hosts contaminated with bradyzoites containing cysts (Dubey, Miller and Frenkel, 1970b). Cysts wall is then digested in the gut by proteolytic enzymes which allows the release of the bradyzoites (Dubey, Lindsay and Speer, 1998), now called trophozoites. They invade intestinal epithelial cells where they move on to the next stage of the cycle inside their parasitophorous vacuole (PV). Repeated cycles of nucleus and organelle replication take place as they increase in size, and form schizonts. The cytoplasm then segregates to form numerous identical daughter cells called merozoites which are then released in the gut. This

leads to the next key phase of the sexual lifecycle of the parasite: formation of gametocytes. Merozoites start their differentiation into microgametes (male) and macrogametes (female), which after fertilization develop into single oocyst (Speer and Dubey, 2005). Millions of oocysts are later excreted into the environment through felid faeces. At this stage, oocysts have not sporulated yet and are non-infective. Sensing drastic changes when released in the external environment, oocysts sporulate resulting in the formation of two sporocysts per oocysts, each containing four sporozoites (Dubey, Lindsay and Speer, 1998). Sporulated oocysts are now infective and will remain in the environment for up to several years until ingested again by felids or mice, repeating the sexual lifecycle (Dubey, Miller and Frenkel, 1970b;Dubey and Frenkel, 1972;Dubey, Lindsay and Speer, 1998), or by other intermediate hosts via contaminated food or water and start their asexual lifecycle.

6.3.2. Lifecycle in the intermediate host

Once ingested by the intermediate host, infective sporulated oocysts begin a strictly asexual lifecycle, which comprises two stages: the lytic cycle, where the parasite goes through multiple rounds of replication within host cells inflicting tissue damage; and the dormant stage, a non-replicative stage where the parasite persists in cysts form (Blader *et al.*, 2015). During the lytic stage, a series of cellular processes occur enabling gliding motility, attachment, invasion into the host cell, and egress of the parasite (Figure 6.2).
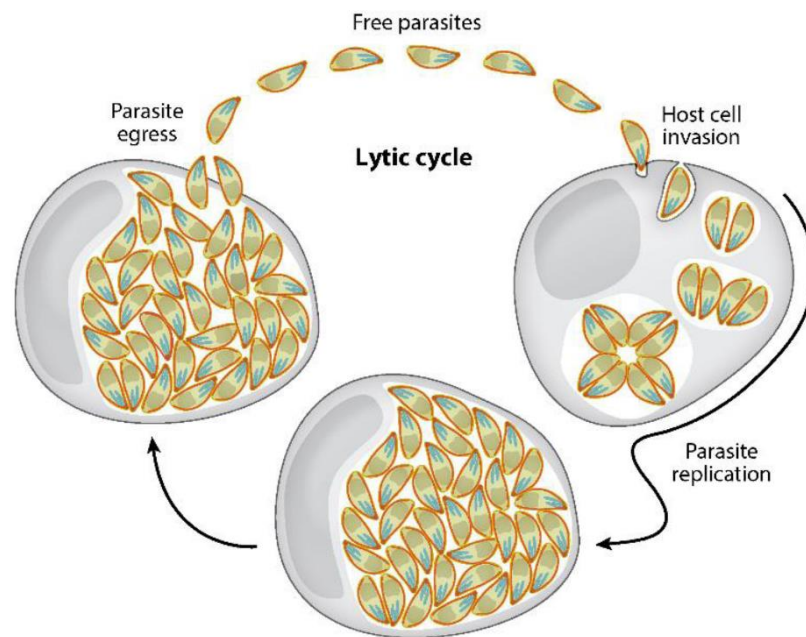
Figure 6.2 The lytic cycle of *T. gondii*
Extracellular tachyzoites use gliding motility to move around within the matrix in the search for a host cell. Once found, the parasite attaches to the host cell, and invades it creating a PV in the process. It will then replicate within the PV by endodyogeny until occupying the whole cytosol of the host cell. The daughter parasites then egress the host cell in the search for another host cell. Reprinted from (Blader *et al.*, 2015). Order license ID 1048105-1.

6.3.3. The lytic cycle

6.3.3.1. Gliding motility, attachment and invasion

In order to migrate through tissue, *T. gondii* uses a particular mode of motility called gliding. *In vitro* studies showed three types of movement on 2D substrates: twirling, circular, and helical (Håkansson *et al.*, 1999). In a 3D matrix, parasites exhibit a left-handed corkscrew type of motility (Leung *et al.*, 2014). This motility is powered by an acto-myosin motor, which is part of a complex called the glideosome, and is located between the inner membrane complex (IMC) and plasma membrane (Frénal *et al.*, 2010). The Myosin A motor protein is anchored to the IMC through the interaction of myosin light chain MLC1 and the glideosome-associated proteins GAP45, GAP50 and GAP40 (Tardieux and Baum, 2016;Frénal, Dubremetz, *et al.*, 2017). The force generated to allow movement occurs when Myosin A pulls on actin filaments. The movement is transferred to surface adhesin proteins secreted from organelles called micronemes, and via a linker, these microneme proteins transfer the movement onto the host cell surface (Carruthers *et al.*, 2000; Huynh *et al.*, 2003). Our understanding of the mechanism of

glideosome function has been evolving over the recent years with studies that demonstrated that the linker, previously believed to be aldolase (Jewett and Sibley, 2003; Shen and Sibley, 2014), is not essential for motility and that another player, a glideosome-associated connector (GAC) mediates this linkage (Jacot *et al.*, 2016). Moreover, short, fast depolymerising actin filaments were shown mediate to traction forces with Myosin A, instead of the canonical long stable actin filaments (Andenmatten *et al.*, 2013; Whitelaw *et al.*, 2017).

Once having reached a host cell, tachyzoites attach to the host cell surface receptors and re-orientate its apical end (Carruthers, Giddings and Sibley, 1999). This is mediated by secreted microneme proteins such as MIC2 and AMA1. Then rhoptry neck (RON) proteins RON2, RON4, RON5, and RON8 are secreted to form a moving junction. RON2 intergrades the host cell plasma membrane, while RON4, RON5, and RON8 cross face the cytosol of the host cell. RON2 interacts with AMA1 at the surface of the parasite as it pulls through the moving junction on the host cell membrane when penetrating the cell (Alexander *et al.*, 2005; Carruthers, Giddings and Sibley, 1999; Carruthers and Boothroyd, 2007; Lamarque *et al.*, 2011; Mital *et al.*, 2005). The parasite enters the host cell through this tight junction which translocates from the apical tip all the way to the basal end and then pinched off by a fission pore. This process retains the host cell plasma membrane surrounding the parasite and which now forms the PV. This process involves other secreted proteins such as Rhoptry bulb proteins (ROP) and Dense Granules proteins (GRA)(Suss-Toby, Zimmerberg and Ward, 1996). The PV is essential for the parasite to build a micro-environment suitable for its survival and replication. Invasion and host cell manipulation allow *T. gondii* to hide from the host cell's defence mechanism, while scavenging metabolites and recruiting mitochondria from the host cell (Jones and Hirsch, 1972; Clough and Frickel, 2017). Interestingly, this close mitochondrial association is only seen in type I parasites, as type II strains lack the MAF1 gene identified to be responsible for this association (Pernas *et al.*, 2014).

6.3.3.2.   Replication and egress

T. gondii tachyzoites start their asexual replication once established in their PV inside the host cell. Replication is done by endodyogeny, which consists in the formation of two daughter cells within the mother cell (Hu *et al.*, 2002).

Tachyzoites replication starts with the replication of the centrioles. The new cytoskeleton forms in collaboration with the centrioles. It defines the daughter cells polarity, and daughter buds start to form. The conoid, spindle poles, and intranuclear microtubules begin to form followed by the generation of the inner membrane complex (IMC) which drives the daughter cell division alongside with the subcellular microtubules (Nishi *et al.*, 2008; Agop-Nersesian *et al.*, 2010; Shaw *et al.*, 2000). The organelles then migrate into the daughter cells, starting with the Golgi apparatus, then apicoplast and nucleus (Hu *et al.*, 2002). In the later phase, the ER and the mitochondrion divide, and reach their final destination inside the new cells (Nishi *et al.*, 2008). Division is complete when all organelles are segregated in both daughter cells and enclosed in their IMC. Secretory organelles are however not inherited from the mother cell but generated *de novo* within the daughter cells. The mother cell's secretory organelles are degraded, and the proteins are recycled by the daughter cells to synthesise their rhoptries and micronemes (Nishi *et al.*, 2008). Parasite replication results in the formation of a residual body (RB) containing degraded maternal secretory organelles and some mitochondrial and nuclear fragments (Nishi *et al.*, 2008). The end of endodyogeny is marked by the disassembly of the mother's cytoskeleton and the incorporation of the plasma membrane to the daughter parasites (Agop-Nersesian *et al.*, 2009). Parasites replicate in an orderly fashion within the PV and are maintained in place via the membranous nanotubular network (MNN), a complex of membranes that connect parasites to one another and to the PV membrane (Sibley *et al.*, 1995; Mercier *et al.*, 2002). This network is maintained throughout the replication rounds until egress, and has been shown to connect the RB to the parasites in the PV, and participate in the exchange of material between parasite via an actin network (Periz *et al.*, 2017).

After a certain number of replication cycles, when the host cell can no longer support parasite division, parasites sense a stress signal from the host cell which triggers a cascade of molecular event leading to an active egress (Frénal *et al.*, 2010). Studies have shown that egress is induced by a rapid surge in calcium (Ca^{2+}) level (Caldas, de Souza and Attias, 2010) which activates the motility complex with the secretion of micronemes. This results in PV and host cell plasma membrane perforation via the micronemal perforin-like protein (PL1) (Kafsack and Carruthers, 2010). This pathway was shown to be dependent on the calcium-

dependent kinase CDPK3 activation (McCoy *et al.*, 2012; Lourido, Tang and Sibley, 2012). Once released in the external environment, the new generation of parasites proceed to repeating the lytic cycle.

6.4. Ultrastructure of *T. gondii* tachyzoites

During the highly proliferative stage, tachyzoite are banana-shaped cells of approximately 6 µm long and 2 µm wide. Being part of the eukaryotic super kingdom, *T. gondii* possesses the conserved organelles such as nucleus which contains a centrally located nucleolus (Dubey, Lindsay and Speer, 1998), mitochondrion, Golgi apparatus and endoplasmic reticulum (Pelletier *et al.*, 2002). It also possesses Apicomplexa specific structures such as the conoid, secretory organelles such as the rhoptries and micronemes (Morrissette and Sibley, 2002), dense granules (Mercier *et al.*, 2005; Kessler *et al.*, 2008; Behnke *et al.*, 2011; Sharma and Chitnis, 2013), and relic plastid called apicolplast (Waller and McFadden, 2005). The parasite's pellicle is composed of a three-layered membranous structure composed of the plasma membrane, and the inner membrane complex (IMC) which is composed of flattened alveolar sacs that underlie the plasma membrane, coupled to a supporting cytoskeletal network.
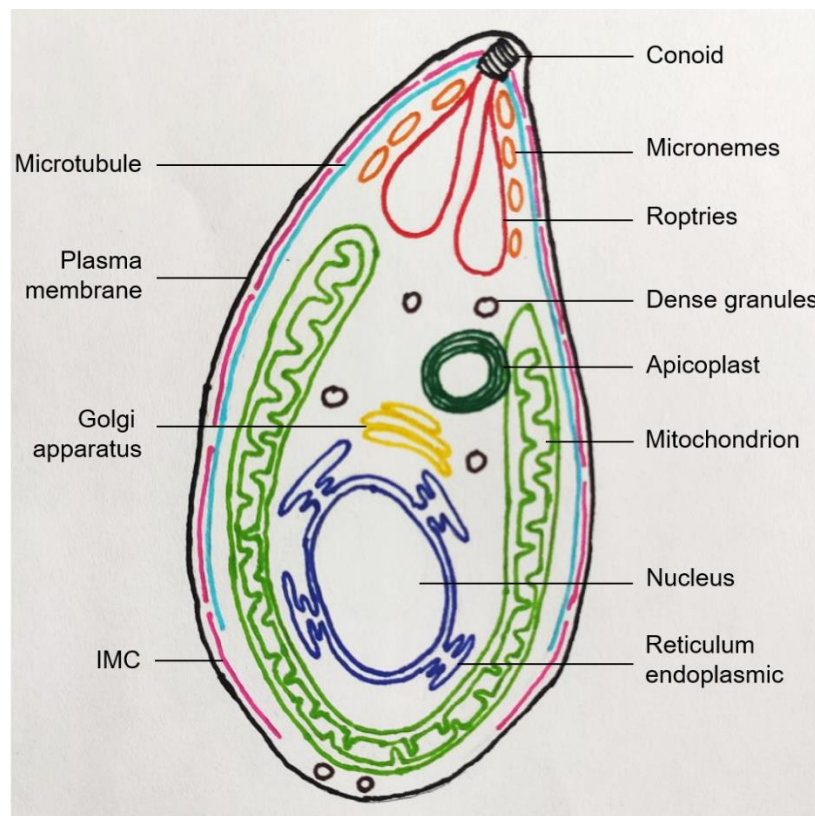
Figure 6.3 *Toxoplasma gondii* ultrastructure
The crescent shape which is characteristic of the parasite is easily distinguishable. The parasite cell is polarised with organelles involved in invasion such as micronemes, conoids and rhoptries which are orientated at the apical end. Other organelles such as dense granules, Golgi apparatus, and the apicoplast are located from middle to the basal end. The mitochondrion goes around the parasite mostly in juxtaposition to the microtubules. The endosymbiotic organelles, mitochondrion and apicoplast, are in close contact with one another. The nucleus, connected to the ER are found in the centre of the parasite, as well as the Golgi apparatus. Dense granules are distributed throughout the parasite. The parasite is surrounded by the plasma membrane, the inner membrane complex (IMC) and microtubules.

6.4.1. The apical complex and secretory organelles

The apical complex, from which the phylum name Apicomplexa originates, is composed of different structures: a set of spirally arranged microtubules called conoid, rhoptries, and one or more polar rings. The conoid, located at the tip of the apical end, is a hollow cone-shaped structure which is thought to be involved in environmental sensing and host cell invasion as it extends in the outside environment when parasites are extracellular (Shaw and Tilney, 1999; Del Carmen et al., 2009). At each extremity of the conoid are a pre-conoidal ring, and a third ring called apical polar ring serve as the microtubule organising centre (MTOC) (Hu, Roos and Murray, 2002). The conoid is the place from where secreted proteins involved in the invasion process exit the parasites (Katris *et al.*, 2014).

T. gondii possesses three different secretory organelles: micronemes, rhoptries and dense granules.

Micronemes are organelles based at the apical end of the parasite in which proteins essential for invasion and egress are stored (Carruthers and Tomley, 2008). To date, there are over 50 micronemal proteins described in the literature. These play a key role in invasion and egress (Carruthers, Giddings and Sibley, 1999).

Rhoptries are elongated sacs-like organelles that extend to the conoid at the apical end (Figure 6.3). There are about 8-10 of these organelles per parasites (Dubremetz, 2007). The neck of the rhoptries, at the most apical end, contains the RON proteins which integrate the host cell plasma membrane allowing the parasite to firmly bind to it via AMA1 which triggers the formation of the tight junction during host cell penetration (Lamarque *et al.*, 2011, 2014). Below the neck is a bulbous compartment in which the ROP proteins are stored. These are

involved in the formation and maintenance of the PV (Figure 6.3) (Carey *et al.*, 2004; El Hajj *et al.*, 2007). Some ROP protein, such as ROP 15/18, also have a role in immunity evasion and are hence considered major virulence factors (Boothroyd and Dubremetz, 2008; Yamamoto *et al.*, 2011; Behnke *et al.*, 2015).

Dense granules are electron-dense organelles that secrete GRA proteins involved in PV formation and maintenance during parasite replication (Mercier *et al.*, 2005), as well as formation of the membranous nanotubular network (MNN) (Mercier *et al.*, 2002). Some of these proteins have also been shown to have a role in host cell response and are considered major virulence factors as well (Bougdour, Tardieux and Hakimi, 2014).

6.4.2. The Inner Membrane Complex

The IMC is composed of flattened membranous sacs located beneath the parasite's plasma membrane called alveoli (Figure 6.3). The IMC is supported by a subpellicular network which connects the IMC to the microtubules (Morrissette, Murray and Roos, 1997), and spreads throughout the whole length of the parasite excluding the parasite polar ends where the conoid and the basal complex reside (Figure 6.3). The space between the plasma membrane and the IMC is where the glideosome complex lays, and gliding associated proteins (GAPs) which are anchored to the IMC connect the two together. GAP45 is believed to be the key factor which holds the two membranes together with a somewhat constant distance of 20 – 30 nm (Kudryashev *et al.*, 2010). Depletion of this protein induces the detachment of the IMC from the plasma membrane plasma membrane (Egarter *et al.*, 2014). In addition, depletion of GAP40 and GAP50 demonstrated their critical role in IMC biogenesis during parasite replication (Harding *et al.*, 2016).

6.4.3. The apicoplast

Many Apicomplexans contain a relic plastid called apicoplast, discovered over 20 years ago (McFadden *et al.*, 1996), except for *Cryptosporidium* spp which likely lost this organelle (Keithly, Marchewka and Zhu, 2000). It is a non-photosynthetic organelle derived from a red alga and was acquired during evolution by secondary endosymbiosis which resulted in this organelle surrounded by four membranes (Waller and McFadden, 2005; Lim and McFadden, 2010). The apicoplast is often

seen in proximity with the mitochondrion (Nishi *et al.*, 2008). Indeed, the apicoplast harbours essential pathways whose end product is either important for mitochondrial functions such as isoprenoid precursors, or requires the collaboration of both organelles to generate the end product such as the haem biosynthesis (See below). This metabolic interdependency, and the microscopy observation of their proximity suggests an association existing between the two organelles, which is further supported by the experimental difficulty to separate both organelles for purification (Kobayashi *et al.*, 2007).

Due to its path of acquisition, the apicoplast is one of the three genome containing compartment in the parasites, the other two being the nucleus and mitochondria. It is 35 kb in size and encodes for the small subunit (SSU) and large subunit (LSU) rRNA (Gajria *et al.*, 2008), as well as for about ~30 gene encoding proteins. The majority encode for organelle gene expression components, including ribosomal proteins (Gupta *et al.*, 2014), the translation elongation factor Tu, and subunits of a eubacterial-like RNA polymerase (Wilson *et al.*, 1996), and a full set of tRNAs which implies that the organelle does not need to import any from the cytosol; the rest of the apicoplast encoded genes are involved in protein import and metabolic pathways.

Although the apicoplast possesses its own genome, the majority of its proteome is encoded in the nucleus. To be functional, these nucleus-encoded apicoplast-targeted (NEAT) proteins must be imported into the organelle. Proper targeting of these proteins is mediated in many cases by a signal peptide followed by a transit peptide at the N-terminal end of NEAT proteins (Nassoury, Wang and Morse, 2005). It is believed that the signal peptide induces co-translational translocation of the protein into the ER and is cleaved off in the ER. Indeed, studies have shown that with the signal peptide from the apicoplast ribosomal protein S9, GFP is targeted to the secretory system (DeRocher *et al.*, 2000; Yung, Unnasch and Lang-Unnasch, 2001). Once in the ER, the transit peptide leads the protein to the apicoplast where it is subsequently cleaved off upon entry (Van Dooren *et al.*, 2002). Within the apicoplast the protein needs to reach its final subcompartment: the outermost, periplastid, second inner, or stromal compartments. However, the mechanism which drives protein sorting to each compartment is not fully understood. Sheiner *et al.*, (2015) showed that protein residing in the stroma often possess aromatic amino acids at the +1 site of the transit peptide, and point

mutation resulted in organelle periphery mislocalisation (Sheiner *et al.*, 2015). However, this is not the case for all stromal proteins. Some lack the bipartite peptides altogether and possess hydrophobic patches or transmembrane domains instead (Agrawal *et al.*, 2009; Karnataki *et al.*, 2009; Sheiner *et al.*, 2011). Apicoplast targeting and subcompartment sorting is hence a complex mechanism, which is not just driven by a define and straightforward sequence motif, and requires further research to figure out what are the determinant factors for a proper localisation.

As in the case of the targeting signals, the complex architecture of the apicoplast affects also the import machinery. Although some pieces of the puzzle are still missing, progress has been made on the characterisation of apicoplast import machinery. The endoplasmic reticulum associated degradation (ERAD) pathway has been shown to play a role in protein import. In the ER, ERAD is involved in protein quality control whereby misfolded proteins are translocated from the ER into the cytoplasm for degradation. It seems that the periplatid membrane of the apicoplast, which originates from an ER-like membrane, re-purposed ERAD to facilitate import (Sommer *et al.*, 2007; Ruggiano, Foresti and Carvalho, 2014). The organellar Der1AP and CDC48AP were shown to allow passage through the periplastid membrane (Agrawal *et al.*, 2009; Fellows *et al.*, 2017). Like in the ER, ubiquitination is proposed to signal for transport through ERAD. In line with this hypothesis, E1AP, E2AP, and E3AP, homologs of E1, E2 and E3 components of the ER ubiquitin pathway respectively, as well as the plastid ubiquitin-like (PUBL) modifier, are required for passing NEAT protein through the periplastid membrane (Hassink *et al.*, 2006; Ernst *et al.*, 2011; Agrawal *et al.*, 2013; Fellows *et al.*, 2017). Passage through the two inner membrane is mediated by homologs of the translocon of the inner and outer chloroplast membrane (TIC/TOC) protein complexes, in line with the origin of those membranes in the primary plastid found in the algal endosymbiont. Homologs of the primary plastid Tic20 (Van Dooren *et al.*, 2008) and Tic22 (Glaser *et al.*, 2012) were both shown to be involved in this process. A homologue of the main pore component of the plant TOC complex, Toc75, was also identified as a role player in translocation of NEAT proteins to the organelle stroma (Sheiner *et al.*, 2015). Further studies are required to discover the rest of the missing pieces of the apicoplast import machinery.

The apicoplast is the centre of three vital metabolic pathways: type II fatty acid biosynthesis (FASII), isoprenoid biosynthesis, and haem biosynthesis. The first pathway, FASII, provides the parasite with essential lipids. Although *T. gondii* can harvest lipids from the host cell (Charron and Sibley, 2002; Nolan, Romano and Coppens, 2017), many essential fatty acids must be synthesised de novo. The FASII pathway meets these needs by synthesising of over 80% of the saturated long-chain fatty acids (LCFA) C14:0 and C16:0, with the acyl carrier protein (ACP) being a core and essential component of the FASII system (Mazumdar *et al.*, 2006).

Another metabolic pathway, the isoprenoid biosynthesis, is an invaluable pathway of the apicoplast, and has been shown to be the only known anabolic pathway present in all parasites possessing an apicoplast, highlighting its essentiality (*T. gondii, N. caninum, P. falciparum, B. bovis, T. parva*) (Seeber, Feagin and Parsons, 2013). Isoprenoids are derivates of isopentenyl pyrophosphate (IPP) or of its isomer dimethylallyl pyrophosphate (DMAPP). They fulfil important cellular functions in signalling processes, in protein prenylation, ubiquinone synthesis for the mitochondrial electron transfer chain (mETC), and for tRNA modifications (Ralph *et al.*, 2004). Similar to bacteria and chloroplasts, the apicoplast harbours the non-mevalonate pathway, the DOXP pathway, for isoprenoid synthesis (Jomaa *et al.*, 1999; Zhu, Marchewka and Keithly, 2000; Seeber and Soldati-Favre, 2010). In another study, IPP was shown to be capable of rescuing the effect of fosmidomycin, as well as restoring the proliferation of apicoplast-less parasites which had been treated with doxycycline (Yeh and DeRisi, 2011), a drug which disrupts apicoplast replication and inheritance during parasite cell division (Dahl *et al.*, 2006). This demonstrated IPP to be the only essential apicoplast product during the blood stage of P. falciparum. This provided an invaluable tool to study apicoplast biology (Yeh and DeRisi, 2011).

The third essential metabolic pathway is the haem biosynthesis (Ramya *et al.*, 2007) which consists in a multistep enzymatic reaction and requires the cooperation of three compartments: the apicoplast, the cytosol and the mitochondrion (Ralph *et al.*, 2004; Van Dooren, Stimmler and McFadden, 2006). Haem is an important prosthetic group on many proteins such as cytochromes which play an essential role in mitochondrial respiration through the electron transport chain in parasites (Tjhin *et al.*, 2020). Throughout the mETC complexes, haem is present in cytochrome b and cytochrome c1 subunits of the complex III,

in CoxI subunit of complex IV, and in the mobile Cytochrome c complex, and allow the transfer of electrons from one complex to another.

The presence of an additional organelle of cyanobacterial origin presents an opportunity for novel drug target discovery with many proteins and pathways not shared by the human host. Many of the current drugs target the apicoplast translation machinery. For example, ribosome inhibitors such as clindamycin, azithromycin and doxycycline, are used as antimalarial drugs or as prophylaxis, with clindamycin also used as a second line drug for toxoplasmosis (Fichera and Roos, 1997). In *Plasmodium* red blood cell (RBC) stage, these drugs seem to only target the apicoplast and not the mitochondrion (Uddin, McFadden and Goodman, 2018). This could either be due to divergent mitoribosome structure (Gupta *et al.*, 2014) and/or to low activity of mitochondrion translation in RBC-stage. These apicoplast targeting drugs induce a phenotype called delayed death (Fichera, Bhopale and Roos, 1995), which consists in the parasites' death only in the second cycle of replication after drug treatment. As the drug blocks essential apicoplast pathways during the parasite replication first cycle, the apicoplast is unable to duplicate as the parasite divides, resulting in daughter cells without apicoplasts. Although the loss of this organelle is lethal, parasites can still replicate as long as at least one apicoplast remains within the vacuole (He *et al.*, 2001). The newly formed parasites lacking apicoplast can then egress and invade neighbouring host cells, but cannot undergo a second cycle of replication (Frénal, Jacot, *et al.*, 2017). Although delayed death is not ideal for clinical application, such drugs are suitable if used in combination with fast acting drugs.

6.5. Mitochondria

6.5.1. Evolution

Mitochondria originate from an endosymbiotic event whereby an α-proteobacterium was engulfed by a larger eukaryotic cell about 1.5 billion years ago (Lang, Gray and Burger, 1999; Andersson *et al.*, 2003; Dyall, Brown and Johnson, 2004). A great deal of the genes from this symbiont were transferred to the host cell's nucleus throughout evolution, which transformed the bacterium from an independent symbiotic organism to a host-dependent organelle. Indeed, most mitochondrial proteins in modern organisms are now nuclear encoded,

translated in the cytosol and imported into the mitochondrion (Wiedemann and Pfanner, 2017a). Mitochondria are found in virtually all eukaryotes (Mokranjac and Neupert, 2009; Karnkowska *et al.*, 2016). They have vital roles in cell signalling, and provide the cell with essential metabolites and energy. However, as evolution continues, divergence started to emerge as consequence of organism adaptation to different niches, and have hence drifted from the canonical mitochondria to mitochondria-like organelles (MLOs).

Regardless of their evolution, mitochondria and MLOs possess some basic common features. Their all have a double membrane: the outer mitochondrial membrane (OMM) and inner mitochondrial membrane (IMM) (Wiedemann and Pfanner, 2017b). The double membranes enclose two compartments: the intermembrane space (IMS) between the outer and inner membrane, and the matrix at the centre of the mitochondrion surrounded by the IMM. All mitochondria possess membrane invaginations emerging from the IMM and form elongated structures called cristae, however, not all MLOs have cristae. Mitochondria and MLOs all appear to harbour at least one pathway, the Fe-S cluster (ISC) assembly pathway.

Depending on the organism lifestyle, some mitochondria degenerated to MLOs, namely hydrogenosomes or mitosomes, through reductive mitochondrial evolution (Burki, 2016)(Burki, 2016). Both hydrogenosomes and mitosomes are structurally and biochemically reduced, in regards to canonical mitochondria. Surprisingly, a recent study reported the existence of a eukaryotic microbe, *Monocercomonoides* sp., for which degenerative evolution has gone as far as to completely loose the organelle (Karnkowska *et al.*, 2016). This was possible by relocating the ISC synthesis to the cytosol, highlighting the indispensable role of mitochondria to provide this pathway in most eukaryotes.

Hydrogenosomes were mainly studied in parasitic trichomonads, diverse free-living and rumen ciliate protozoa, and rumen chytrid fungi (Embley *et al.*, 2003). These organelles do not produce energy through oxidative phosphorylation (OXPHOS) like classic mitochondria do, but rather by fermentation. Substrate-level phosphorylation generates ATP and produces molecular hydrogen as a waste product, giving its name to this organelle. It also produces other metabolites such as formate and acetate (Muller, 1993; Hackstein *et al.*, 2001; Boxma *et al.*, 2004). Organisms possessing hydrogenosomes are the result of adaption to an anaerobic

environment where oxygen is lacking. Due to lack of selective pressure, most of these organelles have lost their genome during hypoxia-driven evolution, as it is the case for organisms such as *P. frontata* or *T. finlayi* (Lewis *et al.*, 2020). This was accompanied with the complete loss of mETC and absence of cristae (Embley and Finlay, 1994). Some organisms, however, have retained a remnant mitochondrial DNA (mtDNA) (*M. contortus, M. es,* and *N. ovalis*). In such cases, although all genes encoding for complex III and IV typically expressed in aerobic ciliates have been lost, hydrogenosomes of these organisms possess genes encoding for complex I subunits and components of the translation machinery. The proton pumping activity of complex I allows them to retain a reduced mitochondrial electron transfer chain (mETC) as well as some level of cristae formation (Finlay and Fenchel, 1989; Lewis *et al.*, 2020). As protein import necessitates a membrane potential (KLINGENBERG and ROTTENBERG, 1977), it is thought that hydrogenosomes deprived of all proton-pumping mETC complexes, including complex I, could use the gradient generated by the organellar production of ATP in exchange for cytosolic ADP. ADP/ATP carrier (AAC) proteins, part of the mitochondrial carrier family (MCF), have been identified in several organisms including *P. frontata* (Lewis *et al.*, 2020).

Mitosomes are the most reduced form of MLOs. The only function known to date is the ISC synthesis, and do not produce any ATP. Yet, they require ATP to import proteins and support activities of ATPases dependent proteins such as Cpn60 and/or mtHsp70 (Dagley *et al.*, no date; Tovar, Fischer and Clark, 1999; Williams *et al.*, 2002; Riordan *et al.*, 2003; Tovar, Cox and Giezen, 2007; Tsaousis *et al.*, 2008). Thus, mitosomes possessing organisms must either produce ATP in the cytosol or import it from host cell, as it is the case of intracellular parasites (Tsaousis *et al.*, 2008). It is thought that import of ATP by mitosomes can occur through a complex of proteins part of the MCF. In classic mitochondria and hydrogenosomes, MCF proteins such as AAC proteins, allow exchange of organellar ATP with cytosolic ADP. In principle, an MCF AAC could operate in reverse and exchange mitosomal ADP for cytosolic ATP (Kunji, 2004). *Entamoeba, E. hystolitica* and *C. parvum* encode for MCF proteins and the Entamoeba MCF protein was shown to transport ATP and ADP using a novel mechanism that does not seem to require a membrane potential (Chan *et al.*, 2005). Overall, mitosome functions remain enigmatic and awaits further studies.

6.5.2. Canonical mitochondria

What is known about mitochondria and their biology emanates from focused research on mainly yeast and mammalian cell models. These "text book" mitochondria are known to be the main site for ATP production through OXPHOS, but also houses other key pathways such as ISC biogenesis, the tricarboxylic acid (TCA) cycle, beta-oxidation of fatty acids, haem biosynthesis, calcium homeostasis, metabolism of certain amino acids and in metazoans they also play a role in apoptosis. Some of those pathways described below, namely the TCA cycle, ISC and haem biosynthesis, have a direct contribution in the respiratory chain function.

6.5.2.1. Oxidative phosphorylation and contributing pathways

OXPHOS is a characteristic process of aerobic cells which is essential for generating the energy the cell need to survive. It consists in series of redox reactions with the transfer of electrons from one carrier to the other along the IMM, which generates an electrochemical gradient that can be used to power the production of ATP. Respiration complex I-IV are the vectors through which electrons flow. Most components of each complex are encoded into the mitochondrial genome. mETC reaction is set in motion by NADH and $FADH_2$ transferring their electrons to complex I and II, respectively. This is coupled with protons being pumped across the IMM into the IMS by complex I. Electrons are then passed on to ubiquinone which is reduced into ubiquinol, and transports its electrons to complex III. As electrons pass through Complex III, more H^+ are pumped across the IMM, and the electrons are passed on to cytochrome C. Cytochrome C transfers the electrons to complex IV, pumping more H^+, and passes the electrons to molecular oxygen, the terminal electron acceptor. Molecular oxygen is split into two oxygen atoms, and accepts H^+ from the matrix to form water. This whole process generates a proton gradient that can be used by the ATP synthase, also called complex V, to make ATP, as well as support protein import into the organelle.

The TCA cycle, is carried out within the matrix of the mitochondrion. It is a series of enzymatic reactions that generate NADH and $FADH_2$ which can in turn be used by the OXPHOS pathway for the generation of ATP. The TCA cycle also generates

precursors to certain amino acids. This ancient pathway, common to all aerobic organisms, is highly conserved across the animal kingdom (Biology *et al.*, 2017). Each TCA cycle produces two molecules of CO_2, three molecules of NADH, three H^+, one molecule of $FADH_2$, and one molecule of GTP. As such each molecule of glucose produces double this (2 CO_2, 6 NADH, 6 hydrogen ions, 2 $FADH_2$ and 2 GTP) (Martínez-Reyes and Chandel, 2020). The TCA cycle is a tightly regulated pathway and its constant feedback with OXPHOS is crucial for cell homeostasis. The maintenance of an acetyl-CoA pool is crucial to sustain the TCA cycle activity (Martínez-Reyes and Chandel, 2020).

Haem is a porphyrin ring complexed with ferrous iron. Haem serves as prosthetic group of many proteins involved in fundamental biological processes like respiration, photosynthesis, and the metabolism and transport of oxygen. Haem containing proteins include haemoglobin and myoglobin, as well as cytochromes of the ETC, catalase, and nitric oxide synthase. Haem biosynthesis involves an eight-step enzymatic pathway which occur in the cytosol and in mitochondria, as well as in the plastid for organisms which possess some, such as plants and apicomplexa parasites.

ISC biosynthesis is another pathway which contribute to the mETC complexes functioning. ISCs are redox-active cofactors with the ability to donate or accept electrons. They are essential components of complexes I, II and III of the respiratory chain and allow electron transfer from one complex to another. ISCs are essential for cell survival and can be found in other cell compartments such as the nucleus (Balk and Lobréaux, 2005; Lill and Mühlenhoff, 2008), and the cytosol (Lill, 2009), and hence take part in many cellular pathways. Moreover, the mitochondrial ISC biogenesis pathway provides the cytosol with essential precursors to the cytosolic ISC assembly pathway involved in apoprotein maturation (Lill *et al.*, 2015).

6.5.2.2.   Mitochondrial genome

Canonical mitochondria have retained a vestigial genome of about 3–100 genes depending on the species. The mtDNA encodes at least some of the essential transmembrane subunits of the OXPHOS complexes. S. cerevisiae mtDNA encodes for 8 proteins of the respiratory chain, 24 tRNAs, the 21S and 15S ribosomal RNAs,

and the 9S RNA component of RNase P (Foury *et al.*, 1998), while human mtDNA encodes for 13 proteins of the respiratory chain, 22 tRNAs, and 2 rRNAs (Dennerlein, Wang and Rehling, 2017)(Dennerlein, Wang and Rehling, 2017), the rest of the mitochondrial proteome is encoded in the nucleus. The respiratory chain being of dual genetic origin, a tight gene expression coordination between the two compartment is key for mitochondrial biogenesis, and prevents wasteful translation and assembly of complex intermediates (Fox *et al.*, 2012; Soto *et al.*, 2012). Studies in yeast have shown that mitochondrial translation regulation upon a nutrient shift was found to be dependent on mitochondrial protein import (Couvillion *et al.*, 2016). Although protein import regulation is not well understood in human mitochondria, some evidence of translation regulation of the mitochondrially encoded COX1 was demonstrated through the translational regulator TACO (Richman *et al.*, 2016)(Richman *et al.*, 2016), suggesting a cross-talk between mitochondria translation needs and import of regulatory factors.

6.5.2.3.   Mitochondrial protein import

Although mitochondria possess their own genome, the majority of the mitochondrial proteome is nuclear encoded. These organelles have thus established a highly specialised import machinery which sorts mitochondrial molecules and enables correct delivery to their final site of action. There are different mitochondrial targeting signals and transport paths which lead precursor proteins to their biologically relevant subcompartment. All targeting signals guide them to the mitochondria upon synthesis in the cytosol, and their different sequences and properties allows recognition by different protein import complexes which ensure their correct subcompartment translocation. The vast majority of precursor proteins enter the mitochondria by going through the main entry gate, the translocase of the outer membrane (TOM), with Tom40 being the core component. Proteins first interact with Tom20 and Tom70 receptors which serve as quality control checkpoints and allows passage based on whether appropriate targeting signal is present or not. For proteins destined to the OMM, small Tim chaperones present in the IMS collect the proteins, transfer them to the Sorting and Assembly Machinery (SAM), where they are integrated into the OMM (Kutik *et al.*, 2008). For IMS proteins, the mitochondrial intermembrane space import and assembly (MIA) machinery is responsible for sorting, and Mia40 forms transient intermolecular disulfides with incoming precursor proteins which traps

them in the IMS. Disulfide bridges are then catalysed within the proteins by Mia40 releasing the protein in the IMS (Chacinska *et al.*, 2004; Müller *et al.*, 2008). IMM carrier proteins, as OMM proteins, are transported through the IMS by small Tim chaperones and subsequently integrated into the inner membrane by the translocase of the inner membrane 22 (TIM22 complex) in a membrane potential ($\Delta\psi$)-driven manner (Rehling *et al.*, 2003). Presequence-carrying preproteins are directly passed on from the TOM complex to the TIM23 complex, both associating into a supercomplex (Pon *et al.*, 1989). Dependent on the presence or absence of additional import signals, the TIM23 complex mediates either the translocation of presequence-carrying precursors into the matrix or their lateral sorting into the inner membrane (Bohnert *et al.*, 2010). Whereas lateral membrane integration depends on $\Delta\psi$ as the sole energy source, complete import into the matrix additionally requires the ATP-driven presequence translocase-associated import motor (PAM) (Strub, Röttgers and Voos, 2002).

6.5.2.4. Mitochondrial tRNA import

Although the vast majority of the mitochondrial proteome is nuclear encoded and imported, the mitochondrial genomes encodes for essential proteins, as mentioned above, and mitochondrial translation is a necessity. Mitochondrial tRNA import (MITI) is a widespread pathway amongst eukaryotes which although is obvious and mandatory for organisms missing mitochondrially encoded tRNAs, it occurs as well in organisms possessing a complete set of mitochondrial tRNA (mt-tRNA) (Lithgow and Schneider, 2010; Rubio and Hopper, 2011; Schneider, 2011). Yeast and human mitochondria are two well-known examples of the latter. Organisms with reduced mitochondrial genomes can lack from one tRNA gene (e.g. the marsupial metazoan Didelphis virginiana) to the complete set of tRNA genes as it is the case for trypanosomatids (e.g., *Trypanosoma brucei*, *Leishmania tarentolae*) and alveolates (e.g., apicomplexans such as *Plasmodia*, *Toxoplasma*) (Salinas-Giegé, Giegé and Giegé, 2015). MITI in *T. brucei* has been demonstrated for all tRNA except tRNA[Met-i] and tRNA[Sec] (Crausaz Esseiva *et al.*, 2004; Bouzaidi-Tiali *et al.*, 2007). For MITI to occur, cytosolic tRNA destined to the mitochondrion need to be recognised, and so must possess some determinants which acts as tRNA import signals. These are thought to be only present in mature tRNAs (Schneider, 2011). MITI usually require the intervention of cytosolic factors to guide the tRNAs to the mitochondria before import. Yeast use the glycolytic enzyme enolase Eno2p

to recruit tRNA$^{Lys(CUU)}$ and transfers it to pre-MSK1, the precursor of the mitochondrial lysyl-tRNA synthetase (Entelis *et al.*, 2006). In plants, no such cytosolic factors have not been identified (Delage *et al.*, 2003; Salinas *et al.*, 2005), although aminoacyl tRNA synthetase (aaRSs) have shown to have a potential role in MITI (Dietrich *et al.*, 1996). In *T. brucei*, tRNAs are targeted to the mitochondrion in association with the cytosolic elongation factor eEF1a (Crausaz Esseiva *et al.*, 2004; Bouzaidi-Tiali *et al.*, 2007). Regarding the tRNA import machinery, there are two categories: (i) one which is dependent on the canonical protein import machinery, and (ii) one that is not. In Leishmania, a putative RNA import complex (RIC) has been identified as a complex necessary for MITI (Mukherjee *et al.*, 2007) but there is some controversy on this topic. This complex is composed of many proteins known to be essential players in the mETC and protein import (Mukherjee *et al.*, 2007), and hence, would places this parasite in the first category. Yeast, interestingly, utilizes the TOM and TIM complexes to translocate tRNA^{lys} into the mitochondria in association with mitochondrial aaRSs (Kolesnikova *et al.*, 2010), but was also shown to import tRNA^{gln} in the absence of cytosolic factors and membrane potential (Rinehart *et al.*, 2005). *S. cerevisiae* therefore belongs in both categories. Plants, however, require the help of the voltage-dependent anion channel (VDAC), a pathway which does not depend on the protein import pathway, and was repurposed to enable the import of tRNA (Salinas *et al.*, 2006). MITI is thus a widespread phenomenon highlighting its functional relevance as it plays a key role in mitochondrial biogenesis in many eukaryotes.

6.5.2.5.   tRNA maturation

In theory, there are two options regarding the state of the mitochondrially imported tRNAs: they can a either be imported in their mature sate – maturation would happen in the cytosol, or in their immature state – maturation, if required, would occur in the mitochondrion. The state of mitochondria imported tRNAs has been a subject of debate in some protist parasites. Studies in trypanosomatids have had some opposing views for. Previous studies have suggested that tRNAs are imported into the mitochondrion as precursors in *T. brucei* (Hancock *et al.*, 1992; LeBlanc, Yermovsky-Kammerer and Hajduk, 1999), while in vivo study suggested that essentially only mature tRNAs are imported (Hauser and Schneider1, 1995; Tan *et al.*, 2002). For *Leishmania*, although a previous study has shown import of

unspliced tRNA^{Tyr} into mitochondria (Sbicego *et al.*, 1998) a consensus seems to have settled on the fact that only mature and fully processed tRNA are imported (BD and L, 1996; Kapushoc *et al.*, 2000; Rubio *et al.*, 2000). This implies that they undergo maturation with editing and processing prior import. tRNAs maturation is a multi-steps process consisting in tRNA splicing and modification which occur in the nucleus and the cytosol. This allow tRNAs to transition from immature pre-tRNAs to mature and functional tRNAs. The location and frequency of modified nucleosides within each tRNA are highly conserved (Grosjean *et al.*, 1995). These modifications help to faithfully decode codons during protein biosynthesis, as well as stabilize tRNA tertiary structure (Lorenz, Lünse and Mörl, 2017). tRNA maturation begins with the cleavage of the 5' end of the tRNA, followed by the 3' end cleavage, addition of the conserved CCA nucleotides on the acceptor stem of the tRNA, and other modification in the nucleus (Hopper, 2013). Pre-tRNA intermediates are exported to the cytosol and traffic to the OMM where splicing of the intron and joint of the two exons occur. Other modifications occur in the cytosol. The resulting mature tRNAs can then either remain in the cytosol and take part in translation or traffic back to the nucleus by retrograde nuclear import for further modifications, then re-exported into the cytosol (Hopper and Nostramo, 2019). Previous studies have also shown that some tRNAs return in the nucleus in their aminoacylated state (Grosshans, Hurt and Simos, 2000; Azad *et al.*, 2001) generating debates on whether translation happens in the nucleus as well (David *et al.*, 2012). In contrast to cytosolic tRNAs, in organisms which possess mitochondrially encoded tRNAs, such as mammalian cells, plants and fungi, tRNA maturation occurs in the mitochondrial matrix (Daoud, Forget and Lang, no date; Rossmanith *et al.*, 1995; Kunzmann, Brennicke and Marchfelder, 1998). Mitochondrial tRNAs are generally synthesized as part of polycistronic transcripts with other genes in between them. Release of tRNAs from these precursors is thus not only required to produce functional components for translation, but also responsible for the maturation of other mitochondrial RNA species such as mitochondrial mRNA and mitochondrial rRNA (Ojala, Montoya and Attardi, 1981). Mitochondrial tRNA maturation is a reduced process compared to cytosolic tRNA maturation (Rossmanith, 2012).

6.5.2.6.   Mitochondrial translation

The mitochondrial translation machinery is composed of mtDNA encoded rRNAs and tRNAs, as well as many nuclear encoded proteins such as initiation, elongation and termination translation factors (Hammarsund *et al.*, 2001; Gaur *et al.*, 2008), mitochondrial ribosomal proteins, and mitochondrial aminoacyl-tRNA synthetases and methionyl-tRNA transformylase. The core component of the mitochondrial translation system, the mitochondrial ribosome, also called mitoribosome (O'Brien, 1970), is assembled inside the mitochondrion. The small and large subunits of the mitoribosome are each composed of many nuclear encoded ribosomal proteins and mitochondrially encoded rRNAs. Mitoribosomes vary in size and in RNA and protein composition depending the organism. The yeast 74S mitoribosome, which is typically about 3 MDa, and the human 55S mitoribosome of 2.7 MDa (Greber and Ban, 2016) are both bigger in size and have a lower RNA to protein ratio compared to the 2.3 MDa bacterial ribosomes with which they share a common ancestor (Amunts *et al.*, 2015). Indeed these mitoribosomes have evolved to facilitate synthesis hydrophobic proteins and their co-translational delivery to the inner membrane (Amunts *et al.*, 2014; Brown *et al.*, 2014; Greber *et al.*, 2014). The mitochondrial translation process possesses some unusual features. Amongst those are the usage of a modified codon decoding system. In humans, the conventional UGA stop codon was reassigned to tryptophan and the two arginine triplets (AGA and AGG) serve as stop codons, and in addition, AUA was recoded to methionine rather than the isoleucine codon. Furthermore, unlike in cytosolic and prokaryotic translation, mitochondrial translation initiation seems to be much more reduced. Only two homologues of the cytosolic initiation factors were retained, IF2 and IF3, with mtIF2 which may have taken on the functions of the prokaryotic IF1 (Grasso *et al.*, 2007; Christian and Spremulli, 2012). Also, initiation and elongation both utilize only one type of tRNA^{Met} (Christian and Spremulli, 2012; Kuzmenko *et al.*, 2014), necessitating that the initiation factor specifically recognizes the formylated version of tRNA^{Met}. In contrast to yeast, mammalian mature mitochondrial mRNAs lack significant untranslated regions (UTRs) which are supposed to flank most open reading frames (ORFs) (Temperley *et al.*, 2010). Although the 3'-termini mature to a poly(A) tail, the 5'-termini are left bare and unstructured which are thought to be preferentially recognised by the specialised mitoribosomes and participate in translation initiation (Sharma *et al.*, 2003; Jones *et al.*, 2008). Elongation proceeds along the mitochondrial mRNA is facilitated by the mtEF-Tu elongation factor which delivers amino-acylated

tRNAs to the mitoribosome (Nagao, Suzuki and Suzuki, 2007), mtEF-Ts which allows the recycling of mtEF-Tu (Xin *et al.*, 1995), and mtEF-G1 which catalyses the translocation step of protein biosynthesis (Bhargava, Templeton and Spremulli, 2004). The termination process has not been fully clarified. Two release factors, mtRF1 and mtRF1a, recognise the stop codon and trigger the release of the protein (Soleimanpour-Lichaei *et al.*, 2007; Nozaki *et al.*, 2008). After release of the newly synthesized protein mtEFG2, initially thought to be involved in elongation, and the ribosome recycling factor mtRRF together enable the dissociation of the mitoribosomal subunits, tRNA and mRNA (Bhargava, Templeton and Spremulli, 2004; Rorbach *et al.*, 2008). It allows making those components to be available for a new round of protein biosynthesis.

6.5.3. Apicomplexan mitochondrion

6.5.3.1.   General mitochondrial structure

T. gondii possesses a single large mitochondrion which is mostly found in close proximity to the cell periphery when intracellular, and only divides in a cell cycle dependant manner (Ovciarikova *et al.*, 2017). This is in sharp contrast with mammalian cells which contain numerous, highly dynamic mitochondria which can autonomously divide according to the cell's physiological demands (Youle and Van Der Bliek, 2012). When extracellular, however, *T. gondii*'s mitochondrion undergoes drastic morphological changes with reduced pellicle contacts (Ovciarikova *et al.*, 2017). However, the reasons behind such morphological contrast between intra and extracellular is not known.

6.5.3.2.   Mitochondrial genome

Apicomplexan parasites possess a divergent mitochondrion with the smallest mitochondrial genome known to date of 6 kb (excluding *Cryptosporidium* spp. which has lost its whole genome). It encodes for only 3 mitochondrial proteins, all conserved and part of the mETC: cytochrome b subunit (Cytb) of complex III, and cytochrome c oxidase subunits I and III (CoxI and III) of complex IV (Suplick *et al.*, 1988; Vaidya, Akella and Suplick, 1989; Feagin, 1992; Lin, Gross and Bohne, 2011; Cinar *et al.*, 2015; Ogedengbe *et al.*, 2015), and also encodes for highly fragmented rRNA (Feagin *et al.*, 2012; Hillebrand *et al.*, 2018). Mitochondrial

genome structure varies from concatemeric to linear form and expresses between 20 to 27 rRNA fragments, depending on the species (Hikosaka, Kita and Tanabe, 2013). Most apicomplexan mtDNA sequences are available, however, progress on solving *T. gondii*'s mtDNA sequence has only very recently been made (Namasivayama *et al.*, 2020). The challenge in sequencing *T. gondii*'s mtDNA lies in the presence of numerous pseudogenes of mitochondrial origin in the nuclear genome making it difficult to discriminate them from the actual mitochondrial genes (Ossorio, Sibley and Boothroyd, 1991). Namasivayam *et al.*, (2020) has tackled this very challenging question and revealed a novel and highly fragmented mtDNA for *T. gondii* composed of 21 non-redundant sequence blocks, none of which individually encode for a full gene of coxI, coxIII and Cytb. This represent an extreme case of DNA fragmentation and evolutionary driftage from conventional mitochondrial genomes. Further studies are need to solve the exact mtDNA topology.

6.5.3.3.   A divergent mETC

The apicomplexan mitochondrion retained many of the canonical functions from model organisms, with some species and life cycle stage specific variations. It has kept its ATP production ability through OXPHOS, although, there are significant differences compared to the canonical OXPHOS complexes. The ATP synthase, also called complex V, is composed of two subcomplexes: the F1 and the Fo sector complex. While the F1 subcomplex components are well conserved across various eukaryotic phyla, Fo is highly divergent and is predicted to contain many unidentified components for which the gene sequences are too divergent to be identified by homology searches (Velours and Arselin, 2000; Meyer *et al.*, 2007). There is, however, on-going progress with the identification of two new indispensable conserved apicomplexan protein (ICAP) subunits in *T. gondii*: ICAP2 and ICAP18 (Huet *et al.*, 2018). Also, apicomplexan parasites lack the canonical complex I and possess a type II non-proton-pumping NADH dehydrogenases (NDH2s) instead (Lin, Gross and Bohne, 2011). NDH2s have been reported in prokaryotes, plants and fungi (Kerscher, 2000), many of which possess the canonical complex I as well, but are absent in mammalian mitochondria. This is why it had been suggested as attractive drug targets against these pathogens (Biagini *et al.*, 2006; Saleh *et al.*, 2007).

6.5.3.4.   Mitochondrial metabolic pathways

Similarly, to canonical mitochondria, apicomplexans have retained the ISC, haem and ubiquinone biosynthesis pathways, and some amino acids metabolism (describe above). Some parasites specific metabolic pathways directly feed into the mitochondrion's own metabolism system, such as dimethylallyl diphosphate and IPP produced by the apicoplast and used in the mitochondrion's ubiquinone biosynthesis (Ling *et al.*, 2007), and the haem biogenesis pathway which requires the mitochondrion, the apicoplast and the cytosol (Seeber and Soldati-Favre, 2010). The close association of the mitochondrion and the apicoplast might simplify metabolite exchange through membrane contact sites. Some mitochondrial pathways are not essential for certain apicomplexans depending on their life stage. For instance, *P. falciparum* asexual blood stage only requires its mitochondrion for pyrimidine biosynthesis (Vaidya and Mather, 2009). Moreover, *Cryptosporidium*'s mitosome only kept two essential functions: the ISC biogenesis and ATP production, with the latter that involves a reduced mitochondrial respiratory chain called alternative oxidase, depending on the species (Vaidya and Mather, 2009; Mogi and Kita, 2010).

6.5.3.5.   Protein import pathway in apicomplexans

Apicomplexan parasites, just like most mitochondria possessing organisms, rely heavily on mitochondrial protein import. Some aspects of protein import are conserved and hence similar to model organisms. This is the case for N-terminal pre-sequences which have been shown to target *T. gondii* proteins to the mitochondrion (Toursel *et al.*, 2000), although some variations exists in terms of the position of the signal within the sequence (Brydges and Carruthers, 2003; Vögtle *et al.*, 2009). However, there are many aspects of targeting sequences which differ significantly. Many matrix proteins do not have the canonical N-terminal signal. This often makes the use of prediction algorithm software, such as MitoProt II, obsolete as these were designed specifically for model organisms. There are other types of targeting signals described in model organisms which are also predicted to have a role in *T. gondii* mitochondrial protein translocation, such as β-barrels (Sheiner *et al.*, 2015; Van Dooren *et al.*, 2016), and tail-anchored signals (Stilger and Sullivan, 2013), however, these have not yet been studied. Protein signals get even more complex with dual targeting to the mitochondrion

and apicoplast, or mitochondrion and cytosol in apicomplexans (Pino *et al.*, 2007, 2010). The apicomplexan protein import machinery is somewhat similar to that of yeast, in regards that it employs homologues of Tom40, Tom22 and Tom7 (Van Dooren *et al.*, 2016), however, lack homologues for Tom70 and Tom20. Despite this, *T. gondii* TOM complex is of similar size to that of the yeast counterpart, namely ~400 kDa (Van Dooren *et al.*, 2016). This suggests that parasite specific components may compensate for these homologues' absence. Homologues of Sam50, which forms the core of the SAM complex in yeast and humans (Kozjak *et al.*, 2003; Kozjak-Pavlovic *et al.*, 2007), have been identified in apicomplexans and experimentally validated for *T. gondii* and *P. falciparum* (Sheiner *et al.*, 2015). However, Sam35 and Sam37 homologues could not be identified. There is also evidence of the use of a MIA machinery in apicomplexans with the presence of Erv1 and other components (Eckers *et al.*, 2013; Van Dooren *et al.*, 2016), however, the Mia40 homologues seems to be lacking. Amongst the IMS small Tim chaperone, only the homologue of the yeast Tim22 was validated (Van Dooren *et al.*, 2016). Finally, the TIM23 machinery, with most of its components, were found *T. gondii* as well as all PAM subunits, highlighting these components to be conserved beyond the narrow spectrum of opisthokonta (Van Dooren *et al.*, 2016).

6.5.3.6.   Mitochondrial tRNA import: an enigma in apicomplexans

Although highly reduced, *T. gondii* possesses a mitochondrial genome that needs to be translated, and with no mitochondrial encoded tRNAs, import of cytosolic tRNA is expected to be an essential for mitochondrial translation. MITI has been mostly studied in model organisms, as mentioned above, and remains obscure for apicomplexan parasites. A handful of *in vitro* studies have provided evidence that MITI happens in *T. gondii* and *P. falciparum* (Esseiva *et al.*, 2004; Pino *et al.*, 2010; Sharma and Sharma, 2014). However, the understanding of the import process and the translocon composition has not yet been solved. *T. brucei, L. tropicana* and yeast perform MITI and use components of the protein import machinery to help with this process, a point which was used for our bioinformatic screen (section 8.3.1). In the specific case of yeast, tRNA[lys] import is facilitated through the protein import channel by the co-import of mitochondrial aaRSs to load free tRNAs with their corresponding amino acids in the organelle and can import tRNA[gln] without aaRS (Figure 6.4.) (Rinehart *et al.*, 2005). As *T. gondii*'s mtDNA does not encodes for any mitochondrial aaRSs nor tRNAs, we hypothesized that it relies on

the import of aminoacylated nuclear encoded tRNA through an import machinery for which components are unknown (Figure 6.4). The fact that tRNAs are essential tools for translation and that mammalian cells do not rely on MITI survival makes this pathway a good lead for drug target discovery.
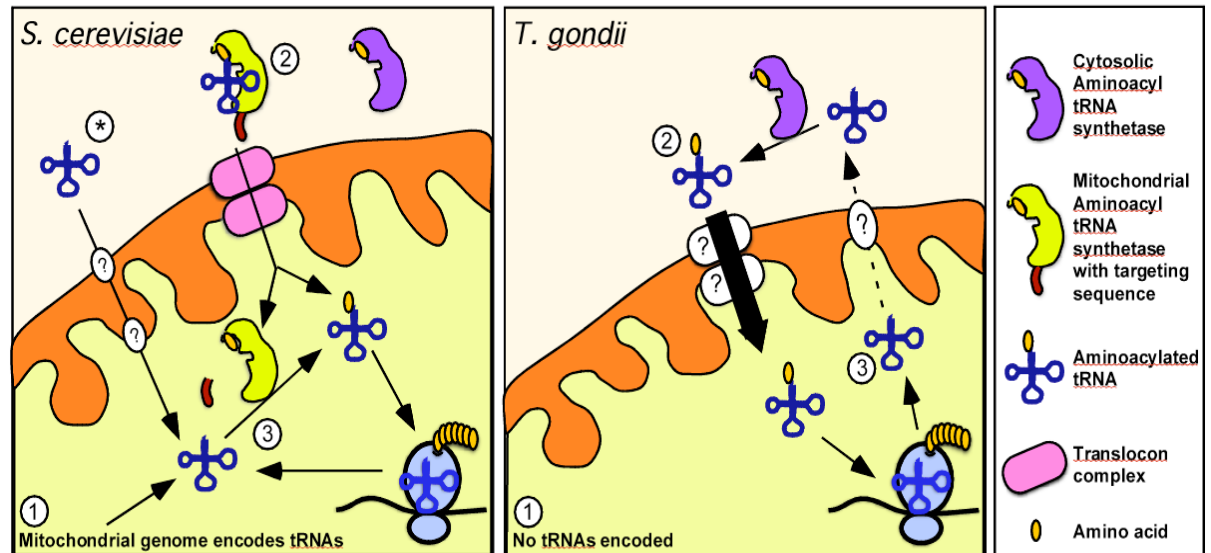

Figure 6.4 Comparison between the *S. cerevisiae and T. gondii* mitochondrial tRNA import. *S. Cerevisiae* can import amino acid loaded tRNA into the mitochondria when coupled with a mitochondrial aminoacyl synthetase and through a translocon complex. Then, it is incorporated to the translation machinery. *T. gondii*, does not possess such an aminoacyl synthetase. It has thus found a way to import amino acid loaded tRNA alone through an unknown tRNA import in order for translation to occur. (Scheme by Dr. Lilach Sheiner)

6.5.3.7.   Mitochondrial translation in apicomplexan

The mitochondrial translation process, including mitoribosome assembly is currently unknown in apicomplexan parasites. Evidence of mitochondrial translation in the literature has mainly been indirect. For instance, the nuclear encoded mtEF-Tu was shown to be targeted to the mitochondrion and Cytb mRNA was found in mitochondrial fractions (Pino *et al.*, 2010), indicating that an active translation machinery is imported from the cytosol. Moreover, a previous study demonstrated that resistance to atovaquone, an antimalarial drug that targets the mETC, can be acquired through mutations within the mitochondrially encoded Cytb subunit gene (Siregar *et al.*, 2008). For *P. falciparum*, a study revealed that during the asexual stages, an active mETC is essential for replenishing ubiquinone, which is necessary to accept electrons from the type 2 dihydroorotate dehydrogenase (DHODH) enzyme for the pyrimidine synthesis pathway (Painter *et al.*, 2007). This was shown by an elegant cross species complementation with the

yeast type 1A DHODH which uses fumarate as the electron acceptor, relocating pyrimidine pathway in the cytosol (Painter *et al.*, 2007). Together, these observations highlight an active mitochondrial translation system which is essential for mitochondrial functioning, and thus vital for parasite. Another recent study by Ke *et al.*, (2018) has shown that depletion of the mitochondrial ribosomal protein L13 in *P. falciparum* induced mitochondrial morphology and mETC defect, and was deleterious to the parasite's survival (Ke *et al.*, 2018). However, Ke et al. (2018) was unsuccessful in rescuing this phenotype by complementation with the yeast DHODH as it was shown in Painter *et al.*, (2007). This raises questions regarding the link between mitochondrial translation and mETC in *P. falciparum*.

6.5.4. Mitochondria purification methods

To study the mitochondrion's genome, proteome, and metabolic functions, its isolation is essential and must be sufficiently pure and intact to adequately represent its function within the cell. Mitochondria purification techniques have been established in well studied organisms, however, there is a lack of equivalent protocols for apicomplexans. It is especially difficult in apicomplexans to separate the mitochondrion from the apicoplast which are physically linked to one another. Yet, this is crucial for studying organelle translation, given that both have a genome and are translationally active.

In general, mitochondria are prepared using differential centrifugation alone for crude mitochondrial preparation or coupled with density gradient ultracentrifugation for pure mitochondrial fractions. For the yeast *S. cerevisiae*, Meisinger et al. (2006) described a protocol for mitochondria enrichments and purification as followed: after digesting of the yeast wall and spheroplast homogenisation, crude mitochondria were obtained by differential centrifugation 1500 x g to remove large debris, nuclei and unbroken cells, followed by a 12,000 x g spin to pellet mitochondria. The crude mitochondria fraction typically contains plasma membranes, vacuole, and ER contaminants (Liao *et al.*, 2018). For highly purified mitochondria, the crude mitochondria fraction was sedimented on a 60%, 32%, 23% and 15% sucrose gradient at ultra-high speed of 134,000 x g for 1h. Purified mitochondria was recovered at the 60%/32% sucrose interface (Liao *et al.*, 2018). Minor variations of this method exist in terms of gradient density percentages and centrifugation speed depending on the organism, but overall this

method is effective, and has been used in many studies to tackle mitochondria biology questions for yeast, as well as in other eukaryotes. A similar method which uses a Percoll density gradient instead of sucrose is also commonly used. This is the case for mitochondria isolation for *Arabidopsis thaliana*. This was performed by grinding the plant tissues in mortar with a pestle and quartz, the lysate was filtered, and similar to the yeast protocol above, a slow and high-speed spin was performed to obtain a crude mitochondrial fraction. The crude mitochondrial pellet can be then loaded onto a continuous linear 50% Percoll gradient (Niehaus *et al.*, 2020) or on different Percoll gradient layers of 43%, 23% and 18% (Sweetlove, Taylor and Leaver, 2007; Carroll, 2017), and centrifuged for 15 min at ~16000 x g. If using a linear gradient, mitochondria will be near the bottom of the tube. With the multiple Percoll densities percentage gradient, mitochondria typically settle between at the 43%/23% interface (Sweetlove, Taylor and Leaver, 2007; Carroll, 2017). Although effective, differential centrifugation followed by density gradient ultracentrifugation requires large amounts of starting material to recover a sufficient quantity of pure mitochondria for downstream applications, and it is quite labour intensive. A recent study in yeast reported a different method which uses paramagnetic beads to immunoprecipitated TOM70 histidine tagged mitochondria from crude mitochondria samples (Liao *et al.*, 2018). Scientists report that mitochondria prepared using this method contain fewer contaminants, and are similar in ultrastructure, protein import and mETC complex activity compared to mitochondria isolated by differential centrifugation. They also mention that this isolation method is suitable for small samples, is faster than differential and density gradient centrifugation, and importantly, it can be applied to any cell type where the genetic modification can be introduced by CRISPR or other methods (Hornig-Do *et al.*, 2009; Franko *et al.*, 2013; Liao *et al.*, 2018). For *T. gondii*, this type of crude mitochondria preparation was performed in previous studies to assess mitochondrial functions, including MITI (Esseiva *et al.*, 2004), mitochondrial translation (Pino *et al.*, 2010), and ATP synthase composition (Huet *et al.*, 2018), however, the quality of such preparation had not been shown.

6.6. Genetic manipulation to study mitochondrial biology in apicomplexan parasites

6.6.1. The tetracycline-inducible system

The tetracycline-transactivator system is a popular tool to study gene function by transcription inhibition of a gene of interest (GOI). This tool originates from the tetracycline-repressor system (TetR) which then was adapted to *T. gondii* (Meissner *et al.*, 2001). The repressor protein TetR is fused to an activation and named tetracycline dependent transactivator domain (TATi) (Meissner et al., 2002), which can bind to the Tet-operator sequence (TetO) placed upstream of a minimal tet-responsive promoter (TRE) which controls the transcription of the GOI. TATi binding to the TetO triggers the recruitment of the transcription machinery and allows transcription of the GOI. However, addition of the tetracycline homologue, anhydrotetracycline (ATc), prevents binding of the transactivator to the TRE and hence down-regulated the expression of the GOI.

Generation of such transgenic lines originally required an arduous tow step genetic manipulation: (1) expressing a repressible copy of the GOI in a TATi-1 expressing line, (2) followed by the knockout of the native gene. This was reduced to a single step process by directly replacing the native promoter of the GOI with a tetracycline repressible promoter fused a DHFR selectable cassette by double homologous recombination, in a ΔKu80 TATi-1 expressing line (Sheiner *et al.*, 2011). Recently, this single step genetic engineering was further improved with the introduction of CRISPR-CAS9 which increases the double homologous recombination efficiency.

6.7. Aim of study

Apicomplexan parasites' mitochondrion is an essential organelle which has undergone a drastic reduction throughout evolution resulting in its driftage from "text book" mitochondria. Plenty of research has been carried out on mitochondrial translation in model organisms, while only very little is known in the case of apicomplexan parasites. Apicomplexan parasites have lost their entire set of mitochondrially encoded tRNA genes which are essential for mitochondrial translation. This implies that these molecules must be imported from the cytosol into the mitochondrion. Mitochondrial tRNA import (MITI) is not unique to apicomplexans. As mentioned above, yeast, mammalian cells, plants and trypanosomatids also import tRNAs. The mode of translocation is not fully

understood, but depending on the organism, some of the components of the MITI machinery have been shown to be either shared with the protein import machinery or not. The composition of the translocon complex in apicomplexans remains, however, unknown; and more generally, there is a gap of knowledge regarding the whole mitochondrial translation pathway. Mitoribosomes, which are the core components of this machinery, again, have been mainly studied in model organisms and in trypanosomatids. These studies have revealed the existence of a wide range of mitoribosomes diversity in terms of size and protein to RNA ratios. Such diversity makes the mitoribosome ideal for drug discovery. Consequently, in this study, we aimed to answer two key research questions:

(1) What is the mechanism which allows the translocation of cytosolic tRNA into the mitochondrion in T. gondii? Answering this question requires identification of the MITI translocon components. In this thesis I aimed at identifying these components via tRNA affinity immunoprecipitation, and by using an in-silico search designed to focus on mitochondrial biogenesis components.

(2) What is the process of mitochondrial translation in T. gondii? The first step to answering this question is to detect the mitoribosome and validate its components, and establish a mitochondrial translation assay. For this, my thesis aimed at detecting the mitoribosome through gene tagging of new mitoribosomal proteins, and elaborating a new protocol to monitor mitochondrial translation.

Lastly, both questions required the use of mitochondria enriched samples. However, given the substantial amount of material necessary, using the appropriate cell lysis method which allows parasite up scaling and minimal mitochondria disruption was essential. Consequently, an additional aim of this study is to set up an appropriate cell lysis protocol which is compatible with our mitochondrial biology studies.

7. Materials and Methods

7.1. Equipment

Applied Biosystems	Real-time PCR light cycler (Prism 7500), MicroAmp® optical 96-well reaction plate, MicroAmp® optical adhesive film
Applied Precision	DeltaVision® Core microscope
BD Biosciences	Syringes, Needles (23-25 gauge)
Beckman Coulter	Cooling centrifuge (Allegra® X-12 Series)
Binder	CO_2 Tissue culture incubator
BioRad	Agarose gel electrophoreses equipment, UV transilluminator, SDS-PAGE system, Blotting apparatus, GenePulser Xcell, electroporation apparatus
GE healthcare	Nitrocellulose membrane (Hybond ECL),
G-Storm	Thermocycler
Heidolph	Orbital Shaker (Rotamax 120), Vortex (Reax top)
Heraeus Instruments	Incubator
Kühner	Shaking incubator (ISF-1-W)
Li-COR	Odyssey CLx
Milipore	MilliQ water deionising facility, 3 µm Millipore filters
Satorius	Analytical weighing scales
Sciquip	Sigma 6K 15 centrifuge (1150 rotor and 12500 rotor)
StarLab	ErgoOne Single & Multi-Channel pipettes
Stuart	Heat block
Syngene	Gel documentation system
Thermo scientific	CO_2 tissue culture incubator, Nanodrop spectrophotometer, Centrifuge (sorvall legend XFR), Table top centrifuge Heraeus Pico 21, cooling table top centrifuge (accuSpin™ Micro R), Pro pipette controller (S1 Pipet Filler)
Zeiss	Axioskop 2 (mot plus) fluorescence microscope with Axiocam MRm CCD camera, Primo Vert (light microscope), Axiovert 40 CFL fluorescence microscope with Axiocam ICc1, Axiovert A1 fluorescence microscope with Axiocam IMc1, ELYRA PS.1 Super-resolution microscope, sCMOS pco SIM camera, Plan Apochromat 63x lens

Table 7.1 Equipment

7.2. Computer Software

Adobe Systems Inc.	Adobe design premium CS4
Carl Zeiss Microscopy	Zen Black and Zen blue
CellProfiler	Cell Profiler 2.1.1 Analyst software
GraphPad software Inc.	GraphPad Prism version 7.3
Li-COR	Image Studio 5.0
Mendeley Desktop	Reference software
Microsoft Corporation	Windows 7, Microsoft Office 2010
National Institute for Biotechnology Information (*NCBI*)	Basic Local Alignment search tool (BLAST) (Altschul *et al.*, 1990)
National Institute of Allergy and	ToxoDB, EuPathDB, PlasmoDB (Gajria *et al.*, 2008)

National Institutes of Health	ImageJ (Schindelin *et al.*, 2015), Fiji (Schindelin *et al.*, 2012)
New England Biolabs (NEB)	NEB tools™: Double Digest Finder, Enzyme Finder, NEBCutter®, NEBBioCalculator®, Tm Calculator
OligoCalc	Oligo Analysis tool (Kibbe, 2007)
Thermo Scientific	Thermo Sientific web tools: Tm Calculator
University of Utah	ApE Plasmid Editor v2.0.53c Copyright© by M. Wayne Davies

Table 7.2 Software

7.3. Consumables, biological and chemical reagent

Life technologies	Phosphate buffered saline 1X (PBS), Trypsin/EDTA (0.05% w/v), DNaseI, NuPage SDS loading buffer and reducing agent, Ultrapure agarose
Marvel	Milk powder (skimmed)
Melford	Agar, dithiothreitol
NEB	DNA ladder (1 kb), all Restriction enzymes and associated buffers, T4 DNA ligase, Taq polymerase, Calf intestinal phosphatase (CIP)
Pheonix Research Products	GelRed nucleic acid stain
Promega	pGEM®-T Easy vectors system, GoTaq® G2 Flexi DNA Polymerase
Roche	$MgSO_4.7H_2O$, potassium hydroxide, paraformaldehyde
Sigma	Ammonium persulfate, Bromophenol blue sodium salt, Dulbecco's Modified Eagle Medium (DMEM), Ficoll, Ethylene glycol tetra-acetic acid, Ponceau S, Isopropanol, Sodium dodecyl sulfate (SDS), dimethyl sulfoxide (DMSO), N,N,N',N'-tetramethylethylenediamine, Triton X- 100, beta mercaptoethanol, Tween20, Giemsa stain, RNase-ZAP, Adenosine 5′-triphosphate disodium salt hydrate, Glutamine, 30% acryl-bisacrylamide mix, Sodium deoxycholate, K_2HPO_4, Magnesium chloride, Ampicillin sodium salt, Penicillin-streptomycin, Chloramphenicol (CAT), Pyrimethamine
Southern Biotech	Fluoromount G (with and without DAPI)
Thermo Scientific	Bovine serum albumin (BSA), Glycine, Methanol, Tris, Sodium chloride, Platinum Taq DNA Polymerase High Fidelity, Restore Western blot stripping buffer
VWR	$CaCl_2.2H_2O$, Glacial acetic acid, Ethanol, HEPES, Potassium chloride, Na_2HPO_4, KH_2PO_4, Potassium chloride, Na_2HPO_4, KH_2PO_4
Zeiss	Immersion oil

Table 7.3 Biological and chemical reagents

7.4. Kits

Qiagen	Spin Mini-prep, Plasmid Midi-prep, MinElute PCR Purification, QIAquick gel extraction kit, DNeasy blood and tissue, RNA extraction kit

Thermo Scientific	Maxima SYBR green

Table 7.4 Nucleic acid extraction and amplification kits

7.5. Buffers, solutions and media

50X TAE buffer	2 M Tris, 0.5 M Na$_2$EDTA, 5.71% glacial acetic acid (v/v)
5X loading die	15% Ficoll (v/v), 20 mM EDTA, 0.25% Bromophenol Blue in H$_2$O
NEB 1 kb DNA ladder	150 µl 1 kb ladder (1 µg/µl), 300 µl 5X DNA loading buffer, 1050 µl H$_2$O

Table 7.5 Buffers for DNA Analysis

4X separating gel buffer	1.5 M Tris-HCl (pH 8.8), 0.4% SDS (w/v)
Separating gel	8-15% of 30% acryl-bisacrylamide, 25% 4X separating gel buffer, 0.1% ammonium persulfate (APS) 10% (w/v), 0.2% N,N,N',N'-tetramethylethane-1,2-diamine (TEMED) (v/v)
4X stacking gel buffer	0.5 M Tris/HCl (pH 6.8), 0.4% SDS (w/v)
Stacking gel	4% of 30% acryl-bisacrylamide, 25% 4X stacking gel buffer (v/v), 0.1% APS 10% (w/v), 0.2% TEMED (v/v)
SDS PAGE running buffer	25 mM Tris, 192 mM glycine, 0.1% SDS (w/v)
Transfer buffer for wet blot	48 mM Tris, 39 mM glycine, 20% methanol (v/v)
Blocking solution	0.2%Tween (v/v), 3% skimmed milk powder (w/v), 0.037% SDS(w/v)
Washing solution or (PBS-Tween)	0.2% tween (v/v) in 1X PBS
1 M DTT	3.085 g 1,4-dithio-DL-threitol (DTT) in 20 ml 10 mM NaAc (pH 5.2)
10 % APS	1 g ammonium persulfate in 10 ml H2O

Table 7.6 Buffers for protein analysis

LB medium	10 g/l tryptone, 5 g/l yeast extract, 5 g/l NaCl
LB agar	1.5% (w/v) agar in LB medium
SOB medium	2% tryptone (w/v), 0.5% yeast extract (w/v), 0.05% NaCl (w/v), 2.5mM KCl, 10mM MgCl2
SOC medium	20 mM glucose in SOB medium
NYZ broth	5 g/l NaCl, 2 g/l MgSO4*7H20, 5 g/l yeast extract, 10 g/l casein hydrolysate, pH adjusted to 7.5 with NaOH
Ampicillin (1000X)	100 mg/ml in H2O

Table 7.7 Buffers and media for bacterial culture

DMEM complete	500 ml DMEM, 10 % fetal bovine serum (FBS) (v/v), 2 mM glutamine, 10 µg/ml penicillin/streptomycin
Electroporation buffer (Cytomix)	10 mM K2HPO4/KH2PO4, 25 mM HEPES, 2mM EGTA pH 7.6, 120 mM KCl, 0.15 mM CaCl2, 5mM MgCl2 with 5 mM KOH adjusted to pH 7.6, 3 mM ATP, 3 mM glutathione (GSH)
Giemsa staining solution	10 % Giemsa stain (v/v) in H2O
Rapamycin (1000X)	50 µM in DMSO
PFA fixing solution	4 % paraformaldehyde (PFA) (w/v) in PBS
Permeabilisation solution	0.2 % Triton X-100 (v/v) in PBS
Blocking solution	2 % bovine serum albumin (BSA) (w/v) in permeabilisation solution

7.6. Antibodies

Name	Species	Dilution		Source
		IFA	WB	
Aldolase	Rabbit??	(-)	1:1000	Meissner, M.
Catalase	Rabbit	(-)	1:3000	Soldati, D.
GAP45	Rabbit	1:1000	(-)	Soldati, D.
GFP	Mouse	1:500	1:2000	Roche
HSP60	Rabbit	1:2000	(-)	Sheiner, L.
IMC1	Mouse	1:1000	(-)	Ward, G.
Mic2	Mouse	1:500	(-)	Carruthers, V.
SAG1 (*Toxoplasma*)	Rabbit	1:1000	(-)	ABCAM
TgMys	Rabbit	1:1000	1:1000	Sheiner, L.
TgTom40	Rabbit	1:2000	1:1000	van Dooren
HA	Rat	1:1000	1:500	Sigma
Myc	Mouse	1:1000	1:1000	Cell signalling
Flag	Mouse	(-)	1:1000	Sigma-Aldrich
Strep	Mouse	(-)	1:4000	IBA

Table 7.9 Primary antibodies

Name	Species	IFA	WB	Source
Alexa Fluor350 anti-mouse	Goat	1:3000	(-)	Life Technologies
Alexa Fluor488 anti-mouse	Goat	1:3000	(-)	Life Technologies
Alexa Fluor594 anti-mouse	Goat	1:3000	(-)	Life Technologies
Alexa Fluor633 anti-mouse	Goat	1:3000	(-)	Life Technologies
Alexa Fluor350 anti-rabbit	Goat	1:3000	(-)	Life Technologies
Alexa Fluor488 anti-rabbit	Goat	1:3000	(-)	Life Technologies
Alexa Fluor594 anti-rabbit	Goat	1:3000	(-)	Life Technologies
Alexa Fluor633 anti-rabbit	Goat	1:3000	(-)	Life Technologies
Alexa Fluor350 anti-rat	Goat	1:3000	(-)	Life Technologies
Alexa Fluor488 anti-rat	Goat	1:3000	(-)	Life Technologies
Alexa Fluor594 anti-rat	Goat	1:3000	(-)	Life Technologies
IRDye800CW anti-Mouse	Goat	(-)	1:5000	Li-Cor
IRDye680RDanti-Rabbit	Goat	(-)	1:5000	Li-Cor
horseradish peroxidase	Mouse		1.10000	Promega
horseradish peroxidase	Rabbit		1.10000	Promega
horseradish peroxidase	Rat		1.10000	Abcam

Table 7.10 Secondary antibodies, fluorescent ligands and stains

7.7. Oligonucleotides

Experiment	Gene ID	Details	Sequence
Localisation	TGME49_203620	TgmS35 endogenous 3xHA tag_fw	TACTTCCAATCCAATTTAATGCCCA ACAAGAGTGGCTGT

	TGME49_203620	TgmS35 endogenous 3xHA tag_rv	TCCTCCACTTCCAATTTTAGCCGCC TTCTTCACCTCTCGC
	TGME49_226280	TgbL28m cDNA-Myc_fw	GGGCAGATCTATGCCGAAGAATCT TAACTTGTGG
	TGME49_226280	TgbL28m cDNA-Myc_rv	GTATCCTAGGAAAGGCACGGTTTTC CCGGTACTTGTG
	TGME49_263680	Endogenous 3xHA tag_fw	TACTTCCAATCCAATTTAATGCGTT CAGTCTCCTGGAGGCCTTTTCG
	TGME49_263680	Endogenous 3xHA tag_rv	TCCTCCACTTCCAATTTTAGCGCGC TGTTTCAAGGTGAAGGGG
	TGME49_201830	TgmL54 endogenous 3xHA tag_rv	TACTTCCAATCCAATTTAATGCGGT CTCCCAAGACACTCCG
	TGME49_201830	TgmL54 endogenous 3xHA tag_fw	TCCTCCACTTCCAATTTTAGCGGCA TCCCAGAAAGCGGCTTCAC
	TGME49_214790	Endogenous 3xHA tag_fw	TACTTCCAATCCAATTTAATGCATG CGGGGATTCCAAGAAACTCGG
	TGME49_214790	Endogenous 3xHA tag_rv	TCCTCCACTTCCAATTTTAGCGTGT TCGACGAACTGAGCGAG
	TGME49_251950	bL12m endogenous TwinStrep_rv	TACTTCCAATCCAATTTAAT
	TGME49_251950	bL12m endogenous TwinStrep_fw	GAATTCCCGTCCTCCACTTCCAATT TTAGC
	TGME49_230050	uL3m endogenous 3xFLAG_rv	TACTTCCAATCCAATTTAAT
	TGME49_230050	uL3m endogenous 3xFLAG_fw	GAATTCCCGTCCTCCACTTCCAATT TTA
	TGME49_257110	cDNA-Myc_fw	CTAAGATCTATGTCGTGCACGGTC GTACCT
	TGME49_257110	cDNA-Myc_rv	CTAGCTAGCTTTCTTGAAAAAGTCA GACGAACCC
Transient disruption via CRISPR/ Cas9	TGME49_214790	sgRNA sequence	GCTCTGCGGTGCTGCGCGAG
	TGME49_226280	TgbL28m sgRNA sequence	GGGGAAGTACCTGCGGCTGG
	TGME49_263680	sgRNA sequence	GTCCTCCACCCCAAGACGGT
	TGME49_233460	SAG1 sgRNA sequence	GAATGTCGCAAGGTGCTCCTAGTTT TAGAGCTAGAAATAGC
Promoter replacement mediated via CRISPR/ Cas9	TGME49_203620	TgmS35 sgRNA sequence	GAAGACAGCATGGGGCCACTTGG
	TGME49_203620	TgmS35 gRNA_fw	AAGTTGAAGACAGCATGGGGCCAC TG
	TGME49_203620	TgmS35 gRNA_rv	AAAACAGTGGCCCCATGCTGTCTTC A
	TGME49_203620	TgmS35 homology region_fw	GACATTAAAGGCAACCACAAGAACA GAGAACATCACAGTGAGAAGACAG CAAGCTTCGCCAGGCTGTAAATCC
	TGME49_203620	TgmS35 homology region_rv	CGACGGACCCCAGCAAGCTGGCCC GAGGACACCCGGCCAAGTGGCCC CATTGGTTGAAGACAGACGAAAGC AGTTG
	TGME49_203620	TgmS35 clone testing_fw	CTTTTCTGGCCTCTGCCTCAGC
	TGME49_203620	TgmS35 clone testing_reverse	CCGAGAAAGCGCGGAGCCAATA
	TGME49_216040	uS15m gRNA sequence	GAATGGCTTCTCTGGCGCGTCGG
	TGME49_216040	uS15m gRNA_fw	AAGTTGAATGGCTTCTCTGGCGCG TG
	TGME49_216040	uS15m gRNA_rv	AAAACACGCGCCAGAGAAGCCATT CA

	TGME49_216040	uS15m homology region_fw	GTCGTCTCCTCCTTCGTCTTCTTCT GCTTCTTCTTCTCTCTTCAAGTGGA AAGCTTCGCCAGGCTGTAAATCC
	TGME49_216040	uS15m homology region_rv	GCCCCCAACGCCTTGGTGGGCGAG AAAATCCGACGCGCCAGAGAAGCC ATTGGTTGAAGACAGACGAAAGCA GTTG
	TGME49_216040	uS15m clone testing_fw	CAGCTTCAAGTCAACTTGCC
		DHFR cassette test_rv	CACGGTTATCAAACCCGAG
		DHFR cassette test_fw	CGGTTCGCTTGAAGAAGG
	TGME49_240270	gRNA sequence	GTCTCTTCTGCTTTTCGCCATGG
	TGME49_240270	gRNA_fw	AAGTTGTCTCTTCTGCTTTTCGCCA G
	TGME49_240270	gRNA _rv	AAAACTGGCGAAAAGCAGAAGAGA CA
	TGME49_240270	Homology region_forwrad	TTTCTCCCCGGCTTTCGCGCTTTTC GCTTCTGTCTCTTCTGCTTTTCGCC AAGCTTCGCCAGGCTGTAAATCC
	TGME49_240270	Homology region_rv	TGGCGCTGCTTGCACTTGTGCTTG CTGCGCTTCCCCTTCGGCACCGCC ATTGGTTGAAGACAGACGAAAGCA GTTG
	TGME49_240270	clone testing_fw	ATCATTTCTCTCGTTCTCTCACC
	TGME49_240270	clone testing_rv	GCTGTCCTTCCTCTTCTTCAGA
	TGME49_214790	Homology region_forwrad	CGCCTTCCCGCCTTTCCCGTGCGT TTTTGCTGTCTCCCCGCCTCATCAC CAAGCTTCGCCAGGCTGTAAATCC
	TGME49_214790	Homology region_rv	AGTGGGGTTTTGGAAGAAAAGAGA CGAAAAACAGAGGCAGAAGTCGCC ATTGGTTGAAGACAGACGAAAGCA GTTG
	TGME49_214790	gRNA_fw	AAGTTCCTCATCACCATGGCGACTT G
	TGME49_214790	gRNA _rv	AAAACAAGTCGCCATGGTGATGAG GA
	TGME49_214790	clone testing_fw	GCAGGAGTCCCTTTCTTCTCGCG
	TGME49_214790	clone testing_rv	GCAGGAACTTCTTGAGGTCGGCG
qRT-PCR	TGME49_203620	TgmS35 expression level	AACCAAGCGCATGTTTACGT
	TGME49_203620	TgmS35 expression level	AGTCGAACCGTTCACTCCTT
	TGME49_240270	Expression level	GCAGCGCCAGTTGATTTACT
	TGME49_240270	Expression level	GCAAATCTTCCTGGCCAGAA
	TGME49_209030	ACT1 (actin)	ATTGGCGGATGAAGAAGTGCAAG
	TGME49_209030	ACT1 (actin)	ATTTAGAAGCACTTGCGGTGGAC
Ribosomal rRNA enrichment assessment	Mitochondrial ApiLSUE rRNA	IP rRNA assessment mito-rRNA_fw	AAGGTGCTCAGGGTCTTACCG
	Mitochondrial ApiLSUE rRNA	IP rRNA assessment mito-rRNA_rv	AGGTAGCAAAATTCCTTGTCG
	TGME49_209030	IP rRNA assessment ACT1 mRNA_fw	ATTGGCGGATGAAGAAGTGCAAG
	TGME49_209030	IP rRNA assessment ACT1 mRNA_rv	ATTTAGAAGCACTTGCGGTGGAC
	TogoCr29	IP rRNA assessment api-rRNA_fw	GCCCGTACTAAAACTGACACAAG
	TogoCr29	IP rRNA assessment api-rRNA_rv	AGGCATCCTTTATCCCGAAG

Table 7.11 Primers and gRNA sequences used in this study.

7.8. Bacterial strains (*Escherichia coli*)

The bacterial strain of *E. coli* used in this study was the chemically competent DH5α™ (New England BioLabs®). It was commercially purchased, and was stored at -80°C.

7.9. Molecular biology

7.9.1. Isolation of genomic DNA from *T. gondii*

Extracellular parasites were collected and centrifuged at 1500 x g for 5 minutes. Parasites' gDNA was extracted by resuspending them in 30-60 µl of lysis buffer (10% Proteinase K in TE buffer (Qiagen)) and incubation at 60°C for 60 minutes, then 95°C for 10 minutes in a thermocycler, and finally cooled to 4°C. gDNA was stored at -20°C. Alternatively, gDNA was extracted using a Qiagen© DNeasy Blood and Tissue kit and following the manufacturer's instructions, with a final elution volume of 100 µl H2O.

7.9.2. Isolation of RNA from *T. gondii*

Parasites lysed from a 6 cm dish (~2x107 parasites) were spun down at 1500 x g for 5 minutes and the pellet was kept on ice. RNA was extracted from the pellet using the Qiagen RNeasy® Mini Kit according to the manufacturer's instruction.

Prior RNA extraction, all equipment and gloves were treated with RNaseZAP™ (Sigma©). Quality of the RNA was assessed by running 1 µl on an agarose gel at 100V for 20 minutes (section 7.9.6). RNA typically generates two bands corresponding to the 28S and 18S RNA (Aranda, Lajoie and Jorcyk, 2012). RNA samples were finally quantified using the NanoDrop™ spectrophotometer (Thermo Scientific©).

7.9.3. cDNA generation

Complementary DNA (cDNA) was generated using 1-2 µg of RNA as a template for reverse transcription. This was performed using the High Capacity RNA-to-cDNA Kit (Thermo Fisher) and following the manufacturer's protocol.

7.9.4. Determination of nucleic acid concentration

DNA and RNA concentration were determined using a NanoDrop™ spectrophotometer following the manufacturer's instructions.

7.9.5. Polymerase chain reaction

Throughout this work, polymerase chain reaction (PCR) was used for multiple purposes such as DNA fragment amplification, checking plasmid integration in transformed bacteria colonies, and screening for transgenic parasites with correct DNA integration. These PCRs were performed using GoTaq®. Super Fidelity Taq DNA Polymerase was utilized for molecular cloning and when generating long homology region for promoter replacement or triple HA tagging using CRISPR by transfection, as high-fidelity polymerases contain proof-reading activity, which reduces the error rate during amplification. PCR reactions were proceeded as followed in Table 7.12 and 7.13.

Component	Volume (µl)
GoTaq mix (2X)	5
10 µM Forwar primer	0.3
10 µM Reverse primer	0.3
Template (10-100 ng)	1
H2O	To 10

Table 7.12 GoTap® reaction

Temperature	Time	Cycles
94ºC	30 sec	1
94ºC	30 sec	
50ºC-60ºC*	30 sec	25-35
72ºC	1 min/kb**	
72ºC	5 min	1
4ºC	Indefinitely	---

Table 7.13 GoTap® PCR thermocycler program
(*) Based on NEB primers Tm
(**) Dependent on the length of the amplicon

Component	Volume (µl)
Super Fidelity Taq DNA Polymerase mix (2X)	5
10 µM Fw primer	0.3
10 µM Rv primer	0.3
Template (100 ng)	1
H2O	To 100

Table 7.14 Super Fidelity Taq DNA Polymerase reaction

Temperature	Time	Cycles
94°C	5 min	1
94°C	45 sec	
53°C	1 min	3
72°C	5 min	
94°C	45 sec	
65°C	1 min	30
72°C	5 min	
72°C	7 min	1
4°C	Indefinitely	---

Table 7.15 Super Fidelity Taq DNA Polymerase thermocycler program

7.9.6. Agarose gel electrophoresis

DNA and RNA were separated according to their size by agarose gel electrophoresis (Lee *et al.*, 2012). Agarose gels were prepared to a final concentration ranging from 1-2% in 1X TAE (w/v) by boiling in a microwave. Addition of 0.01% GelRed allowed nucleic acid visualization under UV light. Samples were added 6X loading dye and loaded on the gel, as well as 5 µl of 1 kb DNA ladder (NEB®) or 1 kb plus DNA ladder (Thermo Scientific™) used as size reference.

7.9.7. Restriction endonuclease digest

Digestion of DNA by endonucleases was performed for plasmid verification and linearization of vectors prior transfection. All restriction processes were done following the standard protocol of 1 hour. Restriction enzymes and buffers were supplied by NEB®. Isolated DNA from bacterial cultures was verified using 200 ng of DNA for diagnostic digests. Stable transfections were done by vector linearization using a single restriction enzyme. For transfections in BioRad© electroporator, 50-70 µg of the plasmid of interest was digested.

7.9.8. Dephosphorylation of digested DNA plasmids

For molecular cloning, the digested plasmids were treated with alkaline calf intestinal phosphatase (CIP), which mediates the dephosphorylation of the 5' end of DNA, to prevent the re-ligation of the backbone. Incubation of 10 U/µl (0.5 µl) of CIP with the sample at 37°C for 1 hour is enough to treat the plasmids before purification.

7.9.9. Purification of DNA

After running the digested plasmid in agarose gels, purification of DNA bands was performed using the QiAquick gel Extraction kit. The desired band was cut from the agarose gel using a sterile scalpel blade over a UV transilluminator. The piece of agarose containing the band was weighed, extracted following the specifications of the manufacturer, and eluted in 10 µl H2O. 0.5 µl elution was run on an agarose gel to assess contamination with other DNA fragments.

7.9.10. Ligation of DNA fragments

T4 DNA ligase (NEB®) was utilised to achieve covalent binding of the insert and plasmid backbone. The formation of phosphodiester bonds connecting the 5' phosphate and 3'hydroxyl ends in dsDNA, was catalysed by this enzyme. 50 ng of backbone was used for this reaction with an insert-to-backbone ratio of 1:3. Incubation of the ligations was performed overnight at ambient temperature with the following additions: 1 µl of T4 DNA Ligase, 1 µl of 10X T4 DNA ligase Buffer and H20 to make up the volume of 10 µl.

7.9.11. Plasmid transformation into bacteria

The ligated reaction was transformed into chemically competent *E. coli* bacteria. To do so, 50 µl of bacteria were used per reaction. The following steps were carried out on ice. 5 µl of the ligation reaction added to the bacteria and incubated for 30 min. the mixture was then was then heat shocked for 45 sec at 42ºC, then placed back on iced for 2 min. To allow the bacteria to recover they were left shaking for 1 hour at 37ºC with 450 µl of NZY rich broth. Bacteria were then plated on LB-ampicillin agar plates overnight at 37ºC, shaking. Positive colonies were checked by PCR or analytical digest and were cultured overnight in the LB broth at 37ºC.

7.9.12. Isolation of plasmid DNA from bacteria

Overnight grown bacteria are pelleted by centrifugation and re-suspended in a buffer solution consisting in part of EDTA and RNase A. Bacteria were lysed using a buffer solution containing SDS and NaOH. NaOH has the additional benefit of de-stabilising hydrogen bonds holding the DNA bases together creating single strand DNA. Potassium acetate is used to neutralize NaOH in the lysis buffer and stop the

lysis reaction. During this process plasmid DNA is able to re-anneal by reforming hydrogen bonds however it is not possible for the longer bacterial genomic DNA to re-anneal. Another round of centrifugation separates the contaminants from the plasmid DNA. Silica columns from either QiAprep spin Miniprep or Midiprep (Qiagen®) were used to purify the plasmid DNA.

7.9.13. DNA sequencing

To verify inserts and final vectors the DNA is sequenced following procedures from GATC© Biotech. 5 µl of primer (5 pmol/µl) and 5 µl of purified DNA (80-100 ng/µl) were prepared and sent to the company.

7.10. Cell biology

7.10.1. *T*. *gondii* tachyzoite and mammalian cell *in vitro* culturing

Human foreskin fibroblast (HFF) monolayers were used as host cells for culturing *T. gondii* tachyzoites. These were cultured in Dulbecco's modified Eagle medium (DNEM), supplemented with 10% (v/v) FBS, 4 mM L-glutamine and 10 µg/ml penicillin/streptomycin. These were incubated in a humidified incubator maintaining a temperature of 37°C and a 5% CO_2 atmosphere. Once freshly egressed, parasites are passed onto new confluent HFFs or artificially released from their host cells by passing them through 23G needles.

7.10.2. Trypsin/EDTA treatment of HHF cells for cell maintenance

Host cells were washed with 1X PBS and trypsin protease was added which detaches HFFs from the bottom of culturing flasks. HHFs were incubated with trypsin at 37°C for 5 min. Gentle taps on the flasks helps to lift cells up from the surface, then one fourth of the cell were placed into a new flask with media.

7.10.3. Cryopreservation of *T*. *gondii*

Four drops of trypsin were added to 6 cm dishes of HFFs heavily infected with *T. gondii* and incubated in the incubator for 3 min. Infected cells in suspension were mixed with 1 ml of FBS and transferred into 2 ml cryotubes. 100 µl of DMSO was

added to the mixture and cells were immediately frozen at -80°C. To recover parasites, frozen samples were thawed at room temperature and the cryotubes content was transferred onto new confluent HFFs.

7.10.4. Transfection of *T. gondii*

7.10.4.1. Bio-Rad© transfections

Transfections with the Bio-Rad© Gene Pulser Xcell™ were conducted in cytomix (Table 2. 8), a buffer which mimics the cytosolic ion composition of the cells, resulting in the best survival rate (Van Den Hoff, Moorman and Lamers, 2902). 50 µg of DNA was linearised and ethanol precipitated. The pelleted DNA was dissolved in cytomix to a volume of 100 µl; parasites were re-suspended in 640 µl of cytomix to which 30 µl ATP (100 mM) and 30 µl GSH (100 mM) was added. This transfection mix was transferred into an electroporation cuvette (BioRad©; 4 mm). Electroporation was conducted using the following settings; mode: square wave, voltage: 1700 V, pulse length: 200 µs, the number of pulses: 2 and interval between pulses: 5 ms.

7.10.4.2. Transient transfections

For transient transfections, circular DNA was used. These do not incorporate into *T. gondii*'s genome and are expressed as additional extra chromosomal copies. They are hence lost after several replication cycles. This method allows rapid gene function/protein localisation assessment without the time-consuming drug selection process for stable transfections. Immediately after electroporation, parasites were inoculated on coverslips containing a confluent monolayer of HFFs and incubated from 24 to 48 hours before fixation.

7.10.4.3. Stable transfections

Insertion of DNA into the parasite genome is required to perform stable transfection, this insertion can either be random or targeted. For random integration, exogenous DNA is incorporated into the genome via the parasite's non-homologous end joining (NHEJ) repair mechanism, this is mediated by the Ku80 enzyme (Donald and Roos, 1993). It is possible to increase the transfection

efficiency during random integration by adding the same restriction enzyme used to linearize the vector to the mixture, the DNA repair mechanism is activated by the enzyme. This method is referred to as the restriction enzyme mediated insertion (REMI) (Black *et al.*, 1995).

Targeted stable transfections based on homologous recombination are carried out in Δku80 parasites: as this parental strain is not able to use the NHEJ repair mechanism, endogenous tagging and DNA sequences replacement with exogenous sequences is highly increased (Fox *et al.*, 2009; Huynh and Carruthers, 2009).

Plasmid must be linearised to be integrated within the parasite's genome. 50 μg of DNA was used for transfection as described above with the BioRad electroporator, into TATiΔku80 (Sheiner *et al.*, 2011). For promoter replacement or HA tagging, the homologous region containing the transgenic promoter/HA tag and selectable cassette sequence was amplified by PCR (Table 7.15) and used directly for transfection with the CRISPR/CAS9 and sgRNA expressing plasmid. Depending of the selectable cassette, the corresponding drug was added either immediately after transfection, or the next day.

7.10.4.4.   Drug-mediated positive selection

Transfected parasites were grown in presence of the drug immediately after transfection with 10 μM chloramphenicol for the chloramphenicol acyl transferase (CAT) resistance cassette (Kim, Soldati and Boothroyd, 1993) which has a delayed action, or the next day with 1 μM pyrimethamine for the dihydrofolate reductase-thymidylate synthase resistance cassette (Donald and Roos, 1993) which has an immediately action. Drugs are kept into the culture media until resistant parasite emerge. At this point, the pool of resistant parasites can be screened by fluorescent microscopy, PCR (Table 7.11) and western blot.

7.10.5.   Isolation of clonal parasite lines by limited dilution

Drug resistant parasites are transferred to 96 well plates of HFF monolayers after confirmation of the pool being positive in order to isolate stable clones. This is performed by serial dilution using multichannel pipettes. Parasites from single

plaque containing wells were collected and transferred to 24 well plates. Clonal lines were tested by PCR, fluorescent microscopy and western blot.

The following material and methods were taken from the Lacombe et al., 2019 publication and is detailed below as it is in this paper with minor modifications.

7.11. *In silico* search for mitochondrial protein identification

The mRNA abundance dataset generated by Behnke *et al.*, (2010) was queried via GeneSpring 11.0. Of the 14 homologs of mitochondrial protein import components (Table 8.3) 3 do not have cyclical expression pattern (Appendix Table 3 - sheet 1). For each of the remaining 11, we searched for other genes with correlating cyclical expression patterns. We ran Euclid and Spearman correlation tests at 0.9 and 0.95 scores and kept lists of correlation that were smaller than 70. This search identified 281 non-overlapping genes (the original search was performed with release 7.2 of ToxoDB, TGME49 strain; the same group of genes now correspond to 279 predicted genes from this strain) (search steps are shown in Appendix Table 3 - sheet 2).

The orthology search leading to the 43 gene list was performed via the ToxoDB link to OrthoMCL. A search strategy queried for *Toxoplasma* genes with orthologs in *Plasmodium* 3D7 and with no orthologs in the three *Cryptosporidium* spp. genomes available. The group of TGME49 genes that comply with these criteria was intersected with the 279-group resulting in 43 genes (Appendix Table 2 – sheet 2).

Fitness phenotypes scores (Appendix Table 4 – columns E-F) were obtained via the ToxoDB tool. All TGME49 genes were converted to their TGGT1 syntenic orthologs and then sorted according to their fitness scores.

The probability of export to the mitochondria (Appendix Table 4 – column B) was assessed using the MitoProt II algorithm (v.1.101) (Claros and Vincens, 1996) (https://ihg.gsf.de/ihg/mitoprot.html).

7.12. Plasmid construct

For ligation independent cloning (LIC), between 500 pb to 1.5 kb homologous region of the 3' end of each gene of interest (GOI) was amplified by PCR from *T. gondii* RH genomic DNA with LIC sequence flanking these regions (primers are in Table 2.11). Products were LIC-cloned into linearised p3HA.LIC.CATΔpac containing a triple HA epitope tag as described previously (Huynh and Carruthers, 2009; Sheiner *et al.*, 2011), or into linearised pTEV.TwinStrep.LIC.CATΔpac or pTEV.TripleFLAG.LIC.CATΔpac, where the triple-HA was replaced with TEV.TwinStrep or TEV.Triple-FLAG using In-Fusion cloning. The vectors were transfected into the TATiΔku80 line (Sheiner *et al.*, 2011) and selected with chloramphenicol.

For expression of tagged exogeneous genes, the corresponding cDNAs were cloned (primers in Table 2.11) into the pDT7S4 expression vector that fuses a C-terminal Myc eptitope tag (Van Dooren *et al.*, 2008) via BglII and AvrII restriction sites.

For promoter replacement, the ChopChoP (http://chopchop.cbu.uib.no/) tool was used to identify gRNAs covering the ATG of each GOI. The corresponding gRNAs were cloned into a U6 promoter and CAS9-GFP expressing vector (Tub-Cas9-YFP-pU6-ccdB-tracrRNA) (Curt-Varesano *et al.*, 2016) using the BsaI restriction site, and the final plasmid was purified by DNA midi-prep (Qiagen) per the manufacturer's protocol. The DHFR selectable cassette and ATc repressible promoter were amplified by PCR from pDT7S4myc (Van Dooren *et al.*, 2008; Sheiner *et al.*, 2011). Parasites were transfected with 50 ug of the gRNA/CAS9 vector-PCR product mixture, and transfectants with integrated cassette were selected with pyrimethamine.

For gene disruption by transient gRNA/CAS9 expression, each gene specific gRNA (sequences in Table 7.11) vector, synthesised by GenScript using backbone vector pU6-SAG1gRNA-DHFR (Serpeloni *et al.*, 2016), was co-transfected with the CAS9-FLAG expressing vector (pU6-universal) (Sidik *et al.*, 2016).

7.13. Immunofluorescence assay and microscopy

Parasites were inoculated onto human foreskin fibroblasts (HFFs) on coverslips for the mentioned time period and fixed with 4% paraformaldehyde (PFA) for 20 minutes at room temperature (RT). The PFA was washed away thrice with

phosphate buffer saline (PBS). Cells were then permeabilised and blocked with blocking buffer (PBS, 0.2% Triton X-100, 2% Bovine Serum Albumin, BSA) for 20 minutes at RT. Cells were then labelled with different sets of primary and secondary antibodies: mouse anti-HA antibody (1:1000, Sigma), rabbit anti-TgMys (1:1000) (Ovciarikova *et al.*, 2017), mouse anti-Myc (1:1000, Cell Signalling), rabbit anti-TgTOM40 (1:2000)(Van Dooren *et al.*, 2016); mouse anti-Strep (1:1000, StrepMAB-Classic, IBA), mouse anti-FLAG (1:1000, Monoclonal ANTI-FLAG® M2, Sigma-Aldrich), mouse anti-GFP (1:2000, Roche), coupled with goat anti-mouse or anti-rabbit fluorescent antibody (AlexaFluor 594 or 488 1:1000 (Invitrogen)). Primary antibodies were incubated for 1 hour at RT. Coverslips were then washed thrice for 5 minutes with PBS-0.2% Triton X-100 and incubated with secondary antibodies for 45 minutes at RT in the dark. Coverslips were washed as above and mounted on microscope slides using DAPI-fluoromountG (Southern Biotech). Images were taken using a Delta Vision microscope as described (Ovciarikova *et al.*, 2017).

7.14. Mitochondrial morphology scoring

CRISPR/Cas9 transient expression - Parasites transiently co-expressing CAS9-FLAG (pU6-universal) (Sidik *et al.*, 2016) and gene specific sgRNA (Serpeloni *et al.*, 2016), for genes TGME49_214790/ 263680 and 226280, were fixed 48 hours post-transfection. The CAS9-FLAG and mitochondria were visualised by immunofluorescence using anti-FLAG and anti-TgMys (mitochondrial marker) as described above. 50 vacuoles of CAS9-FLAG expressing parasites for each gene were then counted and mitochondrial morphology was assessed as followed: mitochondrial morphologies were sorted into two categories: (a) "normal" mitochondrial morphology with vacuoles which contain parasites displaying open-lasso, half-moon, and to a lesser extent, sperm-like mitochondrial morphologies (Figure 8.1; (Ovciarikova *et al.*, 2017)), (b) abnormal morphology which is anything other than open-lasso and sperm-like morphologies, then scored. Dead parasites (displaying one or two balled mitochondria (Ovciarikova *et al.*, 2017)) were not considered. Experiments were performed in triplicate.

Conditional knockdown - rTgmS35-3xHA mutant line was grown in the presence or absence of ATc 0.5 µM for 48 hours, fixed and mitochondria were visualized by

immunofluorescence using anti-TgMys, as described above. Mitochondrial morphology was scored as "normal" if vacuoles have the majority of parasites with open-lasso mitochondrial morphologies (and a few sperm-like shapes) or "abnormal" if vacuoles contained parasites whose majority the mitochondria are in sperm-like shape and anything else). Replicating parasites were excluded. Experiments were performed in triplicate, and a Chi-squared statistical test was performed.

7.15. Plaque assay

1000, 300 and 100 parasites were inoculated in 6-well plates in duplicates, in the presence or absence of ATc 0.5 µM for 9 days. Cells were then fixed with 100% methanol for 30 minutes at RT, washed with PBS and crystal violet dye was added for 2 hours at RT to stain host cells, and then washed with PBS.

7.16. Western Blot

Samples were resuspended in 1X NuPAGE LDS loading dye (Invitrogen) with 5% v/v beta-mercaptoethanol, then boiled at 95°C for 5 minutes and separated by SDS-PAGE. Proteins were transferred under wet conditions (in Towbin buffer (0.025 M TRIS 0.192 M Glycine 10 % Methanol) for 60 minutes at 100 V) to nitrocellulose membrane (0.45 µm Protran™). Blots were labelled with the appropriate set of antibodies: primary rat anti-HA (1:500, Sigma), mouse anti-Myc (1:1000, Cell signalling), mouse anti-Strep (1:4000, StrepMAB-Classic HRP conjugate, IBA), mouse anti-FLAG (1:1000, Monoclonal ANTI-FLAG® M2, Sigma-Aldrich) or rabbit anti-TgTOM40 (1:2000, (Van Dooren *et al.*, 2016)) antibodies coupled to secondary horseradish peroxidase (HRP)(Promega for mouse and rabbit, Abcam for rat) conjugated antibodies (1:10,000) or secondary fluorescent antibodies IRDye® 800CW (1:10000, LIC-COR), and visualised using the Pierce ECL Western Blotting Substrate (Thermo Scientific) or the Odyssey LCX, respectively.

7.17. Protein import assay

Parasites were transfected with the Hsp60L-mDHFR-cMyc vector (Van Dooren *et al.*, 2016) (kind gift from Giel van Dooren), after growth in the presence or absence of 0.5 µM ATc for 24 and 72 hours. Transfected parasites were collected

after an additional 24 hours of growth in their respective treatment, and western blot was performed using the respective parasite pellets as described above. Band intensity was measured using the ImageJ software and the ratio between the mature and pre-processed band intensity was calculated. A 1-way ANOVA statistical test was performed.

7.18. Preparation of mitochondria enriched fraction

Parasites were cultured on HFFs in T150 flasks in the presence or absence of 0.5 µM ATc. Egressed parasites were collected (or, where necessary, parasites were scraped and syringed, e.g. at 96 hours) and filtered through a 3 µm pore size membrane. From this point on, all steps are carried out at 4°C. Parasites were centrifuged at 1500 x g for 15 minutes. Media was discarded and pellets were resuspended in PBS. Parasites in PBS were counted on a Neubauer chamber and centrifuged at 1500 x g for 15 minutes. The supernatant was discarded and the pellet resuspended in lysis buffer (50 mM HEPES-KOH pH 7.4, 210 mM mannitol, 70 mM sucrose, 1 mM EGTA, 5 mM EDTA, 10 mM KCl, 1 mM DTT, 1 protease inhibitor cocktail tablet (Complete Mini, EDTA-free; Roche) per 50 ml) to a concentration of 5×10^8 parasites per ml. Parasites were transferred into a precooled nitrogen cavitation chamber and incubated at a pressure of 2750 psi for 15 minutes on ice. After pressure release and centrifugation at 1500 x g for 15 minutes, the supernatant (lysate) was kept, and the pellet, containing unbroken parasites, was resuspended again at 5×10^8 parasites per ml in lysis buffer. Repeating rounds of nitrogen cavitation were performed until >95% of parasite lysis was achieved (evaluated via counting using Neubauer chamber). Pooled lysates were spun down at 1500 x g to remove any remaining unbroken parasites. The lysate was then aliquoted to the desired amount in microcentrifuge tubes and span down at 16,000 x g for 25 minutes. The supernatant was discarded and the pellet used immediately or stored at -80°C until use.

7.19. Blue-native polyacrylamide gel electrophoresis (BN PAGE)

Whole parasites or previously aliquoted enriched mitochondria fractions were mixed with solubilisation buffer (750 mM aminocaproic acid, 50 mM Bis-Tris–HCl pH 7.0, 0.5 mM EDTA, 1 % (w/v) dodecyl maltoside) and incubated on ice for 5

minutes. The mixture was centrifuged at 16,000 × g at 4°C for 10 minutes. The supernatant containing solubilised membrane proteins was transferred into a new microcentrifuge tube and 0.25% (w/v) Coomassie G250 (final concentration) was added. The anode buffer (50 mM Bis-Tris–HCl pH 7.0) and cathode buffer (50 mM Tricine, 15 mM Bis-Tris–HCl pH 7.0, 0.02% Coomassie G250 (Serva)) were poured into their respective tank compartment and the appropriate amount of protein (55 μg or $5x10^5$ parasites per lane) was loaded on a NativePAGE™ 4-16% or 3-12% Bis-Tris Gel (Novex- Life technologies). 5 μl NativeMark™ (Invitrogen) was used as a molecular weight marker. Gels were run for ~45 minutes at 100 V, 4-10 mA at 4°C with cathode buffer containing 0.02% (w/v) Coomassie G250, then for ~2.5 hours at 250 V, 15 mA with cathode buffer containing 0.002% (w/v) Coomassie G250, until the dye front reached the bottom of the gel. Proteins were transferred onto a PVDF membrane (0.45 μm, Hybond™) using wet transfer in Towbin buffer (0.025 M TRIS 0.192 M Glycine 10 % Methanol) for 60 minutes at 100 V. After transfer and immunolabelling revelation was carried out as described above with Pierce ECL Western Blotting Substrate.

7.20. High resolution clear-native polyacrylamide gel electrophoresis (hrCN PAGE)

Carried out as described previously (Wittig, Karas and Scha, 2007) with minor modifications. Briefly, whole parasites or previously aliquoted mitochondria enriched fraction (75 μg) were mixed with solubilisation buffer (50 mM NaCl, 50 mM imidazole, 2 mM 6-aminohexanoic acid, 1 mM EDTA – HCl pH 7.0, 2% (w/v) n-dodecylmaltoside (DDM)) and incubated on ice for 10 minutes. The mixture was centrifuged at 16,000 × g at 4°C for 15 minutes. A final concentration of 6.25% glycerol and 0.125% Ponceau S was added to the solubilised membrane proteins. The anode buffer was composed of 25 mM imidazole – HCl (pH 7.0) and the cathode buffer of 50 mM Tricine, 7.5 mM Imidazole, 0.02% w/v DDM, 0.05% sodium deoxycholate. Gels were run for 30 minutes at 100 V, 10 mA, then 250-300 V, 15 mA at 4°C until the dye front reached the bottom.

7.21. In-gel activity staining

Activity stains were carried out as described previously (Sabar, Balk and Leaver, 2005). Briefly, gels were equilibrated in buffer without staining reagents for 10 minutes. For complex IV, oxidation activity was shown using 50 mM KH_2PO_4, pH 7.2, 1 mg per ml of cytochrome c, 0.1% (w/v) 3,3'-diaminobenzidine tetrahydrochloride. Stains were visible after 30 minutes. Staining was continued with pictures taken of the stained gels at regular intervals. For complex V, ATP hydrolysis activity was visualised using 35 mM Tris, 270 mM glycine, pH 8.4, 14 mM $MgCl_2$, 11 mM ATP, 0.3% (w/v) $Pb(NO_3)_2$. Stains were visible after 1 hour. Pictures were taken against a black background for optimal visualisation of white lead precipitates.

7.22. Mass spectrometry

Proteins were identified using nanoflow HPLC electrospray tandem mass spectrometry (nLC-ESI.MS/MS) at Glasgow Polyomics. Tryptic peptides, generated using in-gel digest procedure (Williams *et al.*, 2018), were analysed as previously described (Akpunarlieva *et al.*, 2017). Protein identities were assigned using the Mascot search engine (v2.6.2, Matrix Science) to interrogate protein sequences in the *T. gondii* genome sequence dataset, ToxoDB 35 release. During result analysis, only peptides with Mascot score of 20 and above (namely the probability that this match might be a random event is 10^{-2} or lower) were included in the analysis.

7.23. Immunoprecipitation, RNA extraction and RT-PCRs

Parasites were gown in HFF in T175 flasks until lysed ($2\text{-}3\text{x}10^8$ cells), then collected. Dry pellets were stored at -80°C until the day of the experiment. Pellets were lysed on ice for 15 minutes in TBS containing 1% DDM (Thermo Fisher), 0.4 U/ul of RNaseOUT™ Recombinant Ribonuclease Inhibitor (Thermo Fisher) and 1 mM DTT (Sigma). Lysates were spun at 16000 x g 10 minutes at 4°C. Supernatants were transferred to microcentrifuge tubes containing 50ul of washed Pierce® Anti-HA Agarose beads (Thermo scientific). The immunoprecipitation was performed according to the manufacturer's instruction. Elution was performed with 0.1 M glycine, pH 2.6. RNA extraction was carried out using the RNeasy Mini kit (Qiagen) with DNase I treatment (Thermo Fisher). Reverse transcription (RT) reaction was achieved using the High Capacity RNA-to-cDNA Kit (Thermo Fisher). "cDNA" from

the RT reaction was amplified by PCR using primers designed for mitochondrial rRNA sequence (mito-rRNA), apicoplast rRNA sequence (api-rRNA) and actin mRNA (primers sequence in Table 2.11), and was performed with annealing temperature of 51°C and elongation time of 25 seconds for 30 cycles.

7.24. Other cell lysis methods

For detail on parasite lysis by snap freeze and thaw cycles, sonication, dounce homogeniser, and needle, see section 8.1. These methods resulted in poor lysis efficiency and were abandoned for nitrogen cavitation (section 7.18).

7.25. tRNA immuno-affinity assay

50 μl of paramagnetic streptavidin resin (DYNAL Magnetic Beads, Invitrogen), containing 6.7×10^8 beads/ml, was washed 3 times in 500 μl of 1X SSC buffer (150 mM NaCl, 15 mM tri-sodium citrate dihydrate, pH 7.2). The washed resin was resuspended in 500 μl 0.5X SSC, synthetic 5' biotinylated *T. gondii* tRNA^{Ile} or tRNA^{Met-i} (Dharmacon) was added to a final concentration of 2 μM and incubated at 65°C for 10 minutes to form the tRNA-streptavidine affinity resin. After incubation, the tRNA bound resin was washed 3 times with 300 μl of 0.1X SSC and equilibrated in 300 μl of protein binding buffer (PB) (160 mM MOPS, 310 mM sucrose, 6.25 mM MgCl2, 100 mM KCl, 9 mM DTT, 2 units/300 μl of RNAse inhibitor (10U/μl stock), 1 mg/ml BSA). Each of the biological sample was adjusted to 6.0×10^9 cell equivalents, and volumes were adjusted to 300 μl with PB buffer containing 1% Triton X-100. The PB buffer was removed from the beads and replaced by the samples in PB buffer-Triton X-100 1%. Samples were incubated with the tRNA affinity resin for 30 minutes at room temperature on a rotor, unbound proteins were collected, and the tRNA affinity resin was washed 6 times in 500μl of PB buffer. tRNA-bound proteins were eluted in 50ul of elution buffers containing increasing ionic concentrations of NaCl (0.25, 0.5, 0.75, 1M NaCl; 20 mM MOPS, pH 7.2). Protein samples from each elution were TCA precipitated and separated on 8-18% SDS-PAGE. Acrylamide gels were stained with SYPRO™ Orange Protein Gel Stain, silver staining, or Coomassie blue. For LC-MS/MS analysis, bands of interest were cut out of the gel and sent to Polyomics, Glasgow. To evaluate the specificity of binding, this experiment was repeated with synthetic 5'

biotinylated *T. gondii* tRNA^Met-i (Esseiva *et al.*, 2004). Samples were also incubated with paramagnetic streptavidin resin without bound tRNA as a control to identify proteins that bound to the resin non-specifically. The "lab" version of this protocol is available in the Appendix protocol section.

8. Identification of new candidates for components of the mitochondrion tRNA import machinery and examination of their localization

As mentioned in the introduction (section 6.4.3), *T. gondii* has 3 translationally active compartments: the cytosol, the apicoplast and the mitochondrion. The mitochondrial genome is one of the smallest known to date (~6 kb). Only 3 genes remain which encode for essential mitochondrial proteins that are part of the mETC (Vaidya, Akella and Suplick, 1989; Feagin, 1992). The rest of the canonical mitochondrial genes as found in mammals have been transferred to the nucleus, this includes genes encoding for the mitochondrial translation machinery, including all tRNAs. These are translated in the cytosol, then need to be imported into the mitochondrion for mitochondrial translation to occur. Previous studies have demonstrated that some nuclear encoded tRNAs are imported from the cytosol into the mitochondrion (Esseiva *et al.*, 2004) (Figure 8.1). As the mitochondrial genome in mammalian cell encode for all the necessary tRNA genes required for translation, it is expected that mitochondrial tRNA import (MITI) is not essential, as opposed to *T. gondii* for which MITI is an absolute necessity. Consequently, this pathway has potential for drug targeting.
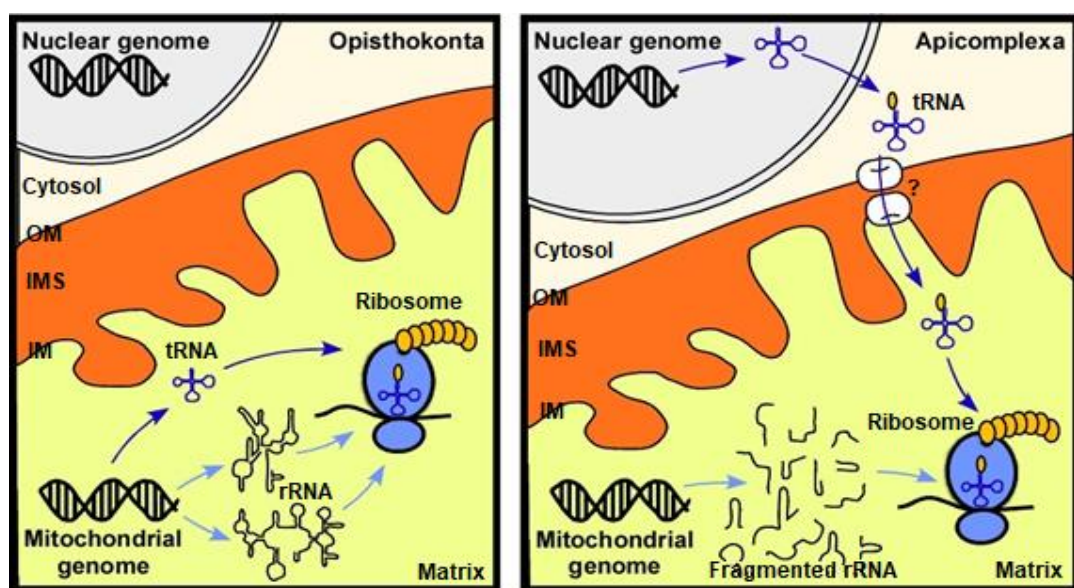
Figure 8.1 Schematic highlighting the mitochondrial translation differences between mammalian cells (left) and apicomplexans (right).

The left panel displays mitochondrial translation in Opisthokonta such as mammalian cells. Their mitochondrial genome encodes for the complete translation machinery including mitochondrial tRNA, hence no import is required. The right panel depicts mitochondrial translation in Apicomplexa where the mitochondrial genome is highly reduced and does not encode for any mitochondrial tRNA and hence, must import them from the cytosol in its aminoacylated state (Pino *et al.*, 2010). OM – outer membrane, IMS – intermembrane space, IM – inner membrane, "?" – refers to the unknown composition of the mitochondrial translocon complex which allows, amongst other things, nuclear encoded mitochondrial tRNA import. (Modified scheme from Dr. Lilach Sheiner)

In this section, we aim at identifying the components involved in MITI. In other systems, there is evidence showing that tRNA import involves the use of components of the canonical mitochondrial protein import machinery (Schneider, 2011). Plants use, amongst others, VDAC, Tom20 and Tom40 to translocate tRNAs into their mitochondria (Salinas *et al.*, 2006). In yeast, Tom40 and Tim44 are required for import of the tRNA (Ivan Tarassov, Entelis and Martin, 1995). In *T. brucei*, Tim17 and HSP70, play a part in tRNA import (Tschopp, Charrière and Schneider, 2011). So, it seems that overall, most organisms use some of the components of the protein import machinery to translocate tRNAs into the mitochondria. However, the current knowledge remains superficial, which makes it challenging to identify *T. gondii* homologs from other systems. Two methods were considered here: (1) tRNA co-immunoprecipitation to pull down protein partners which directly interact with imported tRNAs, (2) a bioinformatic screen which utilizes mRNA expression patterns to identify new mitochondrial proteins.

8.1. Optimisation of parasite lysis: preliminary step towards mitochondrial enrichment

Depending on the purpose of the experiment, there are different methods to break open cells in order to study their content. However, each cell lysis method varies in terms of lysis efficiency and strength, which has a direct impact on the downstream analysis. Different methodologies can be applied as the first step toward subcellular fractionation for organelle enrichment. Apicomplexan parasites are obligate intracellular parasites and must first complete their replication and egress. They can also be mechanically released from host cells. For *T. gondii*, the latter can easily be achieved by passing infected host cells through a 23G syringe followed by filtering to remove host cell debris. Apicomplexan parasites can be broken using techniques which derive from well-established protocols from model organisms (Chen *et al.*, 2016, Gardini, 2017, Zhou and Philips, 2017). Parasites can be lysed by passing them through 27G

needles in a hypotonic buffer (Gardini, 2017), by nitrogen cavitation (Ke *et al.*, 2018), detergent treatment (Esseiva *et al.*, 2004, Lacombe *et al.*, 2019), or sonication (Salunke *et al.*, 2018). Our aim was to identify a scalable method which allows cell breakage with high efficiency and minimal organelle damage.

Due to *T. gondii*'s cytoskeleton structure, breaking the cell open without damaging organelles is a challenge as it is encapsulated in a resistant microtubule cage. In this section, we aim at setting up a cell lysis protocol which allows conservation of mitochondria integrity.

Different approaches were tested. At this point, the focus was put on lysis efficiency. Mitochondrial enrichment and integrity would be assessed once a suitable lysis method was established. The percentage of parasite lysis was assessed, by counting under microscopy.

- *Freeze and thaw*. Parasites were resuspended in SME-20 buffer (250 mM sucrose, 1 mM EDTA, 20 mM MOPS-KOH, pH 7.2), and snap frozen in liquid nitrogen for 30 seconds and immediately thawed in a 37°C water bath for 3 minutes, twelve times. Parasite breakage was assessed by counting parasite under the confocal microscope. This technique was performed twice and allowed 50% lysis.
- *Freeze, thaw and sonication*. In the hope to increase the above lysis efficiency, sonication was performed after freeze-thaw cycles. Parasites were sonicated in the same buffer twice for 5 minutes at 50/60 Hz with 2 minutes recovery on ice in between. It increased the total cell lysis to 60%. This was performed only once. The duration of the freeze/thaw and sonication, and the resulting lysis efficiency made it not worth pursuing.
- *Dounce homogenizer*. Attempts to use a 2 ml glass dounce homogenizer to break parasites in SME-20 buffer, in a 1:8 dilution of SME-20 buffer in HEPES buffer, and in HEPES buffer only, through 15 strokes were completely unsuccessful. This was performed once with each buffer composition.
- *Needle*. Parasites were pushed through 26G needles 15 times in SME-20 buffer. This was performed once and resulted in a 50% cell breakage.
- *Nitrogen cavitation*. This method was the most successful with at least 80% lysis for the 1st round of parasite breaking, and up to 99% lysis by the second

round. It was hence utilized as primary cell lysis method throughout the rest of the study. This method is further detailed in the below (section 8.1.1).

8.1.1. Cell lysis by nitrogen cavitation

Nitrogen cavitation was used as a cell breaking method in other organisms such as *P. falciparum, T. brucei*, and mammalian cells with high lysis efficiency (CHIBBER and CASTLE, 1983; Yermovsky-Kammerer and Hajduk, 1999; Bouzaidi-Tiali *et al.*, 2007; Kobayashi *et al.*, 2007; Mather, Morrisey and Vaidya, 2010; Ke *et al.*, 2018; Hata, Sato and Kita, 2019). The principle is to incubate cells in suspension in a highly pressurized environment containing nitrogen gaz. Due to high pressure, nitrogen molecules solubilize into the solution and penetrate the cells. When the pressure is released, nitrogen molecules re-gasify causing the cell to burst open releasing their organelles in solution. Organelle enrichment can then follow.

Parasite lysis was performed as detailed in Figure 8.2A with all steps performed on ice with equipment and buffers pre-cooled. Briefly, extracellular parasites were filtered, washed in PBS and resuspended in lysis buffer (50 mM HEPES-KOH pH 7.4, 210 mM mannitol, 70 mM sucrose, 1 mM EGTA, 5 mM EDTA, 10 mM KCl, 1 mM DTT, 1 protease inhibitor cocktail tablet (Complete Mini, EDTA-free; Roche) per 50 mL) to a concentration of 5×10^8 parasites/mL. Resuspended parasites were lysed by nitrogen cavitation at 2500 psi for 15 minutes. This step was repeated until over 95% of parasites are broken (typically 2 cycles of nitrogen cavitation is enough). The lysate was then spun down at 1500 x g for 15 minutes to remove unbroken cells and large debris, and the supernatant was spun down at 16,000 x g for 25 minutes to pellet the crude mitochondrial fraction (see section 7.18).

Fractionation quality was assessed by immunoblotting using different cell compartment markers (Table 7.9) such as anti-IMC1 (inner plasma membrane compartment), anti-HSP60 (apicoplast), anti-TgMys (TGME49_215430) (OMM), anti-HA (the line used has a triple HA tagged mitochondrial ribosomal protein named TguL12m which resides in the lumen), anti-ATP-β (for the ATP synthase in the IMM), and anti-aldolase (cytosol) (Figure 8.2B). The anti-ATP-ß antibody was shown in the literature to recognise *T. gondii* ATP synthase in addition to mammalian ATP synthase (Huet *et al.*, 2018; Seidi, Linden S Muellner-Wong, *et al.*, 2018) with the *T. gondii* version having a slightly bigger size of 55 kDa than

the mammalian one (53 kDa). This size difference is observable by western blot and may be used to check for host cell contamination in the samples as presented in Figure 9.6A.
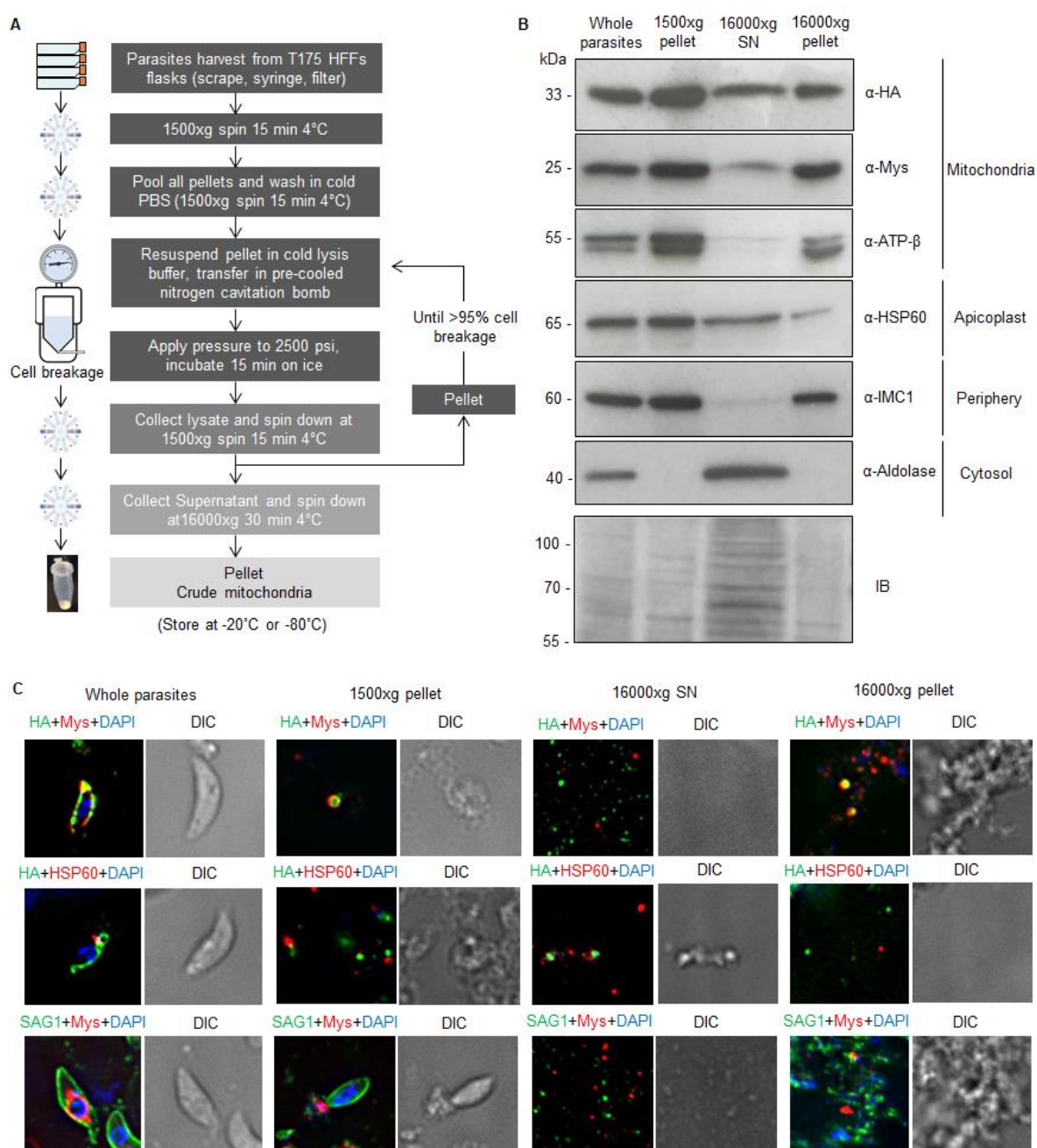
Figure 8.2 Crude mitochondria fraction assessment by western blot and immunofluorescence.
(**A**) Scheme resenting the protocol followed to generate crude mitochondria enrichment. (**B**) Crude mitochondria fraction assessment by western blot. OMM was stained with anti-TgMys, the IMM with anti-ATP-β, the mitochondrial matrix with anti-HA (TguL12m-3HA), the apicoplast with anti-HSP60, the parasite peripheral membrane with anti-IMC1, and the cytosol with anti-aldolase. IB – Instant Blue protein staining serves as loading control. (**C**) IFA of each fraction collected from parasite lysis be N$_2$ cavitation to differential centrifugation. The mitochondrion is stained with anti-TgMys and anti-HA (TguL12m-3HA line), the apicoplast is stained with anti-HSP60, the parasite plasma membrane with anti-SAG1, the nucleus with DAPI and overall shape was visualized by Differential Interference Contrast (DIC).

Western blot and IFA were performed to assess the quality crude mitochondria enrichment. Detection of mitochondria (HA, TgMys and ATP-β signal) can be observed by western blot at each centrifugation step suggesting loss of mitochondria throughout the fractionation process (Figure 8.2B). Substantial mitochondrial loss is observed in the 1500 x g pellet, a centrifugation force which is commonly used for differential centrifugation in yeast and plant crude mitochondria fraction preparation (Liao *et al.*, 2018). There is the possibility that the microtubule cage does not break fully (e.g. parasites broken in two, which will no longer look like cell but still have intact microtubules), and while the cytosol is released, some large organelles, including the mitochondrion, may remain trapped and pellet down at 1500 x g. This is supported by the IMC signal in this pellet. This can be tested by widening our range of antibodies for large organelles (i.e. nucleus, roptries, Golgi apparatus, and ER). Moreover, most protocols for crude mitochondria (Esseiva *et al.*, 2004; Liao *et al.*, 2018), do not show blots of the slow spin pellet as their main focus is on the final mitochondria product, and so we do not have a point of comparison. We would expect this loss to be a common outcome, hence the importance of starting with a sufficient amount of starting material. The mitochondria signal in the 16,000 x g supernatant lane could possibly come from broken mitochondria pieces which have a lower density and hence do not pellet down in the 16,000 x g pellet. Differential centrifugation does not seem to be sufficient to properly separate of all cellular compartments, which was expected and is in line with what was observed in yeast crude mitochondria samples (Liao *et al.*, 2018). Heavy IMC1 contamination can be observed, as well as some apicoplast contamination to a lesser extent. As mentioned above, the anti-ATP-ß antibody can recognise both human and *T. gondii* ATP synthase which can be useful to assess for host cell contaminants. The ATP-β staining indeed reveals the presence of host cell contamination at all steps (lower band) (Figure 8.2B). This, however, varies from one experiment to another. Other experiments showed the *T. gondii* band only, confirming a sample free from host cell material. This means that the filtration using 3 μm pore filters, which are commonly used in the field, cannot be 100% reliable at removing all host cell debris. In addition, it seems like in the presence of human contamination, the fractionation protocol as performed here favours human mitochondria enrichment over *T. gondii*'s, as the band intensity ratio of *T. gondii* vs human mitochondria inverts in the final 16000 x g pellet compared to the whole parasite sample.

Despite the low organelle separation efficiency, this protocol was successful at removing the cytosolic compartment, as described in the yeast protocol (Liao *et al.*, 2018), which is an important achievement for studying mitochondrial translation. Another western blot performed by Dr. McLean, a Sheiner lab postdoc showed similar results (Appendix Figure 1).

The IFA in Figure 8.2C shows sample content at each fractionation step. Samples were stuck to glass slides by incubation in the presence of poly-L-lysine. The mitochondrion is marked with anti-HA and -TgMys (TGME49_215430), the apicoplast with anti-HSP60, the plasma membrane with anti-SAG1 and the nucleus with DAPI (Figure 8.2C). The "whole parasite" panel show healthy extracellular parasites before lysis. After lysis, the 1500 x g pellet, which pellets large cellular debris and unbroken parasites, contains mitochondria and apicolplasts which are often associated with one another (Nishi *et al.*, 2008). The supernatant resulting from the high spin (16000 x g SN) contains mitochondria, apicoplast and plasma membrane. Finally, in the final fraction (16000 x g pellet) contains mitochondria, low abundance of apicoplast, plasma membrane and nuclei. This is all in agreement with the western blot results. All these cellular compartment contaminants are often displayed as clumps in with membranes and pieces of organelles stuck together that pellet down with the mitochondria in the final high spin. Also, mitochondria, after lysis, present a much smaller size with a somewhat spherical shape. This is likely because mitochondria are not inside the cell and there are no more tethers to keep it "open". OMM and mitochondrial matrix signal only can also be observed. TgMys (TGME49_215430) is expected to be lipid binding and thus not fully membrane spanning according to predicted domains. So, it could be that this marker dissociated from the OMM, resulting in the separation of the two signals. It could also be the results of mitochondria damage with ruptured mitochondria ending up in the supernatant of the high spin, although additional testing is needed to validate this.

Taken altogether, these results suggest that nitrogen cavitation breaks parasites open with great efficiency. However, as shown for protocols established for model organisms, differential centrifugation does not allow high quality mitochondria enrichment; however, it does remove the cytosol which the major translationally active compartment, and hence an important step for our mitochondrial translation study. To better validate this protocol, additional organelle markers

can be added to further assess organelle fractionation (micronemes, roptries, ER, Golgi, dense granules, cytoskeleton, and nucleus). Special care should be taken when filtering out host cell from parasites as well, as human mitochondria contamination may occur and cannot be separated from *T. gondii*'s mitochondrion with this protocol. In the future, mitochondrial purification could be attempted using a sucrose or Percoll gradients.

8.2. Identification of MITI partners by tRNA affinity assay

8.2.1. tRNA affinity assay optimization

One way to identify MITI components is to pull down complexes that interact with tRNAs known to be imported into the mitochondrion (Esseiva *et al.*, 2004)(. This experiment was previously performed for *T. brucei* which needs to import all tRNAs into the mitochondria as well (Seidman *et al.*, 2012). In this study, authors pulled down mitochondrial membrane complexes by tRNA affinity purification. They used magnetic beads bound to *T. brucei* biotinylated tRNA[leu] and incubated intact mitochondria with the beads. Once complexes from the outer membrane of the mitochondria are bound, mitochondria were solubilized with 1% Triton X-100, and proteins unspecifically bound were washed out. Elutions were analysed with LC-MS/MS (Liquid Chromatography - Mass Spectrometry and Liquid Chromatography - Tandem Mass Spectrometry). This allowed the identification of several candidate protein with one of them, Tb11.01.4590, being the most promising new protein as its knockdown reduced tRNA import defect. PTP tagging of Tb11.01.4590 confirmed interaction with protein hits from the MS data set, and the recovery of components from the protein import machinery, including Tim17, provides further evidence that the mitochondrial protein import and tRNA import pathways share components (Seidman *et al.*, 2012). These results are in line with previous work from (Tschopp, Charrière and Schneider, 2011) who revealed Tim17 as an important factor for tRNA import, and suggested this component sharing, also shown in yeast (Tarassov *et al.*, 2007) and plants (Salinas *et al.*, 2006), may be a conserved feature in all systems. Seeing these promising results, we decided to adapt the protocol from Seidman *et al.* (2012) for *T. gondii*.

The choice of the tRNAs used in our experiment was based on the work performed by Esseiva *et al.* (2004). In that study, the presence of nuclear encoded tRNAs was

assessed in total cell, crude mitochondria (with apicoplast), and apicoplast only fractions obtained by 0.05% and 0.1% digitonin treatment for the last two fractions, respectively. Northern blots analysis showed that all the tRNAs tested in this study were imported into the mitochondrion of *T. gondii* (tRNA^{Ala}, tRNA^{Ile}, tRNA^{Ser}, tRNA^{Trp}, tRNA^{Gln}, and tRNA^{Met-e}) but not the apicoplast, with the only exception being tRNA^{Met-i} which was systematically recovered in the total cell fraction only, suggesting excusive cytosolic localisation. In a previous study, tRNA^{Met-i} was also reported to be exclusively cytosolic in the unrelated parasite *T. brucei* which requires all tRNAs to be imported (Tan *et al.*, 2002). We hence decided to test one of the imported tRNAs, tRNA^{Ile}, and tRNA^{Met-i} as a negative control for our pull-down assay. Briefly, the experiment was performed as followed (see Appendix for the complete "lab" version protocol). Wild type RH *T. gondii* were cultured in 150 cm^2 flasks and 5x10^8 parasites were lysed using nitrogen cavitation as mentioned above (section 7.18). Differential centrifugation was carried out as above to obtain a crude mitochondrial fraction. Commercially synthetized *T. gondii* biotinylated tRNA^{Ile} and tRNA^{Met-i} (Dharmacon™) using *T. gondii* sequence were bound to magnetic streptavidin beads. Crude mitochondrial samples were then incubated with the tRNA-bound magnetic beads, mitochondria were solubilised with 1% Triton-X100, washed, and proteins were eluted by disrupting hydrophobic protein interaction between tRNAs and mitochondrial membrane protein with 0.25, 0.5, 0.75 and/or 1 M of NaCl elution buffer (Janado *et al.*, 1986). The unbound proteins, washes and elutions were separated by SDS PAGE and stained with Silver staining, Coomassie Blue or SYBR Orange. In our first attempts, the aim was to be able to visualise different band patterns from tRNA^{Ile} compared to controls in order to send the bands of interest for MS analysis. In the attempt presented in Figure 8.3B, the adapted protocol from Seidman *et al.* was utilised, as described above. Crude mitochondria were incubated with "naked" beads serving as control and compared to the tRNA^{Ile} test. Proteins were eluted with 1M NaCl elution buffer, and the gel was stained using Sliver staining, which is a highly sensitive protein staining method. Although Silver staining is not compatible with downstream MS analysis, at this point of the optimisation process, clear protein visualisation on the gel was prioritised. Different protein band patterns between the control and tRNA^{Ile} were expected, with the "naked" beads displaying unspecific bands, and the bands from the tRNA^{Ile} test reflecting specific interactions. However, only a single band was observed at approximately 65 kDa

in both the control and the tRNA^{Ile} test (Figure 8.3B). To figure out if the issue came from the adapted protocol in general, in the next attempt, the protocol from the bead's manufacturer was followed side by side with the adapted Seidman *et al*. protocol for the tRNA^{Ile} only (Figure 8.3C). Proteins were eluted with 0.5M and 1M NaCl elution buffer, and the gel was stained as previously. Results showed the same profile for both protocols with no improvements from to the previous attempt, suggesting that the issue may come from the staining method. For the rest of the experiment, the adapted Seidman *et al*. protocol was used. Proteins were eluted with a gradient of an increasing concentration of NaCl (0.5-1M NaCl) in the elution buffer, an additional lane was loaded with the input (sample before incubation with the tRNA^{Ile}-bound beads), and Coomassie Blue was then used to stain the gel. Finally, bands other than the 65 kDa could be observed as well (Figure 8.3D), which was surprising as Silver staining is meant to be much more sensitive. Perhaps one of the reagents used was expired. Regardless, bands from the elution were too faint to notice any band pattern differences compared to the unbound fraction (Figure 8.3D). Lastly, the experiment was repeated with tRNA^{Ile} and tRNA^{Met-i} and elution was carried out using the salt gradient mentioned above. Elution fractions were pooled together and proteins were trichloroacetic acid (TCA) precipitated before loading on the gel. Proteins were then stained with SYBR Orange, which is compatible with MS analysis of gel slices. The beads and the protein binding buffer were loaded as additional controls for unspecific protein binding and a "no protein" control, respectively (Figure 8.3E). Results show that the predominant band present in all lanes was due to the protein binding buffer which contains bovine serum albumin (BSA) to reduce unspecific binding, and which has a molecular weight (MW) of ~66.5 kDa. Elution lanes show a good protein band resolution, however, bands in the tRNA^{Ile} test are the same as in the tRNA^{Met-i} (Figure 8.3E). Despite this, we cannot exclude the possibility that putative bands of interest are simply too faint to be visualised. We thus decided to proceed with the analysis of these elutions. From the experiments for which bands were the clearest, we initially thought a faint band pattern difference could be observed between 20 and 30 KDa, and so gel slice were cut out between 17-34 KDa and sent to MS. However, this difference could not be observed in the following repetitions. But to remain consistent, the following MS analysis of elution gels were performed on the same 17-34 KDa MW interval. This experiment with the latter conditions

was repeated 5 times. The outcome of this assay is detailed in the below section 8.2.2.
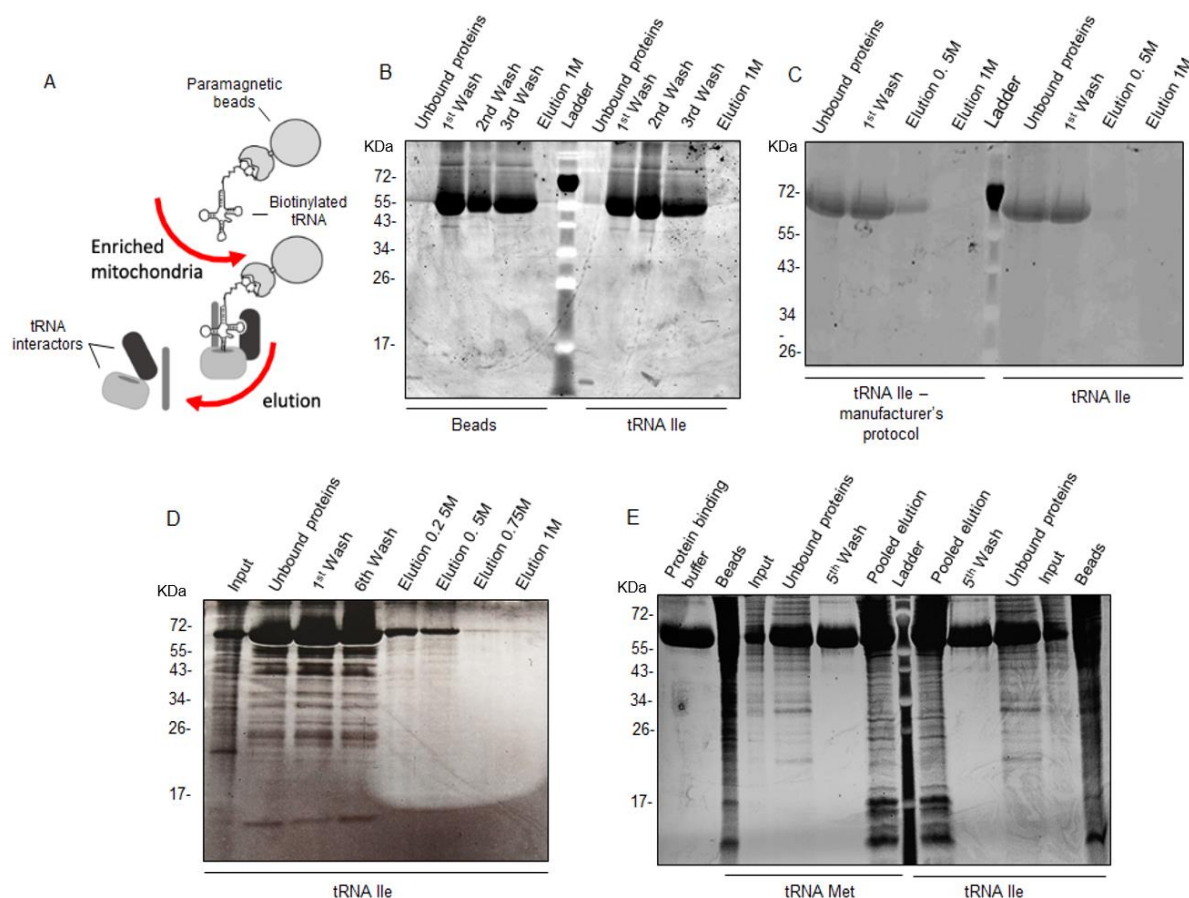
Figure 8.3 Optimization of tRNA Affinity Purification of Mitochondrial Membrane Complexes. (**A**) schematic of the tRNA co-immunoprecipitation (from Dr. Lilach Sheiner). Biotinylated tRNAs are coupled with paramagnetic beads and incubated in the presence of enriched mitochondria samples. tRNA interactors bind the biotinylated tRNA and are then eluted. **B – E**, the different fraction resulting from the co-immunoprecipitation are run and stained using different staining methods: Silver staining (**B and C**), Coomassie (**D**), and SYPRO Orange (**E**).

8.2.2. Analysis and localisation of proteins identified by tRNA co-IP followed by MS

MS was employed to determine the mass and sequence of proteins or peptides from the protein gel, which was used to match to genome datasets (ToxoDB). It typically involves in-gel trypsin digest, extraction of peptides, fractionation by reverse phase high performance liquid chromatography (RP-HPLC) and online nanoelectropsray tandem MS (MS/MS). This was performed by the Polyomics facility in Glasgow. From the list of hits resulting from the MS analysis, were of interest genes which (i) appeared in multiple tRNA^{Ile} repeats, as this was considered to provide support for their validity, and (ii) absent from the tRNA^{Met-i} repeats, as tRNA^{Met-i} being cytosolic only, proteins binding both tRNAs were

considered general binders of tRNAs, and at this point, the focus was on binders of mitochondrial imported tRNA. This sorting generated a list of 7 candidate genes which were found in two tRNA^{Ile} pull-downs and none in tRNA^{Met-i} (Table 8.1, Appendix Table 1). Their predicted localisation was assessed using online prediction tools such as Predotar (https://urgi.versailles.inra.fr/predotar/), Mitoprot (http://ihg.gsf.de/ihg/mitoprot.html), Mitofates (http://mitf.cbrc.jp/MitoFates/cgi-bin/top.cgi), TargetP-2.0 (https://services.healthtech.dtu.dk/service.php?TargetP-2.0), and iPSORT (http://ipsort.hgc.jp/) for mitochondrial localisation and cNLS Mapper (http://nls-mapper.iab.keio.ac.jp/cgi-bin/NLS_Mapper_form.cgi) for nuclear localisation (Table 3.2, Appendix Table 1 – Sheet 2 "Hits found in tRNA^{Ile} only"). Information on (a) their phenotype score (Sidik *et al.*, 2016), and (b) on whether they were found in the mitochondrial matrix proteome (Seidi, Linden S Muellner-Wong, *et al.*, 2018) and (c) hyperLOPIT data (Barylyuk *et al.*, 2020), all available on ToxoDB, was also reviewed as these provide valuable insights on their putative function (Table 8.1, Appendix Table 1 – Sheet 2 "Hits found in tRNA^{Ile} only"). (a) Phenotype scores were generated from a genome-wide CRISPR screen which identified essential genes (Sidik *et al.*, 2016). For this, a sgRNA library for all genes encoded in the nuclear genome was generated and transfected into CAS9 expressing parasites. Parasites which had essential genes disrupted would quickly be lost and over grown by those whose disrupted gene were dispensable. This would hence be reflected in the relative abundance of each integrated sgRNA in the population after a few passages, which was subsequently monitored by next-generation sequencing. According to a specific sgRNA abundance, a phenotype score was assigned to each gene. Genes with scores below -2 are considered essential. (b) To elucidate the mitochondrial matrix proteome, Seidi *et al.* (2018) performed a proximity biotin tagging of matrix proteins using biotin protein ligase (BirA) and ascorbate peroxidase (APEX) which were targeted to the mitochondrial (mt) matrix. Protein biotinylation in mtAPEX and mtBirA expressing lines was triggered by the addition of biotin-phenol and H_2O_2, and biotin, respectively. Biotinylated proteins were affinity purified using streptavidin beads, and analysed by MS. This enable the identification of 421 putative mitochondrial proteins (Seidi, Linden S Muellner-Wong, *et al.*, 2018). (c) Finally, the hyperhyperLOPIT data refers to the work of a recent study by Barylyuk *et al.*, (2020). This study focused on the challenging task of solving the proteome of every compartments and

subcompartments of the cell. The localisation of organelle proteins was assessed by isotope tagging (hyperhyperLOPIT), a spatial proteomic method which allows identification of thousands of proteins with their respective subcompartments. This contributed the expansion of the mitochondrial proteome which includes soluble and membrane proteins from all mitochondrial compartments. A total of 390 putative mitochondrial proteins were identified as a result (Barylyuk *et al.*, 2020).

TGME49_219470, annotated as hypothetical proteins, and TGME49_246540, as cytochrome c1 protein, are predicted to localise to the mitochondrion according to online prediction tools, and mitochondrial matrix proteome and hyperLOPIT data, respectively. TGME49_253740 and TGME49_267660, both hypothetical proteins, and TGME49_259640, annotated as a nucleoporin autopeptidase, are predicted to be nuclear according to the online tools cNLS Mapper and the hyperLOPIT data. TGME49_220950, a hypothetical protein, and TGME49_297780, annotated as a DNA gyrase B, are predicted to localise to another cellular compartment using online tools, and to the dense granules and apicoplast, respectively, according to the hyperLOPIT data. The nucleoporin (TGME49_259640) was recently published as TgNup302 which is involved in nuclear transport (Courjol *et al.*, 2017). The DNA gyrase B protein (TGME49_297780) is an apicoplast protein involved in DNA conformation regulation, and two publications confirm its function and localisation (Lin, Nagano and Gardiner Heddle, 2015; Courjol *et al.*, 2017). The hypothetical protein TGME49_220950 was recently published as the TgMAF1b isoform and was shown to localise to the PV, and is involved in host mitochondria recruitment (Blank *et al.*, 2018). In our experiment, all genes but TGME49_219470 and /220950 have a phenotype score below -2 suggesting that these are essential genes (Table 8.1).

Gene ID (ToxoDB)	Predicted fucntion	Times found in pull-down (out of 5)		Predicted localisation	Phenotype score	Mitochondrial Matrix Proteome	hyperLOPIT
		tRNA^{Ile}	tRNA^{Met-i}				
TGME49_219470	hypothetical protein	2	0	Mitochondrion*	-0.47	no	no
TGME49_220950	hypothetical protein (MAF1b)	2	0	Elsewhere*^	2.13	no'	Dense granules
TGME49_246540	cytochrome c1, heme protein	2	0	Elsewhere*^	-4.36	yes	Mitochondrion - membranes
TGME49_253740	hypothetical protein	2	0	Nucleus*^	-4.72	no'	no
TGME49_259640	nucleoporin autopeptidase (Nup302)	2	0	Nucleus*^	-4.08	no'	Nucleus - chromatin
TGME49_267660	hypothetical protein	2	0	Nucleus*^	-2.76	no	Nucleolus
TGME49_297780	DNA gyrase B	2	0	Elsewhere*^	-2.93	no	Apicolplast
TGME49_284560	ribosomal protein RPL9	3	1	Elsewhere*^	-5.37	yes	60S ribosome
TGME49_207840	ribosomal protein RPS17	2	1	Mitochondrion*	-3.75	yes	40S ribosome
TGME49_245680	ribosomal protein RPL21	2	1	Mitochondrion*	-3.65	no'	60S ribosome
TGME49_248390	ribosomal protein RPL26	2	1	Mitochondrion*	-3.23	no'	60S ribosome
TGME49_266070	ribosomal protein RPL31	2	1	Mitochondrion*	-3.75	no'	60S ribosome
TGME49_267060	ribosomal protein RPL14	2	1	Mitochondrion*	-3.07	no'	60S ribosome

Table 8.1 Putative tRNA interactors obtained from MS analysis of mitochondrial tRNA immunoprecipitation.
*Mitochondrial targeting predictions are done using MitoProt II (https://ihg.gsf.de/ihg/mitoprot.html), Predotar (https://urgi.versailles.inra.fr/predotar/), MitoFates (http://mitf.cbrc.jp/MitoFates/cgi-bin/top.cgi), TargetP-2.0, and iPSORT. ^Nuclear targeting predictions are done using cNLS Mapper (http://nls-mapper.iab.keio.ac.jp/cgi-bin/NLS_Mapper_form.cgi). The fitness score is based on the whole genome CRISPR/CAS9 screen (Sidik *et al.*, 2016). The presence (yes) or absence (no) of the gene product in the proximity tagging based mitochondrial proteome is shown (Seidi, Linden S Muellner-Wong, *et al.*, 2018). Some gene products were found in the mitochondrial proteome data but did not make it to the final 421 gene list (no') (Seidi *et al.*, 2018). Presence or not (no) of the gene product in the hyperLOPIT data (Barylyuk *et al.*, 2020).

In order to confirm the localisation of these candidates, a triple-HA epitope tag was added C-terminal end of the endogenous gene by single homologous recombination (Huynh and Carruthers, 2009; Sheiner *et al.*, 2011). Four out of 7 were successfully tagged: MAF1b protein, TGME49_253740, the nucleoporin TgNup302 and the DNA gyrase B protein, were assessed by IFA (Figure 8.4). All proteins previously published localised to their expected cellular compartment and TGME49_253740 localises to the nucleus. TgNup302 and TGME49_253740 nuclear proteins are both interesting. Indeed, an alternative model of tRNA import could also be a direct passage of tRNA from the nucleus into the mitochondrion. Although tRNA maturation and splicing occur in the cytosol, some travel back into the nucleus by retrograde nuclear import for additional modifications (Chatterjee *et al.*, 2018), moreover, it was proposed that tRNAs are aminoacylated in the nucleus in some systems (e.g. Lund and Dahlberg, 1998; Nathanson and Deutscher, 2000). So, perhaps once back in the nucleus, some of them could be translocated through a direct unknown pathway.
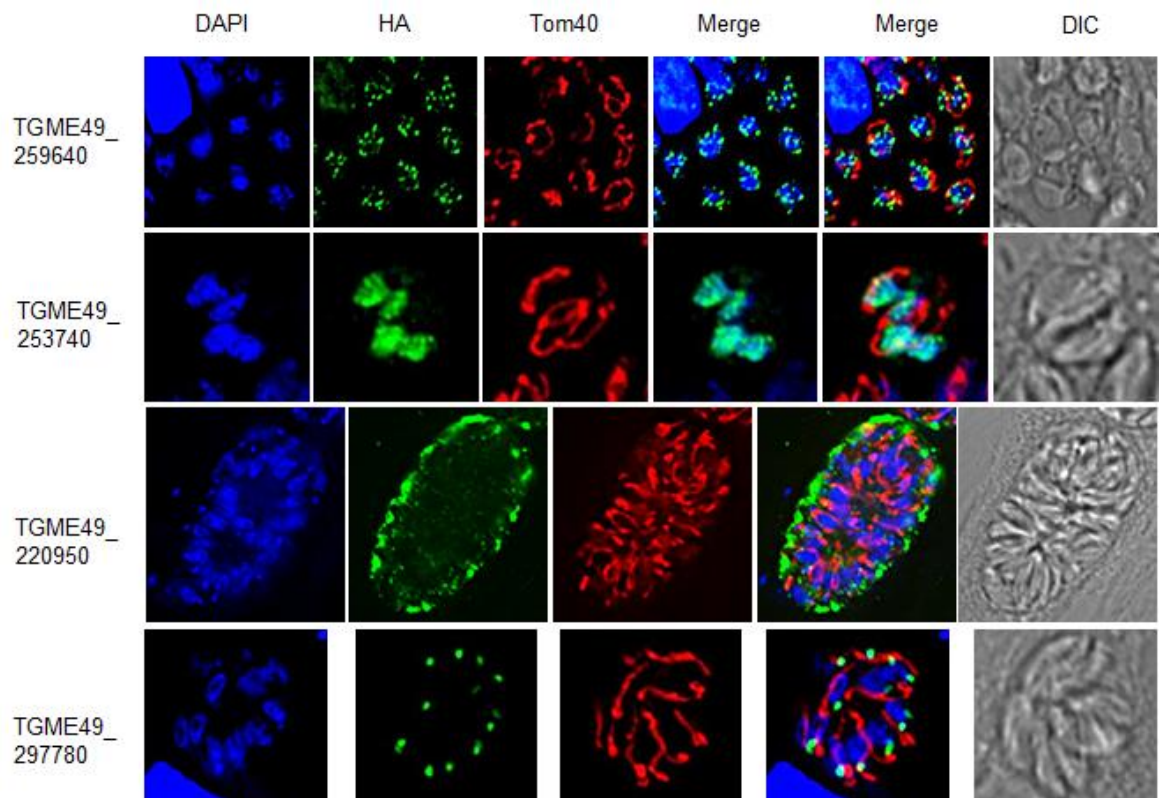
Figure 8.4 Localisation of genes identified by MS from tRNA pull down.
Nucleus is shown in blue stained by DAPI. GOIs in green are stained with anti-HA and in red are mitochondria stained with anti-Tom40. Channels are merged to either see GOI and nucleus co-localisation (blue and green), and/or nucleus, GOI and mitochondrion (blue, green, red), and overall shapes are visualized by Differential Interference Contrast (DIC).

Although the focused was primarily put on proteins which only interact with tRNA^{Ile}, it is possible that interesting hits with a potential role in MITI or mitochondrial translation had been excluded because they had also interacted with tRNA^{Met-i} for the only reason that they can bind to tRNAs, even if some may operate in the mitochondrion. So, we wanted to investigate whether there were any protein function or localization that is enriched in the binders of tRNA^{Ile} compared to the binders of tRNA^{Met-i}. Proteins were assessed on the basis of mitochondrial localisation prediction using online the prediction tools mentioned above, on their presence or not in the matrix proteome data (Seidi, Linden S Muellner-Wong, *et al.*, 2018) and their localisation from the hyperLOPIT data (Barylyuk *et al.*, 2020). Only proteins found in at least two repeats for each tRNA pull down dataset were considered. Results show a moderate enrichment of proteins predicted to be mitochondrial for tRNA^{Ile} (28.7%) compared to tRNA^{Meti-i} (21.4%) as shown in Figure 8.5. This correlates with a higher number of ribosomal proteins predicted to be mitochondrial for tRNA^{Ile} (10%) compared to tRNA^{Meti-i} (4%). These ribosomal proteins, TGME49_207840/245680/248390/266070/267060,

are displayed in Table 3.2. One of them, TGME49_207840, can also be found in the mitochondrial matrix proteome data (Seidi, Linden S Muellner-Wong, *et al.*, 2018). However, these 5 ribosomal proteins cluster also together with the 60S cytosolic ribosome (large SU) or 40S cytosolic ribosomes (small SU) in the hyperLOPIT data, and were not predicted to be part of the mitochondrial ribosome in the Gupta *et.al.*, (2018) study, which provided a list of nuclear encoded mitochondrial ribosomal proteins for apicomplexan parasites including *T. gondii*. These contradicting findings and predictions raise the possibility that these 5 ribosomal proteins may have a bi-modal action as part of both the cytosolic and mitochondrial ribosomes, and hence be shared between the two compartments. The lack of detection in the Seidi *et al.*, (2018) proteomics approach might reflect the low abundance of the mitochondrial ribosomes (Table 8.1). Experimental localisation is needed to test this hypothesis. An additional ribosomal protein, TGME49_284560, although not predicted to be mitochondrial, was added to the Table 3.2 as it was found in at least 3 tRNA^{Ile} repetitions and only once in the tRNA^{Met-i}, and is present in the matrix proteome dataset, and so may be of interest. Many proteins from other cellular compartments were found as well and compose 56% of the proteins identified for tRNA^{Met-i} and ~49% for tRNA^{Ile} (Figure 8.5). Most of these proteins are nuclear, roptries and dense granule proteins (Appendix Table 1 – sheet 1 "All tRNAMet-i hits" and 2 "All tRNAIle hits"), and they are not expected to have any specific interaction with tRNAs. This suggests that this assay may lack specificity, which is a recurrent outcome with IPs where a transient interaction is used to identify binders of a substrate or a molecule.
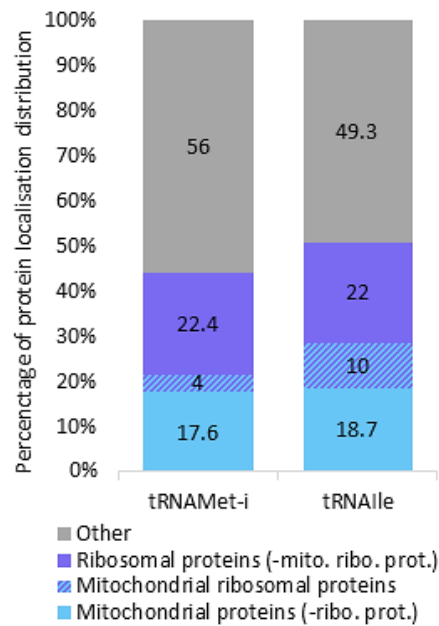
Figure 8.5 Predicted localisation distribution of proteins hits from tRNA^{Met-i} and tRNA^{Ile} immunoprecipitation datasets.
In light blue are the proteins predicted to localise to the mitochondrion, those is dark blue are predicted to be ribosomal proteins, proteins in light and dark blue strips are predicted to be ribosomal proteins and to localise to the mitochondrion, and proteins in grey are those predicted to localise to other cellular compartments such as the nucleus, roptries, dense granules, cytosol, and plasma membrane. Mitochondrial localisation prediction was assessed with prediction algorithms such as Predotar, Mitoprot, Mitofates, TargetP-2.0, and iPSORT, and by search in matrix proteome dataset (Seidi, Linden S Muellner-Wong, *et al.*, 2018). Other cellular localisation predictions were assessed by search in the hyperLOPIT dataset (Barylyuk *et al.*, 2020).

In summary, tRNA immunoprecipitation was used to pull down proteins which likely interact with tRNA^{Ile}, which was previously shown to be imported into the mitochondrion, to identify proteins involved in MITI. Many proteins were found in both tRNA^{Ile} and tRNA^{Met-i} experiments which was expected considering different tRNAs could bind many molecules in common. When applying selection conditions that necessitate hits to be present in at least two repetitions of the tRNA^{Ile} experiments and absent from all tRNA^{Met-I} experiments, only 7 hits came up, but only 2 of the 7 are predicted to be mitochondrial. There are several options of interpretation for this: (1) the non-mitochondrial hits are unspecific and the experiment failed (improvements are discussed in section 11.2), which is likely the case at least for MAF1b and DNA gyrase B. (2) MITI process take place in two parts: recruitment to the mitochondrion, and translocation through the mitochondrial membrane. The non-mitochondrial proteins may be involved in recruitment from the cytosol, or the nucleus. (3) The prediction of localisation is incorrect or that bi-modal targeting takes place. We then also applied a different set of criteria. We analysed protein hits found in at least two repetitions for both tRNA^{Met-i} and tRNA^{Ile}. Among those, ribosomal proteins represent 26% of all proteins

for tRNA^{Met-i} and 32% for tRNA^{Ile}, which is in line with their role in translation, and 7% of the 32% of ribosomal proteins are potentially shared between the cytosol and the mitochondrion, which is in line with the link between tRNA import and mitochondrial translation. This assay, however, has some lack of specificity which should be addressed in the future to increase its robustness (section 11.2).

8.3. Bioinformatic screen identifies new mitochondrial genes

8.3.1. mRNA expression based bioinformatic approach

A new bioinformatic pipeline was used as another independent approach to study MITI. MITI has been demonstrated in many organisms such as in yeast, plant, mammalian cell and trypanosomatids, and can be performed using different components depending on the organism (Rubio and Hopper, 2011). Previous studies have shown in yeast, *Leishmania* and *Trypanosoma* that some components of the protein import system are involved in MITI (Rinehart *et al.*, 2005; Mukherjee *et al.*, 2007; Seidman *et al.*, 2012). We hence use these findings as basis for our bioinformatic screen design. Nishi *et al.*, (2008) have previously demonstrated that organelle biogenesis is a tightly regulated process that occurs in a synchronised manner throughout the cell cycle in *T. gondii*. Each organelle, including the mitochondrion, has a short period of time during cell division in which they can expand (Nishi *et al.*, 2008). This implies that genes involved in the biogenesis for a specific organelle would co-express together. For the mitochondrion, it would include genes encoding for complexes of the mitochondrial protein import machinery which allows the passage of, amongst others, proteins of the mitochondrial translation machinery. Collectively, these proteins are defined in this study as "mitochondrial housekeeping proteins".

The following bioinformatic screen is described of my recent publication (Lacombe *et al.*, 2019) *and is hence presented here as it is in this paper with minor modifications.*

We wished to enlarge the repertoire of known mitochondrial housekeeping proteins with an emphasis on translation components. However, homology searches and the use of mitochondrial targeting prediction software cannot identify of all housekeeping components. Some proteins are too divergent to be

identified by BLAST, some can be unique to *T. gondii*. And although online tools such MitoProt, Predotar and MitoFates are useful to predict mitochondrial localisation by recognising mitochondrial targeting sequence, they hardly recognise these when embedded within the protein sequence as opposed to being at the N or C-terminal end. Previous studies have demonstrated the functional predictive power of mRNA co-expression patterns during the *T. gondii* tachyzoite cell cycle (Huynh and Carruthers, 2009, 2016; Behnke *et al.*, 2010; Sheiner *et al.*, 2011). This was shown for proteins involved in nuclear genome maintenance, microneme adhesins, rhoptry effectors (Behnke *et al.*, 2010), apicoplast biogenesis (Sheiner *et al.*, 2011) and host cell invasion (Huynh and Carruthers, 2016). We therefore reasoned that this strategy could also be applied for genes encoding for mitochondrial housekeeping proteins.

At the time of performing this search, the mitochondrial protein import pathway had the most predicted proteins compared to other housekeeping pathways in apicomplexan parasites. A group of 14 *T. gondii* homologs of these components were hence chosen based on the prediction made by (Van Dooren, Stimmler and McFadden, 2006) (Table 8.2 - top).

14 genes used for mining of the cyclical mRNA expression data[±]				
Protein name	Gene ID of *Plasmodium*[*]	GeneID at time of search (2012)	Current *T. gondii* homolog ID	Recovered in search?
Tim23	PF3D7_1356200	TGME49_014150	TGME49_214150	Y
Tim17	PF3D7_1434700	TGME49_112220	TGME49_312220	Y
Tim50	PF3D7_0726900	TGME49_083590	TGME49_283590	Y
Tim44	PF3D7_1125400	TGME49_027830	TGME49_227830	Y
GrpE	PF3D7_1124700	TGME49_065220	TGME49_265220	Y
Pam18	PF3D7_0724400	TGME49_002810	TGME49_202810	N
Tom40	PF3D7_0617000	TGME49_018280	TGME49_218280	Y
Tim 8	PF3D7_1242900 /PF3D7_1421500	TGME49_054610	TGME49_254610	Y
		TGME49_074090	TGME49_274090	Not used[^]
Tim9	PF3D7_1368600	TGME49_015390	TGME49_215390	Y
		TGME49_060850	TGME49_260850	Not used[^]
Tim 22	PF3D7_0627400	TGME49_025710	TGME49_225710	Y
HSP70	PF3D7_1134000	TGME49_051780	TGME49_251780	Not used[^]
Erv1	PF3D7_1002500	TGME49_032820	TGME49_232815	Y
Additional homologs of mitochondrial import proteins not used as bait				
Cpn10			TGME49_263530[**]	Y
GroS			TGME49_273960[**]	N
Sam50			TGME49_205570[**]	N
Pam16			TGME49_249910[**]	Y
Tim10	PF3D7_1208600		TGME49_215390[**]	Y
Tom22	PF3D7_0524700		Null	N/A

Table 8.2 Toxoplasma genes encoding components of the mitochondrial protein import pathway

In a study from Behnke *et al*. (2010), scientists used synchronised *T. gondii* tachyzoites to generated a microarray data set which was used in the present study to assess the gene expression pattern of the 14 protein throughout the cell cycle. Three genes (TGME49_274090/260850/251780) did not show cyclical expression pattern, so were therefore excluded from the list of baits (Table 8.2 - top). The microarray data was queried for mRNAs expression pattern which correlates with that of each of the 11 remaining baits using either Euclidian distance or Spearman correlation (as described in the Materials and Methods section). This search identified 279 genes (Figure 8.6A, Appendix Table 2 - Sheet 1 - column A). This search criteria were such that each bait was used to query for similar but not identical mRNA expression pattern, in other words: a search with a given bait does not identify itself. Regardless, 10 out of the 11 baits turned up in the overall resulting dataset (Table 8.2, Appendix Table 2 - sheet 1 - columns C-D). This means that queries with specific baits identified the other baits, providing validation for this approach. In addition, 3 other genes encoding protein import components that were not used in the bait list (since they were not predicted at the time the search was performed) were also found in this dataset (Table 8.2 - bottom, Appendix Table 2 - Sheet 1 - columns C-D). As a negative control, 5 different lists of 279 *T. gondii* genes were generated at random (by sorting all the protein encoding genes in ToxoDB by size and selecting lists of 279 random gene IDs from across the size range – see Appendix Table 2 – Sheet 1 – Columns F-J) and examined. The 13 protein import components (10 baits recovered in the search + 3 additional) and the 10 new mitochondrial proteins validated in this study below (Table 8.3) which are all found in the 279 gene dataset, are underrepresented in the five random gene lists (none of them found in four lists, and five are found in one list) (Appendix Table 2- Sheet 1 - columns F-P). These observations provide support for an enrichment of mitochondrial housekeeping proteins in our dataset compared to random datasets of the same size. Moreover, genes involved in other known mitochondrial pathways (metabolic and physiological) which are not expected to co-express with mitochondrial housekeeping genes are underrepresented in the resulting dataset (Figure 8.6B, Appendix Table 2 - sheet 1 - columns R-AA). This provides additional support to

this approach's specificity. False positive evaluation should be carried out in the future to further validate the screen's specificity.
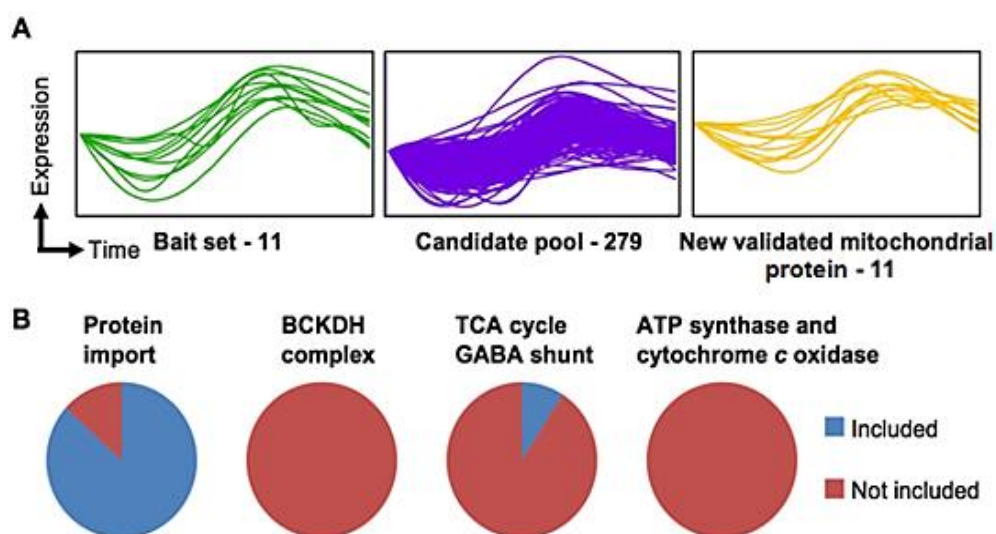
Figure 8.6 *T. gondii* genes with mRNA expression pattern in correlation with mitochondrial protein import components.
(A) Graphs show mRNA abundance profiles of the 11 gene used as baits (left, green), 279 candidate pool (middle, purple) and newly validated mitochondrial proteins (right, yellow) over two consecutive tachyzoite cell-cycles. **(B)** Pie charts depicting the inclusion or exclusion of genes from the candidate pool of 279 in functional groups of mitochondrial proteins (protein import, BCKDH complex, TCA cycle and GABA shunt, and ATP synthase and cytochrome c oxidase) (gene IDs are in Appendix Table 2).

To sharpen our focus on mitochondrial translation, another filter was added to our search: we postulated that *Cryptosporidium* spp, the only known species among the apicomplexans that lost their mitochondrial genome, likely lost their mitochondrial translation pathway, that is otherwise conserved among other apicomplexans. We queried the datasets for genes that do not have orthologs in any of the three genomes available for *Cryptosporidium* spp, but that do have orthologs in the genome of *Plasmodium falciparum* 3D7. This search identified 43 genes (Appendix Table 2 - sheet 2 - column A). Five of the 35 predicted mitochondrial ribosomal proteins (Gupta *et al.*, 2014) were found in this 43-gene dataset, while none of them came up in five randomly generated list of 43 genes (assembled as above) (Appendix Table 2 - sheet 2 - columns C-O).

Attempts to localise 18 genes selected at random from this focused dataset were performed by endogenous tagging whereby, a triple HA tag was fused C-terminally as mentioned above. Where endogenous tagging was unsuccessful, localisation was assessed via expression of 3xMyc tagged or YFP fused cDNA from a heterologous promoter. Among the 16 genes for which we obtained detectable

signal (Table 8.3), 11 were mitochondrial (~70%) (Table 8.3; (Lacombe *et al.*, 2019). Also, 7 of these 11 mitochondrial proteins were either not included in the final mitochondrial proteome dataset from Seidi *et al.*, (2018) or not found in their whole dataset at all. In addition, these same 7 mitochondrial proteins were either not found in the hyperLOPIT data (Barylyuk *et al.*, 2020) or had the wrong localisation. This confirms the usefulness of the bioinformatic screen and its ability to identify mitochondrial proteins that other methods and computational prediction tools have not. And we can expect many more mitochondrial genes to come out of our search if we estimate that about 70% of them could be mitochondrial. This search is therefore a useful contribution to the field by providing additional mitochondrial proteins to the common repertoire, and efforts are made to further localise and characterise more of these proteins.

Gene ID	Predicted product (TGME49)	Localisation Form of tagging	MitoProt	Predotar	Proximity tagging proteome	LOPIT	Phenotype score
TGME49_203620[§]	hypothetical protein	Mitochondrial endogenous	0.9734	0.53	no*	Mitochondrion - soluble	-4.66
TGME49_226270	hypothetical protein	Apicoplast endogenous	0.0402	0.01	no	Endomembrane vesicle	0.23
TGME49_231150	hypothetical protein	Mitochondrial endogenous	0.9986	0.33	yes	Mitochondrion - membranes	-5.21
TGME49_240270[§]	hypothetical protein	Mitochondrial cDNA - YFP	0.2831	0.04	no*	no	-4.65
TGME49_240780	hypothetical protein	Mitochondrial endogenous	0.3871	0.76	no	no	-3.95
TGME49_247740	hypothetical protein	Mitochondrial endogenous	0.0647	0.03	no*	no	0.31
TGME49_257110	hypothetical protein	no signal cDNA - myc	0.6373	0.01	no	Mitochondrion - membranes	-3.21
TGME49_263680	hypothetical protein	Mitochondrial endogenous	0.949	0.52	no*	no	-4.3
TGME49_310500	hypothetical protein	no signal cDNA - myc	0.9211	0.11	no*	Mitochondrion - soluble	-4.1
TGME49_201830	ribosomal protein L54	Mitochondrial endogenous	0.9991	0.43	no	no	-4.94
TGME49_226280	ribosomal protein L28, putative	Mitochondrial endogenous	0.9971	0.65	yes	Mitochondrion - soluble	-4.91
TGME49_214790[§]	glycoprotein	Mitochondrial endogenous	0.8383	0.47	yes	Mitochondrion - soluble	-3.48
TGME49_311750	mago binding protein	Cytosol cDNA - myc	0.198	0.01	no	nucleus - non-chromatin	-0.99
TGME49_312680	60S ribosomal protein L41, putative	Mitochondrial cDNA - myc	0.9388	0.14	no	no	-1.34
TGME49_238000	peptidyl-prolyl isomerase	Mitochondrial endogenous	0.8213	0.53	yes	Nucleolus	-6.27
TGME49_254260	COX19 cytochrome c oxidase assembly family protein	Cytosolic endogenous	0.1621	0,09	yes	Mitochondrion - soluble	-3.34
TGME49_283850	peptidyl-prolyl cis-trans isomerase	Cytosolic endogenous	0.0397	0,01	yes	Cytosol	-1.59
TGME49_286070	hypothetical protein	Cytosolic cDNA - YFP	0.1311	0,01	no	Endomembrane vesicle	-3.36

Table 8.3 Genes from the in silico search whose protein have been localised.

Mitochondrial targeting predictions are done using MitoProt II (https://ihg.gsf.de/ihg/mitoprot.html) and Predotar (https://urgi.versailles.inra.fr/predotar/). The presence (yes) or absence (no) of the gene product in the proximity tagging based mitochondrial proteome is shown (Seidi *et al.,* 2018) (no – no MS data; no* - MS data found but the gene is not included in the final list of 421 genes). Localisation of gene products based on the hyperLOPIT data is shown when available (no – not found in the hyperLOPIT data) (Barylyuk *et al.*, 2020). The fitness score is based on the whole genome CRISPR/CAS9 screen (Sidik *et al.*, 2016) (gene IDs with § - essentiality/importance for fitness confirmed here). In bold are the proteins I personally localised, the rest have been localised by co-workers and can be found in Lacombe *et al.,* (2019).

8.3.2. Localisation of candidate gene from the bioinformatic screen

Amongst the gene products localised from this screen, 16 in total including 11 mitochondrial genes (Table 3.4), I visualized 6 of them by IFA presented in Figure 8.7A (Table 8.3 – in bold). Results show that TGME49_203620, TGME49_240270 and TGME49_238000 are mitochondrial with their signal (green) co-localising with the mitochondrial marker (Tom40 or TgMys (TGME49_215430), both proteins of the OMM, in red). However, TGME49_283850, TGME49_286070 and TGME49_254260 are cytosolic, despite the predicted function of TGME49_254260 as COX19. But predicted functions suggested in ToxoDB do not always correspond to the real function of a gene, thus, only experimental assessment can confirm localisation and function. TGME49_240270 was also observed by super resolution microscopy to get more insight on the protein's sub-compartmental localisation. The green protein signal appears in between the red OMM marker all along the mitochondria, indicating that it resides within the mitochondrial matrix (Figure 8.7B). The molecular weight of the two triple HA tagged mitochondrial proteins was assessed by western blot (Figure 8.7C). Two bands were detected for TGME49_238000: a ~39 kDa band and a ~36 kDa band. These likely represent the immature uncleaved protein which still possesses its mitochondrial signal peptide (39 kDa), and the mature cleaved protein after entry in the mitochondrion (36 kDa) (Figure 8.7C). TGME49_203620 (TgmS35) has a molecular weight of about 38 kDa (Figure 8.7C).
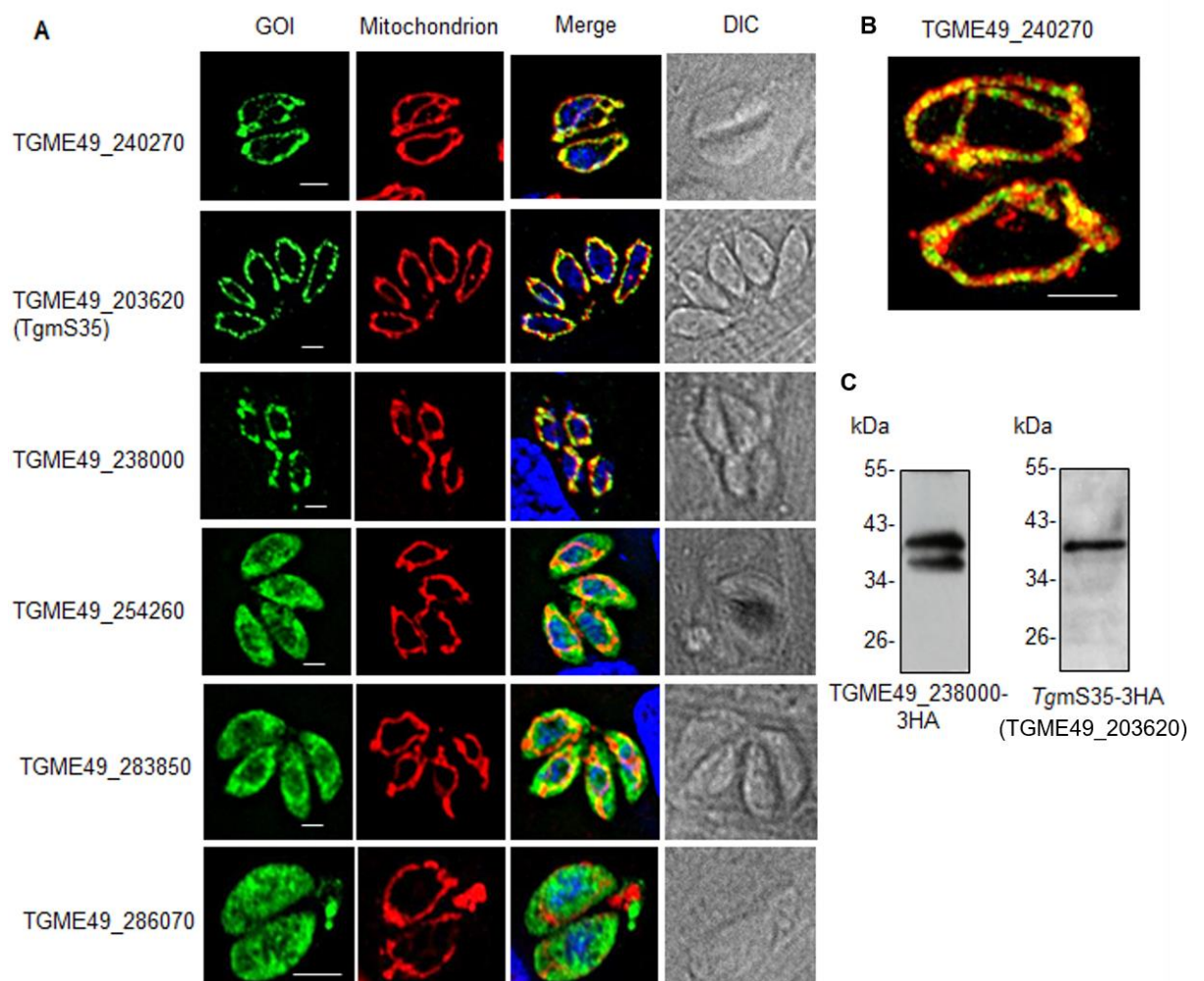
Figure 8.7 Localisation of 6 of the 16 previously uncharacterised proteins by epitope tagging. (A) Localisation through fluorescence microscopy analysis of 6 genes amongst those identified in the bioinformatic search. Mitochondria are stained with anti-TgMys (TGME49_215430) or anti-TOM40 in red, the mentioned GOI (genes of interest) are stained with anti-HA or anti-GFP in green, the nucleus is stained with DAPI in blue, and the parasite shape was visualized by Differential Interference Contrast (DIC); Scale bar 1 µm. (B) TGME49_240270 visualised by super resolution microscopy with the GOI stained with anti-GFP and mitochondrion with anti-TgMys Scale bar 2 µm. (C) Immunoblotting of protein TGEM49_238000-3HA and TgmS35-3HA (TGME49_203620). POIs are stained with anti-HA antibodies.

TGME49_203620, while annotated as hypothetical protein in ToxoDB.org, is a putative homolog of the mitochondrial small subunit 35 (mS35) which has been previously identified (Gupta *et al.*, 2014; Greber and Ban, 2016). A protein alignment of TGME49_203620 protein sequence with that of other apicomplexan sequences, namely *Neospora, Sacrocystis, Eimeria, Plasmodium,* and *Babesia* revealed some sequence conservation among them (Figure 8.8 – blue amino acids and yellow bars). However, only the *Plasmodium* gene PF3D7_1312300 (PlasmoDB.org) is annotated as a putative mS35 protein. Others other are annotated as 3'-5' exoribonuclease CSL4, ribosomal subunit, hypothetical protein, and hypothetical protein for *Neospora, Sacrocystis, Eimeria,* and *Babesia,*

respectively. Yet, a search on InterPro revealed that all sequences possess a conserved mitochondrial ribosomal protein S24/S35 domain (Figure 8.8 - red boxes), as well as for the human (MRPS35) homolog (Appendix Figure 2A-B) (InterPro ID: IPR019349). This provides support for the identity of TGME49_203620 to be a homolog of mS35, and was therefore named TgmS35.

Multiple sequence alignment

```
              10        20        30        40        50        60        70
              |         |         |         |         |         |         |
NCLIV_021400  ------------------------------------------------------------------------
SN3_00201010  ------------------------------------------------------------------------
TGME49_203620 MGPLGRVSSGQLAGVRRHRSCGLIRSTGPLCLSLRQSQSASDSVSSLTPLSLQQRAVCRPVMNADPPCDVISRFVSPDS
ETH_00007530  ------------------------------------------------------------------------
PF3D7_1312300 ------------------------------------------------------------------------
BBOV_III008220 ------------------------------------------------------------------------

Conservation  ------------------------------------------------------------------------
```

```
              80        90        100       110       120       130       140       150
              |         |         |         |         |         |         |         |
NCLIV_021400  ------------------------------------------------------------------------
SN3_00201010  ------------------------------------------------------------------------
TGME49_203620 RLFIFCPRDILRASRGPSDVPAKSQAPTGVSIGSALSRESVTSRSTQPDRARLRLVSLSAAPSLCSTPRLSPCHTRCGAV
ETH_00007530  ------------------------------------------------------------------------
PF3D7_1312300 ------------------------------------------------------------------------
BBOV_III008220 ------------------------------------------------------------------------

Conservation  ------------------------------------------------------------------------
```

```
              160       170       180       190       200       210       220       230
              |         |         |         |         |         |         |         |
NCLIV_021400  -------------------------------------MPPGGLDQAREPEPSPSSSPRSPSFGSAHSRFYSSLVSPHLL
SN3_00201010  -------------------------------------------MKDMRE-------------------------------
TGME49_203620 RDTANASSCVSGPSRSESVLSPQDALHDNLLWLPARRTIRRHNAGATRATLARLPWFSSRFSLPGLHARFYTSSPHGRLL
ETH_00007530  ----------------------------------MATRGCGRLLQQQLQQQLQQQLQQQQQLLERRVSCLMCISPSS
PF3D7_1312300 ------------------------------------------------------------------------
BBOV_III008220 ------------------------------------------------------------------------

Conservation  ------------------------------------------------------------------------
```

```
              240       250       260       270       280       290       300       310
              |         |         |         |         |         |         |         |
NCLIV_021400  CSTL-SFPPSSSSSPSCLRLPTASGLPTRSADSSPTVCVLRAPGA-SLSPPSSPSAPASQVPHESLLPRSSFPLGQARDA
SN3_00201010  ------------------------RREKNQRKKIQNTRRP----------------QRRGDTETPREEN---------
TGME49_203620 SSTTPSQLASPPSPPSPPPLRVPASFFLRASTSAPAISALRASRSSHFSVPGPPSSPMTLFVHASFSRSAGPLLGQARDA
ETH_00007530  PAWTLHPQQQQQQQAGGPWGPRGPQKPRFQAVAAAAAAAAGGPLSSAAGKQRQAAVLQGPCSVDTSLGGSNEKGFGGPPEV
PF3D7_1312300 ----------------------------MYAVKKVNILKPHLWNLPWRKYYENKINKIYKYSYYNEHNVYSFHTFTRYNINNE
BBOV_III008220 ----------------------------------MYCALRNCCVLRNIAFGASDTLSATTS---------

Conservation  ------------------------0000100000000001---01000000000000332127243324 2-------
```

```
              320       330       340       350       360       370       380       390
              |         |         |         |         |         |         |         |
NCLIV_021400  AFDAFVPGG-----GLSWLQVRWKKKRGKKEKIILNAEQVATKTKYDERLGSRRESGFQIDASASPVFRLYERDSGASPL
SN3_00201010  --------HFLRTKYEETGKEKE----DTQREPTSRNAESAVGKEKKSQQSQKEEG---------GAEVADV
TGME49_203620 AVDAFFPGG-----GCSWLQVRWKKKRGKKEKVILNAEQVATKTRLPPIRLEDRITPEPPATVAR---------NIRSQI
ETH_00007530  GALARVGGGPLGSLGCMYTAIRAKKKRGKKEVQKKNAEQLETKASTPPLRLEDYSATPQPPAAVA---------ASIRLET
PF3D7_1312300 IYKDMDVKN----KYYMFNQIRNKKNRKRERVTLNDEQKNTKLKLPIIRLEDRTTVCETPSVIS---------KNIKKEI
BBOV_III008220 ----------QWYFLSQRMGKKKRRKVEKIPKSAEQKECATSMDIIRLHDRVGVPETPQSIA---------QTIRKNV

Conservation  ---------1137544657764474*001758833843454234737627434524373--------0733356
```

```
              400       410       420       430       440       450       460       470
              |         |         |         |         |         |         |         |
NCLIV_021400  TLAVGSSRCRRFDWRTALPRSHPQVWRETFELKSLGLRQVGRQNACSRTEINTD-DDEFTQANSRKRDSQASTSSSASSG
SN3_00201010  DTAVGAWKRR----KSSATGRRPNDRQRNEKLR----RLVG----LTHDID-DEE----NERTRTLGPGSNSSG---
TGME49_203620 SRAVAGWKTK---------RMFTYRNKYRLR----RLVG----MTHDIDSDDEFAQANARTRETNASTSKVSSSG
ETH_00007530  LRALRGRKTS---------RMFAFRNKYRLN----RLLG----LTHDAACSEGPEG---
PF3D7_1312300 LKVCVGKDRTR--------RHFKFRNKYRIRKLLS-----LTHDKE--
BBOV_III008220 RSVQQG-VITR-------KHYARMLQYRTARAMG-------LTHD

Conservation  23863813 45----8362563657 64------5687 00-----
```

```
              480       490       500       510       520       530       540       550
              |         |         |         |         |         |         |         |
NCLIV_021400  GEFKQAAGVKESSMGRKQKRAFAGRTFVTPLTKLQHQAALPRSPLHARFDFPHTFHYDVFWG-PPQVEEEPNKTACWVSP
SN3_00201010  -----------RTSRRVVGRSFVTPLTRLQHQATLPRTPLHVRFNFPHTLSYDVWWG-PPQVEEEPHHSACWVSP
TGME49_203620 CSTEKAEGVNGSTMGRRNRPSFAGRTFVTPLTRLQHQAALPRSPLHARFDFPHTVHYDVFWG-PPQVEEEPNKSGCWVSP
ETH_00007530  ----------SQRKPQGRQFVTPLTRMQHQARLPRSLLHDRFHFRHSLRYSVVWG-PQVAPE-RFSACQVSP
PF3D7_1312300 ----------NIKQKNPSAFITPLTKLQHESTLPRTLDHDRETFPHTHYSIIWHGSSIVDNE-ENNICYFTA
BBOV_III008220 --------NPRSTAPGAFVTPLTRLQHEATLPTTFGQARHNFPHVLRYRVNWLAQASPANLPQTKVTLSP

Conservation  ---------8244257 46*9**99**884-*7953 64-74-5-674-595-3-565745 5-4394977 97
```

```
              560       570       580       590       600       610       620       630
              |         |         |         |         |         |         |         |
NCLIV_021400  HVADLKLSDSQEQRLLDILGPERYDEQTGIACLEADVFPQLNHNAAYLGESDLPSAPISNSGVLPKREARRETHQIRTAC
SN3_00201010  RVADLKLSERQEKRLLDILGEERIDEATGIACIEADLFPQRNQNAAYLGD------------ILQQLMREVRKV---
TGME49_203620 RVADLKLSDSQEQRLLDILGEERIDEQTGVVCLEADVFPQLNHNAAYLGD------------ILQQLMREVKKA-
ETH_00007530  RLKDLNLTAAQQQLKAIVGPERLVG--DFCCLEANIFPELNQNAAFLGD------------SLELLMREIRKV---
PF3D7_1312300 NIKDLSLSSKEKKFIQVLGDERVDLKSQLVCLESNFFNTYNHNAAYLGD-----------ALQLMNKIKTL----
BBOV_III008220 NFNDLGISDEQIRKLKEILGRDNYDESSNIAILQADIFDNLVHNAHYLGD-----------ITERLMKEVKRHE---

Conservation  574**4+9438477864 99-*4976530247 88+8887-6747 6-**49--*9-----------447476 676863----
```

```
              640       650       660       670       680       690       700       710       720
              |         |         |         |         |         |         |         |         |
NCLIV_021400  HPHAEPSPRSCRLTVNVYPVSPARWRYSSTAYARGAKSVNRVTNDTGLAADTGTHTEMKIARTFAGKTWPTAYCVLPCTQQPADFL
SN3_00201010  -------------------------------------------------------------------------------------
TGME49_203620 -------------------------------------------------------------------------------------
ETH_00007530  -------------------------------------------------------------------------------------
PF3D7_1312300 -------------------------------------------------------------------------------------
BBOV_III008220 -------------------------------------------------------------------------------------

Conservation  -------------------------------------------------------------------------------------
```

Figure 8.8 Protein alignment of TgmS35 apicomplexan homologs.
Homologs identified via BLAST in EUpathDB.org. Alignment performed using clustalX pairwise alignment and consensus colours generated via Jalview. NCLIV - *N.caninum*; NS3 - *S.neurona*; TGME49 – T. gondii; ETH - *E.tenella*, , PF3D7 - *P. falciparum*; BBOV - *B.bovis*. Amino acid conservation is shown within the alignment in a blue-scale whereby light-blue is low similarity and dark blue is high similarity. Conservation is also shown as bars at the bottom. Bar colour is yellow-scale, whereby light yellow is high similarity and dark orange/brown is low conservation. Conserved mitochondrial ribosomal protein S24/S35 domains are shown in the red boxes.

8.4. Conclusions

Studies on mitochondrial biology, including MITI and mitochondrial translation, have been hampered by the difficulty to enrich intact mitochondria. This implies the use of a cell lysis protocol that does not compromise mitochondria integrity. For this, different methods were tested, all unsatisfactory except for nitrogen cavitation which resulted in a 95% breakage efficiency or more, and managed to keep some organelle integrity (Figure 8.2). In the future, repeating western blots and IFAs with additional cell compartment markers, as well as assessing mitochondrial membrane potential using MitoTraker and JC1 staining would allow a more robust characterisation of organelle integrity. The high breakage efficiency is also key to maximise the yield of material prior to the enrichment process. A short two step differential centrifugation was performed to pellet down mitochondria. The resulting sample still contains many cell compartment contaminants; however, it successfully removed the cytosol. This level of enrichment has long been considered sufficient in model organisms depending on the sensitivity of the experiment performed. However, when studying mitochondrial translation in apicomplexans, an additional challenge emerges: getting rid of the apicoplast. The described protocol does not allow such separation. Yet, it should have been of sufficient quality for our tRNA affinity assay as tRNA^{Ile} is only meant to be imported in the mitochondrion and not in the apicoplast. Moreover, it allowed us to perform the translation assay which will be discussed in the Discussion section 11.1.

Mitochondrial translation and MITI are two key housekeeping pathways with great potential as drug target, and yet are poorly studied. Previous studies have shown MITI occurs in a diverse array of organism, highlighting the widespread biological relevance of this pathway (Lithgow and Schneider, 2010; Rubio and Hopper, 2011; Schneider, 2011). *T. gondii* is an extreme case where all tRNAs must be imported as a consequence of losing all its corresponding mitochondrial genes. This scenario was demonstrated in *T. brucei* (Tan *et al.*, 2002), and Seidman *et al.* (2012) used

a clever tRNA affinity purification assay to identify components involved in MITI. We decided to apply this technique for *T. gondii*. *T. gondii* tRNA^{Ile,} known to be imported into the mitochondrion, and tRNA^{Met-I}, strictly cytosolic, were bound to magnetic beads and utilized to pull down putative components involved in MITI. After separation on SDS PAGE and gel slice analysis by MS, 7 candidate genes were identified and 4 were experimentally localised. Although more mitochondrial proteins were expected to be found from the IP, two nuclear proteins, with one being a nucleoporin were identified. A direct tRNA transfer from the nucleus to the mitochondrion is a hypothesis that will be discussed in the Discussion (section 11.2), and tested in the future. Many ribosomal proteins were found in both tRNA^{Ile} and tRNA^{Met-i} dataset, which is in line with their function in translation. Some moderate enrichment of ribosomal proteins with possible dual localisation was found for tRNA^{Ile}, which provide further support of the role of tRNA^{Ile} in mitochondrial translation. However, about half of the overall proteins from the tRNA^{Met-i} and tRNA^{Ile} datasets are contaminants of unrelated cell compartments. Together with the fact that only 2 proteins were predicted to be mitochondrial in the first dataset of 7 genes, this raises the question of whether this assay is specific enough. Some controls may be required to make this assay more robust (see in section 11.2).

In a field where the identification of new mitochondrial proteins cannot rely simply on homology searches and computational mitochondrial prediction tools, a bioinformatic screen was established to help overcome these limitations. mRNA expression patterns of genes encoding for protein import components were used to identify new mitochondrial proteins. Eleven out of 16 genes were confirmed as encoding for mitochondrial proteins, including 4 ribosomal proteins, 5 hypothetical proteins, and 2 with other predicted functions (glycoprotein and isomerase). Only 4 of the 11 mitochondrial proteins were part of the final matrix proteome data set from Seidi *et al.*, (2018) and founds in the hyperLOPIT dataset (Barylyuk *et al.*, 2020) supporting the power of this screen to identify genes that would have been missed otherwise. This outcome is not surprising as the bioinformatic screen is not restricted to a particular organelle compartment and hence hits from the mitochondrial matrix, as well as the OMM, IMM, and IMS are expected to be found within the *in-silico* data set. The validation of these genes contributes to the expansion of the mitochondrial proteome available in the field. Altogether, this work presented two independent approaches to identify proteins

involved in MITI and/or mitochondrial translation, and provides a reliable protocol to break parasites open which is compatible with organelle studies (see sections 9 and 10).

9. Functional characterisation of new candidate gene for mitochondrial tRNA import

In the section, we aimed at identifying the most optimal genetic approach to study mitochondrial biogenesis defects.

9.1. Expression of CRISPR-CAS9 as a medium throughput strategy for gene characterisation

Transient expression of CRISPR-CAS9 and single guide RNA (sgRNA) was considered as a strategy to explore if it could be used to provide a rapid read-out assay to detect protein involvement in mitochondrial biogenesis. We hypothesized that abnormal changes in mitochondrial morphology upon gene disruption may be an indicator for a defect in mitochondrial biogenesis.

9.1.1. A previously generated Split-CAS9 line induces mitochondrial and nuclear morphology defects

A line that constitutively expresses an inducible CAS9, where the endonuclease is split into two domains (called "Split-CAS9"), each domain fused to a rapamycin binding domain (FkBP and FRB rapamycin binding domain), was previously generated by Johannes Stortz, a previous PhD student in Prof. Markus Meissner's laboratory at the WCIP/University of Glasgow, and was generously provided by them (Stortz, 2020). This line was originally designed to help overcome the CAS9 cell toxicity (Serpeloni *et al.*, 2016; Sidik *et al.*, 2016; Lacombe *et al.*, 2019) by conditionally activating CAS9, for work that was focused on actin factors and dynamics. Addition of 150 nM of rapamycin to the medium triggers the dimerization of the Split-CAS9 by binding to the FRB and FkBP domain of each halves of the CAS9, which restores its activity. In the presence of sgRNA, the active CAS9 generates a double stranded cut at the precise location where the sgRNA binds in the genome which disrupts the targeted gene. We tested if this line could be used to generate a medium throughput screen which would allow us a rapid assessment of a gene's involvement in mitochondrial biogenesis. In our study, GOI sgRNAs were transiently expressed in the Split-CAS9 line rather than stably expressed to significantly shorten the amount of time needed to obtain results.

Indeed, this strategy would allow multiple gene screening in less than a week, when the process of generating stable lines and gene function assessment usually takes over a month in the fastest case scenario. Genes whose disruption result in mitochondrial morphology defects would then be selected as candidates having a potential role in mitochondrial biogenesis, and would be further studied. To test if this was plausible, 2 genes, TGME49_226280 and TGME49_225710, were assessed as proof of principle. These two genes were chosen at random from the bioinformatic screen list of 43 and 279 genes (see section 8.3.1) as we had no additional means to decide after looking at co-expression and phylogenetic distribution patterns. In our study, Split-CAS9 line was transiently transfected with TGME49_226280 and TGME49_225710 sgRNAs and incubated for 48h with rapamycin before being fixed and analysed by IFA (Figure 9.2). *T. gondii* is known for its highly dynamic mitochondrion. A recent study has shown that upon release into the extracellular environment, the mitochondrion undergoes tremendous morphological changes going from "lasso" shaped, a typical intracellular morphology, to collapsed shape via "sperm-like" shape after a prolonged extracellular period (Ovciarikova *et al.*, 2017). While intracellular, however, the mitochondrion is mainly found in the "lasso", "half-moon" and sometimes "sperm-like" shape, although the latter is not as common (Figure 9.1). An increase in "sperm-like" shaped mitochondria may be seen as an anomaly as it is often a sign that the parasites are undergoing some sort of stress. Abnormal mitochondrial morphologies are displayed as collapsed, fragmented or branched/irregular mitochondria. These appear when parasites are challenged with some biological defects, and is often associated with poor fitness. Of course, there are variations as mitochondria may display intermediate shapes between all illustrated morphologies.
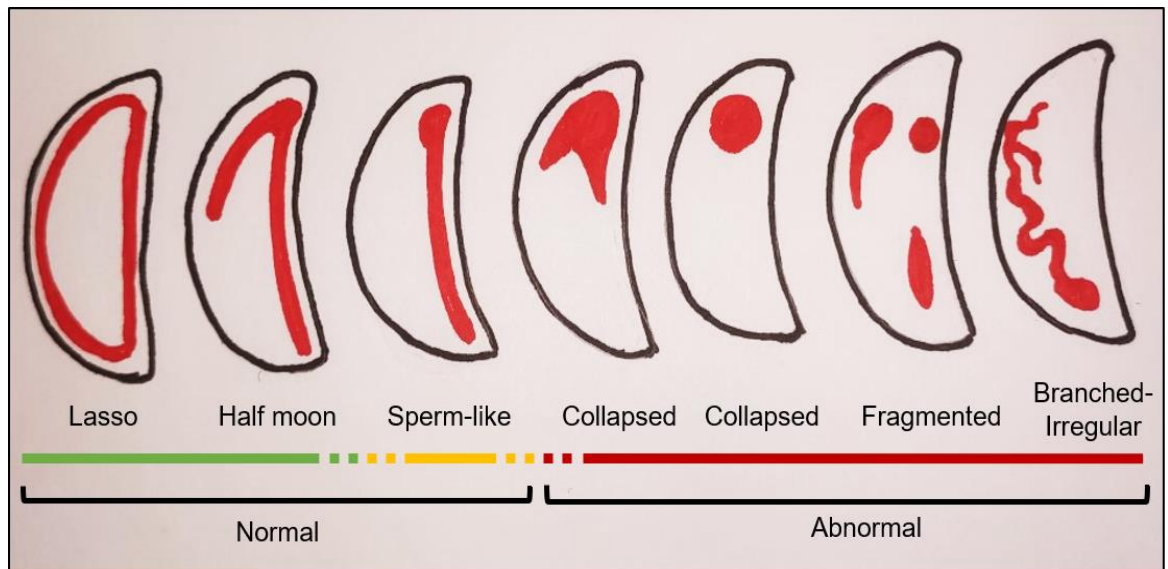
Figure 9.1 Mitochondrial morphology categories for intracellular *T. gondii*.
Scheme illustrating the different mitochondrial morphologies which can be categorised as "normal" or "abnormal", each category comprising in different mitohcndrial shapes. Normal mitochondria are typically in an open "lasso" shape, but can also form an incomplete lasso which we call "half-moon". Normal mitochondria may also be displayed a single elongated line we call "sperm-like" due to its shape often resembling a sperm. Although it is not uncommon to find sperm-like mitochondria in a healthy population, this shape is, however, not as frequent as the two previous ones. An elevated number of "sperm-like" mitochondria is often a sign parasite are undergoing some sort of stress. Mitochondria displaying morphologies in the red right part of the scheme are considered abnormal. Collapsed, fragmented, and branched/irregular morphologies are anomalies, and are the reflection of biological defects, often associated with poor parasite fitness.

Our experiments revealed abnormal mitochondrial morphologies for both genes. These mitochondria did not present any of the morphologies described in the Ovciarikova *et al.*, (2017) study. Instead, they displayed irregular, fragmented shapes with numerous branches (Figure 9.2A and B). However, amongst vacuoles with abnormal mitochondria shapes, some with abnormal nuclei could also be noticed (Figure 9.2C). Although, this analysis is purely qualitative, such unexpected phenotype is worth mentioning and considering when studying mitochondrial biogenesis, as in our experiments, this nuclear phenotype was always accompanied with mitochondrial morphology defect. Nuclear disturbance was reported in Stortz, (2020). He generated lines expressing sgRNATggap40 and sgRNATgsag1 stably in the Split-CAS9 background line. His data revealed unexpected aberrant nuclei phenotype in gene depleted parasites after addition of rapamycin for 1h and 48h, even for SAG1 which was chosen as a control for the system because its depletion should not affect parasite morphology and behaviour (Kim and Boothroyd, 1995; Lekutis *et al.*, 2001). This defect was not observed in Split-CAS9 expressing parasites (not transfected) treated or not with rapamycin. Johannes Stortz suggested this issue to be due to the inability of the parasite to

repair double stranded breaks caused by the activated Cas9 in the presence of sgRNA. This was shown by transiently expressing Cas9-YFP and sag1sgRNA in RH and RHΔku80 strains. As the RHΔku80 strain lacks the ku80 gene which is important in eukaryotes to repair double stranded DNA breaks (Critchlow and Jackson, 1998), he hypothesized that RHΔku80 parasites should not be able to repair the Cas9-mediated double strand break and display the aberrant phenotype as response to Cas9 activity. His result confirmed his hypothesis as almost all transfected RHΔku80 parasites displayed abnormal nuclei compared RH. In order for our observations to become conclusive, our experiments could have been performed with additional factors measured: primarily, monitoring which parasites have been transfected, and counting morphological phenotypes only in transfected ones. However, regardless of the mechanism, the observed artefact by both labs indicated a likely challenge to our study: we would have to discriminate between an abnormal mitochondrial morphology due to mitochondrial biogenesis defect and mitochondrial defect resulting from nuclear damaged. Since this strategy was originally chosen as a way to obtain functional input in a time effective manner, and the encountered obstacle defied that purpose we decided to prioritise assessing other strategies over devoting more time on understanding this morphology phenomenon. Another strategy reported by Sidik *et al.,* (2016) and published after our experiments was performed could be a good alternative to the Split-CAS9. This strategy allows the constitutive expression of CRISPR/CAS9 without deleterious toxicity of its activity by expressing CRISPR/CAS9 as well as a sgRNA that is non-functional against the 3' UTR of NHE1, which serves a decoy. This genetic manipulation is well tolerated by T. gondii and allow a high sgRNA transfection efficiency (Sidik *et al.,* 2016). This is a strategy worth exploring in the future.
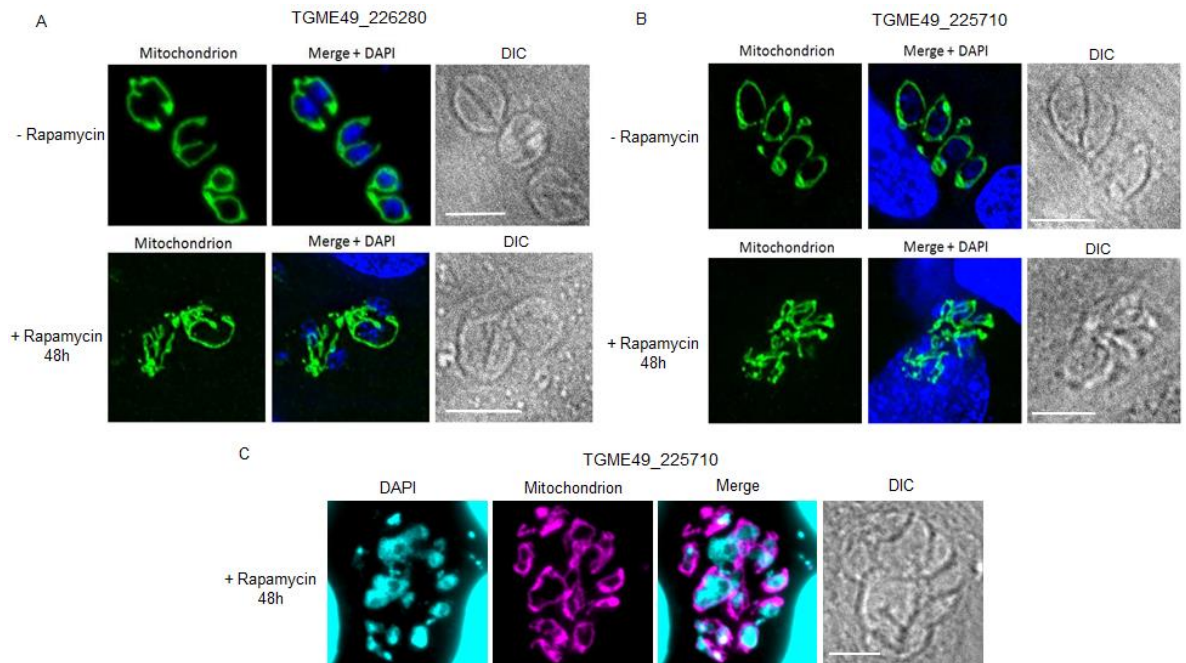
Figure 9.2 Transient expression of specific sgRNA in the Split-CAS9 expressing line results in off target nuclear and mitochondrial phenotypes.
(A) Immunofluorescence showing gene disruption of TGME49_226280 and **(B)** TGME49_225710. Mitochondria in green are stained with anti-TgMys, and the nucleus in blue is stained with DAPI. **(C)** Representative images of vacuoles displaying nuclear (cyan) and mitochondrial (magenta) phenotypes. Scale bar 6 μm. Whole parasites are visualised by Differential Interference Contrast (DIC).

9.1.2. Transient expression of CAS9 results in mitochondrial morphology defects

Three genes from the bioinformatic screen, TGME49_263680/214790 and 226280, were chosen which had previously been validated as encoding for mitochondrial proteins. For each gene, Flag-tagged CAS9 (Sidik *et al.*, 2014) along with a targeting sgRNA were transiently co-expressed (see Table 7.11 for sgRNA sequences). As controls, CAS9-Flag was expressed alone, or with sgRNA for the non-essential *sag1* (*TGME49_233460*) gene for which we do not expect mitochondrial phenotype to be a specific outcome of gene disruption (SAG1sgRNA) because it is not essential. At 48h post co-transfection, mitochondria were visualized as above and morphologies were analysed (Figure 9.3). One example of the 217 images taken is presented in Figure 9.3A. For vacuoles expressing CAS9-Flag with a signal above background fluorescence, normal mitochondria (open or "sperm-like" – Figure 9.1) are circled in green and abnormal (anything other than open or "sperm-like") ones in red. For vacuoles that do not express CAS9-Flag, in yellow are mitochondria with abnormal morphologies and the rest are normal

looking mitochondria. When quantifying mitochondrial morphology, gene disruption was not tested and we assumed that disruption occurred in cell expressing CAS9-Flag. 48h post co-transfection, a significant increase of mitochondrial abnormalities was observed in all conditions tested compared to the non-transfected parasites. While a trend of higher abundance of mitochondrial abnormalities was observed for *TGME49_214790*, the data showed no significant difference with the CAS9-only and CAS9+SAG1sgRNA controls (Figure 9.3B-C). These data suggest that transient expression of CAS9 results in mitochondrial morphological abnormalities, excluding this strategy as a reliable tool for rapid identification of genes involved in mitochondrial biogenesis. As mentioned above, the CAS9-decoy strategy described in the Sidik *et al.,* (2016) is a worth exploring as it has been shown to reduce CAS9 toxicity and hence lower the background phenotype noise. Expressing CAS9 under different *T. gondii* promoter could also be an option to fine-tune the level of CAS9 expression to a level much better tolerated by the parasites.

A CAS9-TGME49_214790

DAPI | FLAG

Mitochondrion | Merge

B

CAS9
DAPI | Mitochondrion | CAS9-Flag | Merge | DIC

CAS9-TGME49_226280
DAPI | Mitochondrion | CAS9-Flag | Merge | DIC

CAS9-SAG1

CAS9-TGME49_263680

CAS9-TGME49_214790

C
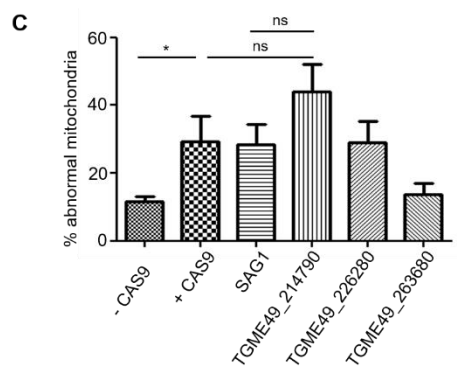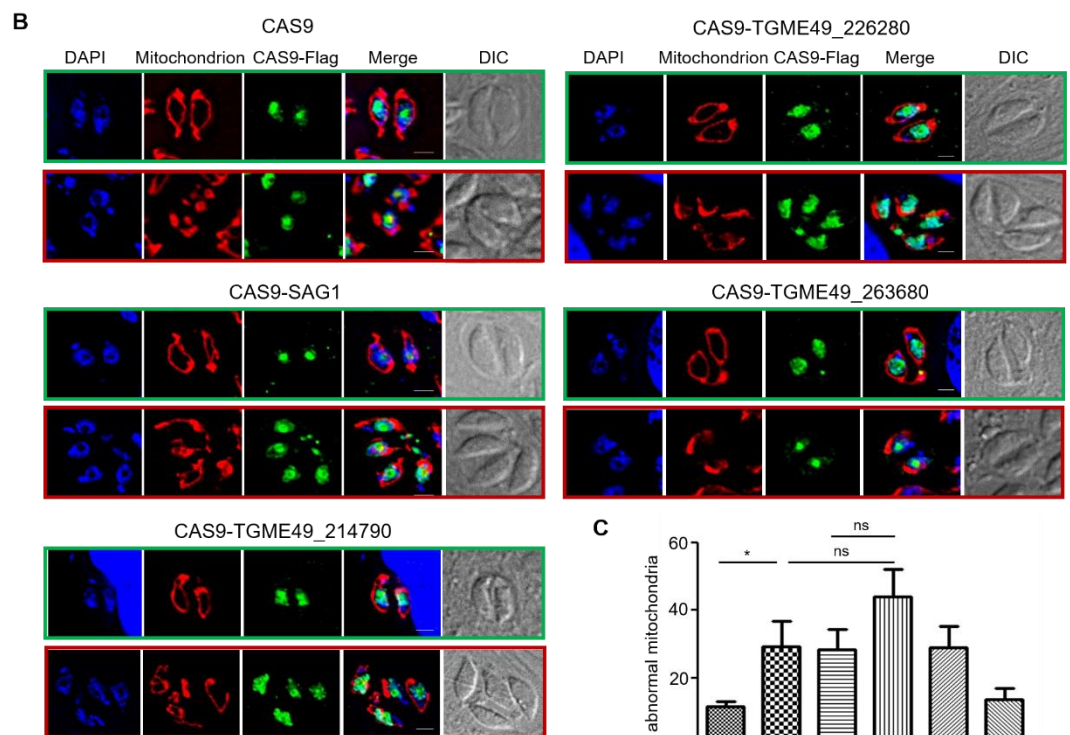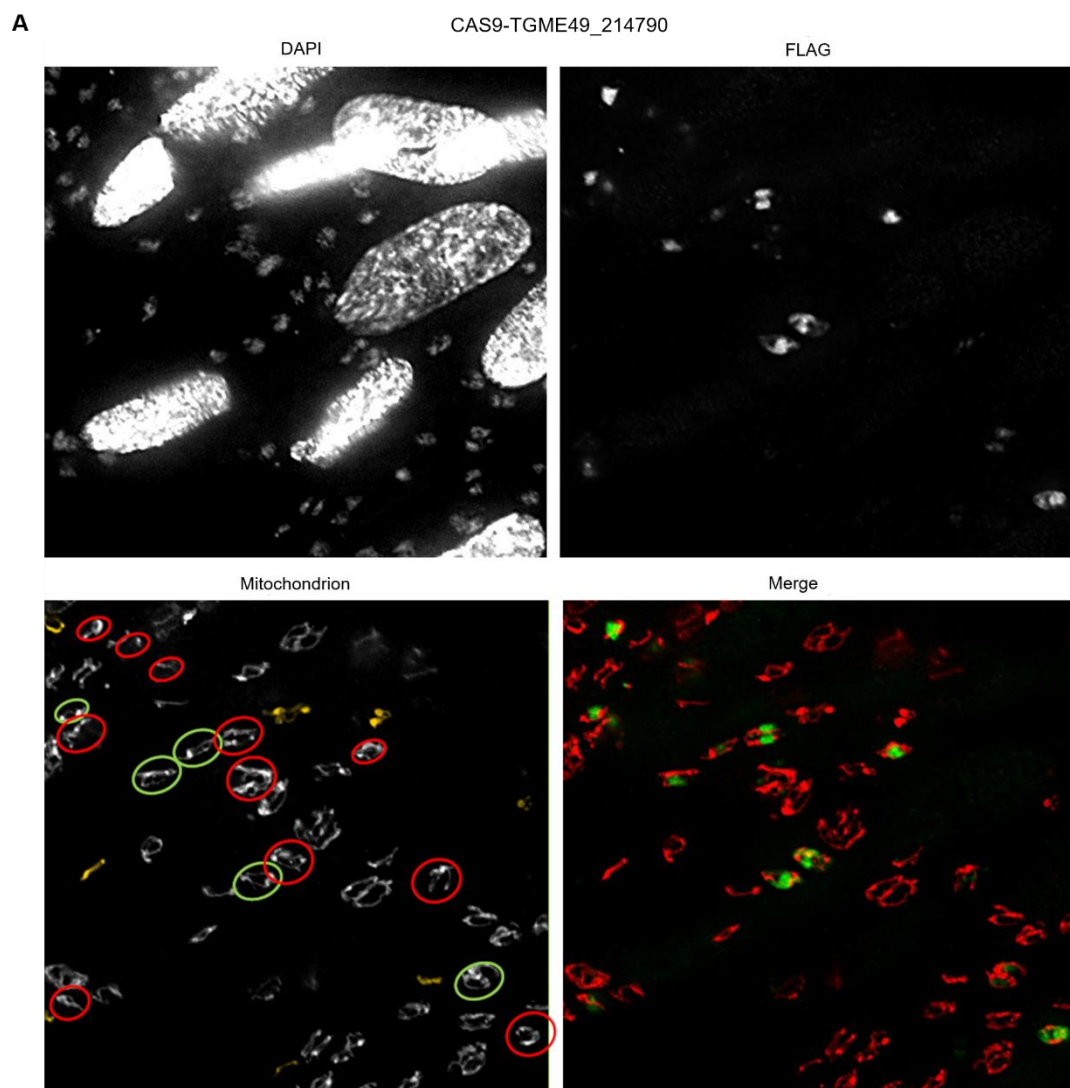
Figure 9.3 Transient expression of Cas9 results in mitochondria morphology defects.
(A) Immunofluorescence presenting the discrimination process of parasites with normal vs abnormal mitochondrial morphologies. Only vacuoles expressing CAS9-Flag were considered. Green circled are vacuoles with normal vacuoles. Circled in red are those with abnormal mitochondrial morphology. Coloured in yellow are abnormal mitochondrial morphology of parasites which do not express CAS9-Flag. Uncoloured are those which have normal mitochondrial morphology. **(B)** Representative immunofluorescence micrographs of parasites transiently expressing CAS9 and sgRNA for the mentioned GOI. Mitochondria in red are marked by anti-TgMys. CAS9-FLAG in green is marked with anti-FLAG. Merge shows DAPI, FLAG and TgMys. Whole parasites are visualised by Differential Interference Contrast (DIC). Green boxes highlight parasites with wild-type looking mitochondria. Red boxes highlight parasites with mitochondria that appear to have a morphological defect herein named "abnormal mitochondria". **(C)** Quantification of vacuole with abnormal mitochondria morphologies for each condition. Bars represent the mean ± SEM (n=3), * p < 0.05 (1-way ANOVA).

9.2. TGME49_214790 and TGME49_240270 are both essential for parasite growth and mitochondrial integrity

Due to the complication encountered in analysing mitochondrial biogenesis defects using transient expression strategies, stable genetic manipulation was considered as means to assess for function. The previously localised TME49_240270 (Figure 8.7 A and B), and TGME49_214790 (Table 8.4, (Lacombe *et al.*, 2019) were chosen to generate conditional knock down (cKD) lines. We decided to choose those genes as TME49_240270 was the first gene for which localisation worked amongst those I localised, and TGME49_214790 was the gene that was the most probable to have an effect on mitochondrial morphology upon depletion from the CAS9 experiment above. cKD lines were generated by replacing the native promoter with a T7S4 anhydrotetracycline (ATc) repressible promoter and DFHR selectable cassette (Figure 9.4A). This manipulation was performed as previously described (Sheiner *et al.*, 2011), with the modification whereby CRISPR/CAS9 was utilised to enhance homologous recombination efficiency (Figure 9.4A). This method overcomes the issue of CAS9 toxicity because CAS9 is only transiently expressed to facilitate promoter replacement. During this time, CAS9 may well have toxicity in the same manner as mentioned above. However, with the repeating parasite replications, the CAS9 (YFP fused) and the expressing plasmid are lost, and any parasites that are critically affected, die off or are overgrown by the healthy population of parasites during selection. At the end of selection, differential dilution is used to choose single clones that no longer express CAS9 and show normal mitochondrial and nuclear morphology. These transgenic lines were performed in the ΔKu80 TATi (transactivator of *T. gondii*) expressing background line (Meissner *et al.*, 2005). This line constitutively expresses the tetracycline-tansactivator, which binds to the T7S4 promoter

allowing constitutive expression of the downstream gene. In the presence of ATc, the trans-activator is unable to bind to the promoter resulting in gene transcription inhibition (Figure 9.4Aiii). Although TGME49_214790 was previously endogenously 3xHA tagged, protein signal was gradually lost overtime until undetectable by IFA. TGME49_240270 was localised by cDNA-YFP transient expression as 3xHA tagging was unsuccessful (section 8.3.2). Hence, for both genes, cKD lines were performed in the untagged TATi expressing line. Obtaining such lines was challenging. The first attempts were either unsuccessful or unexpected signal from the YFP fused CAS9 was observed by IFA, which localised to the nucleolus (Figure 9.4). These lines repressible TME49_240270 and TGME49_214790 lines (rTME49_240270 and rTGME49_214790), were unusually unfavourable and likely acquired some mutation during selection allowing the CAS9 constitutive expression which may well be an inactive CAS9. Promoter replacement confirmation by PCR was performed using 4 primers designed as followed: forward primer 1 anneals to the native sequence upstream of the DHFR selectable cassette; reverse primer 2 anneals to both the DHFR cassette and the T7S4 promoter; forward primer 3 anneals to the T7S4 promoter; and reverse primer 4 anneals to the beginning of the GOI (in the first exon) (Figure 9.4Aiii). Together, primer 1 and 2 confirm the integration of the DHFR resistance cassette and primer 3 and 4 confirm integration of the T7S4 promoter upstream of the GOI. By annealing to the native sequence, after exogenic sequence insertion, primer 1 and 4 are too far apart to generate a PCR product (Figure 9.4A and B). Hence, the absence of PCR products confirms integration of the whole sequence. Clonal lines expressing CAS9-YFP were often displaying a mixed population with a growing number of parasites which lost the CAS9-YfP signal overtime. Still, any clone expressing CAS9-YFP were discarded as we did not want to risk any phenotypical interference.
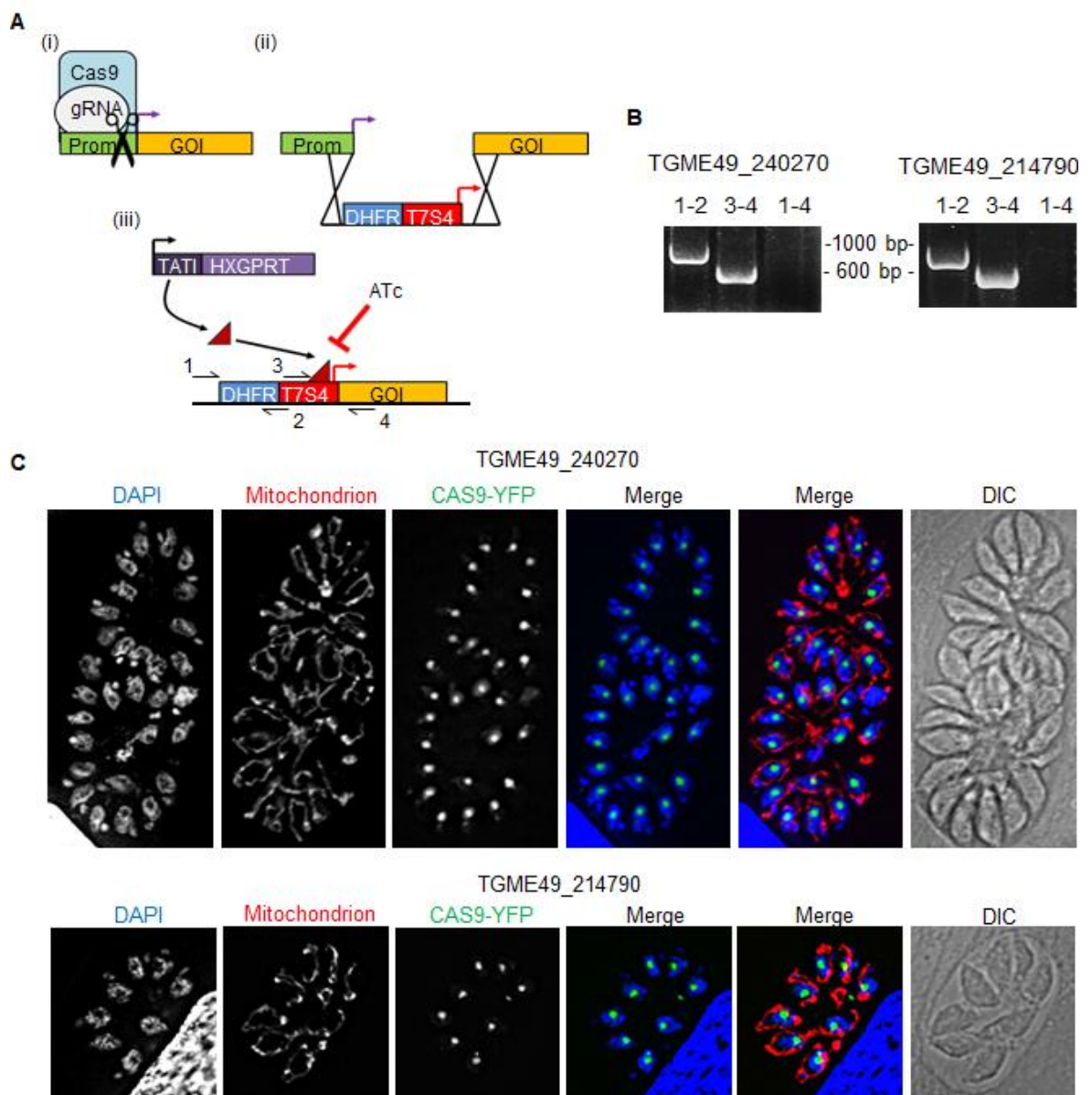
Figure 9.4 Problems with conditional knockdown lines generation with constitutive CAS9-YFP expression for TGME240270 and TGME21470.
(A) Schematic depiction of the promoter replacement strategy allowing knock-down of a gene of interest (GOI) with the addition of anhydrotetracycline (ATc). **(i)** CRISPR/CAS9 guided cut at the predicted promoter/ATG boundary, **(ii)** a repair cassette containing the ATc repressible promoter, the DHFR selection marker, and homology to the promoter/ATG boundary, is inserted between the promoter and GOI, **(iii)** GOI, under the control of ATc repressible promoter, is down regulated when ATc is added. The black arrows represent the four primers used to confirm integration. **(B)** Validation of the promoter integration in the TGME49_240270 and TGME49_214790 locus via PCR analysis using primers 1, 2, 3, and 4. **(C)** Nucleus is shown in blue stained by DAPI, in red are mitochondria stained with anti-TgMys, and in green is CAS9-YFP gene product (no antibodies were used). Merged channels show CAS9-YFP and nucleus colocalization (blue-green), and CSA9-YFP, nucleus and mitochondria (blue-green-red). Overall shapes are visualized by Differential Interference Contrast (DIC).

After 9 other attempts, cKD line was successfully re-generated for TGME49_240270 (Figure 9.5). However, cKD lines for TGME49_214790 was unsuccessful. We decided to choose one clone expressing CAS9-YFP as a mixed population (parasites expressing CAS9-YFP + some that kicked the construct), subcloned it, and selected a subclone without CAS9-YFP signal. Both the subclone and the new

rTGME49_240270 clonal line were PCR checked for promoter replacement with the repressible T7S4 exogenic promoter (Figure 9.5A). ATc induced down-regulation was confirmed by qRT-PCR for rTGME49_240270 (Figure 9.4B). Parasite growth for rTME49_240270 and rTGME49_214790 was monitored by plaque assay which revealed a severe growth defect in response to gene depletion (Figure 9.5C). However, without ATc both rTGME49_240270 and even more so rTGME49_214790 have smaller plaques then the parental RHΔKu80/TaTi line suggesting that promoter replacement affects parasite fitness. This could be due to the T7S4 promoter which likely induces a different level of gene expression as well as a different timing of expression than the endogenous promoter, which creates some level of toxicity to the parasite. Assessing the gene level of expression of the parental line compared to the mutant line without ATc by qPCR will be performed in the future to address this question. Plaque assay will also be repeated to measured plaque sizes to quantify growth rate for the parental line compared to the mutant lines. Mitochondrial morphology abnormality was observed by IFA for both rTGME49_214790 and rTME49_240270 when treated with ATc for 48h, and this defect was not detected for the parental line when treated with ATc for 48 hours (Figure 9.5D). This was quantitatively confirmed for TGME49_240270 by counting normal and abnormal mitochondria morphologies and the numbers were compared to that of the parental ΔKu80/TATi line (Figure 9.5Ei and ii). No qPCR for rTGME49_214790 is shown because this line was abandoned beforehand as it originated from a mutated CAS9 clone, and it was unsure if the much slower growth rate could have had an effect on parasite fitness.

Altogether, these results suggest that TGME49_240270 is important for parasite fitness and mitochondrial integrity and hence, may have a role in mitochondrial biogenesis and is a promising candidate that can be further assessed. TGME49_214790 may be involved in mitochondrial biogenesis, however, these experiments need to be repeated on a new cKD line which does not express CAS9-YFP.
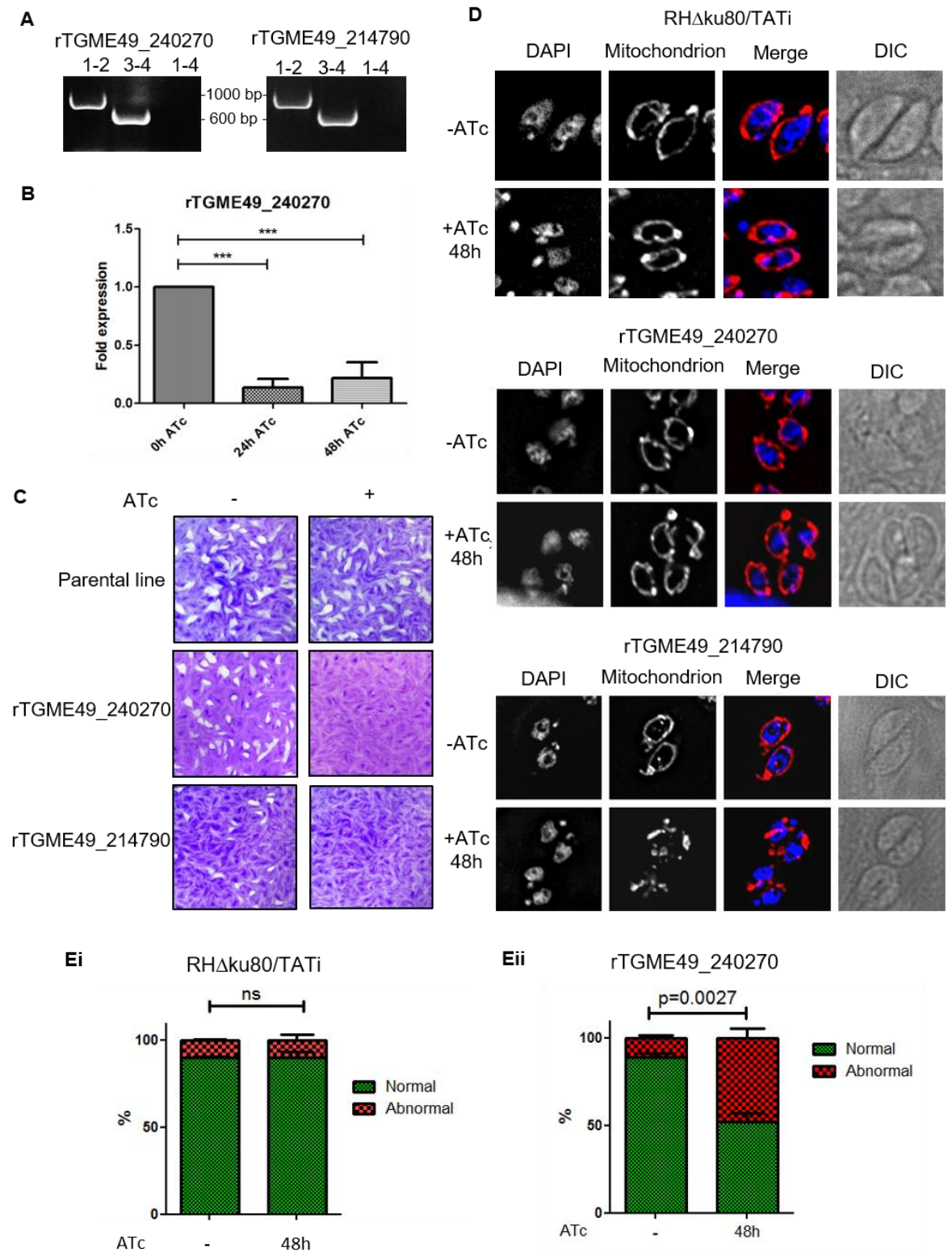
Figure 9.5 Conditional knock-down of TGME49_240270 and TGME49_214790 results in growth defect, and mitochondrial morphology abnormality.
(A) Validation of the promoter integration in the TGME49_240270 and TGME49_214790 locus via PCR analysis using primers 1, 2, 3, and 4. **(B)** Transcript levels of TGME49_240270, analysed by qRT-PCR, in absence (-) or presence of ATc after 24 and 48 hours. Bars represent the mean ± SEM (n=5). ***p< 0.0001. **(C)** Plaque assays performed with parental line (RHΔku80/TATi) or TGME49_240270 and TGME49_214790 parasites grown for 9 days in the absence (-) or presence (+) of ATc. **(D)** Immunofluorescence of the parental line, TGME49_240270 and TGME49_214790 with or without ATc for 48h. Mitochondria in red are stained with anti-TOM40 and the nucleus is visualized with DAPI. Whole parasites are observed by Differential Interference Contrast (DIC). **(E)** Quantification of parasite vacuoles with "normal" (green) vs "abnormal" (red) mitochondrial

morphologies after growth of the RHΔku80/TATi parental **(Ei)** or rTGME49_240270 **(Eii)** lines without (-) or with ATc for 48 hours. Graphs represent mean ± SEM for n = 3 independent experiments; Analysed by t-test.

9.3. A new protocol for the evaluation of mitochondrial translation reveals that TGME49_240270 is not involved in such a function

Following the hypothesis that disrupting mitochondrial translation would influence assembly and activity of mitochondrially encoded mETC complexes, we reasoned we could monitor the above as proxy for their translation. In this case we chose to monitor complex IV which is directly dependent on the translation of mitochondrially encoded CoxI and III by the mitoribosome (arrows and schemes in blue) (Figure 9.7A). This was compared to the assembly and activity of complex V as a negative control, which fully nuclear encoded, translated in the cytosol by the cytosolic translation machinery (arrows and schemes in green) (Figure 9.7A). High resolution clear-native PAGE (hrCN-PAGE) followed by an in-gel complex IV and V catalytic activity assays were performed using the rTGME49_240270 mutant line (Figure 9.7B). If present, each complex can react with the chemicals present in their respective buffers resulting in the generation of a visible precipitate inside the gel. For complex IV, 3,3'-diaminobenzidine (DAB) (reagent) and Cytochrome *c* (substrate) are both part of the gel incubation buffer. The continuous oxidoreduction cycles of Cytochrome *c* triggered its reaction with DAB and complex IV leads to the oxidation and polymerisation of DAB which accumulates as a brown deposit (Seligman *et al.*, 1968; Sabar, Balk and Leaver, 2005). For complex V, the formation of a white precipitate can be visualised at an outcome of the reaction of the compound lead with the inorganic phosphate during ATP hydrolysis.

The band resulting from the complex IV activity assay corresponds to the size reported for *T. gondii* complex IV recently (600 kDa) (Seidi, Linden S Muellner-Wong, *et al.*, 2018), supporting the assay's specificity (Figure 9.7B). To further confirm its identity, we performed mass spectrometry analysis: we cut out the band visualised via the assay and sent it for MS analysis, this was done twice. All components of complex IV were identified but CoxI. This is because CoxI sequence cannot be found in ToxoBD, unlike CoxIII for which a BLAST identified a sequence

match, and so, this was the best outcome we could hope for. The same results were obtained in the Seidi *et al.*, (2018) paper in which their IP identified all complex IV components but CoxI, which supports our data and further validates complex IV's identity (Table 9.1, Appendix Table 5). However, now that the mitochondrial genome is published (Namasivayama *et al.*, 2020), we could search for unassigned sequences and manually search for a matching sequence.

Accession	Name*	Experiment 1			Experiment 2		
		Score	No. of significant matches	No. of significant sequences	Score	No. of significant matches	No. of significant sequences
TGGT1_226590	*Tg*Cox2a	222	9	3	152	5	2
TGGT1_310470	*Tg*Cox2b	257	7	3	155	3	2
TGGT1_209260	*Tg*Cox5b	593	20	10	289	11	7
TGGT1_254030	*Tg*ApiCox13	36	1	1	N/A	N/A	N/A
TGGT1_242840	*Tg*ApiCox14	155	5	3	36	1	1
TGGT1_265370	*Tg*ApiCox16	185	6	4	97	2	2
TGGT1_221510	*Tg*ApiCox18	151	6	3	143	4	3
TGGT1_247770	*Tg*ApiCox19	281	16	4	162	8	5
TGGT1_262640	*Tg*ApiCox23	148	6	4	40	1	1
TGGT1_286530	*Tg*ApiCox24	151	4	3	80	2	2
TGGT1_264040	*Tg*ApiCox25	545	15	8	546	11	7
TGGT1_306670	*Tg*ApiCox26	388	14	5	130	7	5
TGGT1_297810	*Tg*ApiCox30	526	15	10	432	14	9
TGGT1_229920	*Tg*ApiCox35	564	21	10	265	9	7
TGME49_237120	*Tg*CoxIII	67	1	1	57	1	1

Table 9.1 Complex IV components identification from band in complex IV enzymatic assay, by mass spectrometry.
*Name according to (Seidi, Linden S Muellner-Wong, *et al.*, 2018).

For the complex V assay, the same protocol previously reported for *T. gondii* by Salunke *et al.,* (2018) was followed. Additional confirmation to the complex V identity was provided by using an antibody raised against a consensus sequence found in plant, algal and bacterial ATP-β subunit of complex V, and which was shown to cross-react with ATP-β from a variety of organisms including *T. gondii* (Huet *et al.*, 2018; Seidi, Linden S Muellner-Wong, *et al.*, 2018). The cross-reactivity of this antibody with *T. gondii* ATP-β was first demonstrated by SDS-PAGE followed by western blot, which also confirmed the absence of human ATP-β in the parasites lysate after filtration to remove host cells (Figure 9.6A). The filtering process was no different from the one presented in Section 8. Success of removing host cells may be dependant in the force applied when filtering parasites through the filters (e.g. tearing of the membrane), or filter units misassembled (i.e. gaps where parasites and host cells can go through), or it may be an issue of the host cell mitochondrial state when parasites are collected. This issue of inconsistent host mitochondrial contamination in biochemical studies in *Toxoplasma* is something that my project has uncovered and that the Sheiner lab is currently trying to optimise further. Finally, when run under native conditions

by hrCN PAGE, the ATP-β band was observed at a similar size than the one from the enzymatic activity assay (Figure 9.6B).
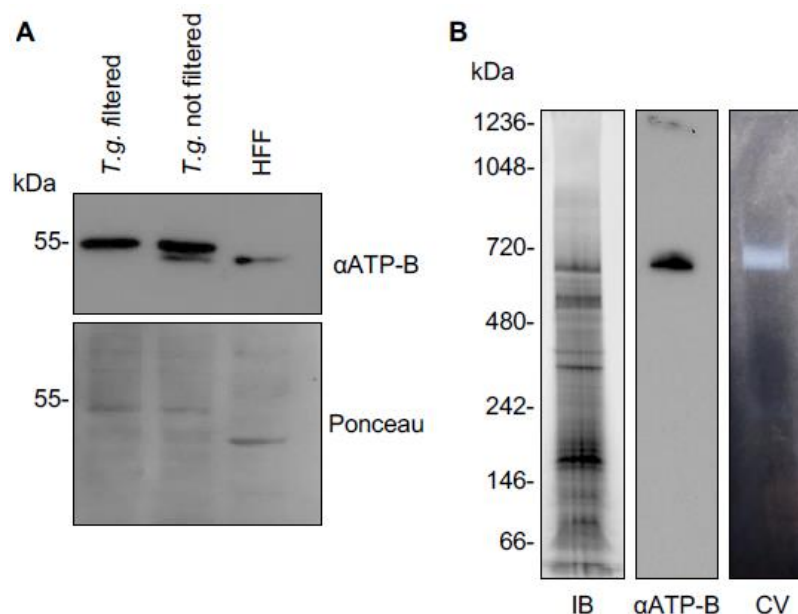
Figure 9.6 Confirmation of band corresponding to complex V activity assay.
(A) Assessment of the cross-reactivity of anti-ATP-β with the *T. gondii* protein. *T. gondii* band seen in lysates from filtered and non-filtered *T. gondii*, while human band appears only in lysates from non-filtered *T. gondii* or human cells. **(B)** Signal from the complex V activity assay and from anti-ATP-β following gel separation under native conditions by hrCN PAGE and BN PAGE provides support for the complex V identity of the activity assay band. IB - Instant blue; CV - complex V.

Complex IV and V catalytic activity assay were performed for the rTGME49_240270 cKD line. After gene down regulation for 96h by ATc addition in the culture medium, crude mitochondrial fractions were used for this assay (Figure 9.7B). Both complex IV and V enzymatic activity were detected with and without ATc, suggesting no effect on mitochondrial translation upon gene depletion. Moreover, as the majority of the mETC complex subunits need to be imported from the cytosol into the mitochondrion, these results also suggest that TGME49_240270 is not involved in mitochondrial protein import, otherwise this would have affected the mETC's activity and hence would have been reflected in the complex IV and V assay. Although band quantification usually allows detection of more subtle variations, this method does not provide sufficient accuracy to quantify the activity because band intensity build up is not linear and it is dependent on how well samples run in the gel (e.g. slightly smeary, bands being wider or narrower, etc.), and this is highly variable. Therefore, we do not read into subtle band intensity variation and rather rely on strong difference (hardly detectable signal vs clear signal) over multiple experiments. Mitochondrial protein import was also

monitored directly; a Myc tagged DHFR fused to the mitochondrial targeting signal of HSP60 (Hsp60$_L$-mDHFR-cMyc (van Dooren et al., 2016) was transiently transfected into the parasites at different time points after TGME49_240270 depletion for 24h, 48h and 96h, or with no ATc. This was carried out as well in the parental line as a control. The localisation of this Hsp60$_L$-mDHFR-cMyc product was visualized by IFA using an anti-Myc antibody (Figure 9.7C). As expected, the Hsp60$_L$-mDHFR-cMyc product (in green) co-localises with the mitochondrion marker (in red) (anti-Mys) for the parental line for all time points, suggesting no protein import defect (Figure 9.7C). The same outcome was observed for TGME49_240270 (Figure 9.7C). For the sake of clarity, population of "normal looking" mitochondrion was chosen to show the co-localization and the number of abnormal mitochondria was not quantified in this experiment. To quantify these results, protein import was monitored by SDS-PAGE followed by western blot (Figure 9.7D). Upon entry into the mitochondrion, the mitochondrial targeting signal is cleaved off generating a smaller sized protein which can be visualised by western blot. If protein import is defective, this cleavage no longer takes place (Van Dooren et al., 2016) and an accumulation of the un-cleaved pro-protein would be observed. The ratio of signal intensities between the cytosolic un-cleaved proteins and the mitochondrial cleaved proteins was calculated for each time point (Table 9.2), this way transfection efficiency variations between samples does not affect the results. This experiment was repeated 4 times. In some cases, a third band can be observed under the mature protein band which may be due to degradation. This band was disregarded; only the bands from the immature and mature proteins were considered. Just like in the parental control, no protein import defect was observed upon gene depletion, confirming the IFA results (Figure 9.7C-E). Moreover, parasites transfected even 4 days (96h) post gene depletion did not show statistically significant mitochondrial import defect (Figure 9.7E; Table 9.2; Appendix Table 6 for statistical analysis detail). This provides validation that, at least for this gene, the outcome of this strategy is not dependent on parasite general fitness, providing that they are still alive. However, a limitation of this strategy is the fact that band intensity quantification using the ImageJ software can be prone to error as the selection of the band surface is done manually. The inclusion of repetition and statistical analysis mitigates this weakness.
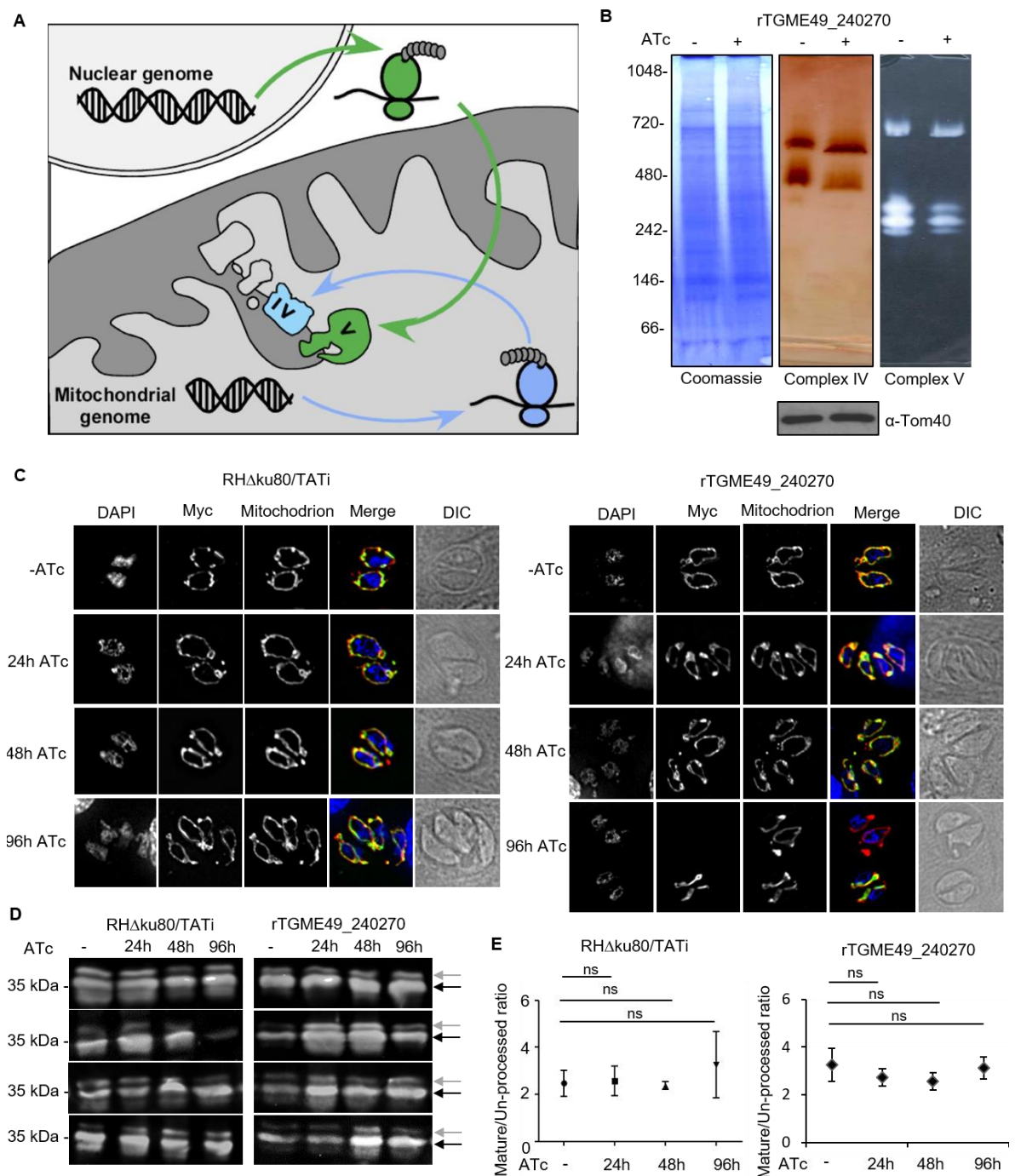
Figure 9.7 Down-regulation of TGME49_240270 does not lead to a defect in respiratory complex IV nor in mitochondrial protein import.
(A) A scheme describing the rational of our assay. Nuclear (grey) encoded proteins translated by the cytosolic ribosome (green) compose complex V, while mitochondrion (blue) encoded proteins translated by the mitochondrial ribosome (blue) are necessary to assemble complex IV. Depletion of a GOI involved in this pathway would result in reduced activity of complex IV but not V. **(B)** Crude mitochondria from TGME49_240270, grown in the absence (-) or presence (+) of ATc for 96 hours, separated by hrCN-PAGE. Complex IV activity was visualised with cytochrome c: DAB staining. Complex V activity was assayed by visualising the precipitation of lead by inorganic phosphate during ATP hydrolysis. Protein immunoblot analysis using anti-TOM40 enriched mitochondria sample was performed as a loading control. **(C)** Immunofluorescence the TGEM49_240270 conditional line and the parental line in the presence or absence (-ATc) for 24, 48, 96 hours followed by transient transfection with Hsp60L-mDHFR-cMyc. The Hsp60L-mDHFR-cMyc protein product was visualised using an anti-Myc antibody, the mitochondrion with anti-Mys antibody, the nucleus was stained with DAPI and whole parasites were visualised by polarised light (DIC). **(D)** Western blot representation of the parasites in the absence (-) or presence of ATc for 24, 48 and 96 hours, using anit-Myc antibody to visualize the immature (grey arrow) and mature (black arrow) of the Hsp60L-mDHFR-cMyc gene product. This was repeated 4 times. **(E)** Graph showing band intensity ratios between the

mature and immature Hsp60L-mDHFR-cMyc product from the western blot shown in (E) on ImageJ software. This import assay was performed for the RHΔku80/TATi parental and rTGME49_240270 cKD line in the absence (-) or presence of ATc for 24, 48 and 96 hours. Bars represent the mean ± SEM (n=4). A one-way ANOVA statistical test was performed for both assays and revealed no statistical differences between the no treatment (-ATc) and treated (+ATc 24h, 48h, 96h) parasites.

		RHΔKu80/TATi - Parental line					rTGME49_240270		
	Treatment	WB band	Mean	Ratio Mature/Immature		Treatment	WB band	Mean	Ratio Mature/Immature
Exp 1	No ATc	Immature	37.428	1.297	Exp 1	No ATc	Immature	8840	5.226
		Mature	48.554				Mature	46200	
	24h ATc	Immature	34.89	1.497		24h ATc	Immature	49100	2.118
		Mature	52.236				Mature	104000	
	48h ATc	Immature	21.542	2.539		48h ATc	Immature	40900	2.836
		Mature	54.701				Mature	116000	
	96h ATc	Immature	29.915	2.201		96h ATc	Immature	18200	3.912
		Mature	65.841				Mature	71200	
Exp 2	No ATc	Mature	48.275	2.001	Exp 2	No ATc	Mature	19.395	2.105
		Immature	24.127				Immature	40.835	
	24h ATc	Mature	37.414	1.928		24h ATc	Mature	19.1	2.497
		Immature	19.409				Immature	47.686	
	48h ATc	Mature	61.896	2.607		48h ATc	Mature	21.875	1.998
		Immature	23.745				Immature	43.713	
	96h ATc	Mature	30.445	7.464		96h ATc	Mature	23.659	1.894
		Immature	4.079				Immature	44.806	
Exp 3	No ATc	Immature	57.682	3.898	Exp 3	No ATc	Immature	20.009	2.412
		Mature	14.796				Mature	8.297	
	24h ATc	Immature	61.893	2.556		24h ATc	Immature	12.809	2.489
		Mature	24.216				Mature	5.147	
	48h ATc	Immature	54.507	1.869		48h ATc	Immature	53.263	3.469
		Mature	29.169				Mature	15.352	
	96h ATc	Immature	57.255	2.142		96h ATc	Immature	13.419	2.905
		Mature	26.734				Mature	4.619	
Exp 4	No ATc	Immature	62.319	2.697	Exp 4	No ATc	Immature	55.792	3.266
		Mature	23.111				Mature	17.084	
	24h ATc	Immature	54.257	4.309		24h ATc	Immature	49.019	3.782
		Mature	12.593				Mature	12.962	
	48h ATc	Immature	27.444	2.442		48h ATc	Immature	52.002	1.974
		Mature	11.237				Mature	26.339	
	96h ATc	Immature	23.967	1.223		96h ATc	Immature	49.425	3.756
		Mature	19.598				Mature	13.159	
		Ratio Average	STDEV	SEM			Ratio Average	STDEV	SEM
	No ATc	2.473	1.109	0.554		No ATc	3.252	1.405	0.702
	24h ATc	2.572	1.236	0.618		24h ATc	2.721	0.729	0.364
	48h ATc	2.364	0.337	0.169		48h ATc	2.570	0.721	0.361
	96h ATc	3.257	2.840	1.420		96h ATc	3.117	0.928	0.464

Table 9.2 . Protein import assay - Quantification of band intensities ratios from the mature and immature Hsp60L-mDHFR-cMyc product for the parental and rTGME49_240270 line.

Taken together, these observations suggest that TGME49_240270 depletion does not affect the assembly and activity of the mitochondrial translation dependent complex IV and hence is unlikely to have a role in mitochondrial translation. As

complex V activity is not affected either, TGME49_240270 is unlikely to have a role in protein import either.

9.4. Conclusions

In this part of the study, we aimed at identifying the most optimal genetic approach to study mitochondrial biogenesis defects. We hypothesized that abnormal changes in mitochondrial morphology upon gene disruption may be an indicator for a defect in mitochondrial biogenesis. First, the CRISPR-CAS9 expression strategy was explored as at the time of performing this assay, CRISPR-CAS9 was quickly ranked as one of the most powerful tools for genetic manipulation and was hence an obvious choice. Transient expression of CRISPR-CAS9 and single guide RNA (sgRNA) was considered as a strategy to explore if it could be used to provide a rapid read-out assay to detect protein involvement in mitochondrial biogenesis. Transient transfection of sgRNA into the Split-CAS9 expressing line (Stortz, 2020), and co-transfection of CAS9 and sgRNA into RH background line were strategies investigated for this purpose. Both strategies lead to defects in mitochondrial morphology even in controls where no defects were expected. J. Stortz reported that in the Split-CAS9 line he generated, CAS9-mediated double-strand breaks in the genome caused DNA damage responsible for aberrant and fragmented nuclei, and overall abnormal cell morphology, which in our study, resulted in mitochondrial morphology defects as well (Stortz, 2020). We also transiently co-expressed CAS9 and sgRNA which resulted in mitochondrial morphology abnormality even in the Sag1sgRNA control and CAS9 alone control, suggesting that in this case, the simple transient expression of CAS9 is enough to induce aberrant mitochondrial morphologies. Studies published around the same time and after my results were produced, have shown that expression of CAS9 alone can induced a severe fitness disadvantage due to the toxicity of its activity, and that expression of sgRNA alongside CAS9 makes CAS9 expression tolerable for the parasite (Sidik *et al.*, 2016; Markus *et al.*, 2019). Another study also showed that stabilisation of conditional ddFKBP-Cas9 for longer than 4h led to aberrant parasite morphology (Serpeloni *et al.*, 2016). Altogether, with these findings reporting that the DNA damage generated by CAS9 activity perturbs the nucleus and the parasite as a whole, it is likely that this undesirable phenomenon is responsible for the observed mitochondrial phenotype as a side effect. This strategy is hence not

compatible with mitochondrial biogenesis studies, and likely with other cellular pathways studies as well. One could also hypothesise that CAS9 could also reach the mitochondrial matrix of the parasite and cause mtDNA damage leading to aberrant mitochondrial morphology, although, this hypothesis has not been tackled yet.

A stable cKD line was generated for TGME49_240270, encoding for a mitochondrial hypothetical protein, by replacing the endogenous promoter replacement with an ATc repressible promoter. This way, issues with CAS9 toxicity is avoided as the CAS9 plasmid is lost after the 1st cycle of replication, which in this strategy, is only used to increase integration efficiency. Gene disruption result in abnormal mitochondrial morphology within 48h, suggesting it may have a role in mitochondrial biogenesis. We established a new protocol to evaluate mitochondrial translation through the assessment of complex IV and V assembly and activity via an in-gel staining assay. Complex IV possesses 2 proteins, CoxI and III, which are encoded in the mitochondrial genome, and so defect in translation would result in defect in activity as a consequence of missing essential SUs. Comparing complex IV activity assay to complex V which is fully nuclear encoded and hence not directly dependent on mitochondrial translation provides specificity for this assay. Lack of interference in both complex IV and V assay suggest that TGME49_240270 is not involved in mitochondrial translation, and likely not involved in mitochondrial protein import either, otherwise both complexes would have been affected. This gene's function remains to be elucidated. RNAseq is a strategy we can go for to look at gene expression changes in the mutant line upon gene down regulation to identify genes whose expression is affected and whose function might provide clues for TGME49_240270 biological role. Identifying counterparts which interact with the hypothetical protein will also a question to be addressed as the function of the interactors may help to figure out its function.

Altogether, this translation assay provides a novel tool for the field to study mitochondrial translation in *T. gondii*, in a less indirect manner than what has been proposed in the literature so far (Esseiva *et al.*, 2004; Pino *et al.*, 2010; Sharma and Sharma, 2014). However, there are limits to the interpretability of the results. Indeed, subtle band intensity difference cannot be accurately quantified due to the non-linear build-up of the staining. Moreover, these assays are tedious and time consuming. In the future, other experiments will be performed to further support results from our mETC complex staining assay. These

experiments include assessing the mitochondrial membrane potential using MitoTracker and JC1 staining. The Sheiner lab will also explore in solution enzymatic assays which would allow a much more precise and linear monitoring of the respiratory complex activity which will be discussed in the Discussion section 11.

10. First characterization of *T. gondii* mitoribosome and establishment of a new mitochondrial translation assay for apicomplexan parasites

10.1. Localisation of 6 putative mitochondrial ribosomal proteins

11 *T. gondii* genes from the bioinformatic search (section 8.3) were localised to the mitochondrion (Lacombe *et al.*, 2019), and 4 of them are predicted to encode mitochondrial ribosomal proteins (Table 8.4, Figure 10.1A). TGME49_201830, 226280, and 312680 are predicted to encode the ribosomal large subunit proteins 54, 28 and 41, respectively, and were hence named TgmL54, TgbL28m and TgmL41, in agreement with the new nomenclature standards (Greber and Ban, 2016). As mentioned earlier in Section 8.3.2, TGME49_203620 was named TgmS35 after its putative mS35 homolog (Gupta *et al.*, 2014; Greber and Ban, 2016). Additional putative ribosomal proteins from Gupta *et al.*, (2014) were selected based on previous use of their homologs in other systems for ribosome IP, with the objective to perform these IPs purify *T. gondii*'s mitoribosome for structural studies in the future. Hence, TgbL12m (TGME49_ 251950) was tagged with either TwinStrep or triple-HA, and TguL3m (TGME49_230050) was tagged with triple-FLAG (Table 10.1); and their mitochondrial localisation was confirmed by IFA (Figure 10.1B). Apart from TgmL54 and TgmL41, most of these ribosomal proteins were found in the mitochondrial proximity tagging proteome (Seidi, Linden S Muellner-Wong, *et al.*, 2018) and/or in the mitochondrion soluble cluster in the hyperLOPIT data (Barylyuk *et al.*, 2020), which is in support with our experimental validation (Table 10.1).
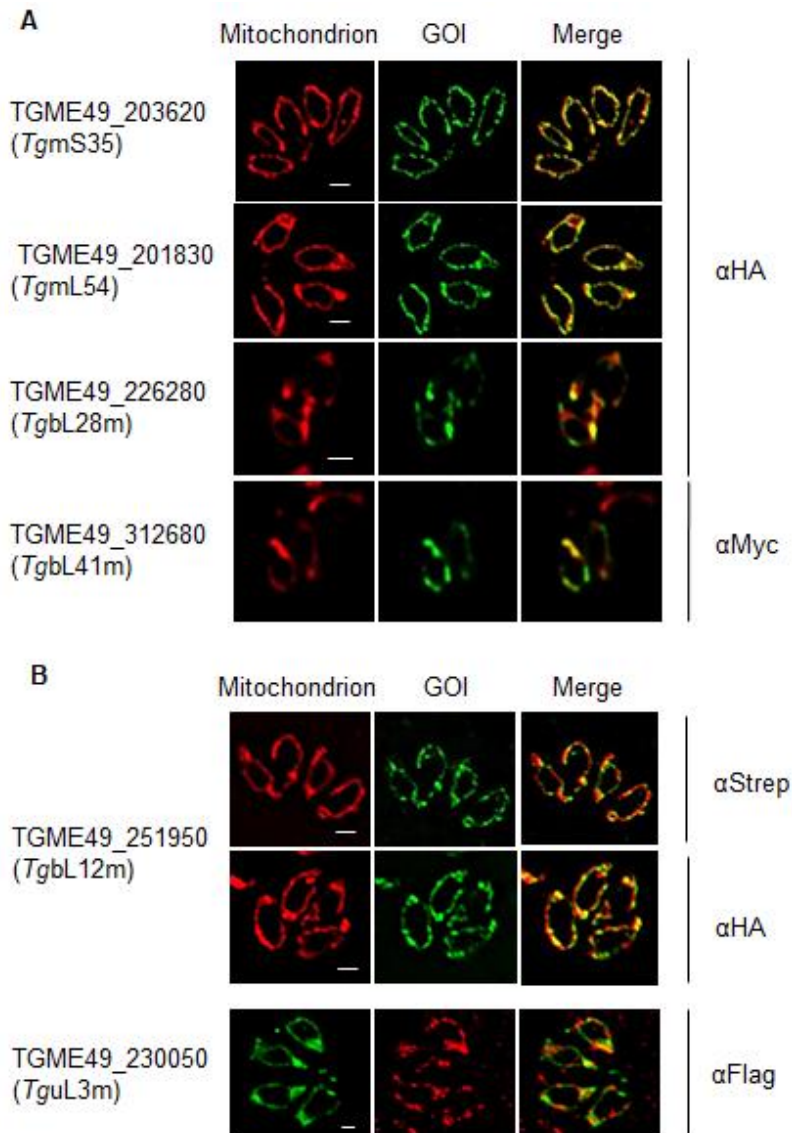
Figure 10.1 Mitochondrial localisation of putative mitochondrial ribosomal proteins by epitope tagging.
(A) Localisation through fluorescence microscopy analysis of 4 gene-products predicted to encode for mitoribosomal proteins identified in our search. **(B)** Localisation of 2 additional gene-products predicted to be mitochondrial ribosomal proteins not found in our search. For both panels, mitochondria are marked with anti-TgMys or anti-TOM40; the mentioned GOI (genes of interest) are marked with anti-HA, anti-FLAG or anti-Strep. Scale bar 2 μm.

Old Name	New Name	Gene ID	SSU/LSU	Mitoprot	CRISPR score	Proximity tagging proteome	LOPIT data
RPS15	uS15m	TGME49_216040	SSU	0.9885	-4.51	Yes	No
RPS35	mS35	TGME49_203620	SSU	0.9734	-4.66	No*	Mitochondrion - soluble
RPL3	uL3m	TGME49_230050	LSU	0.8966	-4.5	Yes	Mitochondrion - soluble
RPL7/L12	bL12m	TGME49_251950	LSU	0.9672	-3.6	Yes	Mitochondrion - soluble
RPL28	bL28m	TGME49_226280	LSU	0.9971	-4.91	Yes	Mitochondrion - soluble
-	mL41	TGME49_312680	LSU	0.9388	-1.34	No	No
-	mL54	TGME49_201830	LSU	0.9991	-4.94	No	No

Table 10.1 Putative mitoribosomal proteins in *T. gondii* assessed in the study.
Putative mitoribosomal proteins identified from Gupta *et al.*, 2014; Seidi *et al.*, 2018 and this study. New names were tentatively assigned based to the new nomenclature for ribosomal proteins (Ban *et al.*, 2014; Greber and Ban, 2016). New mitochondrial targeting predictions are done using MitoProt

II (https://ihg.gsf.de/ihg/mitoprot.html). The presence (yes) or absence (no) of the gene product in the proximity tagging based mitochondrial proteome is shown (Seidi *et al.*, 2018) (no - no mass spectrometry data; no* - mass spectrometry data found but the gene is not included in the final list of 421 genes). Gene localisation from the LOPIT data is shown when available (Barylyuk et al., 2020). The fitness score is based on the whole genome CRISPR/CAS9 screen (Sidik *et al.*, 2016). Genes with scores below -2 are considered essential.

10.2. Detection of the T. gondii mitoribosome

10.2.1.   Mitoribosome megacomplex visualization on blue native PAGE

To date, the apicomplexan mitoribosome has not been detected and this hampered its study. Triple HA tagging of TgmS35 was hence used to detect the mitoribosome and analyse gel migration patterns under native and denaturing condition. An SDS-PAGE followed by immunoblotting revealed that TgmS35 protein migrates around 38 KDa (Figure 10.2A). Whereas in native conditions using blue-native PAGE, it migrates with a high molecular weight (>1000 KDa) complex (Figure 10.2B). Such a size could well coincide with a mitochondrial ribosomal complex, although at this point, due to the lack of knowledge of all mitoribosome components, it is hard to predict if this size corresponds to the full ribosome or to the small subunit. Ribosomes detected in other organism are larger with a size of ~2.3 MDa for bacteria (Amunts *et al.*, 2015), 2.7 MDa and ~3 MDa for mitoribosomes in mammals and yeast, respectively (Greber and Ban, 2016), and even an astonishing 4.5 MDa for *T. brucei* mitoribosome (Ramrath *et al.*, 2018). By comparison, it is tempting to hypothesise that the size observed here corresponds to the SU of the mitoribosome. However, with the growing understanding of the level of diversity amongst mito-ribosomes from different organisms, an exceptionally small mitoribosome cannot be excluded. Finally, it is important to consider that our separation conditions do not provide sufficient resolution to determine an exact size at this point. TgbL12m and TguL3m migrate approximately to their mature protein size under denaturing conditions as predicted on ToxoDB (Figure 10.2A). Separation under native conditions reveals that all three tagged proteins migrate similarly to one another (Figure 10.2B). While, again, at this size, estimation of protein complex molecular weight becomes very approximative and seeming side-by-side migration might be misleading. The results are at this point in agreement with the possibility that all three proteins belong to the same complex, likely the mitoribosome, or that the SSU and LSU complexes are of similar sizes.
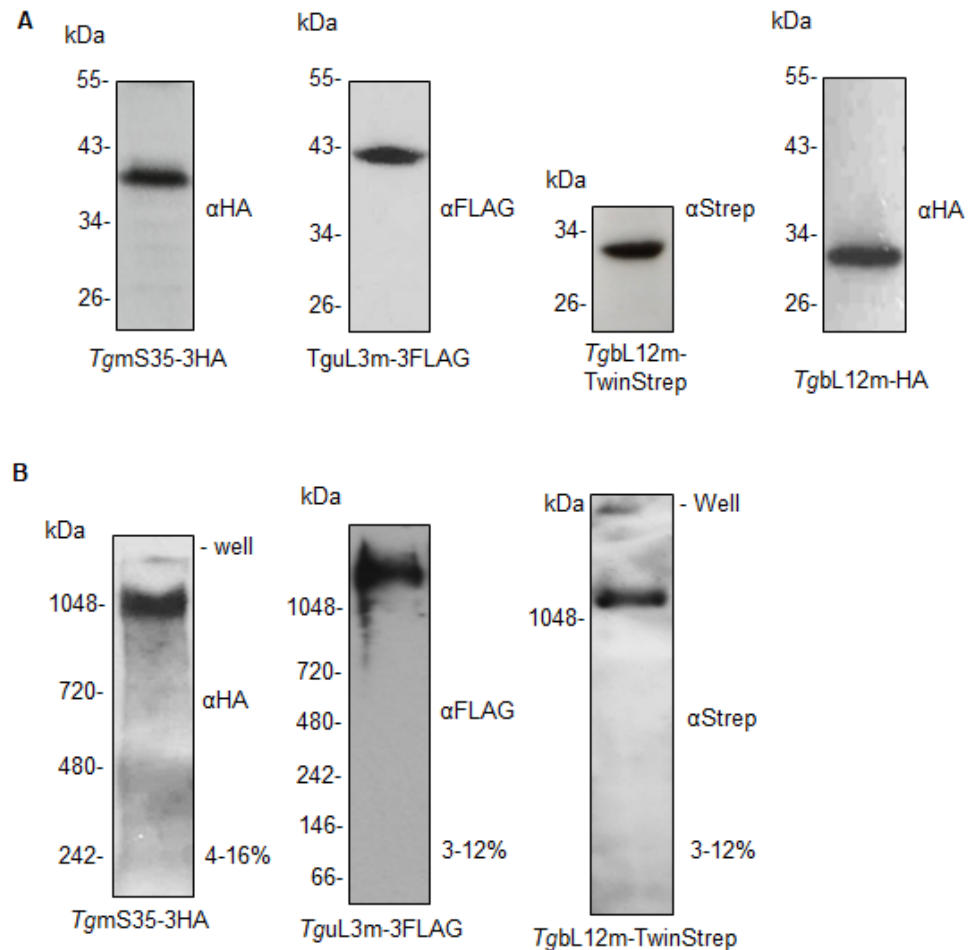
Figure 10.2 Detection of the *T. gondii* mitochondrial ribosome.
(A) Protein immunoblot analysis of endogenously tagged TgmS35, TgbL12m and TguL3m from total cell lysate separated by SDS-PAGE and detected using anti-HA/Strep/FLAG antibodies. **(B)** Total cell lysate separated by blue-native PAGE and immunoblotted to detect TgmS35, TgbL12m and TguL3m with anti-HA/Strep/FLAG antibodies.

10.2.2.   Mitochondrial rRNA enrichment from TgmS35 IP

It is expected that in the case that the observed megacomplex is part of the ribosome, rRNA molecules are included. With this in mind, and to further support the possibility that the observed large complexes are ribosomal complexes, IP experiments using the triple-HA tagged TgmS35 as bait were carried out (Figure 10.4A). The expectation was that the pulled down complex would be enriched with rRNA compared to pull down of non-ribosomal complexes. RNA was thus extracted from the elution fractions to be used as template for PCR. To examine specific mitochondrial rRNA enrichment, the mitochondrial rRNA enriched IP was compared to apicoplast rRNA (api-rRNA, using primers from (Biddau *et al.*, 2018) or to cytosolic mRNA (actin mRNA, using primers from (Melatti *et al.*, 2019). At the time of performing this work the mitochondrial genome of *T. gondii* was unknown (now published - (Namasivayama *et al.*, 2020). Therefore, the PCR of

reverse transcribed mitochondrial encoded rRNA was performed using primers designed to amplify a sequence that is conserved between a coccidian and an haemosporidan, whose mitochondrial DNA genome sequences are published (GenBank accessions: M76611.1 and AB564272.1) (Figure 10.3) (mito-rRNA), under the expectation that sequences that are conserved across those organisms are likely also conserved in *T. gondii*.
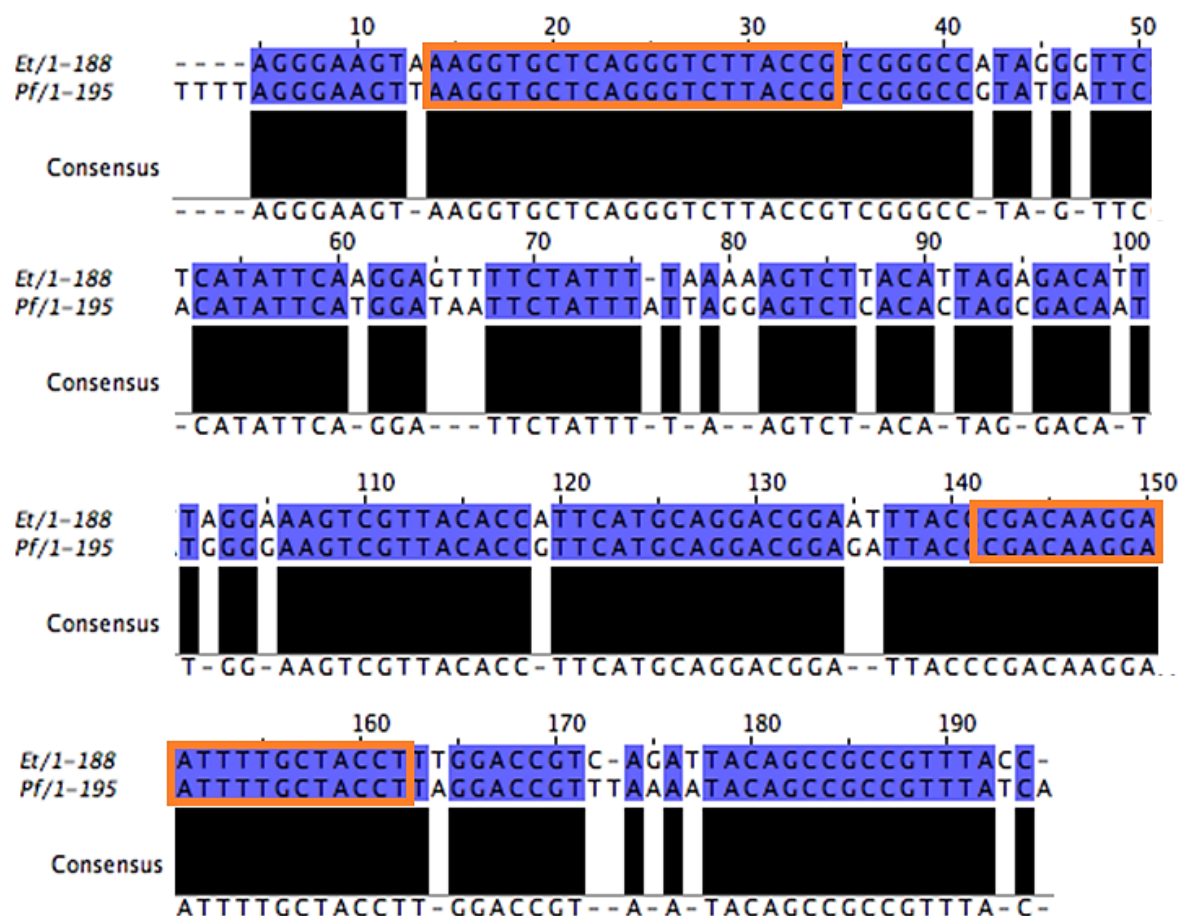
Figure 10.3 Alignments of LSUE ribosomal RNA gene sequences from published mitochondrial genome sequences.
Sequences with GenBank accessions: *Plasmodium falciparum* (M76611) and *Eimeria tenella* (AB564272) were aligned using clustalX pairwise alignment and consensus colours generated via Jalview. Conservation is shown as blue colour on the sequences and black bars at the bottom of the alignment. Consensus based primers (marked with a yellow box) were designed to amplify an rRNA sequence from the *T. gondii* mitochondrial genome.

As negative controls, RNA extracted from IP fractions performed on a line with the mitochondrial protein import component TgTom22 is triple-HA tagged (van Dooren *et al.*, 2016), and from total lysate of the parental line TATiΔku80 were also used as input. We initially wanted to perform RT-qPCR to quantify the amount of rRNA present in each IPs. However, qPCR required to use a precise amount of cDNA, and the amount of RNA extracted from the IPs prior "cDNA" generation was too little to be accurately measured by NanoDrop. We hence decided to carry out

PCR instead, and optimised the number of PCR cycles to be at the minimal detection level of each band so that intensity differences are apparent. 30 PCR cycles gave the best results (Figure 10.4B). PCRs were run on an agarose gel, and band intensities were quantified by calculating the ratio between "mito-rRNA" and "api-rRNA" PCR bands on imageJ (Table 10.2; all PCRs presented in Appendix Figure 3). Results showed that the mito-rRNA PCR product was consistently more abundant than api-rRNA (average mito/api ratio 2.85±0.5, n=7) in TgmS35-3HA IP fractions compared to the controls (0.75±0.13, n=4, from TgTom22-IP and 0.56±0.17, n=5, from total lysate). Figure 10.4D shows a graph summarising data from all the experiments, and Figure 10.4C shows an example of one experiment. In support of the IP specifically enriching for mitochondrial rRNA, the PCR for actin did not amplify products from most of the TgmS35 IP fractions (we could observe a band in one of four Tom22-IP experiments, and in none of seven TgmS35-IP experiments) while consistently amplifying from total RNA (five times of five experiments) (Figure 10.4C). These findings provide additional support for TgmS35 being a part of a ribosomal complex.
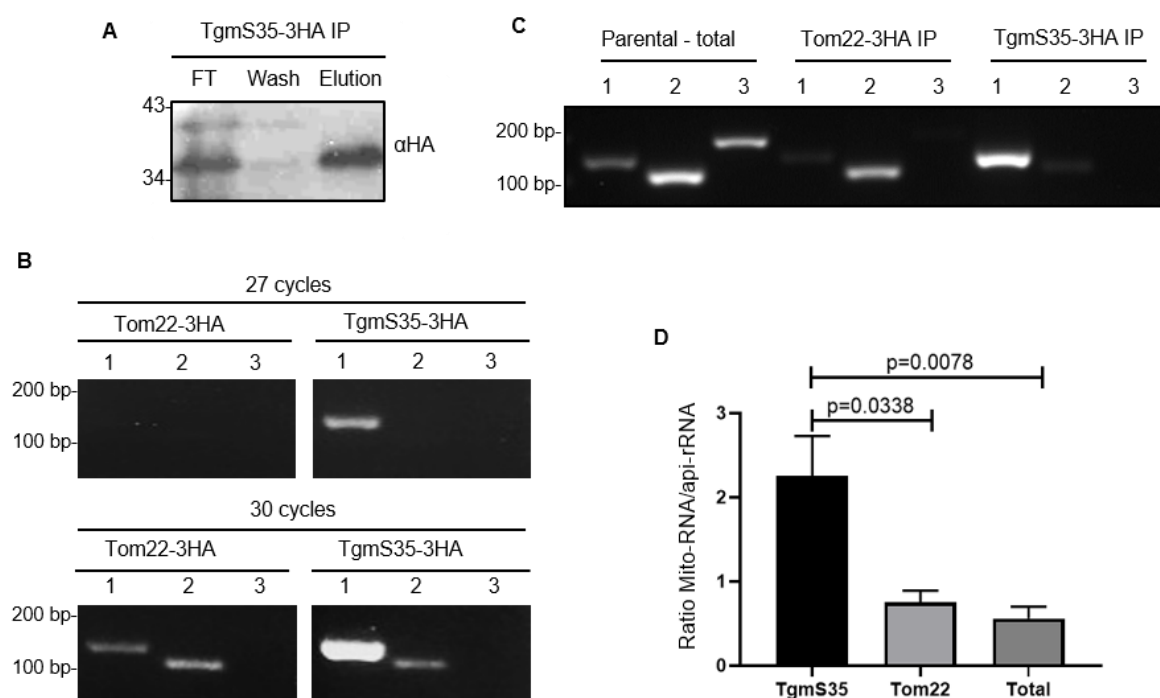
Figure 10.4 Detection of mitochondrial rRNA in TgmS35 immunoprecipitation elutions.
(A) Immunoblotting of the different fraction obtained from the triple HA tagged TgmS35 IP. Anti-HA was used to detect TgmS35 and shows enrichment of the ribosomal protein in the elution compared to the throw through (FT). **(B)** PCR cycle optimisation to reach the minimal detection level of each band. PCRs were performed with primers for a (1) mitochondrial rRNA sequence (mito-rRNA), for an (2) apicoplast rRNA sequence (api-rRNA) and for a (3) cytosolic mRNA (actin). Template is RNA extracted from IP of TgTom22 (Tom22-3HA IP) or from IP of TgmS35 (TgmS35-3HA IP) **(C)** An example PCR experiment performed with primers (1), (2), and (3) as above. Template is RNA extracted from total cell lysate of TATiΔku80 (Parental - total), from IP of TgTom22 (Tom22-IP) or from IP of TgmS35 (TgmS35-IP). **(D)** Comparison of results from PCR performed with primers for a

mitochondrial rRNA sequence (mito-rRNA), for an apicoplast rRNA sequence (api-rRNA) and for a cytosolic mRNA (actin). Template is RNA extracted from total cell lysate of TATiΔku80 (total), from IP of TgTom22 (Tom22) or from IP of TgmS35 (TgmS35). A one-way ANOVA statistical test was performed.

	TgmS35 mito-rRNA	TgmS35 api-rRNA	RT-PCR TgmS35-IP ratio	Tom22 mito-rRNA	Tom22 api-rRNA	RT-PCR TgTom22-IP ratio	Parental - Total mito-rRNA	Parental - Total api-rRNA	RT-PCR Parental - Total ratio
Exp 1	125.233	32.846	3.813	34.288	40.380	0.849	48.593	114.384	0.425
Exp 2	62.163	95.069	0.654	25.469	25.564	0.996	46.656	118.138	0.395
Exp 3	110.048	26.771	4.111	24.493	70.131	0.349	42.724	96.869	0.441
Exp 4	127.351	110.847	1.149	102.972	127.278	0.809	80.315	63.877	1.257
Exp 5	101.466	55.280	1.835				33.843	105.756	0.320
Exp 6	67.524	56.599	1.193						
Exp 7	73.435	30.874	2.379						
Avarage	95.317	58.327	2.859	46.806	65.838	0.751	50.426	99.805	0.568
SEM	10.381	12.459	0.510	18.851	22.479	0.140	7.891	9.704	0.174

Table 10.2 Quantification of mitochondrial rRNA enrichment from TgmS35-3HA IPs in relation to apicoplast rRNA and cytosolic mRNA.
PCR band intensity ratios were calculated by dividing theband intensity value of PCR using mito-rRNA primers (mitochondrial rRNA) by the one using api-rRNA primers (apicoplast rRNA). This was performed for IPs using TgmS35-3HA line, Tom22-3HA line and the TATiΔku80 parental line.

Taken together, the approximate size of the complexes marked by tagged TgmS35, TgbL12m and TguL3m, and the specific enrichment of mitochondrial rRNA in the TgmS35 pull-down are in agreement with the identity of the observed complex as a *T. gondii* mitoribosome complex.

10.3. TgmS35, TguS15m and TgbL12m are crucial for mitochondrial biogenesis and parasite fitness

To study the function of these genes in more detail, conditional knock-down lines were generated. First, we wanted to provide additional support to TgmS35 being part of a mitoribosomal complex. We reasoned that upon disruption of a gene encoding a protein with high homology to another known mitoribosome subunit, TgmS35 expression or stability may be affected. TguS15m is another putative mitochondrial ribosomal protein identified by Gupta *et al*. (2014) as a homolog of the universally conserved uS15m (Table 10.1); it was thus chosen to assess the putative dependency of TgmS35 upon its disruption. Hence, cKD line was generated by replacing TguS15m native promoter with an ATc repressible promoter as described earlier (Figure 9.3A), in the TgmS35-3HA background line. In addition, for the purpose of functional studies, the native promoter of the TgmS35 and TgbL12m was also replaced with an ATc repressible promoter, each

in their respective parental line where the gene is triple HA tagged. These lines were named TgmS35-3HA/rTguS15, rTgmS35-3HA, and rTgbL12m-3HA, respectively. Inducible promoter integration was confirmed by PCR for all 3 genes (Figure 10.5A). ATc induced downregulation was confirmed by qPCR, western blot and IFA for rTgmS35-3HA (Figure 10.5B-C), and loss of protein was verified by IFA for the rTgbL12m-3HA (Figure 10.5E). Interestingly for TgmS35-3HA/rTguS15, immunoblot and IFA analysis showed that downregulation of TguS15m gene results in depletion of the TgmS35 protein (Figure 10.5C and E). These results support the hypothesis that these proteins are part of the same mitoribosomal complex and suggests that they are essential for its stability.

Parasite growth was monitored by plaque assay which revealed a severe growth defect in response to TgmS35 and TguS15m depletion. However, small plaques can still be observed suggesting that these genes are important for fitness, yet not essential (Figure 10.5D), although, this could as well be due to some residual leaky expression from the ATc inducible knock down strategy. Due to lack of time, rTgbL12m-3HA line was not tested for parasite growth and is an assay to be performed in the future, as well as a western blot to assess loss of protein.

In agreement with their potential role in mitochondrial biogenesis, the loss of TgmS35, TguS15m, and TgbL12m induced some mitochondrial morphology abnormalities observable by IFA (Figure 10.5E) with the majority of the parasites on observed fields that displaying mitochondria in "sperm-like" shapes and some fragmented; whereas no morphological defect was observed in the parental line – most parasites displayed open/"half-moon" and lower abundance of "sperm-like" mitochondria (Figure 10.6A). The same criteria for assessing mitochondrial morphology as Figure 9.1 were used here too.
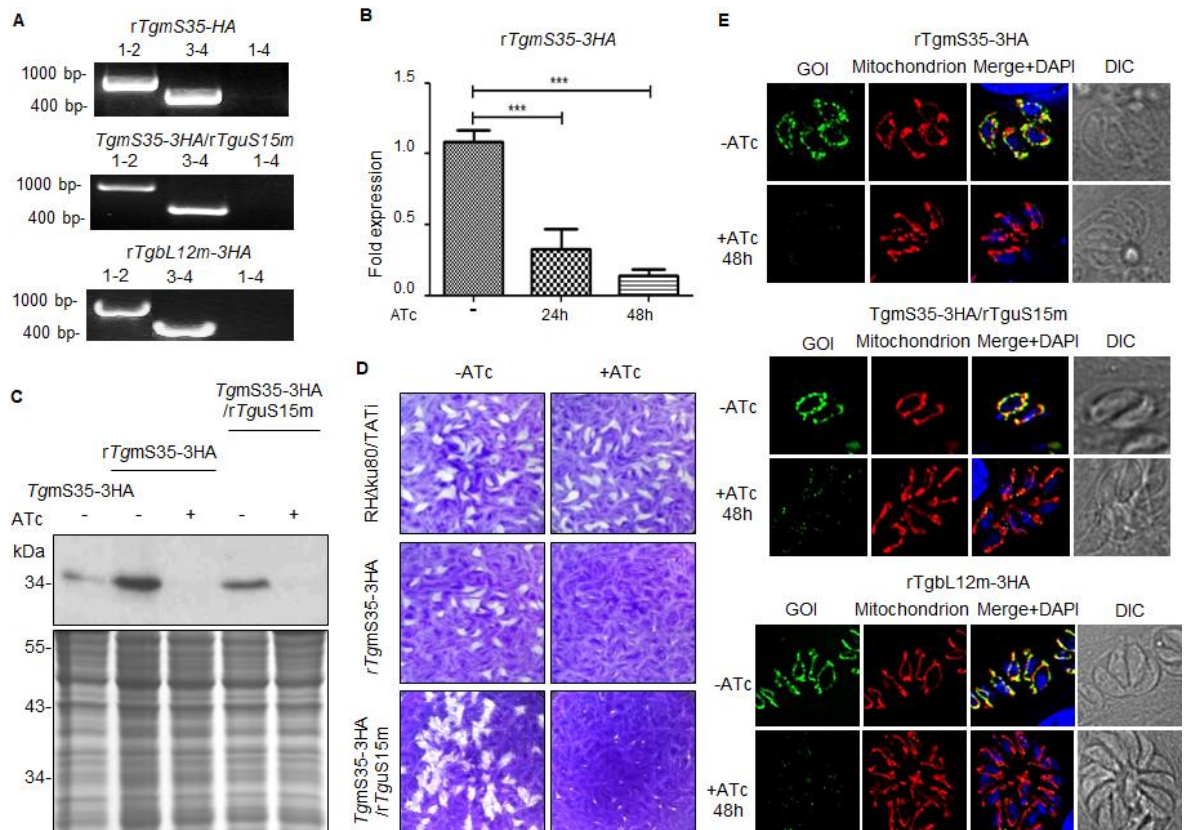
Figure 10.5 Conditional knock-down of TgmS35, TguS15m and TgbL12m results in mitochondrial morphology defect, and growth disturbance for TgmS35, TguS15m as well.
(A) Validation of the promoter integration in the TgmS35, TguS15m and TgbL12m locus via PCR analysis using primers 1, 2, 3, and 4, represented in Figure 9.4A. **(B)** Transcript levels of TgmS35, analysed by qPCR normalised to actin, in absence (-) or presence of ATc after 24 and 48 hours. Bars represent the mean ± SEM (n=5). ***p< 0.0001. **(C)** Western blot (top panel) of TgmS35-3xHA in lines where TgmS35 is under its native promoter (TgmS35-3HA), and where TgmS35 or TguS15m are under regulatable promoters (rTgmS35-3HA and TgmS35-3HA/rTguS15m respectively). Lower panel shows instant blue staining as a loading control. **(D)** Plaque assays performed with parental line (RHΔku80/TATi) (top panel), rTgmS35-3xHA parasites (middle panel) or or rTgmS15 parasites grown for 9 days in the absence (-) or presence (+) of ATc. **(E)** Immunofluorescence assay of rTgmS35-3HA, TgmS35-3HA/rTguS15m and rTgbL12m-3HA parasites in the absence (-ATc) or presence (+ATc) of ATc for 48 hours. GOIs, mitochondria and nuclei were stained with anti-HA, anti-TgMys and DAPI, respectively, and parasites were observed by Differential Interference Contrast (DIC).

To confirm this observation, vacuoles displaying mitochondrial morphological defect were counted in the presence or absence of ATc for 48 hours. IFA analysis for rTgmS35-3HA detected mitochondrial morphological abnormalities with a disproportionate number of mitochondria with "sperm-like", and fragmented and branched-irregular to a lesser extent, upon TgmS35 depletion, and this defect was not detected upon ATc treatment of the parental line (Figure 10.6A-C). Moreover, conditional depletion of a component of an unrelated pathway, a putative ER-mitochondria complex member, EMC1 (TGME49_205740) (Wideman and Muñoz-Gómez, 2016; Ovciarikova and Sheiner, unpublished), while deleterious to the parasites (Lacombe *et al.*, 2019), showed a significantly milder effect on mitochondrial morphology than what was observed upon depletion of TgmS35

(Figure 10.6D) suggesting that this phenotype is not just the result of parasites dying. But as mentioned previously, the timing in which morphological defects events appear is important, and we will perform a detailed time-line analysis in the future to confirm that morphology defects precede other defects to further support our conclusions. Finally, other organelles, such as apicoplast, microneme and nucleus, did not display any significant defect upon TgmS35 depletion (IFA using anti-HSP60 for the apicoplast, anti-Mic2 for micronemes and DAPI for the nucleus) (Figure 10.6E-G). Lack of defect in these organelles is in support of a mitochondrial specific defect in these lines. Together, these results are consistent with TgmS35 being important for parasite fitness and mitochondrial biogenesis.
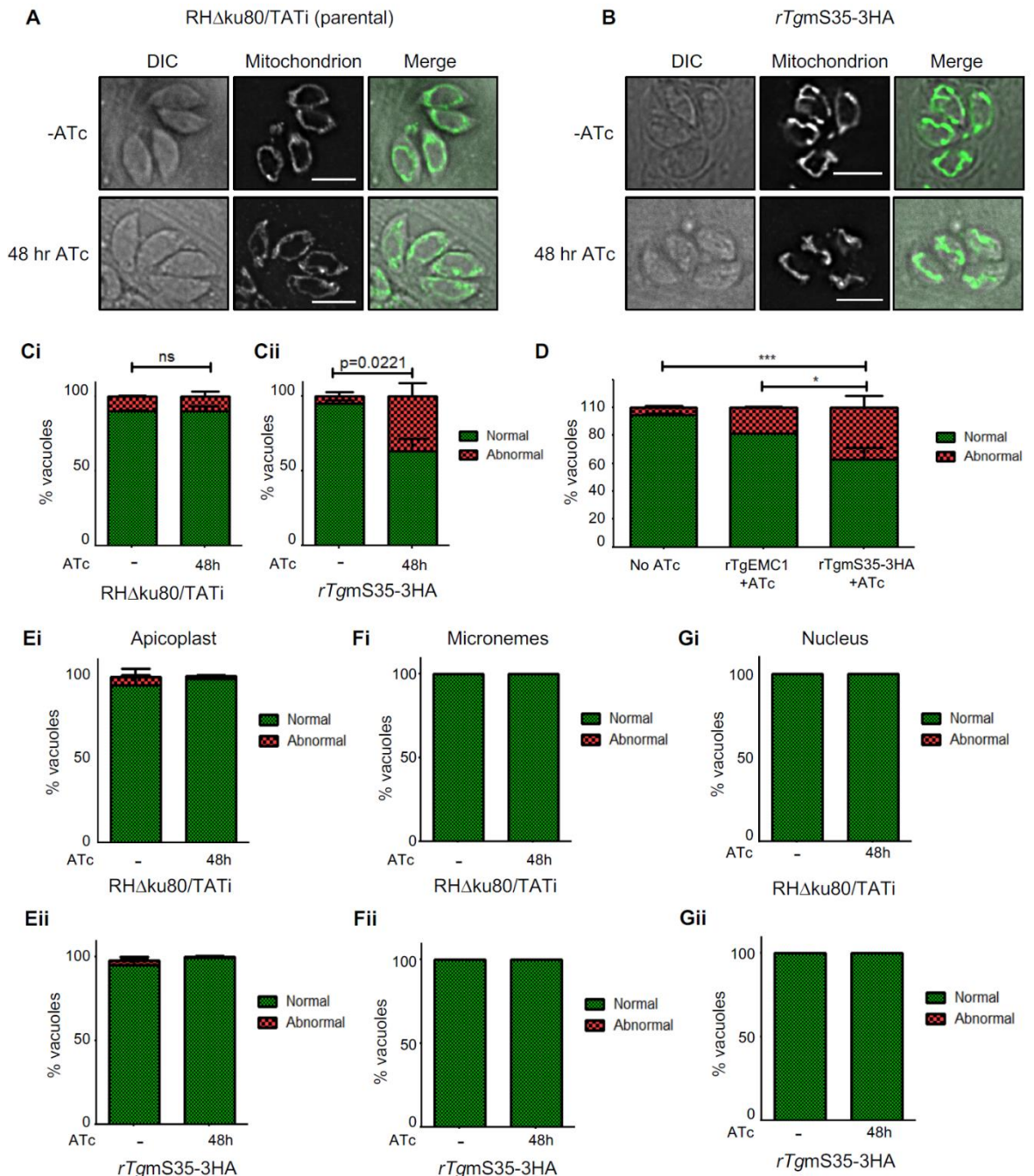
Figure 10.6 Morphological analysis of organelles under TgmS35 depletion.
(A/B) Immunofluorescence micrographs taken with the RHΔku80/TATi parental/rTgmS35-3HA line respectively grown in the presence or absence (-) of ATc for 48h, showing examples for untreated (-ATc) or treated (48h ATc) mitochondrial morphologies. **(C)** Quantification of parasite vacuoles with "normal" (green) vs "abnormal" (red) mitochondrial morphologies after growth of the RHΔku80/TATi parental **(Ci)** or the TgmS35-3HA **(Cii)** lines without (-) or with ATc for 48 hours. Graphs represent mean ± SEM for n = 3 independent experiments; Analysed by t-test. **(D)** Quantification of "normal" vs "abnormal" mitochondria-containing vacuoles after growth of rTgmS35-HA or rTgEMC1 without (-) or with ATc for 48 hours. Graph represents mean ± SEM for n = 3 independent experiments for rTgEMC1 +ATc and rTgmS35-3HA +ATc and n=6 for No ATc where data from rTgEMC1 no ATc and rTgmS35-3HA no ATc were combined; Analysed by ANOVA followed by Tukey's Multiple Comparison Test, * p<0.05 and ***p<0.001. **(E-G)** Quantification of "normal" vs "abnormal" apicoplast/nucleus/microneme after growth of RHΔku80/TATi **(i)** rTgmS35-3HA **(ii)** without (-) or with ATc for 48 hours. Graph for apicoplast represents mean ± SEM for n = 3 independent experiment; Analysed by t-test. Nucleus and microneme morphologies were not analysed statistically as no abnormal morphology was observed.

10.4. TgmS35 is essential for mitochondrial translation

In yeast, mS35 is found at the critical point of mRNA entry into the ribosome (N. *et al.*, 2017). It was hypothesised that depletion of TgmS35 should result in a mitochondrial translation defect. However, the field lacks an assay to directly monitor mitochondrial translation in *T. gondii*. The assembly and activity of complex IV, which is directly dependent on the mitochondrial translation of CoxI and III, was therefore monitored and compared to the assembly and activity of complex V, which in *T. gondii*, does not contain any mitochondrially encoded subunits (Figure 9.7A). Using a crude mitochondrial fraction, obtained from parasites lysed through nitrogen cavitation as described in Section 8.1.1, a hrCN-PAGE followed by in-gel complex IV and V activity assay was performed (Figure 10.7B). As mentioned in Section 9.4.3, both complex VI and V identities were validated (Table 9.1, Figure 9.4). The two assays were performed at 48h and 96h post TgmS35 depletion (Figure 10.7B). A decrease in complex IV activity was observed at 48 hours (decreased band intensity) and complete activity loss by 96 hours (loss of band). Complex V, however, did not display a decrease of activity until 96 hours post gene depletion (Figure 10.7B). These results suggest that TgmS35 likely has a role in mitochondrial translation as activity of mitochondrially encoded complex IV is hampered before nuclear encoded complex V is when TgmS35 is absent. Here again, as in Figure 9.7B, we avoided quantification of subtle differences due to the non-linear staining build-up and sample running variation as it is the case between the complex V assay in Figure 10.7A and 10.7B. The defect seen in complex V at 96h may be the result of a secondary effect, whereby in the absence of mitochondrial translation, complex III (for which one subunit is encoded in the mitochondrial genome) and IV (for which we show a defect) are not functional, as a result the electrochemical gradient is not fully established and protein import to the mitochondrion, which relies on this gradient, is hampered. To explore this possibility, the nuclear encoded TOM complex assembly and protein import were then investigated. Western blot analysis of a native gel from the 96-hour time point showed that TOM40 in the TgmS35 depleted line, migrates at the same size as that of the untreated line (Figure 10.7C). This data suggests that the TOM complex, whose components are not encoded in the mitochondrial genome, continues to assemble. To provide further support for TOM complex assembly, protein import into the mitochondrion

was monitored. As described in Section 9.3., transient transfection of a Myc tagged DHFR fused to the mitochondrial targeting signal of HSP60 (Hsp60L-mDHFR-cMyc (Van Dooren *et al.*, 2016) was carried out at different time points after TgmS35 depletion. Import of this construct was monitored by IFA (Figure 10.7D) and mature/immature band intensity ratio observed by western blot was calculated (Figure 10.7E-F; Table 10.3). In a previous study the depletion of a component of the protein import machinery had resulted in accumulation of pre-mature Hsp60L-mDHFR-cMyc as observed by western blot (Van Dooren *et al.*, 2016). However, in the case of TgmS35 depletion, the western blot analysis showed no significant protein import defect upon, including at the 96-hour time point (no statistical differences compared to absence of ATc) (Figure 10.8E-F; Table 8.5; Appendix Table 6 for statistical analysis detail). The IFA also revealed no mitochondrial import defect, with perfect co-localisation of the Hsp60L-mDHFR-cMyc product (in green) and the TOM40 mitochondrial marker (in red). Taken together, these observations suggest that TgmS35 depletion results in a defect in the assembly and activity specifically of a mitochondrial respiratory complex whose subunits are thought to be encoded in the mitochondrial genome, while other complexes continue to assemble correctly and other mitochondrial biogenesis pathways continue to function.

Figure 10.7 Down-regulation of TgmS35 leads to a defect in rmETC complex IV.
(A) Whole cell (left panel) and enriched mitochondria (middle and right panel) from TgmS35-3xHA
(left panel) and from rTgmS35-3xHA (middle and right panel), grown in the absence (-) or presence
(+) of ATc for 48 hours, separated by high resolution clear- native PAGE. Complex IV activity was
visualised with cytochrome c: DAB staining. Complex V activity was assayed by visualising the
precipitation of lead by inorganic phosphate during ATP hydrolysis. Protein immunoblot analysis

using anti-TOM40 of whole-cell and enriched mitochondria sample was performed as a loading control. **(B)** Mitochondrial enriched fraction from rTgmS35-3xHA grown in the absence (-) or presence (+) of ATc for 96 hours, separated by high resolution clear-native PAGE and stained with Coomassie or for complex IV or complex V activity as above. **(C)** Immunoblot with anti- TOM40 antibody of mitochondrial enriched fraction from rTgmS35-3xHA grown in the absence (-) or presence (+) of ATc for 96 hours, separated by blue-native PAGE. **(D)** Immunofluorescence of rTgmS35-3HA repressible line in the presence or absence (-ATc) for 24, 48, 96 hours followed by transient transfection with Hsp60L-mDHFR-cMyc. The Hsp60L-mDHFR-cMyc protein product was visualised using an anti-Myc antibody, the mitochondrion anti-Tom40 antibody, the nucleus was stained with DAPI and whole parasites were visualised by polarised light (DIC). **(E)** Western blot representation of the parasites in the absence (-) or presence of ATc for 24, 48 and 96 hours, using anit-Myc antibody to visualize the immature (grey arrow) and mature (black arrow) of the Hsp60L-mDHFR-cMyc gene product. This was repeated 4 times. **(F)** Graph showing band intensity ratios between the mature and immature Hsp60L-mDHFR-cMyc product from the western blot shown in (E) on ImageJ software. This import assay was performed for rTgmS35-3xHA line in the absence (-) or presence of ATc for 24, 48 and 96 hours. Bars represent the mean ± SEM (n=4). A one-way ANOVA statistical test was performed and revealed no statistical differences between the no treatment (-ATc) and treated (+ATc 24h, 48h, 96h) parasites.

	Treatment	WB band	Mean	Ratio Mature/Immature
			rTgmS35	
	No ATc	Immature	10200	5.088
		Mature	51900	
	24h ATc	Immature	13000	4.577
		Mature	59500	
Exp 1	48h ATc	Immature	24900	2.257
		Mature	56200	
	96h ATc	Immature	31600	2.516
		Mature	79500	
	No ATc	Mature	20100	3.204
		Immature	64400	
	24h ATc	Mature	19400	3.242
		Immature	62900	
Exp 2	48h ATc	Mature	23400	2.953
		Immature	69100	
	96h ATc	Mature	35400	2.799
		Immature	99100	
	No ATc	Immature	27.047	3.527
		Mature	7.668	
	24h ATc	Immature	24.722	2.647
		Mature	9.338	
Exp 3	48h ATc	Immature	75.592	3.533
		Mature	21.399	
	96h ATc	Immature	49.737	2.343
		Mature	21.226	
	No ATc	Immature	56.26	2.639
		Mature	21.316	
	24h ATc	Immature	64.506	3.063
		Mature	21.063	
Exp 4	48h ATc	Immature	63.127	1.700
		Mature	37.125	
	96h ATc	Immature	31.98	2.299
		Mature	13.912	
		Ratio Average	STDEV	SEM
	No ATc	3.615	1.049	0.524
	24h ATc	3.382	0.834	0.417
	48h ATc	2.611	0.800	0.400
	96h ATc	2.489	0.227	0.113

Table 10.3 Protein import assay - Quantification of band intensities ratios from the mature and immature Hsp60L-mDHFR-cMyc product for the rTgmS35 line.

10.5. Conclusion

Apicomplexans mitochondria are highly divergent from model organisms and have undergone some dramatic reduction in their mitochondrial genome leaving them with only 3 protein encoding genes which encode for subunits of the mETC, and some fragmented rRNA genes (Namasivayama *et al.*, 2020). Very little is known about how these proteins are translated, and up until this work, there were no direct evidence of the assembly of stable mitoribosome complex in apicomplexan parasites. Here, endogenously tagged putative ribosomal proteins TgmS35, TgbL12m and TguL3m were confirmed to localise to the mitochondrion, and the tagged lines allowed the detection of mitoribosome complexes for the first time by BN PAGE (Figure 10.2B). Furthermore, mitochondrial rRNA was enriched after RNA extraction of mitoribosome enriched samples by immunoprecipitating the complex from TgmS35-3HA parasites (Figure 10.4). IP using Tom22-3HA and the parental lines as negative control confirmed that the presence of mitochondrial rRNA was specific to the TgmS35-3HA line (Figure 10.4B and C), which provide further support in the identity of the macromolecular complex. Moreover, conditional knock down of TguS15m in the TgmS35-3HA background line resulted in the loss of the TgmS35 protein by IFA and western blot. This demonstrates that these proteins are both part of the same ribosomal complex and are essential for its stability (Figure 10.5C). Altogether, these data provide compelling evidence of the presence of mitoribosomes in *T. gondii* mitochondrion, and provide another evidence supporting that *T. gondii* mitochondrion is indeed a translationally active organelle.

The generation of conditional knock down lines of ribosomal proteins TgmS35, TguS15m and TgbL12m revealed mitochondrial morphology defect upon gene depletion (Figure 10.5E), while no defects seen in other organelles. Analysis of the knock down further revealed that TgmS35 and TguS15m proteins are crucial for parasite growth (Figure 10.5D). These results fit with their predicted role in mitochondrial biogenesis.

These putative ribosomal proteins are expected to be actively involved in mitochondrial translation. Our complex IV (mitochondrial translation dependent) and complex V (mitochondrial translation independent) activity assay was

developed to monitor this outcome, and revealed early loss of activity of complex IV after TgmS35 depletion and only subsequently loss of complex V upon TgmS35 depletion, which is consistent with a role of TgmS35 in mitochondrial translation. In the absence of other direct methods to study mitochondrial translation in apicomplexans this assay provides a useful proxy, while the lab continues to develop such tools (in the discussion section).

11. Conclusion and discussion

Despite advances in research on mitochondrial biology and diversity across eukaryotes in recent years, knowledge is still focused on a handful of models, such as yeast, mammals and plants. Concentrating on these canonical mitochondria narrows our window of understanding. Indeed, from its first acquisition by endosymbiosis over a billion years ago (Wang and Wu, 2015), the ancestral endosymbiont evolved to give rise to an array of divergent mitochondria and mitochondria-like organelles, and studying these is necessary to have the full picture of mitochondrial biology across life. Learning about mitochondrial biology in organisms outside the Opisthokonta group can help scientists understand mitochondrial functions across eukaryotes and may be of relevance for human diseases caused by e.g. eukaryotic parasites. However, it is the lack of well-developed, tractable, model organisms outside these key groups, as well as the lack of tools to study them, that hampers discoveries. Apicomplexa, which contain the medically important *Plasmodium* and *Toxoplasma* parasites, is such a group where the mitochondria are understudied. The work described here provides crucial advances to the understanding of apicomplexan mitochondrial biology, and especially mitochondrial translation by first investing insubstantial trouble shooting efforts to compare and optimising the cell lysis methods - this works shows that nitrogen cavitation is a powerful technic to break open parasites in a scalable manner, which the Sheiner lab is now using routinely for structural studies as well; then, by characterising the mitochondrial ribosome and by establishing an analytical pipeline to identify mitochondrial translation defects. Finally, characterisation of new ribosomal proteins also provides the field with new validated mitochondrial markers.

11.1. Establishment of a protocol to lyse *T. gondii* in a scalable and efficient manner for crude mitochondrial preparation

To date, studying mitochondrial function has been limited by the lack of protocol that allows good quality, large-scale organelle enrichment. As a result, the field has had to rely on whole cell analysis and biochemistry (e.g. (Ke *et al.*, 2018; Seidi, Linden S Muellner-Wong, *et al.*, 2018), and fluorescence microscopy (e.g.(Garbuz and Arrizabalaga, 2017; Ovciarikova *et al.*, 2017) to address

questions on mitochondrial biology. In model organisms, *in vitro* functional assays performed with isolated mitochondria are extensively used to unravel mitochondrial functions, including translation. However, for *T. gondii,* the parasitology community struggles to isolate mitochondria – firstly due do the tight association with the apicoplast (which remains an issue, and will likely only be solved with apicoplast biogenesis mutants), and secondly due to the nature of this organism's intracellular lifestyle and size, where gathering enough material prior to mitochondria isolation is also a challenge, and cannot be done simply by scaling up axenic culture as it has worked for e.g. *Trypanosomatids*. In this study, we sought to establish a scalable method to break open the parasite with high efficiency which also conserves mitochondrial respiratory complexes intact and active. Different methods, used in model organisms and other parasites, were tested. Most of them resulted in no to moderate success, and are not scalable (Section 8.1). Nitrogen cavitation was the best lysis method tested with an efficiency of up to 99% breakage and capacity (through changing size of chamber and through repeating cycles with unbroken material) to lyse high numbers of parasite cells (so far, the highest number of parasites broken effectively in one experiment in the lab is 5×10^{13} parasites). It is reproducible, reliable, and has the remarkable advantage to allow large scale cell lysis to the point that the only limitation is manpower. Indeed, some on-going experiments designed to solve *T. gondii*'s mitoribosome structure via single particle analysis by cryo-electron microscopy, in collaboration with Prof. Alexey Amunts' laboratory at the university of Stockholm required such quantity of enriched mitochondria that nitrogen cavitation was the obvious and only option capable to meet this requirement.

In this study, differential centrifugation was performed to start removing cellular compartments and enrich samples in mitochondria. A slow spin at 1500 x g aimed at removing unbroken cell and large debris, and a high spin of 16000 x g aimed at pelleting mitochondria. A quality control by western blot and IFA revealed substantial loss of mitochondria in the slow spin pellet, which can possibly be due to organelles and large debris clumping together and being dragged to the bottom of the tube. Slow and high spin differential centrifugation have been used multiple times in the *Toxoplasma* community and routinely for model organisms to generate crude mitochondria samples. However, for such protocols, immunoblots

assessing the quality of the enrichment throughout the centrifugation process is not showed, only the whole cell, end product pellet and supernatant are showed (Liao *et al.*, 2018), when available, and so we do not have points of comparison with other work. So, in some way, our quality control by immunoblotting and IFA is somewhat more thorough than many studies. Nonetheless, it is clear that crude mitochondria samples contain many contaminants, except for the cytosol which is completely removed (Liao *et al.*, 2018). Similarly to these protocols, we were successful at removing the cytosol, which is an essential step to study organellar translation and was the minimum requirement for the tRNA IP experiments (see below). Special care should, be taken while filtering out host cells, as this can impact the quality of the sample preparation. Additional controls to assess mitochondrial integrity can be performed to further validate our lysis and enrichment protocol. Staining with Mitotracker® or JC-1 is a straight forward technique that can tell us if mitochondria are still active as they generated a mitochondrial fluorescent signal when the membrane potential is undisturbed. In model organisms, mitochondrial integrity can also be assessed by measuring complex IV activity through cytochrome c dependent consumption of oxygen, using a Clark-type oxygen electrode (Sweetlove, Taylor and Leaver, 2007). To function, complex IV requires reduced cytochrome c in the IMS as a substrate. As cytochrome c is too large to pass through the OMM, if mitochondria are intact, no complex IV activity should be detected in the presence of reduced cytochrome c in the solution. However, complex IV activity will be detected if the OMM is compromised. Hence, by comparing activity with and without detergent to solubilise the OMM, an estimation of the OMM integrity can be made (Sweetlove, Taylor and Leaver, 2007). Of course, such assay would need to be adapted for *T. gondii* which in itself would be a tedious task. But it is also not guaranteed to work as *T. gondii* being an intracellular parasite, any contamination with host mitochondria would render this assay unusable.

To obtain "cleaner" mitochondria samples, efforts are currently made to optimise mitochondria purification by sucrose and Percoll gradient, which allows a more refined organelle separation by density. Nitrogen cavitation has previously been used for cell lysis followed by mitochondria enrichment in *Plasmodium* (Kobayashi *et al.*, 2007; Mather, Morrisey and Vaidya, 2010; Hata, Sato and Kita, 2019) and in the unrelated single cell eukaryote Trypanosomes (Bouzaidi-Tiali *et al.*, 2007). It

is envisaged that this protocol will be invaluable for future efforts in the field to study *T. gondii* mitochondrial biochemistry, and to characterise other organelles, as it is already the case with the hyperLOPIT study which has made a major step forward in the study of spatial protein sub-compartmental localisation (Barylyuk *et al.*, 2020).

11.2. tRNA IP as a tool to identify putative MITI components: optimisation and protein localisation

Apicomplexan parasite mitochondrial genomes have lost all tRNA genes throughout evolution and hence these mitochondria need to import tRNAs to translate their genome. Previous studies have shown that mitochondrial tRNA import (MITI) occurs in *T. gondii* and *P. falciparum* (Esseiva *et al.*, 2004; Pino *et al.*, 2010; Sharma and Sharma, 2014). In fact, it occurs in many mitochondria possessing organisms including protozoa, fungi, higher plants, and humans (Lithgow and Schneider, 2010; Rubio and Hopper, 2011; Schneider, 2011). *T. brucei* is another example for the extreme case where the complete set of tRNA must be imported into mitochondria (Tan *et al.*, 2002). Seidman *et al.*, (2012) have established a protocol to elucidate the composition of the translocon complex which enables this passage. They used a pull-down approach with synthetic biotinylated tRNA^{leu} (mitochondrial) and tRNA^{Met-i} (strictly cytosolic), bound to paramagnetic beads, to identify components involved in tRNA import. Mass spectrometry (MS) analysis identified candidate proteins, two of which have a role in MITI and one of the two interacts with proteins involved in protein import in the inner mitochondrial membrane (IMM), supporting the hypothesis that tRNA import is performed in collaboration with proteins from the import machinery (Seidman *et al.*, 2012). To try and shed light on the, yet, unknown MITI translocon machinery in *T. gondii*, the same protocol was adapted for our model. Crude mitochondrial fractions were used to pull down proteins which interact with a tRNA known to be imported into the mitochondrion of *T. gondii* (tRNA^{Ile}) (Esseiva *et al.*, 2004); and a strictly cytosolic tRNA (tRNA^{Met-i}), was used as a negative control to subtract unspecific binding and proteins that bind to all tRNAs, from the final result. Elutions were separated on polyacrylamide gels and proteins were stained with different staining methods. Finding a staining method which allowed a clear visualisation of bands was challenging, perhaps due to the low protein yield

at the end of the elution. In experiments for which bands were the clearest on the gel using Coomassie, we initially believed to see a faint band pattern difference between tRNA^{Ile} and tRNA^{Met-i} around the group of proteins which migrated at ~20-30 kDa. As the difference was not very obvious, gel elution lanes were cut within a range of 17 – 34 kDa, and sent for MS analysis. After multiple repetitions, it became clear that there were no consistent band pattern differences between the tRNA^{Ile} and tRNA^{Met-i} elutions. This is perhaps because the proteins of interest represent a very small proportion of the total proteins from the elution and hence are in too low abundance to be visible. Nonetheless, multiple samples had already been sent to MS with this MW range, and so, for consistency purposes, the following repetitions were performed as such, although this meant omitting proteins outside this interval. Five repetitions of gel slices analysis were performed in total, which resulted in the selection of 7 putative candidates which were present in 2 repeats out the 5, and absent from the tRNA^{Met-i} experiments: TGME49_219470/ 220950/ 246540/ 253740/ 259640/ 267660 and /297780. As expected many proteins discovered in the IP bound to both tRNAs ruling them out as candidates according to our criteria. It is important to mention that by exercising these criteria we limited ourselves to miss out on proteins that may have specific role in MITI despite also binding non-mitochondrial tRNAs. However, the finding that only 2 of them are predicted to be mitochondrial suggests the possibility that the others are false positive. The two predicted mitochondrial proteins have not been experimentally confirmed yet: TGME49_219470 (online prediction tools) and TGME49_246540 (found in the mitochondrial membrane cluster from the LOPIT data (Barylyuk *et al.*, 2020). It would be interesting to examine if narrow MW range selection sent for MS had led to us missing other relevant interactions, and this would be another future direction for any follow up work. However, although our main focus was on identifying mitochondrial proteins involved in MITI, tRNAs are also known to traffic from the nucleus to the cytosol (and some even back and forth again) for the purpose of going through their maturation process (Chatterjee *et al.*, 2018), before reaching their final destination. Thus, finding proteins which are predicted to be nuclear led us to consider the possibility of direct nuclear to mitochondrion trafficking. Two of the lists, TGME49_253740 annotated as hypothetical protein, and TGME49_259640 annotated as a nucleoporin autopeptidase protein in ToxoDB, were confirmed nuclear by IFA. TGME49_259640 was published as TgNup302 and

is involved in nuclear transport (Courjol *et al.*, 2017). The finding from our IP, which suggest that these nuclear proteins interact with a mitochondrial tRNA but not with a cytosolic tRNA, may suggest a potential role for nuclear proteins in mediating or controlling MITI. An important future experiment-series to enhance the validity of this finding would include tagging the nuclear proteins and showing that pulling them down recovers only mitochondrial tRNA, and vice versa - confirmation of the interaction of the candidate protein with the imported tRNAs by repeating the tRNA pull down with the TgNup302-3HA tagged line followed by Western blot and doing reverse IPs with the TgNup302-3HA line followed by Northern blot to detect the presence of mitochondrial imported tRNA (and absence of tRNA^{Met-i}). In such a scenario, one possibility is that tRNA traffic from the nucleus into the mitochondrion at sites of nuclear-mitochondrion proximity mediated by components of the nuclear pore. Indeed, examples for exchange of large molecules at sites of proximity between membranes of different organelle (also known as membrane contact sites) are accumulating fast in the field of cell biology in the past years (Prinz, Toulmay and Balla, 2020). Another possibility is that these nuclear proteins are involved in recruitment of tRNA, destined to the mitochondrion, away from the pool of those destined to the cytosol. tRNA recruitment mechanisms have been described before in the yeast (Baleva *et al.*, 2015) and *Trypanosomes* (Bouzaidi-Tiali *et al.*, 2007) MITI pathways, which in both cases, happen in the cytosol. Thus, nuclear tRNA recruitment for MITI would represent a new mechanism. MITI was shown in yeast to occur with tRNAs that are loaded with amino acids (I. Tarassov, Entelis and Martin, 1995). Thus, for either of these possibilities to takes place, amino acylation of the transported tRNA would occur in the nucleus. Nuclear tRNA amino acylation has been detected in different organisms such as yeast (Steiner-Mosonyi and Mangroo, 2004), and mammalian cells (Nathanson and Deutscher, 2000) (e.g. (Lund and Dahlberg, 1998; Nathanson and Deutscher, 2000) but this hasn't been examined in *T. gondii* yet. Future work for this gene includes functional characterisation of conditional knock-down mutants through evaluation of their importance for growth, mitochondrial biogenesis, and translation, as was performed for TgmS35. Further validation would include reproducing the *in vitro* tRNA import assay as described by Esseiva *et al.,* (2004) using these transgenic lines. If validation of this novel idea is achieved through such knock-down characterization and through the above-mentioned validation of the protein-tRNA interaction, a further step would be to

identify the protein partners in the mitochondrial membrane. For this, co-IP or bioID (Roux *et al.*, no date) can also be performed. The hypothesis of a direct tRNA transfer from the nucleus into the mitochondrion widens the area of research to study other complexes which may be indirectly linked to tRNA import, yet essential, such as protein involved in nuclear export of tRNA molecules.

TGME49_220950, while annotated as a hypothetical protein in the genome database, was previously identified as MAF1b (Blank *et al.*, 2018) which is involved in host cell mitochondria recruitment. In support of such role endogenous triple HA tagging confirmed its expected localisation to the PV. In the context of our goal, this finding is surprising as MITI components are expected to be found mainly in the mitochondrion, and so it is likely that this is a false positive of our experiment. Nevertheless, for the completeness of this discussion it is worth considering other scenarios. MAF1b's role in host mitochondrial recruitment and its interaction with the tRNA[Ile] and not tRNA[Met-i] in our experiment, made us wonder about other hypothesis: (1) since MAF1b sequence contains a signal sufficient to interact with human mitochondria through which recruitment occurs, it is possible that the same signal may lead to an interaction with the parasite mitochondrion resulting in be bimodal targeting to the mitochondrion and PV. If such putative mitochondrion interaction occurs rarely, or by a small fraction of the MAF1b molecule population, it may well have been masked by the PV signal detected in the IFA. This possibility could be tested in the future by immuno-electron microscopy or through our parasite crude mitochondria preparation and Western blot. (2) Another intriguing possibility is that host cell mitochondrial recruitment is somehow regulated in respond to availability of tRNA[Ile]? Is there a link between host cell mitochondrial recruitment and parasite mitochondrial translation? This could be tested in the future by performing a MITI assay or by assessing mitochondrial translation in a MAF1 knock out line. However, we acknowledge that both these hypotheses are highly speculative.

For TGME49_246540, annotated as cytochrome c1, triple HA tagging was unsuccessful for now, and attempts at tagging it using different methods (N Terminal tagging, other tagging epitopes or cDNA) are being considered.

TGME49_219470 and /267660 are predicted as hypothetical proteins, and the former is predicted to localise to the mitochondrion. Endogenous tagging of both

genes was attempted twice unsuccessfully. Resistant parasites emerged from drug selection in both cases, however, PCR screen and IFA analysis revealed that none of them incorporated the tag. A likely reason is that the C-terminal tag cannot be tolerated and might interfere with function. N terminal tagging can be envisaged in the future as an alternative.

The whole protein dataset for both tRNA^{Met-I} and tRNA^{Ile} was analysed to find out any differences in terms of overall protein interaction. Results showed that amongst the hits found at least in two repeats, 26.4% and 33% are annotated as ribosomal proteins in ToxoDB for tRNA^{Met-i} and tRNA^{Ile}, respectively, which is in line with their role in translation. Amongst these putative ribosomal proteins, there is 16% more ribosomal proteins predicted to be mitochondrial in the tRNA^{Ile} dataset than in the tRNA^{Met-i} (Figure 8.4; Appendix table 1). This likely reflect the bimodal localisation and function of tRNA^{Ile} in both the cytosol and the mitochondrion, and provide some validation that the approach identifies at least high abundant proteins that interact more specifically with tRNA^{Ile}. Experimental validation by gene tagging will be performed in the future to confirm that these are indeed mitochondrial and if so, their interaction with tRNA^{Ile} will be validated and further assessment of their potential role in mitochondrial translation performed.

Overall, this assay requires further optimisation and controls. Sending total elution fractions instead of gel slices of limited protein size would maximise protein yield. For this, further optimisation of the elution conditions is needed. For example, additional washes with protein buffer without BSA would need to be carried out to avoid heavy BSA contamination in the elution, which would complicate the analysis by MS. The advantage of full elution analysis compared to gel slices is that it also avoids protein loss during the extraction from the gel. Also, using other tRNAs known to be imported into the mitochondrion as controls, such as tRNA^{Ala}, tRNA^{Trp}, and tRNA^{ser} (Esseiva *et al.*, 2004), will allow to address the question of whether there is a separate recognition factor for each tRNAs or it is the same factor which is shared amongst all of them, as it is the case in yeast and Trypanosomes (Rusconi and Cech, 1996; Entelis *et al.*, 2001; Mare, Salinas and Duche, 2008). If the latter is the case, data from IP with various tRNA will also enhance the confidence in the identified factors. Proteins involved in MITI, especially those part of the channel, are expected to have transient and weaker type of interactions with the imported tRNAs. In order to avoid losing these

contacts throughout the experiment and to lower background, crosslinking interaction analysis can be performed which covalently stabilises momentary interactions (Bhattacharyya *et al.*, 2003; Poria and Ray, 2017). Perhaps this could help this assay to be more specific.

Finally, an important control that has not been performed prior the pull-down assay is checking that the synthetic tRNAs are correctly folded and functional, although, this was an assumption made in previous published studies (e.g. Seidman *et al.*, (2012)) which were successful in identifying components of the MITI machinery (Schneider, 2011). There has been some conflicting research about whether tRNAs are imported in their mature state or as precursors. As mentioned in the Introduction, previous studies suggested that in *Trypanosoma* and *Leishmania*, tRNAs can be imported in their precursor form and unsliced form (Hancock *et al.*, 1992; Sbicego *et al.*, 1998; LeBlanc, Yermovsky-Kammerer and Hajduk, 1999), however, later studies refuted these results with evidence that suggested only mature tRNAs are in fact imported (Hauser and Schneider1, 1995; BD and L, 1996; Aphasizhev, Karmarkar and Simpson, 1998; Anne *et al.*, 2000; Kapushoc *et al.*, 2000; Tan *et al.*, 2002). With such ambiguous data, it is difficult to speculate as to how this would be in *T. gondii,* as these questions have not yet been addressed for this model. In light of this, we deemed reasonable to proceed with our tRNA pull down assay as it was performed in the Seidman *et al.*, (2012) study. Nonetheless, this remains a potential point to examine, although, tRNA processing is an entire project altogether. The synthetic biotinylated tRNA we obtained from the Dharmacon company was generated using *T. gondii* sequences which do not have predicted introns. However, these synthetic tRNAs would not possess the many post transcriptional modifications known to be mandatory for tRNA tertiary conformation stability and activity in model organisms. So, their 3D conformation could be tested by tRNA enzymatic probing using nuclease P1 or S1 which cut low complexity regions, and V1 which cuts double-stranded and highly structured regions. This would allow to compare the synthetic tRNA band patterns to the signature bands of mature tRNAs when run on a gel. Using the same enzyme digestion method, interaction with aaRSs can be assessed by performing footprint assays. tRNAs would be incubated with aaRSs before digestion, then band patterns would reflect areas exposed to or protected from the enzymes.

11.3. Bioinformatics screen identified new mitochondrial proteins

Efforts are being made to fill in the gaps of knowledge on mitochondrial biology in apicomplexan parasites, as opposed to the abundance of literature on model organisms such as human, yeast and plants. To fully understand and explore mitochondrial functions it was necessary to create an inventory of experimentally validated mitochondrial proteins. At the beginning of this project no proteomics data such as the mitochondrial proximity tagging based proteome (Seidi, Linden S. Muellner-Wong, *et al.*, 2018) and the LOPIT dataset (Barylyuk *et al.*, 2020) were available. Moreover, even as late at just prior publication of the Lacombe *et al.*, (2019) study, only 88 *Toxoplasma* mitochondrial proteins had been experimentally localised (Mallo *et al.*, 2018) which is expected to be well under the number of mitochondrial proteins based on studies in other organisms. A reason for that is the challenge of establishing a proteome when mitochondria isolation is hindered by its physical association with the apicoplast (Kobayashi *et al.*, 2007; M. Nishi *et al.*, 2008; and unpublished data from Dr. Lilach Sheiner's Laboratory). Strategies to resolve this issue are being explored (Hata, Sato and Kita, 2019), but in the meantime, methods which bypass the reliance on organelle isolation are being explored. Recently, biotin-proximity tagging approaches have made a big step forward by identifying a large proportion of the mitochondrial matrix proteins (Seidi, Linden S. Muellner-Wong, *et al.*, 2018). The number of 421 proposed mitochondrial proteins identified by this method is markedly smaller than the total number of mitochondrial proteins estimated for other species, such as 1060 proteins for *Solanum tuberosum* (potato tubers), 1008 for *T. brucei*, and 1014 for mammalian cells (Panigrahi *et al.*, 2009; Salvato *et al.*, 2014; Marini *et al.*, 2020). Many of the missing proteins are expected to localise to other mitochondrial sub-compartments. In another very recent study, Barylyuk *et al.*, (2020) which assessed the full atlas of organellar proteins in *T. gondii* tachyzoites via localisation of organelle proteins by isotope tagging (hyperLOPIT), a spatial proteomic method which allows identification of thousands of proteins with their respective organelle sub-compartments. Such technique had previously been used for mammalian cells and yeast (Christoforou *et al.*, 2016; Mulvey *et al.*, 2017; Geladaki *et al.*, 2019; Nightingale, Oliver and Lilley, 2019) and was adapted for *T. gondii*. This led to unprecedent advances in the identification of proteins of all cellular compartments and sub-compartments with remarkable accuracy. A total

of 390 mitochondrial proteins were identified, with 8 proteins validated by IFA (Barylyuk *et al.*, 2020). The number of identified mitochondrial proteins still remains smaller than the estimation, and the vast majority still need their localisation to be experimentally validated. In the Sheiner Laboratory, an *in-silico* search utilising a mutual gene-expression pattern and phylogenetic distribution to identify new mitochondrial protein candidates, and tagging was used to validate 11 new *T. gondii* mitochondrial proteins (Figure 8.6A, Lacombe *et al.*, 2019). More than half of them are not present in the Seidi *et al.*, dataset of 421 genes (Table 8.3), as well as in the hyperLOPIT dataset, and 2 of them are not predicted to target the mitochondrion in two different prediction algorithms (Table 8.3). As a result, this search strategy contributes to the ongoing efforts to identify new mitochondrial proteins in the field.

The bioinformatic screen focused on mRNAs that co-express with homologs of the mitochondrial protein import machinery components, some of which were recently validated experimentally (Van Dooren, Stimmler and McFadden, 2006). Authors from this study also identified additional components of the import machinery that were not part our bait list (Van Dooren, Stimmler and McFadden, 2006). Recovering 3 of these 5 new import components in the 279-gene dataset (Table 8.2 bottom) provides support to the power of this strategy to identify mitochondrial protein import components, especially considering none of them are found in five lists of randomly chosen 279 genes from the genome database (Appendix - Table S2 - Sheet 1 - columns F-P). It is hence likely that other proteins known to be involved in protein import may be found in the bioinformatic dataset, which is a point to assess in the future. The study from Van Dooren *et al.*, (2016) also shows that although many canonical protein import homologues can be found in *T. gondii*, with a major component, TgTom40, being of similar size than its yeast counterpart, many cannot be identified via bioinformatics methods, and this is despite the fact the TOM40 complex size as seen by native page is similar to its mammalian homologs (Van Dooren *et al.*, 2016). This finding suggests that it is likely that other unknown components take part in this machinery which may be parasite specific. In the bioinformatic dataset, 109 genes are unique to apicomplexans (Appendix Table 4, column D), providing a pool from which some of those missing pieces may be found. Other characteristics of components of the mitochondrial protein import machinery is absence of a canonical mitochondrial

targeting signal, and presence of transmembrane domains in the membrane integral components. Appendix Table 4 summarises the prediction of these features amongst the 279 genes. Another pathway whose components may co-express with protein import components is MITI (Esseiva *et al.*, 2004; Pino *et al.*, 2010; Sharma and Sharma, 2014), as in some organisms these two pathways are linked (Tschopp, Charrière and Schneider, 2011; Seidman *et al.*, 2012). MITI is likely essential for mitochondrial translation, for which components are enriched in the 43-gene dataset. This dataset was generated by selecting genes from the 279 dataset that have homologs in most apicomplexans and not in *Cryptosporidium* which doesn't have a mitochondrial genome and not expected to perform MITI; and so, we propose these 43 genes as candidate for component of this pathway.

11.4. Defect in mitochondrial morphology is linked with defect in mitochondrial function

In model organisms, organelle morphology and function are tightly linked. The examples for this are numerous, and some classical ones come from the yeast and Drosophila genetics fields where genes were named based on the mitochondrion phenotype of their deletion or over-expression: such as the fusion protein FZO (for "fuzzy onions") (Hales and Fuller, 1997). In another example, a previous study in yeast showed that the protein Mdm10, a subunit of the SAM complex involved in TOM complex assembly, triggers aberrant mitochondrial morphology upon gene deletion (Meisinger *et al.*, 2004). It is hence well accepted that proteins involved in organelle biogenesis influence the organelle's morphology, and protein malfunction typically triggers morphology defect as a result. With plenty of cases like these, we hypothesised that defect in mitochondrial morphology might be a first "marker", or a means to select genes that are likely involved in mitochondrial biogenesis.

Mitochondrial morphology defects were observed qualitatively upon TGME49_214790, TguS15m and TgbL12m depletion, and quantitatively for TGME49_240270 and TgmS35. Given the expected function in mitochondrial translation of TgmS35, which is essential for complex III and IV subunit biogenesis, such phenotype provides support for the relationship between mitochondrial morphology and function in *T. gondii* (Figure 4.3E, Figure 5.5E, Figure 5.6).

Quantitative assessment for TGME49_214790, TguS15m and TgbL12m will be carried out in the future. In addition, with exception of TgbL12 for which no plaque assay was performed due to time constraint, all of these genes were shown to be essential for parasite growth (Figure 9.3D, Figure 10.5D). However, smaller plaques were observed for rTGME49_240270 without ATc compared to the parental line which suggests that the replacement of the native promoter with the repressible one induces some level of toxicity. It would be interesting to assess the basal level of gene expression of the mutant lines compared to the parental line by qPCR as this could be the cause for the loss of fitness. Some genes can also be expressed in a cell cycle dependant manner and replacing them with a constitutive promoter may also affect fitness. By analysing another line where an essential ER protein is depleted, we also demonstrate that this effect is specific to defect in mitochondrial function rather than a general outcome of parasite death (Figure 10.6, Lacombe *et al.*, 2019). Further controls are also being considered for future work to support this, for example analysis of the morphologies of other organelles. Likewise, timing is also a key factor to determine phenotype specificity and the corresponding function. Therefore, assessing parasite growth at earlier time points such as 12, 24, and 48 hours post gene depletion will be carried out in the future.

Overall, as Tgms35 follows the pattern whereby a protein involved in mitochondrial biogenesis would induce a morphology defect upon ablation, observing other proteins with unknown function with such phenotype when depleted may suggests a role in biogenesis as well. In our previous attempts at screening genes from the bioinformatic screen by assessing mitochondrial morphology defect as a "first reporter" for function, it became clear that transient CAS9 expression in *T. gondii* tachyzoites induces mitochondrial morphology defects (Figure 9.1). This observation should be taken into consideration in future studies performed in our field where mitochondrial phenotypes are being analysed under these conditions. Moreover, considering the recent observation of sever nuclear defects resulting from expression of CRISPR-CSA9 (Stortz, 2020), and given that little analysis of other organelles and functions was performed during CRISPR- CSA9 expression, it seems important to execute cautious in any future studies relying on this method.

11.5. Pioneering evidence of the mitoribosome provides support to a translationally active organelle in *T. gondii*

Mitochondrial translation impairment is associated with severe phenotypes in model organisms. In humans, mutations in mitoribosomal proteins, rRNAs, and translation factors are the cause of human multisystemic OXPHOS disorders, such as Leigh's syndrome, sensorineural hearing loss, encephalomyopathy, and hypertrophic cardiomyopathy (Rötig, 2011; De Silva *et al.*, 2015). In plants, mutations in mitochondrial ribosomes have been reported to affect plant growth and development (Robles and Quesada, 2017), and in yeast, this results in growth impairment on non-fermentable carbon sources due to loss of oxygen-consumption capacity (Zeng, Smith and Barrientos, 2018). Needless to say, mitochondrial translation and the role of mitoribosomes in this process is a pivotal pathway and disruptions have severe fitness consequences. This highlights the importance of characterising the mitoribosome of *T. gondii* as it is expected to be just as crucial for the parasite. In addition, there is a wide diversity in the composition and structure-function relationship of mitoribosomes across the eukaryotic tree of life. The plant mitoribosome is much larger and more complex with an expansion of rRNAs and proteins compared to its yeast and mammalian counterpart (Tomal, Kwasniak-Owczarek and Janska, 2019), and certainly compare to its bacterial origin (Greber and Ban, 2016). Yet, an even more unusual mitoribosome was discovered in *T. brucei*. The study showed an evolutionary shift towards a higher ribosome protein and lower RNA content, protein number which surpasses all known eukaryotic organisms, with a total of 127 proteins compared e.g. to 94, 80 and 80 for *A. thaliana, S. cerevisiae and H. sapiens,* respectively (Ramrath *et al.*, 2018; Tomal, Kwasniak-Owczarek and Janska, 2019). This has drastic consequences on the size and structure of these ribosomes. This illustrate the importance of studying basic cellular components in a diverse array of models. These findings further highlight the relevance of studying *T. gondii*'s mitoribosome, firstly as a model for one of the last eukaryotic clade where mitoribosomes have not been assessed, and secondly as a potential therapeutic target due to such diversity as found in trypanosomes.

As a first step towards this aim in apicomplexans, we sought to detect the mitoribosome and validate mitochondrial ribosomal proteins. Amongst 11

mitochondrial confirmed proteins (Figure 8.6A, Figure 10.1A, Lacombe et al., 2019), 4 were predicted to be ribosomal proteins (Table 10.1), and we localised an additional two mitoribosomal predicted proteins (Gupta *et al.*, 2014) (Figure 10.1B, Table 10.1). BN PAGE of endogenously tagged *TgmS35*, *TgbL12m* and *TguL3m* resolved each of them as a part of a macromolecular complex (Figure 10.2B). Although the very high MW makes size estimation approximate, it is clear that both SSU and LSU are a above 1MDa. Co-migration on native PAGE is insufficient to say if the complexes are the same, thus we don't know if the observed size is the size of the full mitoribosome or the size of each SUs which would hence be both of similar sizes. Although, given the size of mitoribosomes from other organisms (2.3 MDa for bacteria, 2.7 MDa for human, 3 MDa for yeast, and 4.5 MDa for *T. brucei*), it is tempting to think that these are the size of each SUs. But with such variations from one organism to another, an exceptionally small mitoribosome should not be excluded. Enrichment of mitochondria encoded rRNA in the TgmS35 IP fraction (Figure 10.4) supports the identity of the mitoribosome observed by BN PAGE. We also show that a co-depletion of *Tg*m*S35* upon depletion of *TguS15m* which reveals that ribosomal protein are essential for the stability of the complexes (Figure 10.5C). These results provide the first direct evidence that, despite the apicomplexan mitochondrial rRNA being fragmented (Namasivayama *et al.*, 2020), mitoribosomes are assembled into stable complexes. This is a major step forward in the study of apicomplexan mitoribosomes which are not well studied and whose composition is not known. While our observation suggests that macro-molecules containing mitochondrial ribosomal proteins form a stable complex, the question of how they assemble and are held together structurally remains open. A recent study identified novel RNA binding proteins in the apicomplexan mitochondrion and proposed the hypothesis that they may participate in ribosome assembly (Hillebrand *et al.*, 2018). The tagged ribosomes we generated here can be used in the future to try tackling the question of mitoribosome structure and function in *T. gondii*. Enrichment of the mitoribosome by IP brings us a step closer to this aim, and function can be assessed with the mutants we generated.

11.6. A new protocol to assess mitochondrial translation in *T. gondii*

Many protocols directly monitoring mitochondrial translation have been established for model organisms. A common method is [^{35}S]methionine/cysteine labelling of newly synthesised mitochondrial polypeptides, in the presence of cytosolic ribosome inhibitors to stop cytosolic translation (Richter *et al.*, 2015). This method cannot be used for apicomplexan parasites due to the presence of the apicoplast, which is an additional translationally active compartment. *In organello* protein synthesis monitoring using isolated intact mitochondria incubated with radiolabeled amino acids is another popular approach in plants, as they also have a translationally active plastid (Kwasniak-Owczarek and Janska, 2014). However, there are no mitochondria isolation protocols in the field that enables the separation of the apicoplast from the mitochondrion. In yeast, a novel system was established which allows monitoring of mitochondrial translation without the use of cytosolic translation inhibitors by inserting a fluorescence-enhanced GFP into the mtDNA. Hence, flow cytometry can be used to analyse mitochondrial translation in live cells (Suhm *et al.*, 2018). Although attractive, this system cannot be adapted to *T. gondii* as well, as there is currently no robust protocol for transfecting apicomplexan mitochondrion. Studying mitochondrial translation in apicomplexans is indeed very challenging. As mentioned above, there are plenty of biological and technical limitations which prevent the establishment of a direct mitochondrial translation assay, and this is a major obstacle to study this important pathway. To date, all evidence in favour of an active mitochondrial translation in apicomplexan mitochondrion are indirect, whether it is MITI (Esseiva *et al.*, 2004; Pino *et al.*, 2010; Sharma and Sharma, 2014), mitochondrially targeted translation factors (Pino *et al.*, 2010), or the finding that atovaquone resistance is acquired through mutation in the mitochondrially encoded Cytb (McFadden *et al.*, 2000). In a recent study, Ke *et al.* (2018) characterised the *P. falciparum* mitochondrial ribosomal protein PfuL13m by monitoring the oxidoreduction catalysed by complex III activity, for which Cytb is mitochondrially encoded, as a read out for mitochondrial translation. PfuL13m depletion, in addition to growth defect, induced a decrease complex III activity, which is reflective of an impaired mitochondrial translation. However, the inability to rescue the growth defect using an mETC bypass route available for the *Plasmodium* asexual stages (Ke *et al.*, 2018) complicates the analysis of phenotype specificity.

In this study, while still indirect, we generated an analytic pipeline which provides specificity for a translation dependent outcome. We established an in-gel complex IV and V activity assay, adapted from yeast protocols (Sabar, Balk and Leaver, 2005), which allows monitoring of translation using mutants. Complex IV activity, for which CoxI and CoxIII are mitochondrially encoded, reflects the mitochondrial translation state, while complex V, entirely nuclear encoded, is used as a control which ensures specificity of the outcome. Results showed that conditional depletion of TgmS35 for 48h results in disruption of the activity of complex IV, while complex V activity remains unchanged (Figure 10.8A). At 96h post TgmS35 depletion, complex IV activity is completely lost which correlates with the disappearance of its corresponding protein band on the Coomassie stained gel, and complex V shows a highly reduced enzymatic activity (Figure 10.8B). These results provide support to the expected role of TgmS35 in translation, and the chronological order of complex IV and V activity disruption validates this assay for detecting translation specific defects. While *TgmS35* depletion disrupts complex IV, the assembly and activity of the TOM complex remains unaffected even 96h after protein loss (Figure 10.8C-E). On the other hand, TGME49_240270 is an example of a gene likely involved in mitochondrial biogenesis, as its depletion affects mitochondrial morphology, but has no role in mitochondrial translation, as complex IV and complex V remain unaffected by its loss (Figure 9.5B).

This set of experiments can, however, be improved. The protein import assay, in particular, has some flaws which are to be discussed. First, a negative control should be added to this experiment in order to interpret the results with more certainty. For instance, repeating this experiment with a mutant for TgTom40 and TgTom22 would give us a reference as to what an impaired import looks like by IFA and western blot (Van Dooren *et al.*, 2016). Second, parasites are transfected with the mitochondrial targeted DHFR construct after initiation of gene knockdown, when the genes studied are essential for parasite fitness. So, one can worry that this could influence the results negatively due to the harsh treatment of parasites already struggling with the loss of an important protein. However, if that had been the case, we would have observed a significant difference between the ratios of cytosolic and mitochondrial product signal of before and after ATc treatment, and results would have most likely shown an import defect. Yet, results have shown that this protocol did not have a negative impact on import.

However, generating stably expressing mitochondrial DHFR construct lines from the mutants would spare parasites additional stress from the electroporation process. Also, the in-gel translation assay cannot provide accurate quantitative measurements due to the non-linear build-up of the signal. There are currently no in solution mETC enzymatic assay for *T. gondii*. Existing assays from other organisms would need to be adapted. Polarographic studies of oxygen consumption and spectrophotometric analysis of the mitochondrial respiratory chain enzymes are classical powerful tools for the biochemical assessment of OXPHOS in cells and mitochondria isolated from cultured cells or tissues in mammalian systems (Barrientos, Fontanesi and Díaz, 2009). These are well-established protocols from which most of our knowledge on the respiratory activity was generated from, and would be helpful for the apicomplexan field. However, the fact that we work with obligated intracellular organisms complicates the experimental design, and although mitochondria isolates are suitable as well, we are still lacking robust methods to achieve high quality mitochondrial purification, which highlights the crucial importance of making this issue a top priority.

Overall, we have established a new specific assay which allows the study of mitochondrial translation in *T. gondii* by assessing respiratory complexes activity directly depend on the translation capacity of the mitochondrion. Activity comparison with that of a complex which does not directly depend on translation ensures specificity of the assay. To our knowledge, this is the first functional characterisation of a mitochondrial ribosomal protein in *T. gondii*. The observations support the role of *Tg*mS35 in the mitochondrial translation machinery. This assay can be used in future studies to assess gene function of proteins with putative roles in mitochondrial translation, as well as the impact of drugs aimed at mitochondrial translation inhibition. It is, however, a laborious protocol which also necessitate an extensive sample preparation, and remains an indirect method to assess mitochondrial translation.

12. Appendix

12.1. Appendix Figures
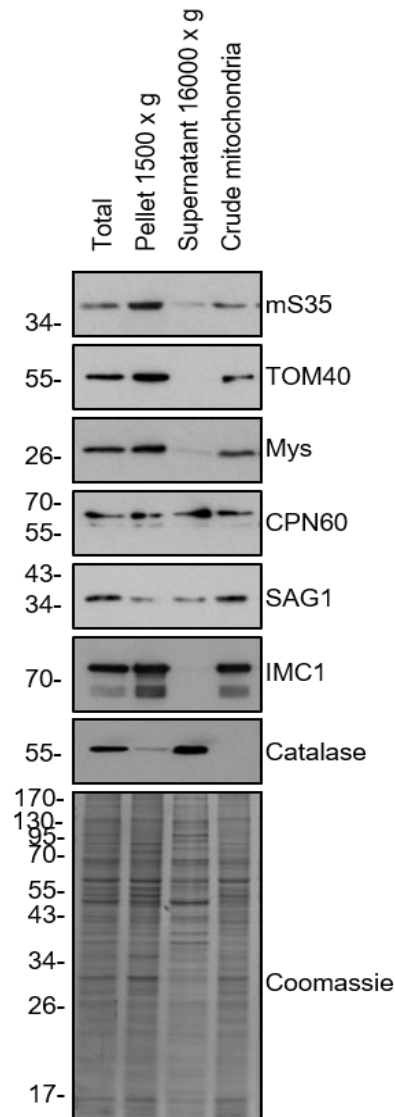
Appendix Figure 12.1 Crude mitochondria fraction assessment by Western blot.
OMM was stained with anti-TgMys and ant-TgTom40, the mitochondrial matrix with anti-HA (TgmS35-3HA), the apicoplast with anti-CPN60, the parasite peripheral membrane with anti-IMC1, and the cytosol with anti-catalase, and plasma membrane with anti-SAG1. Coomassie blue protein staining serves as loading control. This Western blot was performed by Dr. McLean.

A

UniProtKB
P82673 (RT35_HUMAN)
MRPS35

B

```
        10          20          30          40          50
MAAAALPAWL SLQSRARTLR AFSTAVYSAT PVPTPSLPER TPGNERPPRR
        60          70          80          90         100
KALPPRTEKM AVDQDWPSVY PVAAPFKPSA VPLPVRMGYP VKKGVPMAKE
       110         120         130         140         150
GNLELLKIPN FLHLTPVAIK KHCEALKDFC TEWPAALDSD EKCEKHFPIE
       160         170         180         190         200
IDSTDYVSSG PSVRNPRARV VVLRVKLSSL NLDDHAKKKL IKLVGERYCK
       210         220         230         240         250
TTDVLTIKTD RCPLRRQNYD YAVYLLTVLY HESWNTEEWE KSKTEADMEE
       260         270         280         290         300
YIWENSSSER NILETLLQMK AAEKNMEINK EELLGTKEIE EYKKSVVSLK
       310         320
NEEENENSIS QYKESVKRLL NVT
```

Appendix Figure 12.2 Conserved mitochondrial ribosomal protein S24/S35 domain of the human MRS35 protein sequence.
(**A**) Screenshot of the Interpro website search shoeing the conserved S24/S35 domains (InterPro ID: IPR019349). (**B**) MRS35 protein sequence. Red highlight shows the sequence corresponding to the mitochondrial ribosomal protein S24/S35 domain.
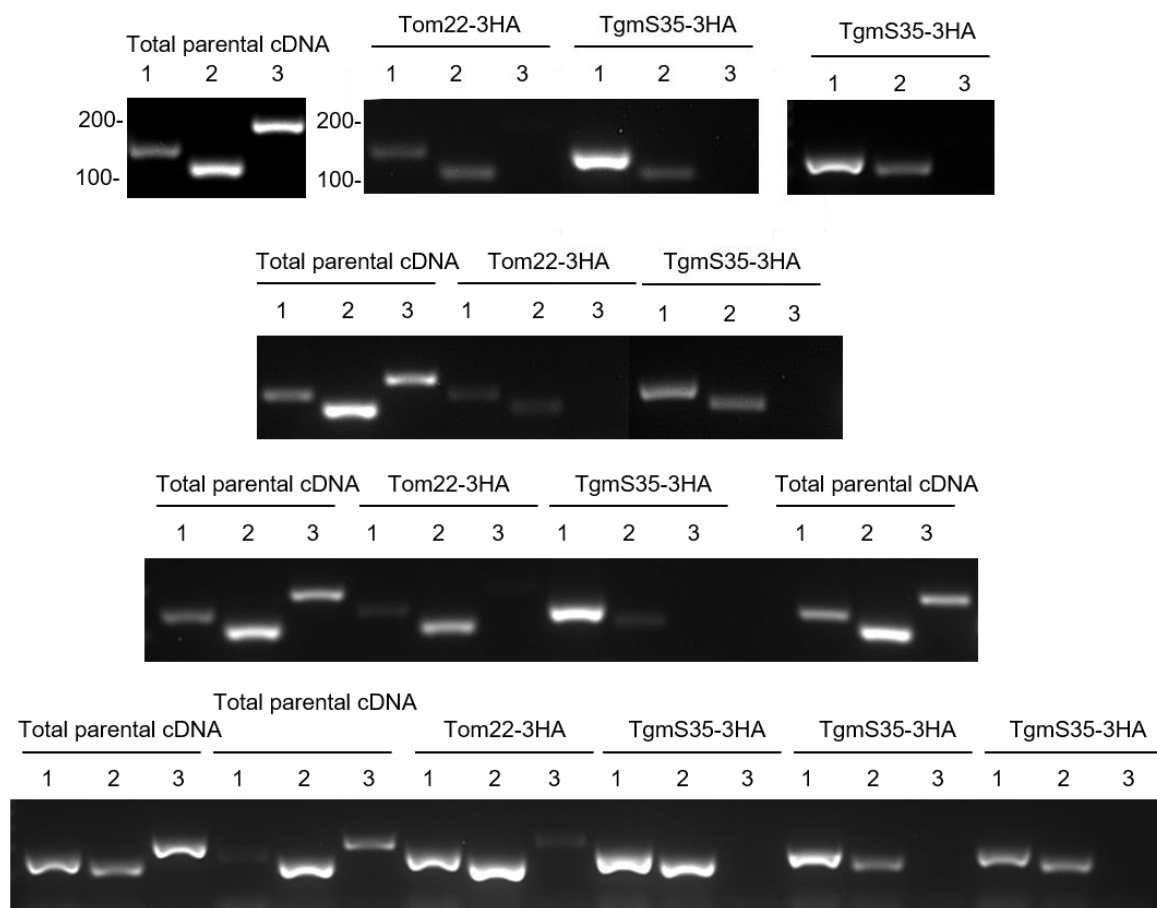
Appendix Figure 12.3 Detection of mitochondrial rRNA in TgmS35 immunoprecipitation elutions.
PCR reactions of all the different repeats of IPs followed by RNA extraction and reverse transcription. PCRs were performed with primers for a (1) mitochondrial rRNA sequence (mito-rRNA), for an (2) apicoplast rRNA sequence (api-rRNA) and for a (3) cytosolic mRNA (actin). Template is RNA extracted from IPs of TgTom22 (Tom22-3HA IP), from IP of TgmS35 (TgmS35-3HA IP) or from total cell lysate of TATiΔku80 (Total parental cDNA)

12.2. Appendix Tables

Appendix Table 1_tRNA affinity IP

Sheet 4 - Met-i & Ile ribosomal protein comparison

Ribosomal protein list									
tRNAMet-i				tRNAIle					
All ribosomal proteins		Mitochondrial ribosomal proteins		All ribosomal proteins		Mitochondrial ribosomal proteins		Mitochondrial ribosomal protein tRNAIle only (minus those found in tRNAMet-i)	
Gene ID	Count	Gene ID	Count	Gene ID	Count	Gene ID	Count	Gene ID	Count
TGME49_215470-t26_1-p1	3	TGME49_288720-t26_1-p1	3	TGME49_254440-t26_1-p1	3	TGME49_288720-t26_1-p1	3	TGME49_207840-t26_1-p1	2
TGME49_288720-t26_1-p1	3	TGME49_238010-t26_1-p1	2	TGME49_262670-t26_1-p1	3	TGME49_207840-t26_1-p1	2	TGME49_245680-t26_1-p1	2
TGME49_299050-t26_1-p1	3	Total	5	TGME49_263050-t26_1-p1	3	TGME49_238010-t26_1-p1	2	TGME49_248390-t26_1-p1	2
TGME49_204020-t26_1-p1	2			TGME49_263700-t26_1-p1	3	TGME49_245680-t26_1-p1	2	TGME49_266070-t26_1-p1	2
TGME49_225080-t26_1-p1	2			**TGME49_284560-t26_1-p1**	**3**	TGME49_248390-t26_1-p1	2	TGME49_267060-t26_1-p1	2
TGME49_226970-t26_1-p1	2			TGME49_288720-t26_1-p1	3	TGME49_266070-t26_1-p1	2	Total	10
TGME49_238010-t26_1-p1	2			TGME49_204020-t26_1-p1	2	TGME49_267060-t26_1-p1	2		
TGME49_242330-t26_1-p1	2			TGME49_205340-t26_1-p1	2	Total	15		
TGME49_245460-t26_1-p1	2			TGME49_207840-t26_1-p1	2				
TGME49_254440-t26_1-p1	2			TGME49_225080-t26_1-p1	2				
TGME49_262670-t26_1-p1	2			TGME49_226970-t26_1-p1	2				
TGME49_263050-t26_1-p1	2			TGME49_238010-t26_1-p1	2				
TGME49_263700-t26_1-p1	2			TGME49_239100-t26_1-p1	2				
TGME49_292130-t26_1-p1	2			TGME49_242330-t26_1-p1	2				
TGME49_314810-t26_1-p1	2			TGME49_245680-t26_1-p1	2				
Total	33			TGME49_248390-t26_1-p1	2				
				TGME49_266070-t26_1-p1	2				
				TGME49_267060-t26_1-p1	2				
				TGME49_292130-t26_1-p1	2				
				TGME49_299050-t26_1-p1	2				
				TGME49_313390-t26_1-p1	2				
				Total	48				

Sheet 1 - All tRNAMet-i hits

	E	F	G	H	I	J	K	L	M	N	O
					Counting of protein occurrence in 5 experiments - tRNAMet-i						
	Accession	**Description**	**Counts**	**Phenotype score**	**Mitochondrial localisation prediction**					**Proteome**	**LOPIT**
					TargetP-2.0	MitoFates	MitoProt	iPSORT	Predotar		
	TGME49_215470-t26_1-p1	ribosomal protein RPL10A	3	-4.94	0	0	0.1747	n	0.01	n*	60S ribosome
	TGME49_227620-t26_1-p1	dense granule protein GRA2	3	2.47	0.0021	0.012	0.0828	n	0.03	n*	Dense granules
	TGME49_230410-t26_1-p1	peroxiredoxin PRX3	3	0.4	0.925	0.572	0.7079	y	0.34	y	mitochondrial membrane/soluble
	TGME49_235402-t26_1-p1	CorA family Mg2+ transporter protein	3	-1.57	0.065	0.065	0.9724	y	0.69	n*	n
	TGME49_247520-t26_1-p1	hypothetical protein	3	0.68	0.0001	0.035	0.1721	y	0.03	n*	Roprties 1
	TGME49_248160-t26_1-p1	hypothetical protein	3	-0.75	0.0001	0.018	0.9997	y	0.01	n	n
	TGME49_288720-t26_1-p1	ribosomal protein RPL10	3	-5.3	0.0044	0.056	0.8855	y	0.18	n*	60S ribosome
	TGME49_292320-t26_1-p1	hypothetical protein	3	-1.16	0	0	0.0371	n	0.01	n	n
	TGME49_299050-t26_1-p1	ribosomal protein RPL17	3	-5.22	0	0.029	0.0649	n	0.01	n*	60S ribosome
	TGME49_300100-t26_1-p1	rhoptry neck protein RON2	3	-4.63	0.0447	0.005	0.8701	n	0.03	n*	Roprties 1
	TGME49_308090-t26_1-p1	rhoptry protein ROP5	3	n	0.0034	0.181	0.8194	n	0.07	n*	Roprties 1
	TGME49_311470-t26_1-p1	rhoptry neck protein RON5	3	-4.34	0.0012	0.042	0.7307	n	0.04	n*	Roprties 1
	TGME49_286630-t26_1-p1	redoxin domain-containing protein	3	1.57	0.2014	0.403	0.9887	y	0.57	n*	Apicoplast
	TGME49_203050-t26_1-p1	AP2 domain transcription factor AP2VIIa-6	2	1.27	0	0	0.1805	n	0.01	n	n
	TGME49_257090-t26_1-p1	NAC domain-containing protein	2	n	0.0004	0.005	0.0402	n	0.01	y	cytosol
	TGME49_257430-t26_1-p1	hypothetical protein	2		0	0	0.0756	n	0.01	n	Apical 1
	TGME49_286420-t26_1-p1	elongation factor 1-alpha (EF-1-ALPHA), p	2		0	0	0.0099	n	0.01	n	n
	TGME49_313380-t26_1-p1	hypothetical protein	2		0	0	0.3062	n	0.04	n*	IMC
	TGME49_313590A-t26_1-p1	**hypothetical protein**	**2**		**0.0073**	**0.055**	**0.0297**	**y**	**0.03**	**n**	**Nucleus - chromatin**
	TGME49_203310-t26_1-p1	**dense granule protein GRA7**	**2**		**0.0008**	**0.003**	**0.1662**	**n**	**0.03**	**n***	**Dense granules**
	TGME49_204020-t26_1-p1	ribosomal protein RPL8	2		0.0683	0.01	0.954	n	0.12	n	60S ribosome
	TGME49_206650-t26_1-p1	zinc finger, c2h2 type domain-containing	2		0	0	0.0214	n	0.01	n	n
	TGME49_214080-t26_1-p1	toxofilin	2		0.0014	0	0.0273	n	0.02	n*	Roprties 1
	TGME49_214770-t26_1-p1	small GTP binding protein rab1a, putative	2		0.0001	0	0.0092	n	0.01	n*	Golgi
	TGME49_215980-t26_1-p1	hypothetical protein	2	2.11	0.0028	0.094	0.0744	n	0.02	n*	Dense granules
	TGME49_217890-t26_1-p1	alkyl hydroperoxide reductase/ Thiol spec	2		0.0009	0	0.9986	y	0.01	n*	Nucleus - non-chromatin
	TGME49_218260-t26_1-p1	histone H3.3	2		0.0009	0.117	0.9986	y	0.11	n	n
	TGME49_220100-t26_1-p1	phosphoribosylpyrophosphate synthetase	2		0.1629	0.345	0.6432	n	0.21	y	Mitochondrion - soluble
	TGME49_224900-t26_1-p1	adenylate kinase, putative	2		0	0	0.0411	n	0.01	n*	Mitochondrion - soluble
	TGME49_225080-t26_1-p1	ribosomal protein RPS18	2		0.002	0.027	0.161	n	0.01	n*	40S ribosome
	TGME49_226970-t26_1-p1	ribosomal protein RPS11	2		0.0002	0.021	0.0475	n	0.01	n*	40S ribosome
	TGME49_227280-t26_1-p1	dense granule protein GRA3	2		0.0047	0.011	0.6987	n	0.01	n*	Dense granules
	TGME49_232410-t26_1-p1	PDI family protein	2		0.0008	0	0.0384	n	0.01	n	Tubulin cytoskeleton
	TGME49_232940-t26_1-p1	heat shock protein HSP20	2		0	0	0.0157	n	0.01	n*	n
	TGME49_238010-t26_1-p1	ribosomal protein RPL23A	2		0.0001	0.03	0.9975	n	0.35	n*	60S ribosome
	TGME49_242330-t26_1-p1	ribosomal protein RPS5	2		0	0	0.0586	n	0.01	n*	40S ribosome
	TGME49_245460-t26_1-p1	ribosomal protein RPS8	2		0	0.007	0.0586	n	0.01	n*	40S ribosome
	TGME49_248880-t26_1-p1	GTPase RAB7	2		0	0.005	0.1029	n	0.01	n*	PM - integral
	TGME49_251810-t26_1-p1	translation initiation factor eIF-5A, putativ	2		0	0	0.021	n	0.01	n*	Cytosol
	TGME49_254440-t26_1-p1	ribosomal protein RPL12	2		0.0002	0.006	0.1688	n	0.01	n*	60S ribosome
	TGME49_261580-t26_1-p1	histone H2AX	2		0.0002	0.017	0.9987	n	0.02	n*	Nucleus - chromatin
	TGME49_262620-t26_1-p1	**RNA recognition motif-containing protein**	**2**		**0**	**0**	**0.111**	**n**	**0.01**	**n***	**Nucleus - non-chromatin**
	TGME49_262670-t26_1-p1	ribosomal protein RPL18A	2		0.0006	0	0.0839	n	0.01	n*	60S ribosome
	TGME49_263050-t26_1-p1	ribosomal protein RPL13	2		0.0015	0.01	0.0294	y	0.01	n*	60S ribosome
	TGME49_263700-t26_1-p1	ribosomal protein RPS14	2		0.0027	0	0.0539	n	0.01	n*	40S ribosome
	TGME49_264040-t26_1-p1	hypothetical protein	2		0.9937	0.921	0.8872	n	0.56	y	mitochondrion - membranes
	TGME49_276140-t26_1-p1	ADP ribosylation factor ARF1	2		0.0003	0.049	0.6436	n	0.03	n*	Nucleus - chromatin
	TGME49_277740-t26_1-p1	zinc finger, C3HC4 type (RING finger) dom	2		0.0002	0	0.0144	n	0.04	n	n
	TGME49_289680-t26_1-p1	Ras-related protein Rab11	2		0	0	0.1504	n	0.01	n*	PM - integral
	TGME49_289750-t26_1-p1	ribosomal-ubiquitin protein RPL40	2		0.0005	0.017	0.0913	n	0.01	n*	Nucleus - chromatin
	TGME49_292130-t26_1-p1	ribosomal protein RPL13A	2		0.0078	0.007	0.0607	n	0.01	n*	60S ribosome
	TGME49_297430-t26_1-p1	hypothetical protein	2		0.0048	0.869	1	n	0.42	n*	Nucleus - non-chromatin
	TGME49_300200-t26_1-p1	histone H2AZ	2		0	0.024	0.8826	n	0.01	n*	Nucleus - chromatin
	TGME49_300280-t26_1-p1	LSM domain-containing protein	2		0.0441	0.199	0.3611	y	0.19	n*	Nucleus - non-chromatin
	TGME49_307810-t26_1-p1	**hypothetical protein**	**2**		**0**	**0**	**0.0416**	**n**	**0.01**	**y**	**Nucleus - chromatin**
	TGME49_314810-t26_1-p1	ribosomal protein RPL7	2		0.0006	0.276	0.2185	n	0.06	n*	60S ribosome

Mitochondrial logarithm prediction

	Sorting		Likely mitochondrial (≥	Possibly mitochondrial (≥	Combined mitochondrial	Elsewhere	All proteins	
			13	14	27	98	125	<-- Count nb
	8.712671 Ch	10.71428571	10.4	11.2	21.6	78.4	100	<-- Count %

Hits found in hyperLOPIT

Mitochondrial	Apicoplast	ribosomes	Nucleus	Roptries		Dense granu	Cytosol	IMC	Plasma m	N/A	Elsewhere	Total	
9	3	33	20	14		9	4	2	4	21	6	125	<-- Count nb
7.2	2.4	26.4	16.0	11.2		7.2	3.2	1.6	3.2	16.8	4.8	100.0	<-- Count %

Ribosomal protein list

All ribosomal proteins		Predicted mitochondrial ribosomal proteins	
Gen ID	count	Gen ID	count
TGME49_215470-t26_	3	TGME49_288720-t26_1-p	3
TGME49_288720-t26_	3	TGME49_238010-t26_1-p	2
TGME49_299050-t26_	3	Total	5
TGME49_204020-t26_	2		
TGME49_225080-t26_	2		
TGME49_226970-t26_	2		
TGME49_238010-t26_	2		
TGME49_242330-t26_	2		
TGME49_245460-t26_	2		
TGME49_254440-t26_	2		
TGME49_262670-t26_	2		
TGME49_263050-t26_	2		
TGME49_263700-t26_	2		
TGME49_292130-t26_	2		
TGME49_314810-t26_	2		
Total	33		

Mitochondrial ribosomal proteins

Count nb	5.00	<-- Count nb
Predicted mitochondri	15.15	<-- Count %
Predicted other compa	84.85	<-- Count %
From all proteins	4.00	<-- Count %
From mitochondrial pr	18.52	<-- Count %

Ribosomal proteins
tRNAMet-i

- Predicted mitochondrial
- Predicted other compartment

Sheet 2 - All tRNAIle hits

Counting of protein occurrence in 5 experiments - tRNAIle

Predicted localisation

Accession	Description	Counts	Phenotype score	TargetP-2.0	MitoFates	MitoProt	iPSORT	Predotar	Proteome	LOPIT
TGME49_235402-t26_1-p1	CorA family Mg2+ transporter prote	5	-1.57	0.065	0.065	0.9724	y	0.69	n*	n
TGME49_248160-t26_1-p1	hypothetical protein	5	-0.75	0	0.018	0.9997	y	0.01	n	n
TGME49_215980-t26_1-p1	hypothetical protein	4	2.11	0.0028	0.094	0.0744	n	0.02	n*	Dense granules
TGME49_292320-t26_1-p1	hypothetical protein	4	-1.16	0	0	0.0371	n	0.01	n	n
TGME49_203050-t26_1-p1	AP2 domain transcription factor AP2	3	1.27	0	0	0.1805	n	0.01	n	n
TGME49_218260-t26_1-p1	histone H3.3	3		0.0009	0.117	0.9986	n	0.11	n	n
TGME49_230410-t26_1-p1	peroxiredoxin PRX3	3	0.4	0.925	0.572	0.7079	y	0.34	y	mitochondrial membrane/soluble
TGME49_232940-t26_1-p1	heat shock protein HSP20	3		0	0	0.0157	n	0.01	n	n
TGME49_254440-t26_1-p1	ribosomal protein RPL12	3		0.0002	0.006	0.1688	n	0.01	n*	60S ribosome
TGME49_261250-t26_1-p1	histone H2A1	3		0.0015	0.003	0.0693	n	0.01	n*	Nucleus
TGME49_261580-t26_1-p1	histone H2AX	3		0.0002	0.017	0.9987	n	0.02	n*	Nucleus - chromatin
TGME49_262670-t26_1-p1	ribosomal protein RPL18A	3		0.0006	0	0.0839	n	0.01	n*	60S ribosome
TGME49_263050-t26_1-p1	ribosomal protein RPL13	3		0.0015	0.01	0.0294	n	0.01	n*	60S ribosome
TGME49_263700-t26_1-p1	ribosomal protein RPS14	3		0.0027	0	0.0539	n	0.01	n*	40S ribosome
TGME49_271050-t26_1-p1	SAG-related sequence SRS34A	3		0.0001		0.1476	n	0.02	n*	PM-peripheral 1
TGME49_284560-t26_1-p1	ribosomal protein RPL9	3	-5.37	0.0005	0.016	0.0453	y	0.01	y	60S ribosome
TGME49_288720-t26_1-p1	ribosomal protein RPL10	3	-5.3	0.0044	0.056	0.8855	y	0.18	n*	60S ribosome
TGME49_289750-t26_1-p1	ribosomal-ubiquitin protein RPL40	3		0.0005	0.017	0.0913	n	0.01	n*	Nucleus - chromatin
TGME49_300200-t26_1-p1	histone H2AZ	3		0	0.024	0.8826	n	0.01	n*	Nucleus - chromatin
TGME49_324600-t26_1-p1	heat shock protein	3		0.0005	0.07	0.4675	n	0.01	n	IMC
TGME49_204020-t26_1-p1	ribosomal protein RPL8	2		0.0683	0.01	0.954	n	0.12	n*	60S ribosome
TGME49_205340-t26_1-p1	ribosomal protein RPS12	2		0	0	0.0345	n	0.01	n*	40S ribosome
TGME49_205580-t26_1-p1	nuclear factor NF4	2		0.023	0	0.4264	y	0.01	y	Nucleus-chromatin
TGME49_207840-t26_1-p1	ribosomal protein RPS17	2	-3.75	0.0252	0.505	0.947	y	0.25	n*	40S ribosome
TGME49_209690-t26_1-p1	small nuclear ribonucleoprotein	2		0.0002	0	0.266	n	0.01	y	Nucleus - non-chromatin
TGME49_214080-t26_1-p1	toxofilin	2		0.0014		0.0273	n	0.01	n*	Roprties 1
TGME49_219470-t26_1-p1	hypothetical protein	2		0.2902	0.156	0.4877	y	0.70	n	n
TGME49_220950-t26_1-p1	hypothetical protein	2		0.0535	0.012	0.0567	n	0.01	y	Dense granules
TGME49_225080-t26_1-p1	ribosomal protein RPS18	2		0.002	0.027	0.161	n	0.01	n*	40S ribosome
TGME49_226000-t26_1-p1	ATP synthase, putative	2		0.9967	0.98	0.5791	y	0.80	y	Mitochondrion - membranes
TGME49_226970-t26_1-p1	ribosomal protein RPS11	2		0.0002	0.021	0.0475	n	0.01	n*	40S ribosome
TGME49_227280-t26_1-p1	dense granule protein GRA3	2		0.0047	0.011	0.6987	n	0.01	n*	Dense granules
TGME49_227620-t26_1-p1	dense granule protein GRA2	2	2.47	0.0021	0.012	0.0828	n	0.03	n*	Dense granules
TGME49_227820-t26_1-p1	hypothetical protein	2		0	0	0.1274	n	0.01	n	Endomembrane vesicles
TGME49_227970-t26_1-p1	histone family DNA-binding protein	2		0.0053	0	0.0165	n	0.01	n*	Apicoplast
TGME49_230160-t26_1-p1	hypothetical protein	2		0.0049	0.054	0.0809	n	0.01	n*	IMC
TGME49_231815-t26_1-p1	hypothetical protein	2		0	0	0.0457	n	0.01	n*	n
TGME49_232410-t26_1-p1	PDI family protein	2		0.0008	0	0.0384	n	0.01	n	Tubulin cytoskeleton
TGME49_238010-t26_1-p1	ribosomal protein RPL23A	2		0.0001	0.03	0.9975	n	0.35	n*	60S ribosome
TGME49_239100-t26_1-p1	ribosomal protein RPS7	2		0.0002	0.005	0.0242	n	0.01	n*	40S ribosome
TGME49_242330-t26_1-p1	ribosomal protein RPS5	2		0	0	0.0586	n	0.01	n*	40S ribosome
TGME49_245680-t26_1-p1	ribosomal protein RPL21	2	-3.65	0.0303	0.807	0.9997	y	0.19	n*	60S ribosome
TGME49_246540-t26_1-p1	cytochrome c1, heme protein	2		0.0001	0.035	0.013	n	0.02	y	Mitochondrion - membranes
TGME49_247520-t26_1-p1	hypothetical protein	2	0.68	0.0001	0.035	0.1721	n	0.03	n*	Roprties 1
TGME49_248390-t26_1-p1	ribosomal protein RPL26	2	-3.23	0.0321	0.176	0.9914	y	0.19	n*	60S ribosome
TGME49_251870-t26_1-p1	histone H2Bb	2		0.0004	0	0.0986	n	0.1	n*	Nucleus - chromatin
TGME49_253740-t26_1-p1	hypothetical protein	2		0	0	0.3953	n	0.01	n*	n
TGME49_259640-t26_1-p1	nucleoporin autopeptidase	2		0.0001	0.003	0.0085	n	0.01	n*	Nucleus - chromatin
TGME49_266070-t26_1-p1	ribosomal protein RPL31	2	-3.75	0.0049	0.107	0.9486	y	0.05	n*	60S ribosome
TGME49_267060-t26_1-p1	ribosomal protein RPL14	2	-3.07	0.0061	0.349	0.0575	y	0.14	n*	60S ribosome
TGME49_267660-t26_1-p1	hypothetical protein	2		0	0	0.0062	n	0.01	n*	Nucleolus
TGME49_286450-t26_1-p1	dense granule protein GRA5	2		0.0015	0.014	0.0435	n	0.03	n	Dense granules
TGME49_286630-t26_1-p1	redox domain-containing protein	2	1.57	0.2014	0.403	0.9887	y	0.57	n*	Apicoplast
TGME49_291960-t26_1-p1	rhoptry kinase family protein ROP40	2		0.0015	0.012	0.3999	n	0.01	n*	Roprties 1
TGME49_292130-t26_1-p1	ribosomal protein RPL13A	2		0.0078	0.007	0.0607	n	0.01	n*	60S ribosome
TGME49_297780-t26_1-p1	ATPase/histidine kinase/DNA gyrase	2		0	0	0.0949	n	0.11	n	Apicolplast
TGME49_299050-t26_1-p1	ribosomal protein RPL17	2	-5.22	0	0.029	0.0649	n	0.01	n*	60S ribosome
TGME49_300100-t26_1-p1	rhoptry neck protein RON2	2	-4.63	0.0447	0.005	0.8701	n	0.19	n*	Roprties 1
TGME49_300280-t26_1-p1	LSM domain-containing protein	2		0.0441	0.199	0.3611	y	0.19	n*	Nucleus - non-chromatin
TGME49_308090-t26_1-p1	rhoptry protein ROP5	2	n	0.0034	0.181	0.8194	n	0.07	n*	Roprties 1
TGME49_313390-t26_1-p1	ribosomal protein RPL6	2		0.0029	0.004	0.0324	n	0.01	n*	60S ribosome
TGME49_315610-t26_1-p1	hypothetical protein	2		0.0011	0.692	0.9996	y	0.20	n*	Nucleolus

Mitochondrial logarithm prediction

	Sorting		Likely mitochondrial (≥3 algorithms with scores of ≥0.5)	Possibly mitochondrial (≥2 algorithms with scores of ≥0.3)	Combined mitochondrial	Elsewhere	All proteins	
	9		20	23	43	107	150	<-- Count nb
	12.90322581	14.51612903	13.33333333	15.33333333	28.66666667	71.33333333	100	<-- Count %

Hits found in hyperLOPIT

Mitochondrial	Apicoplast	ribosomes	Nucleus	Roptries	Dense granules	Cytosol	IMC	Plasma membrane	N/A	Elsewhere	
7	6	48	26	10	12	0	5	3	29	4	150.00 <-- Count nb
4.67	4.00	32.00	17.33	6.67	8.00	0.00	3.33	2.00	19.33	2.67	100.00 <-- Count %

Ribosomal protein list

All ribosomal proteins		Predicted mitochondrial ribosomal proteins	
Gen ID	count	Gen ID	count
TGME49_254440-t26	3	TGME49_288720-t26_1-p1	3
TGME49_262670-t26	3	TGME49_207840-t26_1-p1	2
TGME49_263050-t26	3	TGME49_238010-t26_1-p1	2
TGME49_263700-t26	3	TGME49_245680-t26_1-p1	2
TGME49_284560-t26	3	TGME49_248390-t26_1-p1	2
TGME49_288720-t26	3	TGME49_266070-t26_1-p1	2
TGME49_204020-t26	2	TGME49_267060-t26_1-p1	2
TGME49_205340-t26	2	Total	15
TGME49_207840-t26	2		
TGME49_225080-t26	2		
TGME49_226970-t26	2		
TGME49_238010-t26	2		
TGME49_239100-t26	2		
TGME49_242330-t26	2		
TGME49_245680-t26	2		
TGME49_248390-t26	2		
TGME49_266070-t26	2		
TGME49_267060-t26	2		
TGME49_292130-t26	2		
TGME49_299050-t26	2		
TGME49_313390-t26	2		
Total	48		

Mitochondrial ribosomal proteins		
Count nb	15	<-- Count nb
Predicted mitochond	31.25	<-- Count %
Predicted other com	68.75	<-- Count %
From all proteins	10.0	<-- Count %
From mitochondrial	34.883721	<-- Count %

Ribosomal proteins tRNAIle

- Predicted mitochondrial
- Predicted other compartment

Sheet 3 - Hits found in tRNAIle only

| | | | | | | Ile | | | | Predicted localisation | | | |

Accession	Description	Counts	Sort	Score	Phenotype score (<-2 is essential)	TargetP-2.0	MitoFates	MitoProt	iPSORT	Predotar	cNLS Mapper (>4.5)	Proteome	hyperLOPIT
TGME49_219470-t26_1-p1	hypothetical protein	2	0	15-15	-0.47	0.2902	0.156	0.4877	y	0,70	n	n	n
TGME49_220950-t26_1-p1	hypothetical protein	2	0	73-41	2.13	0.0535	0.012	0.0567	n	0.01	n	n*	Dense granules
TGME49_246540-t26_1-p1	cytochrome c1, heme protein	2	0	18-30	-4.36	0.0001	0.035	0.013	n	0.02	n	y	Mitochondrion - membranes
TGME49_253740-t26_1-p1	hypothetical protein	2	0	23-29	-4.72	0	0	0.3953	n	0.01	y	n*	n
TGME49_259640-t26_1-p1	nucleoporin autopeptidase	2	0	30-22	-4.08	0.0001	0.003	0.0085	n	0.01	y	n*	Nucleus - chromatin
TGME49_267660-t26_1-p1	hypothetical protein	2	0	22-22	-2.76	0	0	0.0062	n	0.01	y	n	Nucleolus
TGME49_297780-t26_1-p1	ATPase/histidine kinase/DNA gyrase B	2	0	37-32	-2.93	0	0	0.0949	n	0,11	n	n	Apicolplast
TGME49_200360-t26_1-p1	hypothetical protein	1	0										
TGME49_203150-t26_1-p1	hypothetical protein	1	0										
TGME49_203200-t26_1-p1	hypothetical protein	1	0										
TGME49_204440-t26_1-p1	cyclic nucleotide-binding domain-contai	1	0										
TGME49_209910-t26_1-p1	histone H2Bv	1	0										
TGME49_212310-t26_1-p1	vacuolar ATP synthetase	1	0										
TGME49_213040-t26_1-p1	hypothetical protein	1	0										
TGME49_214930-t26_1-p1	hypothetical protein	1	0										
TGME49_217740-t26_1-p1	3-ketoacyl-(acyl-carrier-protein) reducta	1	0										
TGME49_221280-t26_1-p1	hypothetical protein	1	0										
TGME49_223050-t26_1-p1	ribosomal protein RPS20	1	0										
TGME49_223920-t26_1-p1	rhoptry neck protein RON3	1	0										
TGME49_225200-t26_1-p1	hypothetical protein	1	0										
TGME49_225790-t26_1-p1	PDI family protein	1	0										
TGME49_226020-t26_1-p1	transporter, major facilitator family prot	1	0										
TGME49_226430-t26_1-p1	reticulon protein	1	0										
TGME49_226790-t26_1-p1	ABC transporter, ATP-binding domain-cc	1	0										
TGME49_231910-t26_1-p1	ATP synthase F1 gamma subunit	1	0										
TGME49_235540-t26_1-p1	eukaryotic initiation factor-2 beta, putat	1	0										
TGME49_236160-t26_1-p1	hypothetical protein	1	0										
TGME49_237860-t26_1-p1	protein kinase domain-containing protei	1	0										
TGME49_244080-t26_1-p1	hypothetical protein	1	0										
TGME49_244720-t26_1-p1	hypothetical protein	1	0										
TGME49_244732-t26_1-p1	hypothetical protein	1	0										
TGME49_245580-t26_1-p1	hypothetical protein	1	0										
TGME49_247610-t26_1-p1	small nuclear ribonucleoprotein E, putat	1	0										
TGME49_253430-t26_1-p1	asparagine synthetase, putative	1	0										
TGME49_254470-t26_1-p1	hypothetical protein	1	0										
TGME49_258480-t26_1-p1	hypothetical protein	1	0										
TGME49_260210-t26_1-p1	DnaJ domain-containing protein	1	0										
TGME49_260800-t26_1-p1	hypothetical protein	1	0										
TGME49_261440-t26_1-p1	ARM repeats containing protein	1	0										
TGME49_262040-t26_1-p1	SAC3/GANP family protein	1	0										
TGME49_262510-t26_1-p1	GTP-binding protein engB, putative	1	0										
TGME49_262880-t26_1-p1	hypothetical protein	1	0										
TGME49_263080-t26_1-p1	hypothetical protein	1	0										
TGME49_264660-t26_1-p1	SAG-related sequence SRS44	1	0										
TGME49_267420-t26_1-p1	mago nashi family protein 2, putative	1	0										
TGME49_269200-t26_1-p1	crooked neck family 1 protein isoform 2	1	0										
TGME49_269350-t26_1-p1	hypothetical protein	1	0										
TGME49_270070-t26_1-p1	synaptobrevin family protein	1	0										
TGME49_273090-t26_1-p1	cell division protein CDC48CY	1	0										
TGME49_273740-t26_1-p1	acetyl-CoA acyltransferase B, putative	1	0										
TGME49_273930-t26_1-p1	DNA topoisomerase domain-containing	1	0										
TGME49_277270-t26_1-p1	NTPase II	1	0										
TGME49_279100-t26_1-p1	hypothetical protein	1	0										
TGME49_282180-t26_1-p1	hypothetical protein	1	0										
TGME49_285830-t26_1-p1	hypothetical protein	1	0										
TGME49_286650-t26_1-p1	hypothetical protein	1	0										
TGME49_286710-t26_1-p1	zinc finger, c2h2 type domain-containin	1	0										
TGME49_288380-t26_1-p1	heat shock protein HSP90	1	0										
TGME49_288750-t26_1-p1	ubiquinol-cytochrome c reductase	1	0										
TGME49_288960-t26_1-p1	hypothetical protein	1	0										
TGME49_290225-t26_1-p1	hypothetical protein	1	0										
TGME49_295350-t26_1-p1	nucleoside diphosphate kinase, putative	1	0										
TGME49_305290-t26_1-p1	vacuolar atp synthase subunit e, putativ	1	0										
TGME49_306460-t26_1-p1	bromodomain-containing protein	1	0										
TGME49_309590-t26_1-p1	rhoptry protein ROP1	1	0										
TGME49_309760-t26_1-p1	hypothetical protein	1	0										
TGME49_310640-t26_1-p1	phosphorylase family protein	1	0										
TGME49_312480-t26_1-p1	uracil phosphoribosyltransferase FUR1,	1	0										
TGME49_312530-t26_1-p1	splicing factor, CC1 family protein	1	0										
TGME49_313070-t26_1-p1	hypothetical protein	1	0										
TGME49_313600-t26_1-p1	DDHD domain-containing protein	1	0										
TGME49_313852-t26_1-p1	hypothetical protein	1	0										
TGME49_314487-t26_1-p1	hypothetical protein	1	0										
TGME49_315720-t26_1-p1	Smg-4/UPF3 family protein	1	0										
TGME49_315830-t26_1-p1	hypothetical protein	1	0										
TGME49_316330-t26_1-p1	superoxide dismutase SOD2	1	0										
TGME49_316540-t26_1-p1	IMC sub-compartment protein ISP3	1	0										
TGME49_323110-t26_1-p1	hypothetical protein	1	0										
TGME49_410370-t26_1-p1	putative transmembrane protein	1	0										
TGME49_411760-t26_1-p1	actin	1	0										
TGME49_202572-t26_1-p1	ribophorin i protein	1	0										
TGME49_212990-t26_1-p1	hypothetical protein	1	0										
TGME49_217800-t26_1-p1	hypothetical protein	1	0										
TGME49_219650-t26_1-p1	transporter, small conductance mechan	1	0										
TGME49_219832-t26_1-p1	cyclin-dependent kinase regulatory subu	1	0										
TGME49_222330-t26_1-p1	hypothetical protein	1	0										
TGME49_223450-t26_1-p1	ubiquitin carboxyl-terminal hydrolase	1	0										
TGME49_223810-t26_1-p1	hypothetical protein	1	0										
TGME49_226330-t26_1-p1	hypothetical protein	1	0										
TGME49_228660-t26_1-p1	Sec7 domain-containing protein	1	0										
TGME49_230110-t26_1-p1	hypothetical protein	1	0										
TGME49_230830-t26_1-p1	ATPase family associated with various c	1	0										
TGME49_231970-t26_1-p1	pre-mRNA processing splicing factor PRI	1	0										
TGME49_234230-t26_1-p1	hypothetical protein	1	0										
TGME49_247700-t26_1-p1	AP2 domain transcription factor AP2XII-	1	0										
TGME49_251460-t26_1-p1	hypothetical protein	1	0										
TGME49_253790-t26_1-p1	zinc finger (CCCH type) motif-containing	1	0										
TGME49_262710-t26_1-p1	Ctr copper transporter family protein	1	0										
TGME49_265190-t26_1-p1	Ulp1 protease family, C-terminal catalyt	1	0										
TGME49_266830-t26_1-p1	Sec7 domain-containing protein	1	0										
TGME49_267855-t26_1-p1	hypothetical protein	1	0										
TGME49_272300-t26_1-p1	hypothetical protein	1	0										
TGME49_275420-t26_1-p1	histone lysine-specific demethylase LSD:	1	0										
TGME49_276155-t26_1-p1	hypothetical protein	1	0										
TGME49_288520-t26_1-p1	ATPase, AAA family protein	1	0										
TGME49_291880-t26_1-p1	hypothetical protein	1	0										
TGME49_293370-t26_1-p1	histone arginine methyltransferase PRM	1	0										
TGME49_294550-t26_1-p1	dynein heavy chain	1	0										
TGME49_295710-t26_1-p1	HECT-domain (ubiquitin-transferase) do	1	0										
TGME49_300140-t26_1-p1	elongation factor 1-gamma, putative	1	0										
TGME49_305890-t26_1-p1	hypothetical protein	1	0										
TGME49_306960-t26_1-p1	phenylalanine--tRNA ligase, beta subuni	1	0										
TGME49_310450-t26_1-p1	myosin heavy chain, putative	1	0										

TGME49_313820-t26_1-p1	dynactin p25, putative	1	0
TGME49_318770-t26_1-p1	aurora kinase(incomplete catalytic triad	1	0
TGME49_320592-t26_1-p1	hypothetical protein	1	0
TGME49_203830-t26_1-p1	FHA domain-containing protein	1	0
TGME491_216290A-t26_1-p1	hypothetical protein	1	0
TGME49_232080-t26_1-p1	hypothetical protein	1	0
TGME49_274000-t26_1-p1	hypothetical protein	1	0
TGME49_235402-t26_1-p1	CorA family Mg2+ transporter protein	5	1
TGME49_248160-t26_1-p1	hypothetical protein	5	1
TGME49_215980-t26_1-p1	hypothetical protein	4	1
TGME49_292320-t26_1-p1	hypothetical protein	4	1
TGME49_203050-t26_1-p1	AP2 domain transcription factor AP2VIIa	3	1
TGME49_218260-t26_1-p1	histone H3.3	3	1
TGME49_230410-t26_1-p1	peroxiredoxin PRX3	3	1
TGME49_232940-t26_1-p1	heat shock protein HSP20	3	1
TGME49_254440-t26_1-p1	ribosomal protein RPL12	3	1
TGME49_261250-t26_1-p1	histone H2A1	3	1
TGME49_261580-t26_1-p1	histone H2AX	3	1
TGME49_262670-t26_1-p1	ribosomal protein RPL18A	3	1
TGME49_263050-t26_1-p1	ribosomal protein RPL13	3	1
TGME49_263700-t26_1-p1	ribosomal protein RPS14	3	1
TGME49_271050-t26_1-p1	SAG-related sequence SRS34A	3	1
TGME49_284560-t26_1-p1	ribosomal protein RPL9	3	1
TGME49_288720-t26_1-p1	ribosomal protein RPL10	3	1
TGME49_289750-t26_1-p1	ribosomal-ubiquitin protein RPL40	3	1
TGME49_300200-t26_1-p1	histone H2AZ	3	1
TGME49_324600-t26_1-p1	heat shock protein	3	1
TGME49_204020-t26_1-p1	ribosomal protein RPL8	2	1
TGME49_205340-t26_1-p1	ribosomal protein RPS12	2	1
TGME49_205580-t26_1-p1	nuclear factor NF4	2	1
TGME49_207840-t26_1-p1	ribosomal protein RPS17	2	1
TGME49_209690-t26_1-p1	small nuclear ribonucleoprotein	2	1
TGME49_214080-t26_1-p1	toxofilin	2	1
TGME49_225080-t26_1-p1	ribosomal protein RPS18	2	1
TGME49_226000-t26_1-p1	ATP synthase, putative	2	1
TGME49_226970-t26_1-p1	ribosomal protein RPS11	2	1
TGME49_227280-t26_1-p1	dense granule protein GRA3	2	1
TGME49_227620-t26_1-p1	dense granule protein GRA2	2	1
TGME49_227820-t26_1-p1	hypothetical protein	2	1
TGME49_227970-t26_1-p1	histone family DNA-binding protein	2	1
TGME49_230160-t26_1-p1	hypothetical protein	2	1
TGME49_231815-t26_1-p1	hypothetical protein	2	1
TGME49_232410-t26_1-p1	PDI family protein	2	1
TGME49_238010-t26_1-p1	ribosomal protein RPL23A	2	1
TGME49_239100-t26_1-p1	ribosomal protein RPS7	2	1
TGME49_242330-t26_1-p1	ribosomal protein RPS5	2	1
TGME49_245680-t26_1-p1	ribosomal protein RPL21	2	1
TGME49_247520-t26_1-p1	hypothetical protein	2	1
TGME49_248390-t26_1-p1	ribosomal protein RPL26	2	1
TGME49_251870-t26_1-p1	histone H2Bb	2	1
TGME49_266070-t26_1-p1	ribosomal protein RPL31	2	1
TGME49_267060-t26_1-p1	ribosomal protein RPL14	2	1
TGME49_286450-t26_1-p1	dense granule protein GRA5	2	1
TGME49_286630-t26_1-p1	redoxin domain-containing protein	2	1
TGME49_291960-t26_1-p1	rhoptry kinase family protein ROP40 (inc	2	1
TGME49_292130-t26_1-p1	ribosomal protein RPL13A	2	1
TGME49_299050-t26_1-p1	ribosomal protein RPL17	2	1
TGME49_300100-t26_1-p1	rhoptry neck protein RON2	2	1
TGME49_300280-t26_1-p1	LSM domain-containing protein	2	1
TGME49_308090-t26_1-p1	rhoptry protein ROP5	2	1
TGME49_313390-t26_1-p1	ribosomal protein RPL6	2	1
TGME49_315610-t26_1-p1	hypothetical protein	2	1
TGME49_201800-t26_1-p1	hypothetical protein	1	1
TGME49_203010-t26_1-p1	aurora kinase	1	1
TGME49_206650-t26_1-p1	zinc finger, c2h2 type domain-containing	1	1
TGME49_207440-t26_1-p1	ribosomal protein RPS4	1	1
TGME49_209030-t26_1-p1	actin ACT1	1	1
TGME49_209260-t26_1-p1	cytochrome c oxidase subunit, putative	1	1
TGME49_209720-t26_1-p1	hypothetical protein	1	1
TGME49_211290-t26_1-p1	rhoptry protein ROP15	1	1
TGME49_212240-t26_1-p1	beta-1 tubulin, putative	1	1
TGME49_214770-t26_1-p1	small GTP binding protein rab1a, putativ	1	1
TGME49_215060-t26_1-p1	small GTP-binding protein sar1, putative	1	1
TGME49_215430-t26_1-p1	hypothetical protein	1	1
TGME49_215470-t26_1-p1	ribosomal protein RPL10A	1	1
TGME49_217890-t26_1-p1	alkyl hydroperoxide reductase/ Thiol spe	1	1
TGME49_218410-t26_1-p1	ribosomal protein RPP0	1	1
TGME49_220100-t26_1-p1	phosphoribosylpyrophosphate synthetas	1	1
TGME49_222880-t26_1-p1	hypothetical protein	1	1
TGME49_224900-t26_1-p1	adenylate kinase, putative	1	1
TGME49_226570-t26_1-p1	hypothetical protein	1	1
TGME49_228630-t26_1-p1	hypothetical protein	1	1
TGME49_229920-t26_1-p1	hypothetical protein	1	1
TGME49_230430-t26_1-p1	vesicle-associated membrane protein, p	1	1
TGME49_231160-t26_1-p1	hypothetical protein	1	1
TGME49_231630-t26_1-p1	alveolin domain containing intermediate	1	1
TGME49_232710-t26_1-p1	ribosomal protein RPS3A	1	1
TGME49_233460-t26_1-p1	SAG-related sequence SRS29B	1	1
TGME49_234380-t26_1-p1	hypothetical protein	1	1
TGME49_234990-t26_1-p1	hypothetical protein	1	1
TGME49_236070-t26_1-p1	pyrroline-5-carboxylate reductase	1	1
TGME49_236640-t26_1-p1	zinc finger, C3HC4 type (RING finger) do	1	1
TGME49_238400-t26_1-p1	endonuclease/exonuclease/phosphatase	1	1
TGME49_239260-t26_1-p1	histone H4	1	1
TGME49_243950-t26_1-p1	prohibitin, putative	1	1
TGME49_244560-t26_1-p1	heat shock protein 90, putative	1	1
TGME49_245460-t26_1-p1	ribosomal protein RPS8	1	1
TGME49_245710-t26_1-p1	phosphatidylinositol-4-phosphate 5-kina	1	1
TGME49_248225-t26_1-p1	PF2 arrest specific protein 8/11, putativ	1	1
TGME49_248340-t26_1-p1	GTP-binding nuclear protein ran/tc4	1	1
TGME49_248880-t26_1-p1	GTPase RAB7	1	1
TGME49_249900-t26_1-p1	adenine nucleotide translocator, putativ	1	1
TGME49_254720-t26_1-p1	dense granule protein GRA8	1	1
TGME49_257430-t26_1-p1	hypothetical protein	1	1
TGME49_257680-t26_1-p1	myosin light chain MLC1	1	1
TGME49_258410-t26_1-p1	photosensitized INA-labeled protein PHI	1	1
TGME49_259630-t26_1-p1	hypothetical protein	1	1
TGME49_262620-t26_1-p1	RNA recognition motif-containing protei	1	1
TGME49_263520-t26_1-p1	microtubule associated protein SPM1	1	1
TGME49_264040-t26_1-p1	hypothetical protein	1	1
TGME49_267500-t26_1-p1	hypothetical protein	1	1
TGME49_270640-t26_1-p1	RNA recognition motif-containing protei	1	1
TGME49_271610-t26_1-p1	pyrroline-5-carboxylate reductase	1	1
TGME49_276140-t26_1-p1	ADP ribosylation factor ARF1	1	1
TGME49_277740-t26_1-p1	zinc finger, C3HC4 type (RING finger) do	1	1
TGME49_286420-t26_1-p1	elongation factor 1-alpha (EF-1-ALPHA),	1	1
TGME49_286720-t26_1-p1	heat shock protein HSP28	1	1
TGME49_288650-t26_1-p1	dense granule protein GRA12	1	1
TGME49_289530-t26_1-p1	ribosomal protein RPL19	1	1

TGME49_289680-t26_1-p1	Ras-related protein Rab11	1	1
TGME49_289970-t26_1-p1	hypothetical protein	1	1
TGME49_293690-t26_1-p1	profilin PRF	1	1
TGME49_297430-t26_1-p1	hypothetical protein	1	1
TGME49_301420-t26_1-p1	hypothetical protein	1	1
TGME49_310070-t26_1-p1	methyltransferase, putative	1	1
TGME49_311470-t26_1-p1	rhoptry neck protein RON5	1	1
TGME49_311720-t26_1-p1	chaperonin protein BiP	1	1
TGME49_312050-t26_1-p1	small GTPase Rab2, putative	1	1
TGME49_313380-t26_1-p1	hypothetical protein	1	1
TGME49_313495-t26_1-p1	hypothetical protein	1	1
TGME49_314810-t26_1-p1	ribosomal protein RPL7	1	1
TGME49_316340-t26_1-p1	hypothetical protein	1	1
TGME49_316400-t26_1-p1	alpha tubulin TUBA1	1	1
TGME49_319920-t26_1-p1	2-oxo acid dehydrogenases acyltransfer	1	1
TGME49_321500-t26_1-p1	RNA recognition motif-containing protei	1	1
TGME49_321570-t26_1-p1	beta-hydroxyacyl-acyl carrier protein de	1	1
TGME49_410360-t26_1-p1	putative transmembrane protein	1	1
TGME49_204560-t26_1-p1	type I fatty acid synthase, putative	1	1
TGME49_208910-t26_1-p1	hypothetical protein	1	1
TGME49_210690-t26_1-p1	ribosomal protein RPS6	1	1
TGME49_211420-t26_1-p1	RNA recognition motif-containing protei	1	1
TGME49_212290-t26_1-p1	ribosomal protein RPS19	1	1
TGME49_213050-t26_1-p1	hypothetical protein	1	1
TGME49_213350-t26_1-p1	ribosomal protein RPS15	1	1
TGME49_214790-t26_1-p1	glycoprotein	1	1
TGME49_214950-t26_1-p1	hypothetical protein	1	1
TGME49_215460-t26_1-p1	ribosomal protein RPS24	1	1
TGME49_216410-t26_1-p1	hypothetical protein	1	1
TGME49_219460-t26_1-p1	hypothetical protein	1	1
TGME49_221210-t26_1-p1	cyclophilin	1	1
TGME49_221220-t26_1-p1	hypothetical protein	1	1
TGME49_227020-t26_1-p1	histone deacetylase SIR2	1	1
TGME49_227600-t26_1-p1	ribosomal protein RPL34	1	1
TGME49_229250-t26_1-p1	ribosomal protein RPL28	1	1
TGME49_229670-t26_1-p1	ribosomal protein RPS23	1	1
TGME49_239760-t26_1-p1	ribosomal protein RPL22	1	1
TGME49_248480-t26_1-p1	ribosomal protein RPS9	1	1
TGME49_250710-t26_1-p1	microneme protein MIC10	1	1
TGME49_251810-t26_1-p1	translation initiation factor eIF-5A, puta	1	1
TGME49_255180-t26_1-p1	ubiquitin carboxyl-terminal hydrolase	1	1
TGME49_257090-t26_1-p1	NAC domain-containing protein	1	1
TGME49_260440-t26_1-p1	nuclear factor NF3	1	1
TGME49_260670-t26_1-p1	centrin, putative	1	1
TGME49_262690-t26_1-p1	ribosomal protein RPL27	1	1
TGME49_262720-t26_1-p1	eukaryotic initiation factor-1A, putative	1	1
TGME49_263040-t26_1-p1	ribosomal protein RPS16	1	1
TGME49_267400-t26_1-p1	ribosomal protein RPL32	1	1
TGME49_268760-t26_1-p1	hypothetical protein	1	1
TGME49_270250-t26_1-p1	dense granule protein GRA1	1	1
TGME49_270380-t26_1-p1	ribosomal protein RPS13	1	1
TGME49_275810-t26_1-p1	ribosomal protein RPS10	1	1
TGME49_294820-t26_1-p1	type I fatty acid synthase, putative	1	1
TGME49_300000-t26_1-p1	ribosomal protein RPL18	1	1
TGME49_306600-t26_1-p1	RNA recognition motif-containing protei	1	1
TGME49_309820-t26_1-p1	ribosomal protein RPL11	1	1
TGME49_310490-t26_1-p1	ribosomal protein RPL27A	1	1
TGME49_313560-t26_1-p1	60S ribosomal protein L7a, putative	1	1
TGME49_314260-t26_1-p1	hypothetical protein	1	1

Appendix Table 2_Bioinformatic screen

Sheet 1

Expression based list	Group of baits (protein import)	Found in our 279?	2-280	1743-2021	4504-4782	7072-7350	7708-7986	Baits group 4	Baits group 5	Baits group 6	Baits group 7	Baits group 8	BCKDH complex	Found in 279?	TCA	Found in 279?	GABA shunt	Found in 279?	ATP synthase	Found in 279?	Cytochrome c oxidase complex	Found in 279?
					5 lists of randomly chosen 279 genes																	
	TGME49_214150	TRUE	TGME49_280660	TGME49_266366	TGME49_261950	TGME49_320780	TGME49_459450	FALSE	FALSE	FALSE	FALSE	FALSE	TGME49_204370	FALSE	TGME49_226730	FALSE	TGME49_208420	FALSE	TGME49_204400	FALSE	TGME49_209260	FALSE
TGME49_201110	TGME49_312220	TRUE	TGME49_313630	TGME49_266367	TGME49_261951	TGME49_321710	TGME49_287450	FALSE	FALSE	FALSE	FALSE	FALSE	TGME49_206470	FALSE	TGME49_268890	FALSE	TGME49_257480	FALSE	TGME49_261950	FALSE	TGME49_221510	FALSE
TGME49_201830	TGME49_283590	TRUE	TGME49_209000	TGME49_266368	TGME49_261952	TGME49_294750	TGME49_291920	FALSE	FALSE	FALSE	FALSE	FALSE	TGME49_235880	FALSE	TGME49_288500	TRUE	TGME49_269110	FALSE	TGME49_231910	FALSE	TGME49_226590	FALSE
TGME49_202180	TGME49_227830	TRUE	TGME49_225745	TGME49_266369	TGME49_261953	TGME49_239640	TGME49_301260	FALSE	FALSE	FALSE	FALSE	FALSE	TGME49_239490	FALSE	TGME49_290600	FALSE	TGME49_280700	FALSE	TGME49_226000	FALSE	TGME49_229920	FALSE
TGME49_203620	TGME49_265220	TRUE	TGME49_248510	TGME49_266370	TGME49_261954	TGME49_459950	TGME49_237120	FALSE	FALSE	FALSE	FALSE	FALSE	TGME49_297850	FALSE	TGME49_309752	FALSE			TGME49_314820	FALSE	TGME49_237120	FALSE
TGME49_203780	TGME49_202810	FALSE	TGME49_232080	TGME49_266371	TGME49_261955	TGME49_460730	TGME49_243360	FALSE	FALSE	FALSE	FALSE	FALSE	TGME49_314400	FALSE	TGME49_313140	FALSE			TGME49_249720	FALSE	TGME49_242840	FALSE
TGME49_204490	TGME49_218280	TRUE	TGME49_294820	TGME49_266372	TGME49_261956	TGME49_273750	TGME49_259100	FALSE	FALSE	FALSE	FALSE	FALSE	TGME49_318560	FALSE	TGME49_318430	FALSE			TGME49_284540	FALSE	TGME49_247770	FALSE
TGME49_205510	TGME49_254610	TRUE	TGME49_203665	TGME49_266373	TGME49_261957	TGME49_215930	TGME49_461460	FALSE	FALSE	FALSE	FALSE	TRUE	TGME49_318660	FALSE					TGME49_310360	FALSE	TGME49_254030	FALSE
TGME49_206360	TGME49_274090	FALSE	TGME49_295710	TGME49_266374	TGME49_261958	TGME49_325100	TGME49_203100	FALSE	FALSE	FALSE	FALSE	TRUE	TGME49_319920	FALSE					TGME49_231410	FALSE	TGME49_262640	FALSE
TGME49_207640	TGME49_215390	TRUE	TGME49_242625	TGME49_266375	TGME49_261959	TGME49_229250	TGME49_212060	FALSE	FALSE	FALSE	FALSE	TRUE							TGME49_268830	FALSE	TGME49_264040	FALSE
TGME49_207710	TGME49_260850	FALSE	TGME49_266010	TGME49_266376	TGME49_261960	TGME49_257572	TGME49_216770	FALSE	FALSE	FALSE	FALSE	FALSE							TGME49_223040	FALSE	TGME49_265370	FALSE
TGME49_207760	TGME49_225710	TRUE	TGME49_306020	TGME49_266377	TGME49_261961	TGME49_457980	TGME49_271310	FALSE	FALSE	FALSE	FALSE	FALSE							TGME49_247410	FALSE	TGME49_286530	FALSE
TGME49_207820	TGME49_251780	FALSE	TGME49_224870	TGME49_266378	TGME49_261962	TGME49_200310	TGME49_207360												TGME49_260180	FALSE	TGME49_297810	FALSE
TGME49_207940	TGME49_232815	TRUE	TGME49_210700	TGME49_266379	TGME49_261963	TGME49_253530	TGME49_240260	FALSE	FALSE	FALSE	FALSE	TRUE							TGME49_218940	FALSE	TGME49_306670	FALSE
TGME49_208200	Other protein import components		TGME49_268370	TGME49_266380	TGME49_261964	TGME49_274700	TGME49_458730	FALSE	FALSE	FALSE	FALSE	FALSE							TGME49_282180	FALSE	TGME49_310470	FALSE
TGME49_209020	TGME49_268370		TGME49_304630	TGME49_266381	TGME49_261965	TGME49_236130	TGME49_209112	FALSE	FALSE	FALSE	FALSE	FALSE							TGME49_285510	FALSE	TGME49_322600	FALSE
TGME49_209240	TGME49_263530	TRUE	TGME49_253750	TGME49_266382	TGME49_261966	TGME49_242350	TGME49_230122	FALSE	FALSE	FALSE	FALSE	TRUE							TGME49_215610	FALSE	TGME49_323400	FALSE
TGME49_209430	TGME49_273960	FALSE	TGME49_202070	TGME49_266383	TGME49_261967	TGME49_321700	TGME49_243220												TGME49_290030	FALSE		
TGME49_209680	TGME49_205570	TRUE	TGME49_292020	TGME49_266384	TGME49_261968	TGME49_458030	TGME49_276820												TGME49_310180	FALSE		
TGME49_209790	TGME49_249910	TRUE	TGME49_270595	TGME49_266385	TGME49_261969	TGME49_460930	TGME49_313318															
	TGME49_215390	TRUE	TGME49_216335	TGME49_266386	TGME49_261970	TGME49_293740	TGME49_458880												TGME49_214930	FALSE		
New mitochondrial proteins found and validated in this study																						
TGME49_210360	TGME49_203620	TRUE	TGME49_226810	TGME49_266387	TGME49_261971	TGME49_248430	TGME49_259680	FALSE	FALSE	FALSE	FALSE	FALSE							TGME49_245450	FALSE		
TGME49_211240	TGME49_231150	TRUE	TGME49_268780	TGME49_266388	TGME49_261972	TGME49_251530	TGME49_292290	FALSE	FALSE	FALSE	FALSE	FALSE							TGME49_208440	FALSE		
TGME49_211310	TGME49_240270	TRUE	TGME49_286270	TGME49_266389	TGME49_261973	TGME49_257340	TGME49_314560	FALSE	FALSE	FALSE	FALSE	FALSE							TGME49_201800	FALSE		
TGME49_211410	TGME49_240780	TRUE	TGME49_291180	TGME49_266390	TGME49_261974	TGME49_292270	TGME49_327800	FALSE	FALSE	FALSE	FALSE	FALSE							TGME49_225730	FALSE		
TGME49_211710	TGME49_247740	TRUE	TGME49_262825	TGME49_266391	TGME49_261975	TGME49_309540	TGME49_243770	FALSE	FALSE	FALSE	FALSE	FALSE							TGME49_263080	FALSE		
TGME49_211870	TGME49_263680	TRUE	TGME49_306660	TGME49_266392	TGME49_261976	TGME49_229230	TGME49_253680	FALSE	FALSE	FALSE	FALSE	FALSE							TGME49_263990	FALSE		
TGME49_213410	TGME49_201830	TRUE	TGME49_212880	TGME49_266393	TGME49_261977	TGME49_230100	TGME49_258618	FALSE	FALSE	FALSE	FALSE	FALSE							TGME49_270360	FALSE		
TGME49_214150	TGME49_226280	TRUE	TGME49_228690	TGME49_266394	TGME49_261978	TGME49_258462	TGME49_284680	FALSE	FALSE	FALSE	FALSE	FALSE							TGME49_258060	FALSE		
TGME49_214320	TGME49_214790	TRUE	TGME49_230000	TGME49_266395	TGME49_261979	TGME49_231920	TGME49_322130															
TGME49_214790	TGME49_312680	TRUE	TGME49_315860	TGME49_266396	TGME49_261980	TGME49_255380	TGME49_231450															
TGME49_214870			TGME49_239885	TGME49_266397	TGME49_261981	TGME49_294760	TGME49_281660															
TGME49_215260			TGME49_205562	TGME49_266398	TGME49_261982	TGME49_328500	TGME49_226820	none	none	none	none	5										
TGME49_215390			TGME49_278205	TGME49_266399	TGME49_261983	TGME49_213430	TGME49_251860															
TGME49_215400			TGME49_304720	TGME49_266400	TGME49_261984	TGME49_218940	TGME49_218940															
TGME49_215430			TGME49_234230	TGME49_266401	TGME49_261985	TGME49_251940	TGME49_283570															
TGME49_215490			TGME49_229630	TGME49_266402	TGME49_261986	TGME49_289660	TGME49_283800						None in 279		1 in 279		none in 279		none in 279		none in 279	
TGME49_216120			TGME49_264140	TGME49_266403	TGME49_261987	TGME49_240530	TGME49_461260															
TGME49_216210			TGME49_203320	TGME49_266404	TGME49_261988	TGME49_240940	TGME49_227330															
TGME49_216490			TGME49_321450	TGME49_266405	TGME49_261989	TGME49_301330	TGME49_227630															
TGME49_216770			TGME49_288940	TGME49_266406	TGME49_261990	TGME49_304480	TGME49_228640															
TGME49_216830			TGME49_283702	TGME49_266407	TGME49_261991	TGME49_460010	TGME49_260330															
TGME49_216900			TGME49_216210	TGME49_266408	TGME49_261992	TGME49_262810	TGME49_293410															
TGME49_217820			TGME49_295610	TGME49_266409	TGME49_261993	TGME49_458090	TGME49_251390															
TGME49_217890			TGME49_206430	TGME49_266410	TGME49_261994	TGME49_459230	TGME49_267630															
TGME49_218230			TGME49_313430	TGME49_266411	TGME49_261995	TGME49_212910	TGME49_270830															
TGME49_218280			TGME49_236930	TGME49_266412	TGME49_261996	TGME49_243550	TGME49_461240															
TGME49_219140			TGME49_288440	TGME49_266413	TGME49_261997	TGME49_247930	TGME49_216420															
TGME49_220140			TGME49_224260	TGME49_266414	TGME49_261998	TGME49_273650	TGME49_240820															
TGME49_222070			TGME49_271145	TGME49_266415	TGME49_261999	TGME49_267610	TGME49_269470															
TGME49_222090			TGME49_234900	TGME49_266416	TGME49_262000	TGME49_211080	TGME49_291970															
TGME49_222170			TGME49_287480	TGME49_266417	TGME49_262001	TGME49_329500	TGME49_255990															
TGME49_222860			TGME49_294550	TGME49_266418	TGME49_262002	TGME49_267610	TGME49_269470															
TGME49_223140			TGME49_205130	TGME49_266419	TGME49_262003	TGME49_211080	TGME49_291970															
TGME49_223710			TGME49_211890	TGME49_266420	TGME49_262004	TGME49_256792	TGME49_259280															
TGME49_223970			TGME49_204560	TGME49_266421	TGME49_262005	TGME49_264150	TGME49_279430															
TGME49_225710			TGME49_285140	TGME49_266422	TGME49_262006	TGME49_207420	TGME49_312120															
TGME49_225800			TGME49_264790	TGME49_266423	TGME49_262007	TGME49_265340	TGME49_325600															
TGME49_225930			TGME49_316680	TGME49_266424	TGME49_262008	TGME49_322020	TGME49_313418															
TGME49_226270			TGME49_279320	TGME49_266425	TGME49_262009	TGME49_255320	TGME49_277830															
TGME49_226280			TGME49_206580	TGME49_266426	TGME49_262010	TGME49_259690	TGME49_457870															
TGME49_226430																						

Column groups:
- Column A: 279 (current number of 281 found by mRNA expression)
- Columns C–D: Enrichments of known mitochondrial proteins, likely housekeeping
- Columns F–J: 5 lists of randomly chosen 279 genes (2-280, 1743-2021, 4504-4782, 7072-7350, 7708-7986 in the transcript size list)
- Columns L–P: known and putative mitochondrial housekeeping proteins are enriched in our 279 list compared to randomly chosen 279 genes (Baits found in group 4, 5, 6, 7, 8)
- Columns R–AA: Non-housekeeping mitochondrial pathways are mainly excluded from the 279 (BCKDH complex, TCA, GABA shunt, ATP synthase, Cytochrome c oxidase complex)

TGME49_227060	TGME49_212810	TGME49_266427	TGME49_262011	TGME49_263430	TGME49_302060
TGME49_227830	TGME49_316430	TGME49_266428	TGME49_262012	TGME49_216270	TGME49_259540
TGME49_229180	TGME49_209880	TGME49_266429	TGME49_262013	TGME49_262800	TGME49_261770
TGME49_230050	TGME49_288190	TGME49_266430	TGME49_262014	TGME49_266040	TGME49_277780
TGME49_230450	TGME49_207480	TGME49_266431	TGME49_262015	TGME49_296340	TGME49_459420
TGME49_230555	TGME49_206550	TGME49_266432	TGME49_262016	TGME49_235440	TGME49_459790
TGME49_230580	TGME49_240380	TGME49_266433	TGME49_262017	TGME49_240550	TGME49_287460
TGME49_230840	TGME49_311230	TGME49_266434	TGME49_262018	TGME49_233850	TGME49_204090
TGME49_230990	TGME49_213300	TGME49_266435	TGME49_262019	TGME49_252410	TGME49_309150
TGME49_231020	TGME49_246190	TGME49_266436	TGME49_262020	TGME49_255270	TGME49_324100
TGME49_231150	TGME49_230830	TGME49_266437	TGME49_262021	TGME49_295750	TGME49_203560
TGME49_231750	TGME49_219660	TGME49_266438	TGME49_262022	TGME49_315390	TGME49_229800
TGME49_232520	TGME49_223080	TGME49_266439	TGME49_262023	TGME49_242330	TGME49_253770
TGME49_232640	TGME49_209650	TGME49_266440	TGME49_262024	TGME49_268230	TGME49_301218
TGME49_232815	TGME49_253870	TGME49_266441	TGME49_262025	TGME49_268810	TGME49_459890
TGME49_233100	TGME49_269075	TGME49_266442	TGME49_262026	TGME49_276830	TGME49_263720
TGME49_233190	TGME49_224540	TGME49_266443	TGME49_262027	TGME49_310122	TGME49_273940
TGME49_233260	TGME49_228120	TGME49_266444	TGME49_262028	TGME49_229320	TGME49_458100
TGME49_233720	TGME49_246170	TGME49_266445	TGME49_262029	TGME49_263350	TGME49_313322
TGME49_234530	TGME49_223480	TGME49_266446	TGME49_262030	TGME49_211660	TGME49_233842
TGME49_235560	TGME49_307860	TGME49_266447	TGME49_262031	TGME49_459740	TGME49_240490
TGME49_235970	TGME49_295658	TGME49_266448	TGME49_262032	TGME49_212420	TGME49_460090
TGME49_236580	TGME49_301270	TGME49_266449	TGME49_262033	TGME49_233150	TGME49_208080
TGME49_237100	TGME49_269290	TGME49_266450	TGME49_262034	TGME49_237810	TGME49_216230
TGME49_237290	TGME49_254370	TGME49_266451	TGME49_262035	TGME49_203070	TGME49_324800
TGME49_237460	TGME49_214960	TGME49_266452	TGME49_262036	TGME49_461180	TGME49_457310
TGME49_238000	TGME49_311625	TGME49_266453	TGME49_262037	TGME49_218740	TGME49_459210
TGME49_238240	TGME49_223985	TGME49_266454	TGME49_262038	TGME49_228500	TGME49_460530
TGME49_239610	TGME49_241850	TGME49_266455	TGME49_262039	TGME49_318380	TGME49_207020
TGME49_239790	TGME49_267030	TGME49_266456	TGME49_262040	TGME49_310110	TGME49_264250
TGME49_239890	TGME49_301400	TGME49_266457	TGME49_262041	TGME49_461340	TGME49_461190
TGME49_240200	TGME49_223725	TGME49_266458	TGME49_262042	TGME49_236880	TGME49_459120
TGME49_240210	TGME49_272155	TGME49_266459	TGME49_262043	TGME49_263590	TGME49_231230
TGME49_240270	TGME49_309980	TGME49_266460	TGME49_262044	TGME49_271892	TGME49_235590
TGME49_240400	TGME49_311070	TGME49_266461	TGME49_262045	TGME49_297440	TGME49_460440
TGME49_240440	TGME49_280390	TGME49_266462	TGME49_262046	TGME49_459080	TGME49_200700
TGME49_240590	TGME49_250690	TGME49_266463	TGME49_262047	TGME49_254310	TGME49_217951
TGME49_240780	TGME49_203135	TGME49_266464	TGME49_262048	TGME49_460120	TGME49_459370
TGME49_240810	TGME49_306338	TGME49_266465	TGME49_262049	TGME49_263170	TGME49_214930
TGME49_240820	TGME49_263610	TGME49_266466	TGME49_262050	TGME49_270380	TGME49_288970
TGME49_240890	TGME49_232010	TGME49_266467	TGME49_262051	TGME49_228310	TGME49_315330
TGME49_242415	TGME49_242055	TGME49_266468	TGME49_262052	TGME49_314570	TGME49_457830
TGME49_242610	TGME49_266435	TGME49_266469	TGME49_262053	TGME49_459570	TGME49_243900
TGME49_243530	TGME49_243265	TGME49_266470	TGME49_262054	TGME49_227920	TGME49_268940
TGME49_243760	TGME49_254160	TGME49_266471	TGME49_262055	TGME49_275590	TGME49_307620
TGME49_244120	TGME49_309250	TGME49_266472	TGME49_262056	TGME49_286170	TGME49_311820
TGME49_244140	TGME49_235920	TGME49_266473	TGME49_262057	TGME49_310990	TGME49_261580
TGME49_244310	TGME49_237425	TGME49_266474	TGME49_262058	TGME49_233200	TGME49_254780
TGME49_244380	TGME49_214840	TGME49_266475	TGME49_262059	TGME49_261700	TGME49_264260
TGME49_244440	TGME49_218560	TGME49_266476	TGME49_262060	TGME49_255490	TGME49_326300
TGME49_245470	TGME49_216430	TGME49_266477	TGME49_262061	TGME49_228620	TGME49_200110
TGME49_245520	TGME49_214140	TGME49_266478	TGME49_262062	TGME49_258130	TGME49_324500
TGME49_245650	TGME49_203180	TGME49_266479	TGME49_262063	TGME49_225460	TGME49_461090
TGME49_246730	TGME49_297210	TGME49_266480	TGME49_262064	TGME49_217560	TGME49_458250
TGME49_246920	TGME49_216620	TGME49_266481	TGME49_262065	TGME49_267060	TGME49_228140
TGME49_247390	TGME49_229310	TGME49_266482	TGME49_262066	TGME49_291910	TGME49_239760
TGME49_247550	TGME49_236970	TGME49_266483	TGME49_262067	TGME49_298590	TGME49_258828
TGME49_247740	TGME49_264485	TGME49_235670	TGME49_262068	TGME49_325800	TGME49_263642
TGME49_248200	TGME49_316510	TGME49_306500	TGME49_262069	TGME49_261018	TGME49_305050
TGME49_248960	TGME49_291980	TGME49_216870	TGME49_262070	TGME49_303450	TGME49_321270
TGME49_249010	TGME49_235420	TGME49_225000	TGME49_262071	TGME49_235870	TGME49_210220
TGME49_249215	TGME49_226660	TGME49_243610	TGME49_262072	TGME49_267000	TGME49_327300
TGME49_249410	TGME49_311510	TGME49_310080	TGME49_262073	TGME49_258880	TGME49_265100
TGME49_249510	TGME49_264670	TGME49_269320	TGME49_262074	TGME49_316550	TGME49_271178
TGME49_249650	TGME49_214600	TGME49_315270	TGME49_262075	TGME49_239320	TGME49_281040
TGME49_249910	TGME49_270720	TGME49_226390	TGME49_262076	TGME49_258220	TGME49_320660
TGME49_249920	TGME49_206450	TGME49_232100	TGME49_262077	TGME49_285820	TGME49_274030
TGME49_249950	TGME49_224270	TGME49_238930	TGME49_262078	TGME49_460400	TGME49_226640
TGME49_251170	TGME49_315190	TGME49_280560	TGME49_262079	TGME49_230118	TGME49_306860
TGME49_251500	TGME49_242780	TGME49_204350	TGME49_262080	TGME49_238480	TGME49_313840
TGME49_251550	TGME49_243635	TGME49_274160	TGME49_262081	TGME49_319690	TGME49_327000

TGME49_251690	TGME49_254940	TGME49_244630	TGME49_262082	TGME49_239660	TGME49_210100
TGME49_251760	TGME49_203710	TGME49_254135	TGME49_262083	TGME49_262020	TGME49_272630
TGME49_252230	TGME49_261080	TGME49_311490	TGME49_262084	TGME49_238450	TGME49_297488
TGME49_252340	TGME49_286932	TGME49_205300	TGME49_262085	TGME49_329700	TGME49_315630
TGME49_252480	TGME49_208050	TGME49_261990	TGME49_262086	TGME49_281030	TGME49_263530
TGME49_253510	TGME49_267855	TGME49_269390	TGME49_262087	TGME49_309180	TGME49_272450
TGME49_253780	TGME49_207120	TGME49_262390	TGME49_262088	TGME49_314820	TGME49_312850
TGME49_254260	TGME49_289520	TGME49_203200	TGME49_262089	TGME49_235600	TGME49_240460
TGME49_254280	TGME49_256920	TGME49_211450	TGME49_262090	TGME49_248480	TGME49_270540
TGME49_254610	TGME49_310530	TGME49_242030	TGME49_262091	TGME49_258810	TGME49_290010
TGME49_254770	TGME49_255180	TGME49_315280	TGME49_262092	TGME49_460420	TGME49_459000
TGME49_254810	TGME49_283550	TGME49_270190	TGME49_262093	TGME49_267830	TGME49_272560
TGME49_254940	TGME49_266830	TGME49_213770	TGME49_262094	TGME49_227040	TGME49_461130
TGME49_255320	TGME49_320080	TGME49_209800	TGME49_262095	TGME49_310020	TGME49_458500
TGME49_256760	TGME49_297330	TGME49_213610	TGME49_262096	TGME49_210682	TGME49_459770
TGME49_256990	TGME49_226755	TGME49_312050	TGME49_262097	TGME49_249520	TGME49_279540
TGME49_257110	TGME49_202490	TGME49_288350	TGME49_262098	TGME49_310590	TGME49_295140
TGME49_257150	TGME49_210781	TGME49_270570	TGME49_262099	TGME49_323400	TGME49_305830
TGME49_258100	TGME49_276200	TGME49_207040	TGME49_262100	TGME49_260660	TGME49_201750
TGME49_258210	TGME49_280540	TGME49_265270	TGME49_262101	TGME49_263330	TGME49_316580
TGME49_258390	TGME49_296010	TGME49_218830	TGME49_262102	TGME49_267010	TGME49_321280
TGME49_259690	TGME49_261022	TGME49_202040	TGME49_262103	TGME49_459360	TGME49_457820
TGME49_260300	TGME49_249840	TGME49_281580	TGME49_262104	TGME49_460600	TGME49_459160
TGME49_260440	TGME49_211270	TGME49_282210	TGME49_262105	TGME49_289810	TGME49_229190
TGME49_261260	TGME49_221400	TGME49_202470	TGME49_262106	TGME49_273080	TGME49_279560
TGME49_261480	TGME49_247390	TGME49_224620	TGME49_262107	TGME49_286480	TGME49_460030
TGME49_261520	TGME49_242700	TGME49_314340	TGME49_262108	TGME49_251550	TGME49_200600
TGME49_261600	TGME49_294840	TGME49_243990	TGME49_262109	TGME49_281560	TGME49_327400
TGME49_261690	TGME49_208070	TGME49_277710	TGME49_262110	TGME49_260010	TGME49_266600
TGME49_262040	TGME49_237290	TGME49_294640	TGME49_262111	TGME49_306050	TGME49_327500
TGME49_263070	TGME49_311030	TGME49_202750	TGME49_262112	TGME49_310090	TGME49_461060
TGME49_263260	TGME49_219260	TGME49_224220	TGME49_262113	TGME49_273060	TGME49_203430
TGME49_263340	TGME49_228070	TGME49_237210	TGME49_262114	TGME49_255360	TGME49_203460
TGME49_263420	TGME49_215910	TGME49_252250	TGME49_262115	TGME49_230640	TGME49_240620
TGME49_263440	TGME49_315760	TGME49_266320	TGME49_262116	TGME49_232230	TGME49_242840
TGME49_263530	TGME49_314875	TGME49_284530	TGME49_262117	TGME49_314760	TGME49_288300
TGME49_263680	TGME49_221280	TGME49_289020	TGME49_262118	TGME49_458440	TGME49_325400
TGME49_263760	TGME49_231815	TGME49_235150	TGME49_262119	TGME49_263990	TGME49_457780
TGME49_264060	TGME49_274010	TGME49_260470	TGME49_262120	TGME49_309610	TGME49_220400
TGME49_264200	TGME49_268010	TGME49_218310	TGME49_262121	TGME49_459500	TGME49_457520
TGME49_264790	TGME49_242415	TGME49_218950	TGME49_262122	TGME49_297492	TGME49_458900
TGME49_265110	TGME49_203050	TGME49_321600	TGME49_262123	TGME49_316270	TGME49_459650
TGME49_265220	TGME49_208020	TGME49_280400	TGME49_262124	TGME49_289270	TGME49_325700
TGME49_265280	TGME49_265090	TGME49_266785	TGME49_262125	TGME49_259050	TGME49_221860
TGME49_265990	TGME49_311380	TGME49_267570	TGME49_262126	TGME49_264110	TGME49_283770
TGME49_266750	TGME49_239420	TGME49_205370	TGME49_262127	TGME49_269850	TGME49_322800
TGME49_266950	TGME49_319610	TGME49_290880	TGME49_262128	TGME49_226500	TGME49_459990
TGME49_267390	TGME49_236560	TGME49_260800	TGME49_262129	TGME49_277700	TGME49_258930
TGME49_268640	TGME49_225960	TGME49_209060	TGME49_262130	TGME49_225102	TGME49_300780
TGME49_268820	TGME49_249540	TGME49_218500	TGME49_262131	TGME49_207110	TGME49_311050
TGME49_268840	TGME49_223880	TGME49_306220	TGME49_262132	TGME49_257160	TGME49_270290
TGME49_269650	TGME49_210345	TGME49_307790	TGME49_262133	TGME49_259620	TGME49_322900
TGME49_269740	TGME49_214610	TGME49_313570	TGME49_262134	TGME49_223010	TGME49_214860
TGME49_270150	TGME49_209500	TGME49_212820	TGME49_262135	TGME49_271220	TGME49_237060
TGME49_270650	TGME49_213060	TGME49_309280	TGME49_262136	TGME49_272300	TGME49_258940
TGME49_271178	TGME49_201820	TGME49_220600	TGME49_262137	TGME49_254670	TGME49_264230
TGME49_271182	TGME49_234410	TGME49_260580	TGME49_262138	TGME49_249980	TGME49_293200
TGME49_271280	TGME49_274000	TGME49_297150	TGME49_262139	TGME49_263660	TGME49_328400
TGME49_271300	TGME49_242750	TGME49_313110	TGME49_262140	TGME49_298960	TGME49_215610
TGME49_272010	TGME49_309890	TGME49_315600	TGME49_262141	TGME49_311640	TGME49_289218
TGME49_272410	TGME49_218000	TGME49_225900	TGME49_262142	TGME49_274290	TGME49_460640
TGME49_272490	TGME49_227780	TGME49_240340	TGME49_262143	TGME49_281600	TGME49_231990
TGME49_272695	TGME49_277895	TGME49_267670	TGME49_262144	TGME49_289030	TGME49_278522
TGME49_272740	TGME49_264860	TGME49_248120	TGME49_262145	TGME49_207210	TGME49_294030
TGME49_273460	TGME49_294740	TGME49_311880	TGME49_262146	TGME49_277240	TGME49_324200
TGME49_273520	TGME49_253170	TGME49_237470	TGME49_262147	TGME49_310510	TGME49_297300
TGME49_273640	TGME49_245560	TGME49_202650	TGME49_262148	TGME49_310690	TGME49_328200
TGME49_274190	TGME49_242640	TGME49_239870	TGME49_262149	TGME49_205080	TGME49_459910
TGME49_275490	TGME49_252880	TGME49_216660	TGME49_262150	TGME49_231860	TGME49_211060
TGME49_278270	TGME49_247700	TGME49_301410	TGME49_262151	TGME49_254440	TGME49_244900
TGME49_278900	TGME49_222800	TGME49_309220	TGME49_262152	TGME49_261590	TGME49_260850

TGME49_279330	TGME49_293170	TGME49_213870	TGME49_262153	TGME49_260670	TGME49_457470	
TGME49_282190	TGME49_312300	TGME49_261230	TGME49_262154	TGME49_226930	TGME49_459730	
TGME49_283590	TGME49_208910	TGME49_264070	TGME49_262155	TGME49_243520	TGME49_203630	
TGME49_283850	TGME49_321340	TGME49_299080	TGME49_262156	TGME49_285790	TGME49_224560	
TGME49_285670	TGME49_223450	TGME49_222400	TGME49_262157	TGME49_261220	TGME49_232770	
TGME49_285720	TGME49_253380	TGME49_257760	TGME49_262158	TGME49_234550	TGME49_325500	
TGME49_285840	TGME49_314920	TGME49_288050	TGME49_262159	TGME49_215050	TGME49_267990	
TGME49_286070	TGME49_255700	TGME49_215440	TGME49_262160	TGME49_299220	TGME49_307060	
TGME49_286420	TGME49_281440	TGME49_206600	TGME49_262161	TGME49_263630	TGME49_227870	
TGME49_286550	TGME49_233430	TGME49_265240	TGME49_262162	TGME49_254340	TGME49_230598	
TGME49_288500	TGME49_273780	TGME49_311500	TGME49_262163	TGME49_220720	TGME49_244930	
TGME49_288510	TGME49_242890	TGME49_214520	TGME49_262164	TGME49_233140	TGME49_313740	
TGME49_288580	TGME49_253930	TGME49_228080	TGME49_262165	TGME49_251900	TGME49_319988	
TGME49_289650	TGME49_217860	TGME49_294560	TGME49_262166	TGME49_460500	TGME49_275390	
TGME49_290040	TGME49_239910	TGME49_225780	TGME49_262167	TGME49_265160	TGME49_295970	
TGME49_290570	TGME49_248720	TGME49_278060	TGME49_262168	TGME49_458590	TGME49_311850	
TGME49_290840	TGME49_293000	TGME49_205500	TGME49_262169	TGME49_313890	TGME49_459100	
TGME49_291080	TGME49_306300	TGME49_267460	TGME49_262170	TGME49_213860	TGME49_264182	
TGME49_291150	TGME49_226620	TGME49_290190	TGME49_262171	TGME49_232280	TGME49_283870	
TGME49_291590	TGME49_234300	TGME49_265230	TGME49_262172	TGME49_270820	TGME49_290710	
TGME49_292010	TGME49_242435	TGME49_321540	TGME49_262173	TGME49_275810	TGME49_307080	
TGME49_293700	TGME49_245510	TGME49_262700	TGME49_262174	TGME49_225210	TGME49_460700	
TGME49_294050	TGME49_313860	TGME49_255970	TGME49_262175	TGME49_233350	TGME49_264240	
TGME49_294350	TGME49_288000	TGME49_295370	TGME49_262176	TGME49_307840	TGME49_288850	
TGME49_294420	TGME49_277260	TGME49_243930	TGME49_262177	TGME49_316390	TGME49_328300	
TGME49_294980	TGME49_310970	TGME49_221250	TGME49_262178	TGME49_319980	TGME49_206910	
TGME49_295010	TGME49_234250	TGME49_294690	TGME49_262179	TGME49_458190	TGME49_219828	
TGME49_295960	TGME49_308890	TGME49_211280	TGME49_262180	TGME49_217490	TGME49_274280	
TGME49_296950	TGME49_219710	TGME49_291950	TGME49_262181	TGME49_222080	TGME49_461170	
TGME49_297170	TGME49_306060	TGME49_297180	TGME49_262182	TGME49_255200	TGME49_264748	
TGME49_297880	TGME49_210300	TGME49_276210	TGME49_262183	TGME49_266980	TGME49_240790	
TGME49_299210	TGME49_211720	TGME49_312510	TGME49_262184	TGME49_293520	TGME49_202060	
TGME49_299270	TGME49_209440	TGME49_217688	TGME49_262185	TGME49_293290	TGME49_244950	
TGME49_301390	TGME49_310190	TGME49_278850	TGME49_262186	TGME49_320770	TGME49_326700	
TGME49_305460	TGME49_319370	TGME49_222370	TGME49_262187	TGME49_321900	TGME49_458220	
TGME49_305490	TGME49_227610	TGME49_249215	TGME49_262188	TGME49_207780	TGME49_461390	
TGME49_305750	TGME49_311920	TGME49_242670	TGME49_262189	TGME49_215540	TGME49_222260	
TGME49_306290	TGME49_285830	TGME49_246510	TGME49_262190	TGME49_232700	TGME49_459010	
TGME49_306380	TGME49_213370	TGME49_202460	TGME49_262191	TGME49_460320	TGME49_225098	
TGME49_306610	TGME49_273800	TGME49_269920	TGME49_262192	TGME49_229240	TGME49_326000	
TGME49_306650	TGME49_215080	TGME49_236080	TGME49_262193	TGME49_258720	TGME49_266460	
TGME49_306950	TGME49_248540	TGME49_214800	TGME49_262194	TGME49_458510	TGME49_275750	
TGME49_307650	TGME49_299000	TGME49_272500	TGME49_262195	TGME49_262040	TGME49_306940	
TGME49_308950	TGME49_224670	TGME49_232970	TGME49_262196	TGME49_253760	TGME49_324400	
TGME49_308990	TGME49_281400	TGME49_212090	TGME49_262197	TGME49_319890	TGME49_250350	
TGME49_309570	TGME49_214230	TGME49_220510	TGME49_262198	TGME49_217178	TGME49_268170	
TGME49_310050	TGME49_238880	TGME49_294870	TGME49_262199	TGME49_218390	TGME49_263030	
TGME49_310320	TGME49_264752	TGME49_288040	TGME49_262200	TGME49_243700	TGME49_320140	
TGME49_310400	TGME49_245720	TGME49_295020	TGME49_262201	TGME49_300090	TGME49_283470	
TGME49_310500	TGME49_204380	TGME49_228240	TGME49_262202	TGME49_459290	TGME49_269442	
TGME49_310850	TGME49_228660	TGME49_239010	TGME49_262203	TGME49_219750	TGME49_291160	
TGME49_311030	TGME49_247790	TGME49_266890	TGME49_262204	TGME49_273630	TGME49_274090	
TGME49_311240	TGME49_309910	TGME49_236650	TGME49_262205	TGME49_254030	TGME49_286070	
TGME49_311430	TGME49_231480	TGME49_293730	TGME49_262206	TGME49_264680	TGME49_301190	
TGME49_311750	TGME49_319860	TGME49_264880	TGME49_262207	TGME49_214160	TGME49_322200	
TGME49_311870	TGME49_234430	TGME49_207900	TGME49_262208	TGME49_302450	TGME49_307450	
TGME49_312220	TGME49_271370	TGME49_240310	TGME49_262209	TGME49_303050	TGME49_309830	
TGME49_312340	TGME49_247050	TGME49_266080	TGME49_262210	TGME49_322400	TGME49_460510	
TGME49_312350	TGME49_288960	TGME49_231170	TGME49_203610	TGME49_324900	TGME49_457910	
TGME49_312480	TGME49_232190	TGME49_239540	TGME49_227970	TGME49_281360	TGME49_252090	
TGME49_312490	TGME49_205615	TGME49_247590	TGME49_222940	TGME49_283882	TGME49_460590	
TGME49_312530	TGME49_229260	TGME49_289110	TGME49_266630	TGME49_227880	TGME49_261470	
TGME49_312680	TGME49_268035	TGME49_212110	TGME49_315970	TGME49_231620	TGME49_461430	
TGME49_313230	TGME49_239700	TGME49_219860	TGME49_208780	TGME49_322120	TGME49_232840	
TGME49_313350	TGME49_248290	TGME49_240070	TGME49_279450	TGME49_300080	TGME49_241310	
TGME49_313520	TGME49_249810	TGME49_305620	TGME49_312980	TGME49_312090	TGME49_298080	
TGME49_314480	TGME49_280800	TGME49_294770	TGME49_315730	TGME49_322210	TGME49_306692	
TGME49_314710	TGME49_275420	TGME49_246950	TGME49_318430	TGME49_326900	TGME49_459640	
TGME49_314800	TGME49_226470	TGME49_259260	TGME49_242600	TGME49_305010	TGME49_215390	
TGME49_316350	TGME49_248710	TGME49_214280	TGME49_285220	TGME49_255910	TGME49_254600	
TGME49_316450	TGME49_221320	TGME49_294240	TGME49_289910	TGME49_261540	TGME49_313650	

TGME49_316900		TGME49_265780	TGME49_321640	TGME49_310230	TGME49_250900	TGME49_284630
TGME49_318310		TGME49_280590	TGME49_266400	TGME49_201760	TGME49_260340	TGME49_270080
TGME49_320550		TGME49_213255	TGME49_271990	TGME49_202690	TGME49_320710	TGME49_460760
TGME49_321310		TGME49_223060	TGME49_226920	TGME49_215360	TGME49_206520	TGME49_293372
TGME49_321640		TGME49_246760	TGME49_297650	TGME49_285240	TGME49_258890	TGME49_327100
TGME49_321680						

Sheet 2

A	C	D	E	F	G	I	H	K	L	M	N	O
Phylogeny filter list	**5 lists of randomaly chosen 43 genes**					**Ribosomal proteins are enriched in our 43 list compared to randomly choosen 43 genes**						
279 + must be in *Plasmodium* 3D7 + must not be in any *Cryptosporidium*	7709-7751 in the transcript size list	7752-7794 in the transcript size list	7795-7837 in the transcript size list	7838-7880 in the transcript size list	7881-7923 in the transcript size list	Ribosomal components	Found in group 1?	Found in group 2?	Found in group 3?	Found in group 4?	Found in group 5?	Found in our list?
	TGME49_287450	TGME49_293410	TGME49_459210	TGME49_313840	TGME49_459650	TGME49_202350	FALSE	FALSE	FALSE	FALSE	FALSE	FALSE
TGME49_201830	TGME49_291920	TGME49_251390	TGME49_460530	TGME49_327000	TGME49_325700	TGME49_203620	FALSE	FALSE	FALSE	FALSE	FALSE	TRUE
TGME49_203620	TGME49_301260	TGME49_267630	TGME49_207020	TGME49_210100	TGME49_221860	TGME49_207940	FALSE	FALSE	FALSE	FALSE	FALSE	TRUE
TGME49_206360	TGME49_290250	TGME49_270830	TGME49_264250	TGME49_272630	TGME49_283770	TGME49_216010	FALSE	FALSE	FALSE	FALSE	FALSE	FALSE
TGME49_207940	TGME49_237120	TGME49_461240	TGME49_461190	TGME49_297488	TGME49_322800	TGME49_216040	FALSE	FALSE	FALSE	FALSE	FALSE	FALSE
TGME49_214320	TGME49_243360	TGME49_216420	TGME49_459120	TGME49_315630	TGME49_459990	TGME49_219770	FALSE	FALSE	FALSE	FALSE	FALSE	FALSE
TGME49_214790	TGME49_259100	TGME49_240820	TGME49_231230	TGME49_263530	TGME49_258930	TGME49_220150	FALSE	FALSE	FALSE	FALSE	FALSE	FALSE
TGME49_215260	TGME49_461460	TGME49_255990	TGME49_235590	TGME49_272450	TGME49_300780	TGME49_222990	FALSE	FALSE	FALSE	FALSE	FALSE	FALSE
TGME49_223970	TGME49_203100	TGME49_269470	TGME49_460440	TGME49_312850	TGME49_311050	TGME49_223660	FALSE	FALSE	FALSE	FALSE	FALSE	FALSE
TGME49_225800	TGME49_212060	TGME49_291970	TGME49_200700	TGME49_240460	TGME49_270290	TGME49_225240	FALSE	FALSE	FALSE	FALSE	FALSE	FALSE
TGME49_226270	TGME49_216770	TGME49_259280	TGME49_217951	TGME49_270540	TGME49_322900	TGME49_225250	FALSE	FALSE	FALSE	FALSE	FALSE	FALSE
TGME49_226280	TGME49_271310	TGME49_279430	TGME49_459370	TGME49_290010	TGME49_214860	TGME49_226280	FALSE	FALSE	FALSE	FALSE	FALSE	TRUE
TGME49_230050	TGME49_273300	TGME49_312120	TGME49_214930	TGME49_459000	TGME49_237060	TGME49_230050	FALSE	FALSE	FALSE	FALSE	FALSE	TRUE
TGME49_231150	TGME49_207360	TGME49_325600	TGME49_288970	TGME49_272560	TGME49_258940	TGME49_231120	FALSE	FALSE	FALSE	FALSE	FALSE	FALSE
TGME49_237100	TGME49_240260	TGME49_313418	TGME49_315330	TGME49_461130	TGME49_264230	TGME49_244580	FALSE	FALSE	FALSE	FALSE	FALSE	FALSE
TGME49_238000	TGME49_458730	TGME49_277830	TGME49_457830	TGME49_458500	TGME49_293200	TGME49_251950	FALSE	FALSE	FALSE	FALSE	FALSE	FALSE
TGME49_240210	TGME49_209112	TGME49_457870	TGME49_243900	TGME49_459770	TGME49_328400	TGME49_253800	FALSE	FALSE	FALSE	FALSE	FALSE	FALSE
TGME49_240270	TGME49_230122	TGME49_302060	TGME49_268940	TGME49_279540	TGME49_215610	TGME49_254380	FALSE	FALSE	FALSE	FALSE	FALSE	FALSE
TGME49_240780	TGME49_243220	TGME49_259540	TGME49_307620	TGME49_295140	TGME49_289218	TGME49_260660	FALSE	FALSE	FALSE	FALSE	FALSE	FALSE
TGME49_243530	TGME49_276820	TGME49_261770	TGME49_311820	TGME49_305830	TGME49_460640	TGME49_261380	FALSE	FALSE	FALSE	FALSE	FALSE	FALSE
TGME49_247740	TGME49_313318	TGME49_277780	TGME49_261580	TGME49_201750	TGME49_231990	TGME49_263110	FALSE	FALSE	FALSE	FALSE	FALSE	FALSE
TGME49_251550	TGME49_458880	TGME49_459420	TGME49_254780	TGME49_316580	TGME49_278522	TGME49_263550	FALSE	FALSE	FALSE	FALSE	FALSE	FALSE
TGME49_253510	TGME49_259680	TGME49_459790	TGME49_264260	TGME49_321280	TGME49_294030	TGME49_273060	FALSE	FALSE	FALSE	FALSE	FALSE	FALSE
TGME49_253780	TGME49_292290	TGME49_287460	TGME49_326300	TGME49_457820	TGME49_324200	TGME49_277700	FALSE	FALSE	FALSE	FALSE	FALSE	FALSE
TGME49_254260	TGME49_314560	TGME49_204090	TGME49_200110	TGME49_459160	TGME49_297300	TGME49_284660	FALSE	FALSE	FALSE	FALSE	FALSE	FALSE
TGME49_257110	TGME49_327800	TGME49_309150	TGME49_324500	TGME49_229190	TGME49_328200	TGME49_285970	FALSE	FALSE	FALSE	FALSE	FALSE	FALSE
TGME49_259690	TGME49_243770	TGME49_324100	TGME49_461090	TGME49_279560	TGME49_459910	TGME49_293310	FALSE	FALSE	FALSE	FALSE	FALSE	FALSE
TGME49_263680	TGME49_253680	TGME49_203560	TGME49_458250	TGME49_460030	TGME49_211060	TGME49_297170	FALSE	FALSE	FALSE	FALSE	FALSE	TRUE
TGME49_266750	TGME49_258618	TGME49_229800	TGME49_228140	TGME49_200600	TGME49_244900	TGME49_308930	FALSE	FALSE	FALSE	FALSE	FALSE	FALSE
TGME49_268840	TGME49_284680	TGME49_253770	TGME49_239760	TGME49_327400	TGME49_260850	TGME49_310118	FALSE	FALSE	FALSE	FALSE	FALSE	FALSE
TGME49_270650	TGME49_322130	TGME49_301218	TGME49_258828	TGME49_266600	TGME49_457470	TGME49_310122	FALSE	FALSE	FALSE	FALSE	FALSE	FALSE
TGME49_283850	TGME49_231450	TGME49_459890	TGME49_263642	TGME49_327500	TGME49_459730	TGME49_310490	FALSE	FALSE	FALSE	FALSE	FALSE	FALSE
TGME49_285670	TGME49_281660	TGME49_263720	TGME49_305050	TGME49_461060	TGME49_203630	TGME49_310710	FALSE	FALSE	FALSE	FALSE	FALSE	FALSE
TGME49_285840	TGME49_226820	TGME49_273940	TGME49_321270	TGME49_203430	TGME49_224560	TGME49_313960	FALSE	FALSE	FALSE	FALSE	FALSE	FALSE
TGME49_286070	TGME49_251860	TGME49_458100	TGME49_210220	TGME49_203460	TGME49_232770	TGME49_318420	FALSE	FALSE	FALSE	FALSE	FALSE	FALSE

TGME49_289650		TGME49_254040	TGME49_313322	TGME49_327300	TGME49_240620	TGME49_325500
TGME49_290040		TGME49_283570	TGME49_233842	TGME49_265100	TGME49_242840	TGME49_267990
TGME49_290840		TGME49_283800	TGME49_240490	TGME49_271178	TGME49_288300	TGME49_307060
TGME49_297170		TGME49_461260	TGME49_460090	TGME49_281040	TGME49_325400	TGME49_227870
TGME49_310500		TGME49_227330	TGME49_208080	TGME49_320660	TGME49_457780	TGME49_230598
TGME49_311750		TGME49_227630	TGME49_216230	TGME49_274030	TGME49_220400	TGME49_244930
TGME49_312680		TGME49_228640	TGME49_324800	TGME49_226640	TGME49_457520	TGME49_313740
TGME49_318310		TGME49_260330	TGME49_457310	TGME49_306860	TGME49_458900	TGME49_319988
TGME49_201110						

Appendix Table 3_Bioinformatic screen
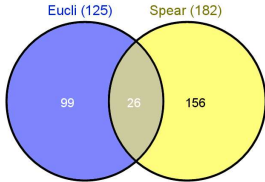
Sheet 1

1-Expression data for 14 genes encoding components of the mitochodnrial protein import machinery

log2 values

Genbank	fold change	Peak time	Genbank	0.00	0.20	0.41	0.61	0.81	1.02	1.22	1.42	1.63	1.83	2.03	2.24	2.44	2.64	2.85	3.05	3.25	3.46	3.66	3.86	4.07	4.27	4.47	4.68	4.88	5.08	5.29	5.49	5.69	5.90	6.10	6.31	6.51	6.71	6.92	7.12	7.32	7.53	7.73	7.93	8.14	8.34	8.54	8.75	8.95
TGME49_054610	3.18	6.31	TGME49_054610	9.76	9.64	9.52	9.41	9.31	9.22	9.15	9.10	9.06	9.03	9.01	9.01	9.02	9.04	9.08	9.13	9.19	9.27	9.37	9.47	9.57	9.69	9.80	9.91	10.02	10.12	10.21	10.29	10.35	10.39	10.42	10.42	10.41	10.38	10.33	10.28	10.22	10.16	10.08	10.01	9.92	9.84	9.75	9.67	9.59
TGME49_060850	2.76	8.95	TGME49_060850	4.49	4.49	4.50	4.50	4.50	4.50	4.50	4.50	4.50	4.51	4.51	4.51	4.51	4.51	4.51	4.52	4.52	4.52	4.52	4.53	4.53	4.53	4.53	4.53	4.53	4.54	4.54	4.54	4.54	4.54	4.55	4.55	4.55	4.55	4.55	4.56	4.56	4.56	4.56	4.56	4.56
TGME49_032820	3.28	5.69	TGME49_032820	9.17	9.07	8.97	8.87	8.76	8.65	8.53	8.41	8.31	8.24	8.22	8.25	8.32	8.43	8.55	8.68	8.81	8.93	9.04	9.15	9.25	9.36	9.45	9.54	9.61	9.68	9.72	9.75	9.77	9.76	9.73	9.69	9.62	9.56	9.49	9.44	9.39	9.36	9.33	9.30	9.25	9.19	9.12	9.03	8.93
TGME49_074090	2.95	0.20	TGME49_074090	8.11	8.09	8.08	8.07	8.05	8.04	8.03	8.01	8.00	7.99	7.98	7.96	7.95	7.94	7.92	7.91	7.90	7.88	7.87	7.86	7.84	7.83	7.82	7.80	7.79	7.78	7.76	7.75	7.74	7.72	7.71	7.69	7.68	7.66	7.64	7.63	7.61	7.60	7.58	7.56	7.55	7.53	7.51	7.49	7.48
TGME49_027830	3.20	6.10	TGME49_027830	6.32	6.28	6.25	6.21	6.18	6.14	6.11	6.08	6.05	6.03	6.03	6.03	6.05	6.08	6.11	6.16	6.22	6.28	6.35	6.43	6.51	6.60	6.68	6.76	6.84	6.90	6.95	6.98	7.00	7.01	7.02	7.01	7.00	6.98	6.95	6.93	6.90	6.87	6.84	6.81	6.77	6.74	6.70	6.66	6.63
TGME49_025710	3.03	6.10	TGME49_025710	6.45	6.43	6.41	6.39	6.38	6.37	6.36	6.35	6.35	6.35	6.35	6.36	6.38	6.40	6.42	6.45	6.48	6.52	6.56	6.60	6.65	6.70	6.75	6.81	6.86	6.91	6.95	6.98	7.01	7.02	7.03	7.03	7.02	7.00	6.98	6.95	6.92	6.89	6.85	6.81	6.77	6.72	6.67	6.63	6.58
TGME49_014150	3.22	5.90	TGME49_014150	7.10	7.04	6.99	6.93	6.89	6.85	6.82	6.80	6.78	6.78	6.80	6.82	6.85	6.90	6.95	7.01	7.08	7.15	7.22	7.30	7.39	7.49	7.58	7.68	7.76	7.83	7.88	7.92	7.93	7.93	7.92	7.89	7.85	7.80	7.75	7.70	7.64	7.59	7.54	7.49	7.44	7.39	7.35	7.32	7.29
TGME49_015390	3.29	6.31	TGME49_015390	8.17	8.01	7.87	7.73	7.60	7.48	7.39	7.31	7.26	7.22	7.19	7.18	7.19	7.21	7.24	7.29	7.35	7.42	7.50	7.58	7.68	7.78	7.89	7.99	8.10	8.20	8.29	8.38	8.45	8.51	8.55	8.56	8.56	8.55	8.52	8.49	8.45	8.41	8.37	8.32	8.26	8.20	8.13	8.06	7.99
TGME49_112220	3.01	5.69	TGME49_112220	7.84	7.83	7.81	7.80	7.79	7.78	7.77	7.77	7.77	7.78	7.79	7.82	7.85	7.89	7.93	7.98	8.03	8.08	8.14	8.20	8.26	8.33	8.39	8.45	8.50	8.53	8.56	8.57	8.57	8.57	8.55	8.52	8.50	8.46	8.43	8.39	8.36	8.33	8.29	8.26	8.24	8.21	8.19	8.17	8.15
TGME49_018280	3.19	6.31	TGME49_018280	9.87	9.75	9.64	9.53	9.43	9.33	9.25	9.17	9.11	9.07	9.04	9.05	9.07	9.12	9.18	9.25	9.34	9.44	9.54	9.66	9.77	9.90	10.02	10.13	10.24	10.32	10.39	10.44	10.47	10.49	10.50	10.50	10.50	10.50	10.48	10.47	10.45	10.42	10.38	10.34	10.28	10.22	10.15	10.08	10.01
TGME49_083590	3.21	6.10	TGME49_083590	6.91	6.87	6.83	6.79	6.75	6.72	6.69	6.67	6.66	6.66	6.67	6.69	6.73	6.77	6.82	6.88	6.95	7.01	7.09	7.17	7.25	7.33	7.42	7.50	7.57	7.64	7.69	7.72	7.75	7.76	7.77	7.76	7.75	7.74	7.72	7.70	7.67	7.65	7.62	7.59	7.56	7.52	7.49	7.45	7.41
TGME49_002810	3.12	5.69	TGME49_002810	7.30	7.30	7.29	7.29	7.28	7.27	7.25	7.24	7.23	7.22	7.23	7.25	7.28	7.30	7.31	7.29	7.25	7.19	7.15	7.13	7.17	7.28	7.43	7.61	7.79	7.94	8.05	8.10	8.11	8.08	8.01	7.90	7.78	7.65	7.54	7.46	7.41	7.40	7.41	7.42	7.42	7.40	7.35	7.30	7.24
TGME49_051780	2.75	6.71	TGME49_051780	10.46	10.47	10.47	10.47	10.48	10.48	10.49	10.49	10.50	10.50	10.50	10.50	10.51	10.51	10.52	10.52	10.53	10.53	10.53	10.54	10.54	10.55	10.55	10.55	10.55	10.56	10.56	10.56	10.56	10.57	10.57	10.57	10.57	10.57	10.57	10.57	10.57	10.57	10.57	10.57	10.57	10.56	10.56	10.56	10.56
TGME49_065220	3.15	6.10	TGME49_065220	7.70	7.66	7.62	7.58	7.54	7.49	7.45	7.41	7.38	7.34	7.32	7.30	7.29	7.29	7.31	7.33	7.36	7.41	7.47	7.54	7.62	7.73	7.84	7.95	8.06	8.15	8.23	8.29	8.34	8.36	8.37	8.36	8.33	8.30	8.26	8.22	8.18	8.14	8.10	8.06	8.02	7.98	7.94	7.90	7.86

3 are non-cyclical
TGME49_074090
TGME49_060850
TGME49_051780

A	B	D	E	G H I J	L	M	O

Column A / B header: 1. The cell cycle transcriptome {Benhke, 2010}n=2869 genes was queried for "like" genes, using either euclidian distance or Spearmann correlation, cutoff 0.9. This was done for each of the 11 baits, generating a list of total 395 genes with similar mRNA expression profile. Of those we identified the non-redundant genes.

Column D / E header: 2. We Keept only unique instances in each list

Column G header: 3. a Venn diagram was used to to identify overlaping genes between the two methods

Column L header: 4. List of Uniqe genes (281)

Column O header: 5. Convert to current geneID and anontation

Euclidian (143 V5)	Spearmann (203 V5)	Euclidian (125 uniq V5)	Spearmann (182 V5)	Uniq281	origin	(current geneID)
TGME49_016490	TGME49_045650	TGME49_016490	TGME49_045650	TGME49_007940;TGME49_007950	Spearmann	TGME49_201110
TGME49_088580	TGME49_016490	TGME49_088580	TGME49_016490	TGME49_011240;TGME49_011250	Euclidian	TGME49_201830
TGME49_048960	TGME49_088580	TGME49_048960	TGME49_088580	TGME49_011300;TGME49_011310	Both	TGME49_202180
TGME49_026280	TGME49_048960	TGME49_026280	TGME49_048960	TGME49_042410;TGME49_042420	Spearmann	TGME49_203620
TGME49_105750	TGME49_026280	TGME49_105750	TGME49_026280	TGME49_058090;TGME49_058100	Both	TGME49_203780
TGME49_049920	TGME49_049920	TGME49_049920	TGME49_049920	TGME49_072690;TGME49_072700	Spearmann	TGME49_204490
TGME49_051760	TGME49_025930	TGME49_051760	TGME49_025930	TGME49_094980;TGME49_094990	Spearmann	TGME49_205510
TGME49_054610	TGME49_107650	TGME49_054610	TGME49_107650	TGME49_108990;TGME49_109000	Euclidian	TGME49_206360
TGME49_011300;TGME49_011310	TGME49_051760	TGME49_011300;TGME49_011310	TGME49_051760	TGME49_112610;TGME49_112620	Spearmann	TGME49_207640
				TGME49_105750	Euclidian	TGME49_207710
TGME49_095010	TGME49_046920	TGME49_095010	TGME49_046920	TGME49_042610	Euclidian	TGME49_207760
TGME49_032820	TGME49_016770	TGME49_032820	TGME49_016770	TGME49_005510	Euclidian	TGME49_207820
TGME49_006360	TGME49_110400	TGME49_006360	TGME49_110400	TGME49_085720	Euclidian	TGME49_207940
TGME49_027830	TGME49_054610	TGME49_027830	TGME49_054610	TGME49_040890	Euclidian	TGME49_208200
TGME49_042610	TGME49_016830	TGME49_042610	TGME49_016830	TGME49_091110	Euclidian	TGME49_209020
TGME49_005510	TGME49_011300;TGME49_011310	TGME49_005510	TGME49_011300;TGME49_011310	TGME49_033260	Euclidian	TGME49_209240
TGME49_014150	TGME49_054810	TGME49_014150	TGME49_054810	TGME49_110320	Euclidian	TGME49_209430
TGME49_072010	TGME49_064060	TGME49_072010	TGME49_064060	TGME49_114710	Euclidian	TGME49_209680
TGME49_085720	TGME49_112340	TGME49_085720	TGME49_112340	TGME49_099270	Euclidian	TGME49_209790
TGME49_040890	TGME49_083850	TGME49_040890	TGME49_083850	TGME49_026430	Euclidian	TGME49_210360
TGME49_091110	TGME49_048960	TGME49_091110	TGME49_048200	TGME49_007820	Euclidian	TGME49_211240
TGME49_033260	TGME49_048200	TGME49_033260	TGME49_063340	TGME49_011410	Euclidian	TGME49_211310
TGME49_110320	TGME49_063340	TGME49_114710	TGME49_095010	TGME49_049510	Euclidian	TGME49_211410
TGME49_114710	TGME49_110320	TGME49_099270	TGME49_079330	TGME49_031750	Euclidian	TGME49_211710
TGME49_099270	TGME49_095010	TGME49_026430	TGME49_070650	TGME49_045470	Euclidian	TGME49_211870
TGME49_026430	TGME49_079330	TGME49_007820	TGME49_110850	TGME49_007710	Euclidian	TGME49_213410
TGME49_007820	TGME49_070650	TGME49_011410	TGME49_007710	TGME49_069740	Euclidian	TGME49_214150
TGME49_011410	TGME49_026430	TGME49_049510	TGME49_071280	TGME49_094350	Euclidian	TGME49_214320
TGME49_049510	TGME49_110850	TGME49_031750	TGME49_116900	TGME49_112680	Euclidian	TGME49_214790
TGME49_031750	TGME49_071280	TGME49_045470	TGME49_038000	TGME49_061260	Euclidian	TGME49_214870
TGME49_045470	TGME49_116900	TGME49_108990;TGME49_109000	TGME49_061690	TGME49_040270	Euclidian	TGME49_215260
TGME49_108990;TGME49_109000	TGME49_049510	TGME49_007710	TGME49_105490	TGME49_027060	Euclidian	TGME49_215390
TGME49_007710	TGME49_038000	TGME49_069740	TGME49_114480	TGME49_058210	Euclidian	TGME49_215400
TGME49_069740	TGME49_061690	TGME49_094350	TGME49_111030	TGME49_043760	Euclidian	TGME49_215430
TGME49_094350	TGME49_105490	TGME49_112680	TGME49_007760	TGME49_060300	Euclidian	TGME49_215490
TGME49_112680	TGME49_114480	TGME49_061260	TGME49_071180	TGME49_054940	Euclidian	TGME49_216120
TGME49_061260	TGME49_111030	TGME49_040270	TGME49_086550	TGME49_014870	Euclidian	TGME49_216210
TGME49_040270	TGME49_007760	TGME49_027060	TGME49_067390	TGME49_009240	Euclidian	TGME49_216490
TGME49_027060	TGME49_094350	TGME49_058210	TGME49_061520	TGME49_013410	Euclidian	TGME49_216770
TGME49_058210	TGME49_071180	TGME49_043760	TGME49_018230	TGME49_011870	Euclidian	TGME49_216830
TGME49_043760	TGME49_086550	TGME49_060300	TGME49_114800	TGME49_065280	Euclidian	TGME49_216900
TGME49_060300	TGME49_067390	TGME49_054940	TGME49_111870	TGME49_058390	Euclidian	TGME49_217820
TGME49_054940	TGME49_061520	TGME49_014870	TGME49_009430	TGME49_017820	Euclidian	TGME49_217890
TGME49_014870	TGME49_018230	TGME49_009240	TGME49_093700	TGME49_037100	Euclidian	TGME49_218230
TGME49_009240	TGME49_114800	TGME49_013410	TGME49_040400	TGME49_111240	Euclidian	TGME49_218280
TGME49_013410	TGME49_043760	TGME49_011870	TGME49_016120	TGME49_020140	Euclidian	TGME49_219140
TGME49_011870	TGME49_111870	TGME49_065280	TGME49_033720	TGME49_112350	Euclidian	TGME49_220140
TGME49_065280	TGME49_009430	TGME49_058390	TGME49_112610;TGME49_112620	TGME49_047740	Euclidian	TGME49_222070
TGME49_058390	TGME49_093700	TGME49_017820	TGME49_009790	TGME49_066950	Euclidian	TGME49_222090
TGME49_017820	TGME49_040400	TGME49_037100	TGME49_055320	TGME49_106610	Euclidian	TGME49_222170
TGME49_037100	TGME49_016120	TGME49_065220	TGME49_049950	TGME49_040210	Euclidian	TGME49_222860
TGME49_065220	TGME49_033720	TGME49_111240	TGME49_049910	TGME49_057150	Euclidian	TGME49_223140
TGME49_111240	TGME49_011870	TGME49_020140	TGME49_106290	TGME49_106380	Euclidian	TGME49_223710
TGME49_020140	TGME49_112610;TGME49_112620	TGME49_112350	TGME49_031020	TGME49_090040	Euclidian	TGME49_223970
TGME49_112350	TGME49_009790		TGME49_032640	TGME49_049210	Euclidian	TGME49_225710
	TGME49_055320		TGME49_101390			TGME49_225800
	TGME49_049950					
	TGME49_049910					
	TGME49_106290					
	TGME49_111240					
	TGME49_031020					
	TGME49_032640					

Venn diagram (Column G–J): Eucli (125) — Spear (182); 99 | 26 | 156

Only 26 genes are common to both methods, highlighting their complementarities

Thus, we have 281 unique genes

TGME49_047740	TGME49_101390	TGME49_047740	TGME49_016210	TGME49_063760	Euclidian	TGME49_225930
TGME49_097880	TGME49_016210	TGME49_097880	TGME49_036580	TGME49_037290	Euclidian	TGME49_226270
TGME49_066950	TGME49_036580	TGME49_066950	TGME49_072740	TGME49_008200	Euclidian	TGME49_226280
TGME49_049650	TGME49_072740	TGME49_049650	TGME49_032820	TGME49_044140	Euclidian	TGME49_226430
TGME49_106610	TGME49_032820	TGME49_106610	TGME49_111430	TGME49_091590	Euclidian	TGME49_227060
TGME49_040210	TGME49_111430	TGME49_040210	TGME49_072490	TGME49_092010	Euclidian	TGME49_227830
TGME49_057150	TGME49_072490	TGME49_057150	TGME49_039790	TGME49_086070	Euclidian	TGME49_229180
TGME49_040820	TGME49_039790	TGME49_040820	TGME49_110500	TGME49_030840	Euclidian	TGME49_230050
TGME49_023710	TGME49_110500	TGME49_023710	TGME49_029180	TGME49_054240	Euclidian	TGME49_230450
TGME49_073460	TGME49_029180	TGME49_073460	TGME49_006360	TGME49_016900	Euclidian	TGME49_230555
TGME49_018280	TGME49_006360	TGME49_018280	TGME49_015400	TGME49_085670	Euclidian	TGME49_230580
TGME49_106380	TGME49_015400	TGME49_106380	TGME49_054280	TGME49_096950	Euclidian	TGME49_230840
TGME49_090040	TGME49_054280	TGME49_090040	TGME49_030450	TGME49_070150	Euclidian	TGME49_230990
TGME49_049210	TGME49_030450	TGME49_049210	TGME49_032520	TGME49_086420	Euclidian	TGME49_231020
TGME49_030990	TGME49_032520	TGME49_030990	TGME49_022090	TGME49_082190	Euclidian	TGME49_231150
TGME49_031750	TGME49_022090	TGME49_063760	TGME49_035560	TGME49_040200	Euclidian	TGME49_231750
TGME49_063760	TGME49_035560	TGME49_037290	TGME49_004490	TGME49_030550	Euclidian	TGME49_232520
TGME49_037290	TGME49_004490	TGME49_008200	TGME49_116350	TGME49_094050	Euclidian	TGME49_232640
TGME49_008200	TGME49_016830	TGME49_044140	TGME49_094420	TGME49_075490	Euclidian	TGME49_232815
TGME49_044140	TGME49_016830	TGME49_091590	TGME49_059690	TGME49_106650	Euclidian	TGME49_233100
TGME49_091590	TGME49_094420	TGME49_092010	TGME49_068640	TGME49_068820	Euclidian	TGME49_233190
TGME49_092010	TGME49_059690	TGME49_086070	TGME49_073640	TGME49_090570	Euclidian	TGME49_233260
TGME49_086070	TGME49_068640	TGME49_030840	TGME49_078270	TGME49_064790	Euclidian	TGME49_233720
TGME49_030840	TGME49_073640	TGME49_054240	TGME49_030990	TGME49_034530	Euclidian	TGME49_234530
TGME49_112680	TGME49_078270	TGME49_016900	TGME49_056990	TGME49_044120	Euclidian	TGME49_235560
TGME49_054240	TGME49_016900	TGME49_085670	TGME49_014790	TGME49_120550	Euclidian	TGME49_235970
TGME49_016900	TGME49_056990	TGME49_011240;TGME49_011250	TGME49_056760	TGME49_033190	Euclidian	TGME49_236580
TGME49_085670	TGME49_014790	TGME49_096950	TGME49_061600	TGME49_065110	Euclidian	TGME49_237100
TGME49_011240;TGME49_011250	TGME49_096950	TGME49_070150	TGME49_121310	TGME49_010360	Euclidian	TGME49_237290
TGME49_096950	TGME49_061600	TGME49_086420	TGME49_063530	TGME49_049410	Euclidian	TGME49_237460
TGME49_070150	TGME49_121310	TGME49_082190	TGME49_121640	TGME49_113350	Euclidian	TGME49_238000
TGME49_086420	TGME49_063530	TGME49_040200	TGME49_074190	TGME49_065990	Euclidian	TGME49_238240
TGME49_082190	TGME49_121640	TGME49_030550	TGME49_027830	TGME49_031150	Euclidian	TGME49_239610
TGME49_040200	TGME49_074190	TGME49_094050	TGME49_051500	TGME49_030050	Euclidian	TGME49_239790
TGME49_030550	TGME49_027830	TGME49_075490	TGME49_112490	TGME49_009680	Euclidian	TGME49_239890
TGME49_094050	TGME49_051500	TGME49_106650	TGME49_073460	TGME49_088510	Euclidian	TGME49_240200
TGME49_009240	TGME49_112490	TGME49_068820	TGME49_015490	TGME49_078900	Euclidian	TGME49_240210
TGME49_075490	TGME49_073460	TGME49_090570	TGME49_007640	TGME49_106950	Euclidian	TGME49_240270
TGME49_106650	TGME49_015490	TGME49_064790	TGME49_069650	TGME49_039890	Euclidian	TGME49_240400
TGME49_037100	TGME49_007640	TGME49_034530	TGME49_089650	TGME49_040780	Euclidian	TGME49_240440
TGME49_068820	TGME49_069650	TGME49_044120	TGME49_052480	TGME49_049010	Euclidian	TGME49_240590
TGME49_090570	TGME49_089650	TGME49_120550	TGME49_043530	TGME49_068840	Euclidian	TGME49_240780
TGME49_064790	TGME49_052480	TGME49_033190	TGME49_003620	TGME49_046730	Euclidian	TGME49_240810
TGME49_097880	TGME49_043530	TGME49_065110	TGME49_061480	TGME49_001830	Euclidian	TGME49_240820
TGME49_066950	TGME49_003620	TGME49_053510	TGME49_053510	TGME49_009020	Euclidian	TGME49_240890
TGME49_034530	TGME49_061480	TGME49_010360	TGME49_051690	TGME49_022170	Euclidian	TGME49_242415
TGME49_044120	TGME49_057110	TGME49_049410	TGME49_025800	TGME49_015430	Euclidian	TGME49_242610
TGME49_120550	TGME49_049410	TGME49_113350	TGME49_044440	TGME49_091150	Euclidian	TGME49_243530
TGME49_040820	TGME49_051690	TGME49_065990	TGME49_085840	TGME49_063680	Euclidian	TGME49_243760
TGME49_033190	TGME49_025800	TGME49_031150	TGME49_113300	TGME49_071300	Euclidian	TGME49_244120
TGME49_065110	TGME49_044050	TGME49_030050	TGME49_033100	TGME49_111750	Euclidian	TGME49_244140
TGME49_049210	TGME49_033100	TGME49_009680	TGME49_040810	TGME49_016490	Both	TGME49_244310
TGME49_053510	TGME49_063260	TGME49_088510	TGME49_058090;TGME49_058100	TGME49_088580	Both	TGME49_244380
TGME49_010360	TGME49_040810	TGME49_078900	TGME49_121680	TGME49_048960	Both	TGME49_244440
TGME49_108990;TGME49_109000	TGME49_058090;TGME49_058100	TGME49_106950	TGME49_025710	TGME49_026280	Both	TGME49_245470
TGME49_049410	TGME49_121680	TGME49_039890	TGME49_047550	TGME49_049920	Both	TGME49_245520
TGME49_113350	TGME49_025710	TGME49_040780	TGME49_044310	TGME49_051760	Both	TGME49_245650
TGME49_112680	TGME49_047550	TGME49_049010	TGME49_113230	TGME49_054610	Both	TGME49_246730
TGME49_040270	TGME49_044270	TGME49_001110	TGME49_054770	TGME49_095010	Both	TGME49_246920
TGME49_065990	TGME49_044440	TGME49_025710	TGME49_003780	TGME49_032820	Both	TGME49_247390
TGME49_065110	TGME49_113230	TGME49_068840	TGME49_014150	TGME49_006360	Both	TGME49_247550
TGME49_043760	TGME49_054770	TGME49_046730	TGME49_042410;TGME49_042420	TGME49_027830	Both	TGME49_247740
TGME49_082190	TGME49_003780	TGME49_054260	TGME49_112480	TGME49_014150	Both	TGME49_248200
TGME49_031150	TGME49_009430	TGME49_001830	TGME49_063440	TGME49_072010	Both	TGME49_248960

TGME49_030050	TGME49_014150	TGME49_009020	TGME49_023970	TGME49_065220	Both	TGME49_249010
TGME49_009680	TGME49_042410;TGME49_042420	TGME49_022170	TGME49_015390	TGME49_097880	Both	TGME49_249215
TGME49_088510	TGME49_121680	TGME49_015430	TGME49_019140	TGME49_049650	Both	TGME49_249410
TGME49_078900	TGME49_112480	TGME49_091150	TGME49_051550	TGME49_040820	Both	TGME49_249510
TGME49_037100	TGME49_063440	TGME49_063680	TGME49_017890	TGME49_023710	Both	TGME49_249650
TGME49_106950	TGME49_023970	TGME49_071300	TGME49_072690;TGME49_072700	TGME49_073460	Both	TGME49_249910
TGME49_064790	TGME49_073640	TGME49_111750	TGME49_091080	TGME49_018280	Both	TGME49_249920
TGME49_057150	TGME49_015390		TGME49_040820	TGME49_030990	Both	TGME49_249950
TGME49_039890	TGME49_019140		TGME49_090840	TGME49_053510	Both	TGME49_251170
TGME49_040780	TGME49_051550		TGME49_051170	TGME49_001110	Both	TGME49_251500
TGME49_049010	TGME49_017890		TGME49_109570	TGME49_025710	Both	TGME49_251550
TGME49_001110	TGME49_072690;TGME49_072700		TGME49_112220	TGME49_054260	Both	TGME49_251690
TGME49_025710	TGME49_091080		TGME49_072010	TGME49_045650	Spearmann	TGME49_251760
TGME49_068840	TGME49_090840		TGME49_038240	TGME49_025930	Spearmann	TGME49_252230
TGME49_046730	TGME49_051170		TGME49_044380	TGME49_107650	Spearmann	TGME49_252340
TGME49_054260	TGME49_109570		TGME49_062040	TGME49_046920	Spearmann	TGME49_252480
TGME49_001830	TGME49_112220		TGME49_023140	TGME49_016770	Spearmann	TGME49_253510
TGME49_009020	TGME49_072010		TGME49_054260	TGME49_110400	Spearmann	TGME49_253780
TGME49_022170	TGME49_038240		TGME49_035970	TGME49_016830	Spearmann	TGME49_254260
TGME49_015430	TGME49_044380		TGME49_015260	TGME49_054810	Spearmann	TGME49_254280
TGME49_091150	TGME49_062040		TGME49_052340	TGME49_064060	Spearmann	TGME49_254610
TGME49_063680	TGME49_023140		TGME49_023710	TGME49_112340	Spearmann	TGME49_254770
TGME49_071300	TGME49_054260		TGME49_052230	TGME49_083850	Spearmann	TGME49_254810
TGME49_111750	TGME49_056990		TGME49_047390	TGME49_048200	Spearmann	TGME49_254940
TGME49_065220	TGME49_035970		TGME49_060440	TGME49_063340	Spearmann	TGME49_255320
	TGME49_015260		TGME49_037460	TGME49_079330	Spearmann	TGME49_256760
	TGME49_014790		TGME49_112530	TGME49_070650	Spearmann	TGME49_256990
	TGME49_052340		TGME49_002180	TGME49_110850	Spearmann	TGME49_257110
	TGME49_121640		TGME49_022070	TGME49_071280	Spearmann	TGME49_257150
	TGME49_023710		TGME49_088500	TGME49_116900	Spearmann	TGME49_258100
	TGME49_112490		TGME49_018280	TGME49_038000	Spearmann	TGME49_258210
	TGME49_052230		TGME49_063070	TGME49_061690	Spearmann	TGME49_258390
	TGME49_073460		TGME49_011710	TGME49_105490	Spearmann	TGME49_259690
	TGME49_047390		TGME49_064200	TGME49_114480	Spearmann	TGME49_260300
	TGME49_060440		TGME49_063420	TGME49_111030	Spearmann	TGME49_260440
	TGME49_037460		TGME49_049650	TGME49_007760	Spearmann	TGME49_261260
	TGME49_112530		TGME49_022860	TGME49_071180	Spearmann	TGME49_261480
	TGME49_002180		TGME49_026270	TGME49_086550	Spearmann	TGME49_261520
	TGME49_022070		TGME49_105460	TGME49_067390	Spearmann	TGME49_261600
	TGME49_052480		TGME49_118310	TGME49_061520	Spearmann	TGME49_261690
	TGME49_088500		TGME49_073520	TGME49_018230	Spearmann	TGME49_262040
	TGME49_018280		TGME49_040440	TGME49_114800	Spearmann	TGME49_263070
	TGME49_063070		TGME49_014320	TGME49_111870	Spearmann	TGME49_263260
	TGME49_011710		TGME49_108950	TGME49_009430	Spearmann	TGME49_263340
	TGME49_064200		TGME49_095960	TGME49_093700	Spearmann	TGME49_263420
	TGME49_063420		TGME49_113520	TGME49_040400	Spearmann	TGME49_263440
	TGME49_016770		TGME49_083590	TGME49_016120	Spearmann	TGME49_263530
	TGME49_057110		TGME49_110050	TGME49_033720	Spearmann	TGME49_263680
	TGME49_049650		TGME49_072410	TGME49_009790	Spearmann	TGME49_263760
	TGME49_022860		TGME49_030580	TGME49_055320	Spearmann	TGME49_264060
	TGME49_026270		TGME49_007940;TGME49_007950	TGME49_049950	Spearmann	TGME49_264200
	TGME49_105460		TGME49_099210	TGME49_049910	Spearmann	TGME49_264790
	TGME49_118310		TGME49_053510	TGME49_106290	Spearmann	TGME49_265110
	TGME49_073520		TGME49_094980;TGME49_094990	TGME49_031020	Spearmann	TGME49_265220
	TGME49_040440		TGME49_045520	TGME49_032640	Spearmann	TGME49_265280
	TGME49_014320		TGME49_039610	TGME49_101390	Spearmann	TGME49_265990
	TGME49_108950		TGME49_001110	TGME49_016210	Spearmann	TGME49_266750
	TGME49_095960		TGME49_066750	TGME49_036580	Spearmann	TGME49_266950
	TGME49_113520		TGME49_040590	TGME49_072740	Spearmann	TGME49_267390
	TGME49_083590		TGME49_116450	TGME49_111430	Spearmann	TGME49_268640
	TGME49_110050		TGME49_053780	TGME49_072490	Spearmann	TGME49_268820
	TGME49_072410		TGME49_065220	TGME49_039790	Spearmann	TGME49_268840
	TGME49_083590		TGME49_097880	TGME49_110500	Spearmann	TGME49_269650
			TGME49_097170	TGME49_029180	Spearmann	TGME49_269740

TGME49_030580		
TGME49_007940;TGME49_007950		
TGME49_099210		
TGME49_053510		
TGME49_094980;TGME49_094990		
TGME49_045520		
TGME49_039610		
TGME49_001110		
TGME49_066750		
TGME49_040590		
TGME49_056990		
TGME49_116450		
TGME49_074190		
TGME49_053780		
TGME49_113520		
TGME49_112490		
TGME49_043530		
TGME49_065220		
TGME49_057110		
TGME49_097880		
TGME49_097170		

TGME49_015400	Spearmann	TGME49_270150
TGME49_054280	Spearmann	TGME49_270650
TGME49_030450	Spearmann	TGME49_271178
TGME49_032520	Spearmann	TGME49_271182
TGME49_022090	Spearmann	TGME49_271280
TGME49_035560	Spearmann	TGME49_271300
TGME49_004490	Spearmann	TGME49_272010
TGME49_116350	Spearmann	TGME49_272410
TGME49_094420	Spearmann	TGME49_272490
TGME49_059690	Spearmann	TGME49_272695
TGME49_068640	Spearmann	TGME49_272740
TGME49_073640	Spearmann	TGME49_273460
TGME49_078270	Spearmann	TGME49_273520
TGME49_056990	Spearmann	TGME49_273640
TGME49_014790	Spearmann	TGME49_274190
TGME49_056760	Spearmann	TGME49_275490
TGME49_061600	Spearmann	TGME49_278270
TGME49_121310	Spearmann	TGME49_278900
TGME49_063530	Spearmann	TGME49_279330
TGME49_121640	Spearmann	TGME49_282190
TGME49_074190	Spearmann	TGME49_283590
TGME49_051500	Spearmann	TGME49_283850
TGME49_112490	Spearmann	TGME49_285670
TGME49_015490	Spearmann	TGME49_285720
TGME49_007640	Spearmann	TGME49_285840
TGME49_069650	Spearmann	TGME49_286070
TGME49_089650	Spearmann	TGME49_286420
TGME49_052480	Spearmann	TGME49_286550
TGME49_043530	Spearmann	TGME49_288500
TGME49_003620	Spearmann	TGME49_288510
TGME49_061480	Spearmann	TGME49_288580
TGME49_057110	Spearmann	TGME49_289650
TGME49_051690	Spearmann	TGME49_290040
TGME49_025800	Spearmann	TGME49_290570
TGME49_044440	Spearmann	TGME49_290840
TGME49_085840	Spearmann	TGME49_291080
TGME49_033100	Spearmann	TGME49_291150
TGME49_063260	Spearmann	TGME49_291590
TGME49_040810	Spearmann	TGME49_292010
TGME49_121680	Spearmann	TGME49_293700
TGME49_047550	Spearmann	TGME49_294050
TGME49_044310	Spearmann	TGME49_294350
TGME49_113230	Spearmann	TGME49_294420
TGME49_054770	Spearmann	TGME49_294980
TGME49_003780	Spearmann	TGME49_295010
TGME49_112480	Spearmann	TGME49_295960
TGME49_063440	Spearmann	TGME49_296950
TGME49_023970	Spearmann	TGME49_297170
TGME49_015390	Spearmann	TGME49_297880
TGME49_019140	Spearmann	TGME49_299210
TGME49_051550	Spearmann	TGME49_299270
TGME49_017890	Spearmann	TGME49_301390
TGME49_091080	Spearmann	TGME49_305460
TGME49_090840	Spearmann	TGME49_305490
TGME49_051170	Spearmann	TGME49_305750
TGME49_109570	Spearmann	TGME49_306290
TGME49_112220	Spearmann	TGME49_306380
TGME49_038240	Spearmann	TGME49_306610
TGME49_044380	Spearmann	TGME49_306650
TGME49_062040	Spearmann	TGME49_306950
TGME49_023140	Spearmann	TGME49_307650
TGME49_035970	Spearmann	TGME49_308950
TGME49_015260	Spearmann	TGME49_308990
TGME49_052340	Spearmann	TGME49_309570

TGME49_052230	Spearmann	TGME49_310050
TGME49_047390	Spearmann	TGME49_310320
TGME49_060440	Spearmann	TGME49_310400
TGME49_037460	Spearmann	TGME49_310500
TGME49_112530	Spearmann	TGME49_310850
TGME49_002180	Spearmann	TGME49_311030
TGME49_022070	Spearmann	TGME49_311240
TGME49_088500	Spearmann	TGME49_311430
TGME49_063070	Spearmann	TGME49_311750
TGME49_011710	Spearmann	TGME49_311870
TGME49_064200	Spearmann	TGME49_312220
TGME49_063420	Spearmann	TGME49_312340
TGME49_022860	Spearmann	TGME49_312350
TGME49_026270	Spearmann	TGME49_312480
TGME49_105460	Spearmann	TGME49_312490
TGME49_118310	Spearmann	TGME49_312530
TGME49_073520	Spearmann	TGME49_312680
TGME49_040440	Spearmann	TGME49_313230
TGME49_014320	Spearmann	TGME49_313350
TGME49_108950	Spearmann	TGME49_313520
TGME49_095960	Spearmann	TGME49_314480
TGME49_113520	Spearmann	TGME49_314710
TGME49_083590	Spearmann	TGME49_314800
TGME49_110050	Spearmann	TGME49_316350
TGME49_072410	Spearmann	TGME49_316450
TGME49_030580	Spearmann	TGME49_316900
TGME49_099210	Spearmann	TGME49_318310
TGME49_045520	Spearmann	TGME49_320550
TGME49_039610	Spearmann	TGME49_321310
TGME49_066750	Spearmann	TGME49_321640
TGME49_040590	Spearmann	TGME49_321680
TGME49_116450	Spearmann	
TGME49_053780	Spearmann	
TGME49_097170	Spearmann	

Appendix Table 4_Bioinformatic screen

Sheet 1

	A	B	C	D	E	F	G	H
	Starting list	Localization	Phylogeny		Essentiality		TMDs	
	279 (current number of 281 found by mRNA expression)	Prediction of canonical mitochondrial targeting signal	279 + must be in all Plasmodium species = 144	279 unique apicomplexan = 109	step 1 - transform to TGGT1	Step 2 - CRISPR screen scores >-6.8 and <-2 = 176	50 genes from the 279 that have predicted TMDs	# TM Domains
	TGME49_201110	0.563	TGME49_201110	TGME49_201110	TGGT1_201110	TGGT1_201110	TGME49_201110	1
	TGME49_201830	0.9991	TGME49_201830	TGME49_201830	TGGT1_201830	TGGT1_201830	TGME49_207710	4
	TGME49_202180	0.8951	TGME49_203620	TGME49_202180	TGGT1_202180	TGGT1_202180	TGME49_209790	1
	TGME49_203620	0.9734	TGME49_205510	TGME49_203620	TGGT1_203620	TGGT1_203620	TGME49_211240	1
	TGME49_203780	0.077	TGME49_206360	TGME49_204490	TGGT1_203780	TGGT1_203780	TGME49_211710	3
	TGME49_204490	0.2057	TGME49_207640	TGME49_207940	TGGT1_204490	TGGT1_205510	TGME49_211870	1
	TGME49_205510	0.0529	TGME49_207760	TGME49_208200	TGGT1_205510	TGGT1_207640	TGME49_214150	1
	TGME49_206360	0.5919	TGME49_207820	TGME49_209020	TGGT1_206360	TGGT1_207710	TGME49_214320	12
	TGME49_207640	0.9939	TGME49_207940	TGME49_209680	TGGT1_207640	TGGT1_207760	TGME49_215490	12
	TGME49_207710	0.2017	TGME49_209240	TGME49_211310	TGGT1_207710	TGGT1_207820	TGME49_216770	2
	TGME49_207760	0.6445	TGME49_209430	TGME49_211710	TGGT1_207760	TGGT1_207940	TGME49_222090	2
	TGME49_207820	0.0142	TGME49_209790	TGME49_211870	TGGT1_207820	TGGT1_208200	TGME49_225710	1
	TGME49_207940	0.2581	TGME49_210360	TGME49_215430	TGGT1_208200	TGGT1_210360	TGME49_226270	7
	TGME49_208200	0.2035	TGME49_211240	TGME49_215490	TGGT1_209020	TGGT1_211870	TGME49_226430	3
	TGME49_209020	0.8218	TGME49_211410	TGME49_216120	TGGT1_209240	TGGT1_213410	TGME49_230555	3
	TGME49_209240	0.9423	TGME49_213410	TGME49_216210	TGGT1_209430	TGGT1_213930	TGME49_230840	5
	TGME49_209430	0.165	TGME49_214150	TGME49_216490	TGGT1_209680	TGGT1_214150	TGME49_233100	1
	TGME49_209680	0.9805	TGME49_214320	TGME49_216770	TGGT1_209790	TGGT1_214870	TGME49_234530	2
	TGME49_209790	0.042	TGME49_214790	TGME49_218230	TGGT1_210360	TGGT1_215400	TGME49_239610	1
	TGME49_210360	0.0809	TGME49_215260	TGME49_220140	TGGT1_211240	TGGT1_215430	TGME49_239890	1
	TGME49_211240	0.0069	TGME49_215430	TGME49_222070	TGGT1_211310	TGGT1_215490	TGME49_240210	11
	TGME49_211310	0.1385	TGME49_215490	TGME49_222170	TGGT1_211410	TGGT1_216120	TGME49_240440	1
	TGME49_211410	0.0989	TGME49_216900	TGME49_226430	TGGT1_211710	TGGT1_216210	TGME49_240780	1
	TGME49_211710	0.8377	TGME49_217820	TGME49_227060	TGGT1_211870	TGGT1_216900	TGME49_240810	10
	TGME49_211870	0.4508	TGME49_217890	TGME49_230555	TGGT1_213410	TGGT1_217820	TGME49_243760	3
	TGME49_213410	0.6752	TGME49_218280	TGME49_230580	TGGT1_213930	TGGT1_218280	TGME49_244140	1
	TGME49_214150	0.1705	TGME49_222860	TGME49_230840	TGGT1_214150	TGGT1_220140	TGME49_244440	10
	TGME49_214320	0.0367	TGME49_223140	TGME49_230990	TGGT1_214320	TGGT1_222140	TGME49_249510	1
	TGME49_214790	0.8383	TGME49_223710	TGME49_231020	TGGT1_214790	TGGT1_222170	TGME49_252340	11
	TGME49_214870	0.9776	TGME49_223970	TGME49_231750	TGGT1_214870	TGGT1_222860	TGME49_253510	8
	TGME49_215260	0.0313	TGME49_225710	TGME49_232815	TGGT1_215260	TGGT1_223710	TGME49_260300	2
	TGME49_215390	0.0322	TGME49_225930	TGME49_234530	TGGT1_215390	TGGT1_223970	TGME49_261480	9
	TGME49_215400	0.981	TGME49_226270	TGME49_235560	TGGT1_215400	TGGT1_225260	TGME49_263260	11
	TGME49_215430	0.5146	TGME49_226280	TGME49_237100	TGGT1_215430	TGGT1_225800	TGME49_264200	2
	TGME49_215490	0.1881	TGME49_227830	TGME49_237290	TGGT1_215490	TGGT1_225930	TGME49_266750	7
	TGME49_216120	0.333	TGME49_229180	TGME49_237460	TGGT1_216120	TGGT1_226280	TGME49_268820	4
	TGME49_216210	0.0031	TGME49_230050	TGME49_238000	TGGT1_216210	TGGT1_226960	TGME49_272695	1
	TGME49_216490	0.0276	TGME49_230450	TGME49_239610	TGGT1_216490	TGGT1_227830	TGME49_273460	2
	TGME49_216770	0.3362	TGME49_231150	TGME49_240200	TGGT1_216770	TGGT1_229180	TGME49_285670	6
	TGME49_216830	0.0612	TGME49_232520	TGME49_240270	TGGT1_216830	TGGT1_230050	TGME49_290840	1
	TGME49_216900	0.2566	TGME49_233100	TGME49_240400	TGGT1_216900	TGGT1_230580	TGME49_294050	1
	TGME49_217820	0.0232	TGME49_233190	TGME49_240440	TGGT1_217820	TGGT1_230990	TGME49_294980	1
	TGME49_217890	0.0354	TGME49_233720	TGME49_240780	TGGT1_217890	TGGT1_231020	TGME49_296950	10
	TGME49_218230	0.0122	TGME49_235970	TGME49_240810	TGGT1_218230	TGGT1_231750	TGME49_297880	1
	TGME49_218280	0.5333	TGME49_236580	TGME49_240820	TGGT1_218280	TGGT1_232520	TGME49_308990	13
	TGME49_219140	0.0409	TGME49_237100	TGME49_242415	TGGT1_219140	TGGT1_232640	TGME49_310320	2
	TGME49_220140	0.0226	TGME49_238000	TGME49_243760	TGGT1_220140	TGGT1_232815	TGME49_313520	1
	TGME49_222070	0.0552	TGME49_238240	TGME49_244120	TGGT1_222070	TGGT1_233100	TGME49_316450	6
	TGME49_222090	0.4911	TGME49_239790	TGME49_244140	TGGT1_222140	TGGT1_233190	TGME49_321310	1
	TGME49_222170	0.0183	TGME49_240210	TGME49_245520	TGGT1_222170	TGGT1_233500	TGME49_321640	1
	TGME49_222860	0.0078	TGME49_240590	TGME49_245650	TGGT1_222860	TGGT1_233720		
	TGME49_223140	0.0624	TGME49_240780	TGME49_247390	TGGT1_223140	TGGT1_235560		
	TGME49_223710	0.0453	TGME49_240890	TGME49_247740	TGGT1_223150	TGGT1_235970		
	TGME49_223970	0.0166	TGME49_243530	TGME49_249215	TGGT1_223710	TGGT1_236580		
	TGME49_225710	0.0468	TGME49_244310	TGME49_249410	TGGT1_223970	TGGT1_237100		
	TGME49_225800	0.0035	TGME49_244380	TGME49_249910	TGGT1_225260	TGGT1_238000		
	TGME49_225930	0.1421	TGME49_246730	TGME49_251170	TGGT1_225710	TGGT1_238240		
	TGME49_226270	0.0402	TGME49_246920	TGME49_252230	TGGT1_225800	TGGT1_239610		
	TGME49_226280	0.9971	TGME49_247550	TGME49_252340	TGGT1_225930	TGGT1_239790		
	TGME49_226430	0.0719	TGME49_247740	TGME49_252480	TGGT1_226270	TGGT1_240270		
	TGME49_227060	0.0193	TGME49_248200	TGME49_254280	TGGT1_226280	TGGT1_240440		
	TGME49_227830	0.9942	TGME49_248960	TGME49_254810	TGGT1_226430	TGGT1_240590		
	TGME49_229180	0.0306	TGME49_249010	TGME49_261690	TGGT1_226960	TGGT1_240780		
	TGME49_230050	0.8966	TGME49_249650	TGME49_263260	TGGT1_227060	TGGT1_240810		
	TGME49_230450	0.0107	TGME49_249920	TGME49_263340	TGGT1_227830	TGGT1_242415		
	TGME49_230555	0.0491	TGME49_249950	TGME49_263440	TGGT1_229180	TGGT1_243480		
	TGME49_230580	0.0815	TGME49_251550	TGME49_263680	TGGT1_230050	TGGT1_243530		
	TGME49_230840	0.0613	TGME49_251690	TGME49_263760	TGGT1_230450	TGGT1_244140		
	TGME49_230990	0.1332	TGME49_251760	TGME49_264200	TGGT1_230555	TGGT1_244310		
	TGME49_231020	0.015	TGME49_253510	TGME49_264790	TGGT1_230580	TGGT1_244380		
	TGME49_231150	0.9986	TGME49_253780	TGME49_265280	TGGT1_230840	TGGT1_245520		
	TGME49_231750	0.2746	TGME49_254260	TGME49_265990	TGGT1_230990	TGGT1_245650		
	TGME49_232520	0.9501	TGME49_254770	TGME49_266950	TGGT1_231020	TGGT1_246730		
	TGME49_232640	0.0072	TGME49_255320	TGME49_268820	TGGT1_231150	TGGT1_247390		
	TGME49_232815	0.1263	TGME49_256760	TGME49_270150	TGGT1_231750	TGGT1_247550		
	TGME49_233100	0.2118	TGME49_256990	TGME49_272490	TGGT1_232520	TGGT1_248200		
	TGME49_233190	0.7096	TGME49_257110	TGME49_272695	TGGT1_232640	TGGT1_249215		
	TGME49_233260	0.01	TGME49_257150	TGME49_273640	TGGT1_232815	TGGT1_249910		
	TGME49_233720	0.0917	TGME49_258210	TGME49_275490	TGGT1_233100	TGGT1_249920		
	TGME49_234530	0.0671	TGME49_258390	TGME49_285840	TGGT1_233190	TGGT1_249950		
	TGME49_235560	0.7776	TGME49_259690	TGME49_286070	TGGT1_233260	TGGT1_251500		
	TGME49_235970	0.0271	TGME49_260440	TGME49_288510	TGGT1_233500	TGGT1_251690		
	TGME49_236580	0.9575	TGME49_261480	TGME49_290570	TGGT1_233720	TGGT1_252340		
	TGME49_237100	0.8551	TGME49_261520	TGME49_291080	TGGT1_234530	TGGT1_252465		
	TGME49_237290	0.2109	TGME49_261600	TGME49_291150	TGGT1_235560	TGGT1_252480		
	TGME49_237460	0.1857	TGME49_262040	TGME49_291590	TGGT1_235970	TGGT1_253510		
	TGME49_238000	0.8213	TGME49_263070	TGME49_294050	TGGT1_236580			
	TGME49_238240	0.0464	TGME49_263420	TGME49_294420	TGGT1_237100			
	TGME49_239610	0.647	TGME49_263530	TGME49_294980				
	TGME49_239790	0.6368	TGME49_263680					

TGME49	value	TGME49	TGME49	TGGT1	TGGT1
TGME49_239890	0.1928	TGME49_264060	TGME49_295960	TGGT1_237290	TGGT1_254260
TGME49_240200	0.3525	TGME49_265110	TGME49_296950	TGGT1_237460	TGGT1_254280
TGME49_240210	0.0203	TGME49_265220	TGME49_297170	TGGT1_238000	TGGT1_254810
TGME49_240270	0.2831	TGME49_266750	TGME49_297880	TGGT1_238240	TGGT1_254940
TGME49_240400	0.0206	TGME49_267390	TGME49_299270	TGGT1_239610	TGGT1_255320
TGME49_240440	0.4388	TGME49_268640	TGME49_306650	TGGT1_239790	TGGT1_256760
TGME49_240590	0.558	TGME49_268840	TGME49_306950	TGGT1_239890	TGGT1_256990
TGME49_240780	0.3871	TGME49_269650	TGME49_308950	TGGT1_240200	TGGT1_257110
TGME49_240810	0.096	TGME49_270650	TGME49_310500	TGGT1_240210	TGGT1_257150
TGME49_240820	0.0135	TGME49_271300	TGME49_311030	TGGT1_240270	TGGT1_257290
TGME49_240890	0.0616	TGME49_272010	TGME49_312340	TGGT1_240400	TGGT1_257530
TGME49_242415	0.039	TGME49_272740	TGME49_312350	TGGT1_240440	TGGT1_258110
TGME49_242610	0.0958	TGME49_273460	TGME49_312490	TGGT1_240590	TGGT1_258210
TGME49_243530	0.8919	TGME49_273520	TGME49_313520	TGGT1_240780	TGGT1_258390
TGME49_243760	0.0693	TGME49_278270	TGME49_314710	TGGT1_240810	TGGT1_259690
TGME49_244120	0.0122	TGME49_278900	TGME49_314800	TGGT1_240820	TGGT1_260170
TGME49_244140	0.9767	TGME49_279330	TGME49_316350	TGGT1_240890	TGGT1_261480
TGME49_244310	0.0713	TGME49_283590	TGME49_320550	TGGT1_242415	TGGT1_261520
TGME49_244380	0.0476	TGME49_283850	TGME49_321310	TGGT1_242610	TGGT1_263070
TGME49_244440	0.0133	TGME49_285670		TGGT1_243480	TGGT1_263440
TGME49_245470	0.1006	TGME49_285720		TGGT1_243530	TGGT1_263530
TGME49_245520	0.1202	TGME49_285840		TGGT1_243760	TGGT1_263680
TGME49_245650	0.0681	TGME49_286420		TGGT1_244120	TGGT1_263760
TGME49_246730	0.1258	TGME49_286550		TGGT1_244140	TGGT1_264060
TGME49_246920	0.7867	TGME49_288500		TGGT1_244310	TGGT1_264200
TGME49_247390	0.0023	TGME49_289650		TGGT1_244380	TGGT1_264610
TGME49_247550	0.9722	TGME49_290040		TGGT1_244440	TGGT1_265110
TGME49_247740	0.0647	TGME49_291080		TGGT1_245470	TGGT1_265220
TGME49_248200	0.9925	TGME49_292010		TGGT1_245520	TGGT1_265280
TGME49_248960	0.0389	TGME49_294350		TGGT1_245650	TGGT1_267390
TGME49_249010	0.1819	TGME49_295010		TGGT1_246730	TGGT1_268640
TGME49_249215	0.9509	TGME49_297170		TGGT1_246920	TGGT1_268840
TGME49_249410	0.0226	TGME49_299210		TGGT1_247390	TGGT1_270150
TGME49_249510	0.9279	TGME49_301390		TGGT1_247550	TGGT1_271280
TGME49_249650	0.4835	TGME49_305460		TGGT1_247740	TGGT1_271300
TGME49_249910	0.7797	TGME49_305750		TGGT1_248200	TGGT1_272490
TGME49_249920	0.0042	TGME49_306290		TGGT1_248960	TGGT1_272740
TGME49_249950	0.0919	TGME49_306650		TGGT1_249010	TGGT1_273090
TGME49_251170	0.4465	TGME49_307650		TGGT1_249215	TGGT1_273460
TGME49_251500	0.0316	TGME49_309570		TGGT1_249410	TGGT1_273520
TGME49_251550	0.405	TGME49_310850		TGGT1_249510	TGGT1_273960
TGME49_251690	0.053	TGME49_311240		TGGT1_249650	TGGT1_274190
TGME49_251760	0.1895	TGME49_311750		TGGT1_249910	TGGT1_275490
TGME49_252230	0.001	TGME49_311870		TGGT1_249920	TGGT1_278270
TGME49_252340	0.7575	TGME49_312220		TGGT1_249950	TGGT1_278900
TGME49_252480	0.258	TGME49_312530		TGGT1_250955	TGGT1_279330
TGME49_253510	0.0105	TGME49_312680		TGGT1_251170	TGGT1_283590A
TGME49_253780	0.0367	TGME49_313230		TGGT1_251500	TGGT1_283590B
TGME49_254260	0.1621	TGME49_313350		TGGT1_251550	TGGT1_283890
TGME49_254280	0.0162	TGME49_314480		TGGT1_251690	TGGT1_285720
TGME49_254610	0.0195	TGME49_316450		TGGT1_251760	TGGT1_285840
TGME49_254770	0.0227	TGME49_316900		TGGT1_252190	TGGT1_286070
TGME49_254810	0.0854	TGME49_318310		TGGT1_252230	TGGT1_286420B
TGME49_254940	0.0481	TGME49_321640		TGGT1_252340	TGGT1_286550
TGME49_255320	0.6866			TGGT1_252465	TGGT1_290570
TGME49_256760	0.3764			TGGT1_252480	TGGT1_291080
TGME49_256990	0.9946			TGGT1_253510	TGGT1_292000
TGME49_257110	0.6373			TGGT1_253780	TGGT1_292010
TGME49_257150	0.0139			TGGT1_254260	TGGT1_293700
TGME49_258100	0.9624			TGGT1_254280	TGGT1_294050
TGME49_258210	0.0034			TGGT1_254610	TGGT1_294350
TGME49_258390	0.1292			TGGT1_254770	TGGT1_294420
TGME49_259690	0.0795			TGGT1_254810	TGGT1_295010
TGME49_260300	0.5609			TGGT1_254940	TGGT1_297170
TGME49_260440	0.0227			TGGT1_255320	TGGT1_299210
TGME49_261260	0.5853			TGGT1_256760	TGGT1_300320
TGME49_261480	0.1389			TGGT1_256990	TGGT1_301390
TGME49_261520	0.0247			TGGT1_257110	TGGT1_305460
TGME49_261600	0.9549			TGGT1_257150	TGGT1_305750
TGME49_261690	0.0945			TGGT1_257290	TGGT1_306290
TGME49_262040	0.0677			TGGT1_257530	TGGT1_306610
TGME49_263070	0.9043			TGGT1_258110	TGGT1_306950
TGME49_263260	0.3945			TGGT1_258210	TGGT1_309000
TGME49_263340	0.009			TGGT1_258390	TGGT1_310500
TGME49_263420	0.0085			TGGT1_259660	TGGT1_310850
TGME49_263440	0.1005			TGGT1_259690	TGGT1_311030
TGME49_263530	0.2184			TGGT1_260170	TGGT1_311240
TGME49_263680	0.949			TGGT1_260300	TGGT1_311430
TGME49_263760	0.656			TGGT1_260440	TGGT1_311870
TGME49_264060	0.8158			TGGT1_260850	TGGT1_313230
TGME49_264200	0.9684			TGGT1_261260A	TGGT1_313520
TGME49_264790	0.0168			TGGT1_261260B	TGGT1_314480
TGME49_265110	0.075			TGGT1_261480	TGGT1_316900
TGME49_265220	0.9636			TGGT1_261520	TGGT1_321640
TGME49_265280	0.0264			TGGT1_261600	TGGT1_356300
TGME49_265990	0.2381			TGGT1_261690	TGGT1_409260
TGME49_266750	0.1475			TGGT1_262040	
TGME49_266950	0.0533			TGGT1_263070	
TGME49_267390	0.0181			TGGT1_263260	
TGME49_268640	0.0885			TGGT1_263340	
TGME49_268820	0.0045			TGGT1_263420	
TGME49_268840	0.027			TGGT1_263430	
TGME49_269650	0.1083			TGGT1_263440	
TGME49_269740	0.2249			TGGT1_263530	
TGME49_270150	0.9859			TGGT1_263680	
TGME49_270650	0.5708			TGGT1_263760	
TGME49_271178	0.0243			TGGT1_264060	

TGME49_271182	0.3764	TGGT1_264200
TGME49_271280	0.0943	TGGT1_264610
TGME49_271300	0.1507	TGGT1_264790
TGME49_272010	0.9247	TGGT1_265110
TGME49_272410	0.9931	TGGT1_265220
TGME49_272490	0.997	TGGT1_265280
TGME49_272695	0.0248	TGGT1_265990
TGME49_272740	0.0495	TGGT1_266750
TGME49_273460	0.0054	TGGT1_266950
TGME49_273520	0.0505	TGGT1_267390
TGME49_273640	0.0178	TGGT1_268640
TGME49_274190	0.0331	TGGT1_268820
TGME49_275490	0.0206	TGGT1_268840
TGME49_278270	0.2301	TGGT1_269650
TGME49_278900	0.0372	TGGT1_269740
TGME49_279330	0.01	TGGT1_270150
TGME49_282190	0.1652	TGGT1_270650
TGME49_283590	0.9955	TGGT1_271178
TGME49_283850	0.0397	TGGT1_271280
TGME49_285670	0.022	TGGT1_271300
TGME49_285720	0.6991	TGGT1_272010
TGME49_285840	0.9678	TGGT1_272410
TGME49_286070	0.1311	TGGT1_272490
TGME49_286420	0.0121	TGGT1_272640
TGME49_286550	0.0063	TGGT1_272695
TGME49_288500	0.9872	TGGT1_272740
TGME49_288510	0.0369	TGGT1_273090
TGME49_288580	0.007	TGGT1_273460
TGME49_289650	0.969	TGGT1_273520
TGME49_290040	0.0524	TGGT1_273640
TGME49_290570	0.0116	TGGT1_273960
TGME49_290840	0.0609	TGGT1_274190
TGME49_291080	0.0855	TGGT1_275490
TGME49_291150	0.0565	TGGT1_277850
TGME49_291590	0.019	TGGT1_278270
TGME49_292010	0.9504	TGGT1_278900
TGME49_293700	0.0101	TGGT1_279330
TGME49_294050	0.936	TGGT1_282190
TGME49_294350	0.011	TGGT1_283590A
TGME49_294420	0.0298	TGGT1_283590B
TGME49_294980	0.7202	TGGT1_283850
TGME49_295010	0.2861	TGGT1_283890
TGME49_295960	0.1895	TGGT1_285670
TGME49_296950	0.0838	TGGT1_285720
TGME49_297170	0.9926	TGGT1_285840
TGME49_297880	0.8927	TGGT1_286070
TGME49_299210	0.1422	TGGT1_286420A
TGME49_299270	0.1724	TGGT1_286420B
TGME49_301390	0.089	TGGT1_286550
TGME49_305460	0.0785	TGGT1_288500
TGME49_305490	0.0593	TGGT1_288510
TGME49_305750	0.418	TGGT1_288580
TGME49_306290	0.0019	TGGT1_289650
TGME49_306380	0.0895	TGGT1_290040
TGME49_306610	0.0111	TGGT1_290570
TGME49_306650	0.9127	TGGT1_290840
TGME49_306950	0.1597	TGGT1_291080
TGME49_307650	0.5893	TGGT1_291150
TGME49_308950	0.7586	TGGT1_291590
TGME49_308990	0.0088	TGGT1_292000
TGME49_309570	0.2575	TGGT1_292010
TGME49_310050	0.0748	TGGT1_293700
TGME49_310320	0.1792	TGGT1_294050
TGME49_310400	0.0535	TGGT1_294350
TGME49_310500	0.9211	TGGT1_294420
TGME49_310850	0.1292	TGGT1_294800A
TGME49_311030	0.7379	TGGT1_294800B
TGME49_311240	0.0168	TGGT1_294980
TGME49_311430	0.9866	TGGT1_295010
TGME49_311750	0.198	TGGT1_295935
TGME49_311870	0.0486	TGGT1_295950
TGME49_312220	0.0377	TGGT1_295960
TGME49_312340	0.0424	TGGT1_296950
TGME49_312350	0.0424	TGGT1_297170
TGME49_312480	0.0405	TGGT1_297880
TGME49_312490	0.9255	TGGT1_299210
TGME49_312530	0.0207	TGGT1_299270
TGME49_312680	0.9388	TGGT1_300320
TGME49_313230	0.0265	TGGT1_301390
TGME49_313350	0.0336	TGGT1_305120
TGME49_313520	0.0168	TGGT1_305460
TGME49_314480	0.9664	TGGT1_305490
TGME49_314710	0.0187	TGGT1_305750
TGME49_314800	0.2764	TGGT1_306290
TGME49_316350	0.0253	TGGT1_306380
TGME49_316450	0.0896	TGGT1_306610
TGME49_316900	0.692	TGGT1_306650
TGME49_318310	0.0126	TGGT1_306950
TGME49_320550	0.5151	TGGT1_307650
TGME49_321310	0.8598	TGGT1_308950
TGME49_321640	0.0047	TGGT1_308990
TGME49_321680	0.3494	TGGT1_309000
		TGGT1_309210
		TGGT1_309570
		TGGT1_309730
		TGGT1_310050
		TGGT1_310320

TGGT1_310400
TGGT1_310500
TGGT1_310850
TGGT1_311030
TGGT1_311240
TGGT1_311430
TGGT1_311750
TGGT1_311870
TGGT1_312220
TGGT1_312340
TGGT1_312350
TGGT1_312480
TGGT1_312490
TGGT1_312530
TGGT1_312680
TGGT1_313230
TGGT1_313350
TGGT1_313520
TGGT1_314480
TGGT1_314710
TGGT1_314800
TGGT1_316350
TGGT1_316450
TGGT1_316900
TGGT1_318310
TGGT1_320490
TGGT1_320550
TGGT1_321310
TGGT1_321640
TGGT1_321680
TGGT1_323020
TGGT1_356300
TGGT1_358440
TGGT1_359490
TGGT1_366530
TGGT1_409260

Appendix Table 5_Complex IV proteomics

Sheet 1 - Gel 1

Family	Accession	Score	Mass	Num. of matches	Num. of significant matches	Num. of sequences	Num. of significant sequences	emPAI	Description
1	TGGT1_235470-t26_1-p1	1303	93901	41	41	28	28	4.26	myosin A
2	TGGT1_232830-t26_1-p1	853	1E+05	18	18	13	13	1.01	putative vacuolar proton translocating ATPase subunit A
3	TGGT1_311720-t26_1-p1	744	73379	17	17	16	16	1.8	chaperonin protein BiP
3	TGGT1_273760-t26_1-p1	130	72703	2	2	2	2	0.14	heat shock protein HSP70
4	TGGT1_308090-t26_1-p1	669	60966	20	20	13	13	2.73	rhoptry protein ROP5
4	TGME49_308090-t26_1-p1	515	61292	16	16	10	10	1.94	rhoptry protein ROP5
4	TGGT1_411430-t26_1-p1	489	51646	14	14	9	9	1.99	rhoptry protein ROP5
5	TGGT1_240600-t26_1-p1	620	72464	20	20	16	16	1.84	putative chaperonin cpn60
6	TGGT1_259010-t26_1-p1	594	45150	14	14	12	12	2.5	putative vacuolar ATP synthase subunit d
7	TGGT1_209260-t26_1-p1	593	35188	20	20	10	10	7.49	putative cytochrome c oxidase subunit
8	TGGT1_229920-t26_1-p1	564	34990	21	21	10	10	4.75	hypothetical protein
9	TGGT1_232350-t26_1-p1	555	36095	17	17	10	10	4.45	lactate dehydrogenase LDH1
10	TGGT1_230350-t26_1-p1	553	1E+05	18	18	11	11	0.55	hypothetical protein
11	TGGT1_264040-t26_1-p1	545	24760	15	15	8	8	13.17	hypothetical protein
12	TGGT1_297810-t26_1-p1	526	29778	15	15	10	10	6.79	hypothetical protein
13	TGGT1_219320-t26_1-p1	522	46805	11	11	8	8	1.47	acid phosphatase GAP50
14	TGGT1_310750-t26_1-p1	433	65050	11	11	9	9	0.92	emp24/gp25L/p24 family protein
15	TGGT1_208370-t26_1-p1	412	1E+05	14	14	13	13	0.63	putative myosin heavy chain
16	TGGT1_233460-t26_1-p1	402	35605	12	12	9	9	2.28	SAG-related sequence SRS29B
17	TGGT1_263630-t26_1-p1	401	15535	9	9	5	5	7.14	hypothetical protein
18	TGGT1_306670-t26_1-p1	388	26159	14	14	5	5	2.5	hypothetical protein
19	TGGT1_230420-t26_1-p1	377	1E+05	8	8	7	7	0.37	sarco/endoplasmic reticulum Ca2+-ATPase
20	TGGT1_209800-t26_1-p1	337	44945	7	7	5	5	0.88	formate/nitrite transporter protein
21	TGGT1_291890-t26_1-p1	303	49668	10	10	8	8	1.35	microneme protein MIC1
22	TGGT1_249270-t26_1-p1	295	60698	8	8	6	6	0.59	putative protein disulfide isomerase-related protein (provisional)
23	TGGT1_223940-t26_1-p1	284	27643	6	6	3	3	1.34	GAP45 protein
24	TGGT1_247770-t26_1-p1	281	19291	16	16	4	4	3.27	hypothetical protein
25	TGGT1_288650-t26_1-p1	259	48110	8	8	7	7	0.99	dense granule protein GRA12
26	TGGT1_309590-t26_1-p1	257	49683	9	9	4	4	0.77	rhoptry protein ROP1
27	TGGT1_310470-t26_1-p1	257	21386	7	7	3	3	1.4	putative cytochrome C oxidase subunit IIb
28	TGGT1_244560-t26_1-p1	256	97779	9	9	7	7	0.4	putative heat shock protein 90
29	TGGT1_257680-t26_1-p1	251	24393	8	8	6	6	3.64	myosin light chain MLC1
30	TGGT1_249900-t26_1-p1	246	35461	7	7	7	7	1.53	putative adenine nucleotide translocator
31	TGGT1_228170-t26_1-p1	246	2E+05	8	8	8	8	0.23	inner membrane complex protein IMC2A
32	TGGT1_209030-t26_1-p1	231	42166	6	6	5	5	0.75	actin ACT1
33	TGGT1_308000-t26_1-p1	226	84008	5	5	4	4	0.25	Gpi16 subunit, GPI transamidase component protein
34	TGGT1_324600-t26_1-p1	224	20424	6	6	4	4	2.14	heat shock protein
35	TGGT1_226590-t26_1-p1	222	34694	9	9	3	3	0.97	putative cytochrome C oxidase subunit IIa
36	TGGT1_306390-t26_1-p1	215	21488	4	4	3	3	0.92	hypothetical protein
37	TGGT1_237250-t26_1-p1	198	28772	4	4	3	3	0.92	hypothetical protein
38	TGGT1_232180-t26_1-p1	195	2E+05	7	7	5	5	0.12	UBA/TS-N domain-containing protein
39	TGGT1_231930-t26_1-p1	193	87118	5	5	4	4	0.24	hypothetical protein
40	TGGT1_286420A-t26_1-p1	193	49988	7	7	5	5	0.76	putative elongation factor 1-alpha (EF-1-ALPHA)
41	TGGT1_262880-t26_1-p1	191	3E+05	6	6	6	6	0.1	hypothetical protein
42	TGGT1_263180-t26_1-p1	189	91793	3	3	3	3	0.17	myosin D
43	TGGT1_265370-t26_1-p1	185	16478	6	6	4	4	4.49	hypothetical protein
44	TGGT1_319560-t26_1-p1	184	42440	5	5	4	4	0.74	microneme protein MIC3
45	TGGT1_290720-t26_1-p1	184	1E+05	6	6	5	5	0.22	putative vacuolar proton translocating ATPase subunit
46	TGGT1_218520-t26_1-p1	183	37773	3	3	3	3	0.45	microneme protein MIC6
47	TGGT1_289690-t26_1-p1	174	53989	4	4	4	4	0.42	glyceraldehyde-3-phosphate dehydrogenase GAPDH1
48	TGGT1_316255-t26_1-p1	173	10197	6	6	3	3	5.09	hypothetical protein
49	TGGT1_311240-t26_1-p1	172	47989	3	3	1	1	0.1	putative DnaJ family chaperone
50	TGGT1_363030-t26_1-p1	168	64277	6	6	5	5	0.44	rhoptry protein ROP8
51	TGGT1_251690-t26_1-p1	162	54683	5	5	5	5	0.54	putative seryl-tRNA synthetase, cytoplasmic
52	TGGT1_286630-t26_1-p1	161	31500	2	2	1	1	0.16	redoxin domain-containing protein
53	TGGT1_242840-t26_1-p1	155	13952	5	5	3	3	2.78	membrane protein
54	TGGT1_221510-t26_1-p1	151	18073	6	6	3	3	1.81	hypothetical protein
55	TGGT1_286530-t26_1-p1	151	25648	4	4	3	3	1.08	hypothetical protein
56	TGGT1_262640-t26_1-p1	148	23859	6	6	4	4	1.67	Cg8 family protein
57	TGGT1_306650-t26_1-p1	148	31792	4	4	3	3	0.56	hypothetical protein
58	TGGT1_205010-t26_1-p1	147	2E+05	3	3	2	2	0.06	putative U2 small nuclear ribonucleoprotein family protein
59	TGGT1_278660-t26_1-p1	145	1E+05	3	3	3	3	0.1	putative P-type ATPase4
60	TGME49_234380-t26_1-p1	137	38746	4	4	3	3	0.44	hypothetical protein
61	TGGT1_295125-t26_1-p1	136	40398	4	4	4	4	0.59	rhoptry protein ROP4
61	TGGT1_295110-t26_1-p1	117	63659	3	3	3	3	0.25	rhoptry protein ROP7
62	TGGT1_268590-t26_1-p1	132	73221	2	2	1	1	0.14	rhomboid protease ROM4
63	TGGT1_267840-t26_1-p1	127	39005	4	4	2	2	0.44	tetratricopeptide repeat-containing protein
64	TGGT1_205740-t26_1-p1	126	1E+05	4	4	3	3	0.11	hypothetical protein
65	TGGT1_313080-t26_1-p1	126	50066	6	6	6	6	0.76	hypothetical protein
66	TGGT1_278990-t26_1-p1	124	53856	4	4	3	3	0.3	putative phosphate carrier
67	TGGT1_289880-t26_1-p1	124	1E+05	6	6	6	6	0.21	hypothetical protein
68	TGGT1_301210-t26_1-p1	123	1E+05	3	3	3	3	0.11	putative NAD(P) transhydrogenase subunit beta
69	TGGT1_204160-t26_1-p1	121	2E+05	4	4	4	4	0.11	GYF domain-containing protein
70	TGGT1_308810B-t26_1-p1	121	1E+05	4	4	4	4	0.18	rhoptry neck protein RON9
71	TGGT1_246580-t26_1-p1	115	43022	2	2	2	2	0.24	hypothetical protein
72	TGGT1_297470-t26_1-p1	114	40916	3	3	3	3	0.41	putative myosin light chain 2
73	TGGT1_238100-t26_1-p1	112	27217	5	5	4	4	0.99	transmembrane protein
74	TGGT1_209150-t26_1-p1	109	67796	2	2	2	2	0.15	non-proton pumping type-II NADH dehydrogenase I
75	TGGT1_204310-t26_1-p1	108	2E+05	5	5	4	4	0.1	hypothetical protein
76	TGGT1_255260-t26_1-p1	105	64064	2	2	1	1	0.16	apical membrane antigen AMA1
77	TGGT1_258580-t26_1-p1	105	69296	2	2	1	1	0.07	rhoptry protein ROP17
78	TGGT1_297970-t26_1-p1	104	56545	3	3	3	3	0.28	aspartyl aminopeptidase
79	TGGT1_319300-t26_1-p1	102	1E+05	5	5	4	4	0.18	hypothetical protein
80	TGGT1_223920-t26_1-p1	100	2E+05	5	5	5	5	0.11	rhoptry neck protein RON3
81	TGGT1_227280-t26_1-p1	97	24284	3	3	3	3	0.78	dense granule protein GRA3
82	TGGT1_275440-t26_1-p1	93	23396	2	2	1	1	0.49	dense granule protein GRA6
83	TGGT1_290670-t26_1-p1	91	84163	3	3	3	3	0.18	leucyl aminopeptidase LAP
84	TGGT1_224900-t26_1-p1	90	28771	1	1	1	1	0.18	putative adenylate kinase
85	TGGT1_225850-t26_1-p1	89	2E+05	1	1	1	1	0.03	peptidase, M28 family protein
86	TGGT1_230510-t26_1-p1	88	39816	4	4	4	4	0.6	hypothetical protein
87	TGGT1_312160-t26_1-p1	87	22702	2	2	1	1	0.23	hypothetical protein
88	TGGT1_270865-t26_1-p1	86	2E+05	1	1	1	1	0.02	putative adenylate cyclase
89	TGGT1_248160-t26_1-p1	84	1E+05	6	6	1	1	0.04	hypothetical protein
90	TGGT1_220240-t26_1-p1	83	54192	1	1	1	1	0.09	hypothetical protein
91	TGGT1_203310-t26_1-p1	83	25899	4	4	4	4	1.07	dense granule protein GRA7
92	TGGT1_252440-t26_1-p1	81	60099	3	3	2	2	0.17	peptidase c13 family protein
93	TGGT1_215590-t26_1-p1	80	73429	2	2	2	2	0.14	flavoprotein subunit of succinate dehydrogenase

94	TGGT1_279420-t26_1-p1	77	1E+05	2	2	2	2	0.07	hypothetical protein
95	TGGT1_253290-t26_1-p1	76	1E+05	1	1	1	1	0.04	valyl-tRNA synthetase
96	TGGT1_243390-t26_1-p1	75	37026	2	2	2	2	0.29	hypothetical protein
97	TGGT1_308020-t26_1-p1	73	42545	2	2	2	2	0.25	SAG-related sequence SRS57
98	TGGT1_274060-t26_1-p1	71	35277	1	1	1	1	0.14	2-oxoglutarate/malate translocase OMT
99	TGGT1_258826-t26_1-p1	69	1E+05	1	1	1	1	0.04	hypothetical protein
100	TGGT1_204050-t26_1-p1	69	85785	3	3	2	2	0.12	subtilisin SUB1
101	TGGT1_212240-t26_1-p1	69	50476	1	1	1	1	0.1	putative beta-1 tubulin
102	TGME49_237120-t26_1-p1	67	18270	1	1	1	1	0.29	hypothetical protein
103	TGGT1_288380-t26_1-p1	64	82281	2	2	2	2	0.12	heat shock protein HSP90
104	TGGT1_224980-t26_1-p1	64	1E+05	1	1	1	1	0.04	hypothetical protein
105	TGGT1_205250-t26_1-p1	62	62702	3	3	3	3	0.25	rhoptry protein ROP18
106	TGGT1_251630-t26_1-p1	61	98981	2	2	1	1	0.05	slc30a2 protein
107	TGGT1_290160-t26_1-p1	60	1E+05	2	2	2	2	0.09	putative sortilin
108	TGGT1_229010-t26_1-p1	60	1E+05	1	1	1	1	0.04	rhoptry neck protein RON4
109	TGGT1_209950-t26_1-p1	59	48112	1	1	1	1	0.1	putative thioredoxin
110	TGGT1_213670-t26_1-p1	58	85898	2	2	2	2	0.12	hypothetical protein
111	TGGT1_256980-t26_1-p1	57	1E+05	1	1	1	1	0.04	glycerol-3-phosphate-acyltransferase
112	TGGT1_280410-t26_1-p1	57	1E+05	2	2	2	2	0.08	3'5'-cyclic nucleotide phosphodiesterase domain-containing protein
113	TGGT1_275568-t26_1-p1	56	61363	1	1	1	1	0.08	GPI transamidase subunit PIG-U protein
114	TGGT1_289750-t26_1-p1	56	14961	2	2	2	2	0.86	ribosomal-ubiquitin protein RPL40
115	TGGT1_207830-t26_1-p1	52	40037	1	1	1	1	0.12	MORN repeat-containing protein
116	TGGT1_305050-t26_1-p1	52	15439	1	1	1	1	0.35	putative calmodulin
117	TGGT1_312630-t26_1-p1	51	3E+05	2	2	2	2	0.03	putative anonymous antigen-1
118	TGGT1_227620-t26_1-p1	50	19887	2	2	2	2	0.6	dense granule protein GRA2
119	TGGT1_249850-t26_1-p1	50	43624	1	1	1	1	0.11	GAP40 protein
120	TGGT1_256760-t26_1-p1	50	58120	2	2	2	2	0.18	pyruvate kinase PyK1
121	TGGT1_299210-t26_1-p1	49	71752	2	2	2	2	0.14	CTP synthase
122	TGGT1_301130-t26_1-p1	48	13841	1	1	1	1	0.4	hypothetical protein
123	TGGT1_312150-t26_1-p1	47	61088	1	1	1	1	0.08	hypothetical protein
124	TGGT1_315930-t26_1-p1	46	18147	1	1	1	1	0.29	putative integral membrane protein, DUF56 family protein
125	TGGT1_261950-t26_1-p1	46	60107	1	1	1	1	0.08	ATP synthase beta subunit ATP-B
126	TGGT1_290660-t26_1-p1	46	48437	1	1	1	1	0.1	RNA recognition motif-containing protein
127	TGGT1_297430-t26_1-p1	46	25322	1	1	1	1	0.2	hypothetical protein
128	TGGT1_261750-t26_1-p1	45	91961	2	2	2	2	0.11	rhoptry neck protein RON10
129	TGGT1_293570-t26_1-p1	45	45726	1	1	1	1	0.11	putative translocation protein sec62
130	TGGT1_316240-t26_1-p1	44	75893	1	1	1	1	0.06	hypothetical protein
131	TGGT1_318160-t26_1-p1	43	26016	4	4	1	1	0.2	MSP (Major sperm protein) domain-containing protein
132	TGGT1_269442-t26_1-p1	43	9774	2	2	1	1	0.6	putative calmodulin
133	TGGT1_289580-t26_1-p1	43	49757	1	1	1	1	0.1	strictosidine synthase subfamily protein
134	TGGT1_286650-t26_1-p1	42	20450	1	1	1	1	0.26	hypothetical protein
135	TGGT1_293440-t26_1-p1	42	59840	1	1	1	1	0.08	hypothetical protein
136	TGGT1_309560-t26_1-p1	42	29485	1	1	1	1	0.17	nmda receptor glutamate-binding chain
137	TGGT1_230960-t26_1-p1	41	1E+05	1	1	1	1	0.04	putative splicing factor 3b, subunit 3
138	TGGT1_254720-t26_1-p1	41	28509	1	1	1	1	0.18	dense granule protein GRA8
139	TGGT1_252630-t26_1-p1	41	15299	1	1	1	1	0.36	hypothetical protein
140	TGGT1_235420-t26_1-p1	41	1E+05	1	1	1	1	0.04	CorA family Mg2+ transporter protein
141	TGGT1_231630-t26_1-p1	40	50596	1	1	1	1	0.1	alveolin domain containing intermediate filament IMC4
142	TGGT1_259000-t26_1-p1	40	24485	1	1	1	1	0.21	hypothetical protein
143	TGGT1_225555-t26_1-p1	40	7368	2	2	2	2	2.48	hypothetical protein
144	TGGT1_219682-t26_1-p1	39	82936	1	1	1	1	0.06	putative pyruvate dehydrogenase kinase
145	TGGT1_253700-t26_1-p1	38	1E+05	1	1	1	1	0.03	transporter, major facilitator family protein
146	TGGT1_215280-t26_1-p1	37	39384	2	2	2	2	0.27	succinate dehydrogenase [ubiquinone] iron-sulfur protein
147	TGGT1_254030-t26_1-p1	36	13666	1	1	1	1	0.41	zinc finger CDGSH-type domain-containing protein
148	TGGT1_222910-t26_1-p1	36	56254	1	1	1	1	0.09	phosphoglycerate mutase
149	TGGT1_244390-t26_1-p1	35	34480	1	1	1	1	0.15	coatomer epsilon subunit protein
150	TGGT1_217890-t26_1-p1	35	21936	2	2	1	1	0.24	putative alkyl hydroperoxide reductase/ Thiol specific antioxidant/ Mal allergen
151	TGGT1_286580-t26_1-p1	34	1E+05	1	1	1	1	0.04	hypothetical protein
152	TGGT1_225080-t26_1-p1	34	17826	1	1	1	1	0.3	ribosomal protein RPS18
153	TGGT1_230410-t26_1-p1	34	30729	2	2	2	2	0.36	peroxiredoxin PRX3
154	TGGT1_206480-t26_1-p1	33	22850	1	1	1	1	0.23	hypothetical protein
155	TGGT1_220100-t26_1-p1	33	61572	1	1	1	1	0.08	phosphoribosylpyrophosphate synthetase
156	TGGT1_247550-t26_1-p1	33	61388	1	1	1	1	0.08	heat shock protein HSP60
157	TGGT1_263700-t26_1-p1	33	16349	1	1	1	1	0.33	ribosomal protein RPS14
158	TGGT1_236070-t26_1-p1	33	36744	1	1	1	1	0.14	pyrroline-5-carboxylate reductase
159	TGGT1_280560-t26_1-p1	32	1E+05	1	1	1	1	0.03	selenide, water dikinase
160	TGGT1_203240-t26_1-p1	31	80954	1	1	1	1	0.06	hypothetical protein
161	TGGT1_211040-t26_1-p1	31	10154	1	1	1	1	0.58	Sec61beta family protein
162	TGGT1_270620-t26_1-p1	31	1E+05	1	1	1	1	0.05	DEAD/DEAH box helicase domain-containing protein
163	TGGT1_212310-t26_1-p1	31	17579	1	1	1	1	0.3	vacuolar ATP synthetase
164	TGGT1_262620-t26_1-p1	30	31911	1	1	1	1	0.16	RNA recognition motif-containing protein
165	TGGT1_200310-t26_1-p1	30	18804	2	2	1	1	0.28	hypothetical protein
166	TGGT1_287500-t26_1-p1	28	59895	1	1	1	1	0.08	putative T complex chaperonin
167	TGGT1_292320-t26_1-p1	27	99683	1	1	1	1	0.05	hypothetical protein
168	TGME49_255060-t26_1-p1	25	45697	1	1	1	1	0.11	cytochrome b(N-terminal)/b6/petB subfamily protein
169	TGGT1_257160-t26_1-p1	25	16651	1	1	1	1	0.32	hypothetical protein
170	TGGT1_238180-t26_1-p1	25	47990	1	1	1	1	0.1	putative 26s proteasome regulatory complex subunit
171	TGGT1_236510-t26_1-p1	25	1E+05	1	1	1	1	0.04	hypothetical protein
172	TGGT1_271888-t26_1-p1	25	38203	1	1	1	1	0.13	putative 3-ketoacyl-CoA reductase
173	TGGT1_313070-t26_1-p1	24	35865	1	1	1	1	0.14	hypothetical protein
174	TGGT1_209060-t26_1-p1	24	96777	1	1	1	1	0.05	thrombospondin type 1 domain-containing protein
175	TGGT1_309910-t26_1-p1	24	2E+05	1	1	1	1	0.02	hypothetical protein
176	TGGT1_235150-t26_1-p1	23	61312	1	1	1	1	0.08	transporter, major facilitator family protein
177	TGGT1_207710-t26_1-p1	23	28076	1	1	1	1	0.18	putative phosphatidylinositol synthase
178	TGGT1_221220-t26_1-p1	22	2E+05	1	1	1	1	0.02	hypothetical protein
179	TGGT1_229180-t26_1-p1	22	1E+05	1	1	1	1	0.03	HEAT repeat-containing protein
180	TGGT1_315127-t26_1-p1	22	1E+05	1	1	1	1	0.05	hypothetical protein
181	TGGT1_201150-t26_1-p1	21	2E+05	1	1	1	1	0.02	heavy metal translocating P-type ATPase subfamily protein
182	TGGT1_411660-t26_1-p1	21	14466	1	1	1	1	0.38	hypothetical protein
183	TGGT1_272475-t26_1-p1	20	3E+05	1	1	1	1	0.02	protein kinase domain-containing protein
184	TGGT1_294050-t26_1-p1	19	62479	1	1	1	1	0.08	hypothetical protein
185	TGGT1_290700-t26_1-p1	19	34568	1	1	1	1	0.15	hypothetical protein
186	TGGT1_218410-t26_1-p1	19	34250	1	1	1	1	0.15	ribosomal protein RPP0
187	TGGT1_311220-t26_1-p1	18	2E+05	1	1	1	1	0.03	hypothetical protein
188	TGGT1_226540-t26_1-p1	18	55054	1	1	1	1	0.09	protein kinase
189	TGGT1_232750-t26_1-p1	17	66803	1	1	1	1	0.07	putative 23S rRNA (adenine(1618)-N(6))-methyltransferase
190	TGME49_272370-t26_1-p1	16	3E+05	1	1	1	1	0.02	hypothetical protein
191	TGGT1_275420-t26_1-p1	14	3E+05	1	1	1	1	0.01	histone lysine-specific demethylase

Sheet 2 - Gel 2

Family	Accession	Score	Mass	Num. of matches	Num. of significant matches	Num. of sequences	Num. of significant sequences	emPAI	Description
1	TGGT1_235470-t26_1-p1	2198	93901	68	68	31	31	10.21	myosin A
2	TGGT1_232830-t26_1-p1	1114	1E+05	24	24	17	17	1.65	putative vacuolar proton translocating ATPase subunit A
3	TGGT1_230350-t26_1-p1	1003	1E+05	25	25	20	20	1.03	hypothetical protein
4	TGGT1_319560-t26_1-p1	850	42440	19	19	8	8	2.39	microneme protein MIC3
5	TGGT1_308090-t26_1-p1	711	60966	24	24	18	18	4.5	rhoptry protein ROP5
5	TGGT1_411430-t26_1-p1	553	51646	17	17	12	12	2.94	rhoptry protein ROP5
5	TGME49_308090-t26_1-p1	551	61292	17	17	13	13	2.43	rhoptry protein ROP5
6	TGGT1_240600-t26_1-p1	687	72464	19	19	14	14	1.84	putative chaperonin cpn60
7	TGGT1_259010-t26_1-p1	672	45150	22	22	12	12	4.31	putative vacuolar ATP synthase subunit d
8	TGGT1_291890-t26_1-p1	660	49668	18	18	12	12	3.57	microneme protein MIC1
9	TGGT1_264040-t26_1-p1	546	24760	11	11	7	7	7.03	hypothetical protein
10	TGGT1_219320-t26_1-p1	513	46805	15	15	10	10	2.35	acid phosphatase GAP50
11	TGGT1_257680-t26_1-p1	483	24393	13	13	7	7	7.26	myosin light chain MLC1
12	TGGT1_297810-t26_1-p1	432	29778	14	14	9	9	5.65	hypothetical protein
13	TGGT1_205740-t26_1-p1	424	1E+05	15	15	12	12	0.6	hypothetical protein
14	TGGT1_308000-t26_1-p1	424	84008	10	10	9	9	0.75	Gpi16 subunit, GPI transamidase component protein
15	TGGT1_249900-t26_1-p1	410	35461	11	11	9	9	3.31	putative adenine nucleotide translocator
16	TGGT1_230420-t26_1-p1	378	1E+05	11	11	9	9	0.48	sarco/endoplasmic reticulum Ca2+-ATPase
17	TGGT1_308810B-t26_1-p1	367	1E+05	9	9	8	8	0.39	rhoptry neck protein RON9
18	TGGT1_310750-t26_1-p1	355	65050	9	9	8	8	0.79	emp24/gp25L/p24 family protein
19	TGGT1_223940-t26_1-p1	355	27643	9	9	4	4	2.28	GAP45 protein
20	TGGT1_258580-t26_1-p1	355	69296	9	9	6	6	0.73	rhoptry protein ROP17
21	TGGT1_311720-t26_1-p1	353	73379	9	9	9	9	0.79	chaperonin protein BiP
21	TGGT1_273760-t26_1-p1	139	72703	3	3	3	3	0.22	heat shock protein HSP70
22	TGGT1_232180-t26_1-p1	298	2E+05	8	8	6	6	0.15	UBA/TS-N domain-containing protein
23	TGGT1_218520-t26_1-p1	298	37773	5	5	5	5	0.87	microneme protein MIC6
24	TGGT1_208370-t26_1-p1	294	1E+05	7	7	7	7	0.3	putative myosin heavy chain
25	TGGT1_209260-t26_1-p1	289	35188	11	11	7	7	2.33	putative cytochrome c oxidase subunit
26	TGGT1_249850-t26_1-p1	275	43624	8	8	4	4	0.91	GAP40 protein
27	TGGT1_309590-t26_1-p1	268	49683	12	12	6	6	1.35	rhoptry protein ROP1
28	TGGT1_229920-t26_1-p1	265	34990	9	9	7	7	1.56	hypothetical protein
29	TGGT1_306390-t26_1-p1	263	21488	6	6	3	3	1.96	hypothetical protein
30	TGGT1_223920-t26_1-p1	258	2E+05	9	9	8	8	0.18	rhoptry neck protein RON3
31	TGGT1_228170-t26_1-p1	239	2E+05	9	9	8	8	0.23	inner membrane complex protein IMC2A
32	TGGT1_295110-t26_1-p1	227	63659	7	7	6	6	0.56	rhoptry protein ROP7
32	TGGT1_295125-t26_1-p1	192	40398	6	6	6	6	1.01	rhoptry protein ROP4
33	TGGT1_288650-t26_1-p1	226	48110	9	9	8	8	1.42	dense granule protein GRA12
34	TGGT1_204310-t26_1-p1	219	2E+05	7	7	7	7	0.15	hypothetical protein
35	TGGT1_209800-t26_1-p1	216	44945	5	5	3	3	0.52	formate/nitrite transporter protein
36	TGGT1_230510-t26_1-p1	215	39816	6	6	4	4	0.81	hypothetical protein
37	TGGT1_290720-t26_1-p1	194	1E+05	6	6	6	6	0.27	putative vacuolar proton translocating ATPase subunit
38	TGGT1_286420A-t26_1-p1	188	49988	5	5	4	4	0.6	putative elongation factor 1-alpha (EF-1-ALPHA)
39	TGGT1_246580-t26_1-p1	186	43022	2	2	2	2	0.24	hypothetical protein
40	TGGT1_227280-t26_1-p1	172	24284	3	3	3	3	0.78	dense granule protein GRA3
41	TGGT1_262880-t26_1-p1	168	3E+05	5	5	5	5	0.08	hypothetical protein
42	TGGT1_313080-t26_1-p1	163	50066	4	4	4	4	0.46	hypothetical protein
43	TGGT1_247770-t26_1-p1	162	19291	8	8	5	5	3.27	hypothetical protein
44	TGGT1_289880-t26_1-p1	160	1E+05	9	9	9	9	0.33	hypothetical protein
45	TGGT1_203310-t26_1-p1	160	25899	6	6	5	5	1.48	dense granule protein GRA7
46	TGGT1_261750-t26_1-p1	157	91961	4	4	4	4	0.23	rhoptry neck protein RON10
47	TGGT1_310470-t26_1-p1	155	21386	3	3	2	2	0.55	putative cytochrome C oxidase subunit IIb
48	TGGT1_319300-t26_1-p1	154	1E+05	4	4	3	3	0.18	hypothetical protein
49	TGGT1_226590-t26_1-p1	152	34694	5	5	2	2	0.5	putative cytochrome C oxidase subunit IIa
50	TGGT1_263180-t26_1-p1	147	91793	4	4	3	3	0.23	myosin D
51	TGGT1_221510-t26_1-p1	143	18073	4	4	3	3	1.17	hypothetical protein
52	TGGT1_244560-t26_1-p1	141	97779	6	6	4	4	0.21	putative heat shock protein 90
53	TGGT1_311240-t26_1-p1	139	47989	3	3	2	2	0.22	putative DnaJ family chaperone
54	TGGT1_263630-t26_1-p1	139	15535	2	2	2	2	0.82	hypothetical protein
55	TGGT1_324600-t26_1-p1	135	20424	5	5	5	5	2.14	heat shock protein
56	TGGT1_209030-t26_1-p1	135	42166	5	5	4	4	0.56	actin ACT1
57	TGGT1_306670-t26_1-p1	130	26159	7	7	5	5	2.5	hypothetical protein
58	TGGT1_251690-t26_1-p1	121	54683	2	2	2	2	0.19	putative seryl-tRNA synthetase, cytoplasmic
59	TGGT1_274060-t26_1-p1	112	35277	3	3	3	3	0.49	2-oxoglutarate/malate translocase OMT
60	TGGT1_279420-t26_1-p1	112	1E+05	3	3	3	3	0.1	hypothetical protein
61	TGGT1_215590-t26_1-p1	108	73429	1	1	1	1	0.07	flavoprotein subunit of succinate dehydrogenase
62	TGGT1_312270-t26_1-p1	107	45158	3	3	2	2	0.23	rhoptry protein ROP13
63	TGGT1_301210-t26_1-p1	106	1E+05	4	4	3	3	0.15	putative NAD(P) transhydrogenase subunit beta
64	TGGT1_316255-t26_1-p1	104	10197	3	3	3	3	2.88	hypothetical protein
65	TGGT1_252440-t26_1-p1	104	60099	3	3	2	2	0.17	peptidase c13 family protein
66	TGME49_204160-t26_1-p1	102	2E+05	4	4	4	4	0.1	GYF domain-containing protein
67	TGGT1_243390-t26_1-p1	98	37026	3	3	3	3	0.46	hypothetical protein
68	TGGT1_297970-t26_1-p1	97	56545	4	4	2	2	0.18	aspartyl aminopeptidase
69	TGGT1_265370-t26_1-p1	97	16478	2	2	2	2	0.76	hypothetical protein
70	TGGT1_306650-t26_1-p1	96	31792	2	2	2	2	0.34	hypothetical protein
71	TGGT1_268590-t26_1-p1	92	73221	1	1	1	1	0.07	rhomboid protease ROM4
72	TGGT1_305050-t26_1-p1	90	15439	3	3	3	3	1.47	putative calmodulin
73	TGGT1_269450-t26_1-p1	88	39809	2	2	1	1	0.13	hypothetical protein
74	TGGT1_289690-t26_1-p1	87	53989	2	2	2	2	0.19	glyceraldehyde-3-phosphate dehydrogenase GAPDH1
75	TGGT1_286450-t26_1-p1	87	12969	2	2	1	1	0.43	dense granule protein GRA5
76	TGGT1_288380-t26_1-p1	86	82281	2	2	2	2	0.12	heat shock protein HSP90
77	TGGT1_252630-t26_1-p1	86	15299	1	1	1	1	0.36	hypothetical protein
78	TGGT1_229010-t26_1-p1	85	1E+05	1	1	1	1	0.04	rhoptry neck protein RON4
79	TGGT1_233460-t26_1-p1	85	35605	4	4	4	4	0.7	SAG-related sequence SRS29B
80	TGGT1_275568-t26_1-p1	84	61363	3	3	3	3	0.26	GPI transamidase subunit PIG-U protein
81	TGGT1_286530-t26_1-p1	80	25648	2	2	2	2	0.44	hypothetical protein
82	TGGT1_224980-t26_1-p1	77	1E+05	1	1	1	1	0.04	hypothetical protein
83	TGGT1_233110-t26_1-p1	75	59352	1	1	1	1	0.08	IMP dehydrogenasa

#	ID								Description
84	TGGT1_212310-t26_1-p1	72	17579	3	3	3	3	1.22	vacuolar ATP synthetase
85	TGGT1_315930-t26_1-p1	70	18147	2	2	2	2	0.68	putative integral membrane protein, DUF56 family protein
86	TGGT1_237250-t26_1-p1	69	28772	3	3	3	3	0.63	hypothetical protein
87	TGGT1_289750-t26_1-p1	67	14961	3	3	3	3	1.54	ribosomal-ubiquitin protein RPL40
88	TGGT1_248160-t26_1-p1	62	1E+05	6	6	1	1	0.04	hypothetical protein
89	TGGT1_249310-t26_1-p1	61	36624	1	1	1	1	0.14	hypothetical protein
90	TGGT1_278990-t26_1-p1	59	53856	1	1	1	1	0.09	putative phosphate carrier
91	TGME49_237120-t26_1-p1	57	18270	1	1	1	1	0.29	hypothetical protein
92	TGGT1_301130-t26_1-p1	56	13841	1	1	1	1	0.4	hypothetical protein
93	TGGT1_205010-t26_1-p1	56	2E+05	2	2	1	1	0.03	putative U2 small nuclear ribonucleoprotein family protein
94	TGGT1_235402-t26_1-p1	54	1E+05	2	2	1	1	0.04	CorA family Mg2+ transporter protein
95	TGGT1_232300-t26_1-p1	53	29018	1	1	1	1	0.18	ribosomal protein RPS3
96	TGGT1_251630-t26_1-p1	52	98981	2	2	1	1	0.05	slc30a2 protein
97	TGGT1_275440-t26_1-p1	51	23396	4	4	2	2	0.82	dense granule protein GRA6
98	TGGT1_278660-t26_1-p1	51	1E+05	1	1	1	1	0.03	putative P-type ATPase4
99	TGGT1_261450-t26_1-p1	49	1E+05	1	1	1	1	0.04	hypothetical protein
100	TGGT1_269442-t26_1-p1	49	9774	1	1	1	1	0.6	putative calmodulin
101	TGGT1_248340-t26_1-p1	48	26095	1	1	1	1	0.2	GTP-binding nuclear protein ran/tc4
102	TGGT1_263700-t26_1-p1	47	16349	1	1	1	1	0.33	ribosomal protein RPS14
103	TGGT1_204050-t26_1-p1	45	85785	2	2	2	2	0.12	subtilisin SUB1
104	TGGT1_203240-t26_1-p1	45	80954	1	1	1	1	0.06	hypothetical protein
105	TGGT1_207710-t26_1-p1	42	28076	1	1	1	1	0.18	putative phosphatidylinositol synthase
106	TGME49_215775-t26_1-p1	41	66043	1	1	1	1	0.07	rhoptry protein ROP8
107	TGGT1_293440-t26_1-p1	41	59840	1	1	1	1	0.08	hypothetical protein
108	TGGT1_206480-t26_1-p1	40	22850	1	1	1	1	0.23	hypothetical protein
109	TGGT1_218280-t26_1-p1	40	50708	1	1	1	1	0.1	putative eukaryotic porin
110	TGGT1_262640-t26_1-p1	40	23859	1	1	1	1	0.22	Cg8 family protein
111	TGGT1_215430-t26_1-p1	39	27594	1	1	1	1	0.19	hypothetical protein
112	TGGT1_281980-t26_1-p1	39	1E+05	1	1	1	1	0.04	phosphatidate cytidylyltransferase
113	TGGT1_297470-t26_1-p1	38	40916	2	2	2	2	0.26	putative myosin light chain 2
114	TGGT1_231930-t26_1-p1	37	87118	2	2	2	2	0.11	hypothetical protein
115	TGGT1_238100-t26_1-p1	37	27217	1	1	1	1	0.19	transmembrane protein
116	TGGT1_311290-t26_1-p1	37	30942	1	1	1	1	0.16	protein tyrosine phosphatase family protein, ptpla protein
117	TGGT1_227620-t26_1-p1	37	19887	2	2	2	2	0.6	dense granule protein GRA2
118	TGGT1_242840-t26_1-p1	36	13952	1	1	1	1	0.39	membrane protein
119	TGGT1_216890-t26_1-p1	35	1E+05	1	1	1	1	0.04	hypothetical protein
120	TGGT1_293180-t26_1-p1	35	64784	1	1	1	1	0.08	NADP-specific glutamate dehydrogenase
121	TGGT1_312150-t26_1-p1	35	61088	1	1	1	1	0.08	hypothetical protein
122	TGGT1_201150-t26_1-p1	35	2E+05	1	1	1	1	0.02	heavy metal translocating P-type ATPase subfamily protein
123	TGGT1_247550-t26_1-p1	34	61388	1	1	1	1	0.08	heat shock protein HSP60
124	TGGT1_292320-t26_1-p1	34	99683	1	1	1	1	0.05	hypothetical protein
125	TGGT1_220100-t26_1-p1	33	61572	1	1	1	1	0.08	phosphoribosylpyrophosphate synthetase
126	TGGT1_313630-t26_1-p1	32	1E+06	1	1	1	1	0	hypothetical protein
127	TGGT1_270620-t26_1-p1	32	1E+05	1	1	1	1	0.05	DEAD/DEAH box helicase domain-containing protein
128	TGGT1_316240-t26_1-p1	31	75893	1	1	1	1	0.06	hypothetical protein
129	TGGT1_259000-t26_1-p1	30	24485	1	1	1	1	0.21	hypothetical protein
130	TGGT1_314020-t26_1-p1	29	2E+05	1	1	1	1	0.03	hypothetical protein
131	TGGT1_312630-t26_1-p1	29	3E+05	1	1	1	1	0.02	putative anonymous antigen-1
132	TGGT1_207830-t26_1-p1	29	40037	1	1	1	1	0.12	MORN repeat-containing protein
133	TGGT1_267430-t26_1-p1	29	49418	1	1	1	1	0.1	DnaJ domain-containing protein
134	TGGT1_411760-t26_1-p1	27	32380	1	1	1	1	0.16	actin
135	TGGT1_321620-t26_1-p1	27	96157	1	1	1	1	0.05	dynamin-related protein DRPB
136	TGGT1_286650-t26_1-p1	26	20450	1	1	1	1	0.26	hypothetical protein
137	TGGT1_263300-t26_1-p1	26	31617	1	1	1	1	0.16	eukaryotic porin protein
138	TGGT1_280560-t26_1-p1	25	1E+05	1	1	1	1	0.03	selenide, water dikinase
139	TGGT1_215100-t26_1-p1	24	3E+05	1	1	1	1	0.02	PP-loop family protein
140	TGGT1_209060-t26_1-p1	24	96777	1	1	1	1	0.05	thrombospondin type 1 domain-containing protein
141	TGGT1_291900-t26_1-p1	24	60275	1	1	1	1	0.08	Ydr279p family (RNase H2 complex component) protein
142	TGGT1_225080-t26_1-p1	23	17826	1	1	1	1	0.3	ribosomal protein RPS18
143	TGGT1_300260-t26_1-p1	23	96909	1	1	1	1	0.05	threonyl-tRNA synthetase family protein
144	TGGT1_253710-t26_1-p1	22	1E+05	1	1	1	1	0.04	hypothetical protein
145	TGGT1_209755B-t26_1-p1	22	66436	1	1	1	1	0.07	hypothetical protein
146	TGGT1_216730-t26_1-p1	21	1E+05	1	1	1	1	0.04	MCM2/3/5 family protein
147	TGGT1_219710-t26_1-p1	20	2E+05	1	1	1	1	0.02	hypothetical protein
148	TGGT1_200310-t26_1-p1	19	18804	1	1	1	1	0.28	hypothetical protein
149	TGGT1_290700-t26_1-p1	19	34568	1	1	1	1	0.15	hypothetical protein
150	TGGT1_216500-t26_1-p1	19	3E+05	1	1	1	1	0.02	putative tRNA synthetase
151	TGGT1_286580-t26_1-p1	19	1E+05	1	1	1	1	0.04	hypothetical protein
152	TGGT1_314770-t26_1-p1	18	56539	1	1	1	1	0.09	tRNA (guanine-N1)-methyltransferase

Appendix Table 6_Protein import assay_ parental-rTgmS35-rTGME49_240270

Sheet 1 - Protein import assay

RHΔKu80/TATi - Parental line

Exp	Treatment	WB band	Mean	Ratio Mature/Immature
Exp 1	No ATc	Immature	37.428	1.297
		Mature	48.554	
	24h ATc	Immature	34.89	1.497
		Mature	52.236	
	48h ATc	Immature	21.542	2.539
		Mature	54.701	
	96h ATc	Immature	29.915	2.201
		Mature	65.841	
Exp 2	No ATc	Mature	48.275	2.001
		Immature	24.127	
	24h ATc	Mature	37.414	1.928
		Immature	19.409	
	48h ATc	Mature	61.896	2.607
		Immature	23.745	
	96h ATc	Mature	30.445	7.464
		Immature	4.079	
Exp 3	No ATc	Immature	57.682	3.898
		Mature	14.796	
	24h ATc	Immature	61.893	2.556
		Mature	24.216	
	48h ATc	Immature	54.507	1.869
		Mature	29.169	
	96h ATc	Immature	57.255	2.142
		Mature	26.734	
Exp 4	No ATc	Immature	62.319	2.697
		Mature	23.111	
	24h ATc	Immature	54.257	4.309
		Mature	12.593	
	48h ATc	Immature	27.444	2.442
		Mature	11.237	
	96h ATc	Immature	23.967	1.223
		Mature	19.598	

Treatment	Ratio Average	STDEV	SEM
No ATc	2.473	1.109	0.554
24h ATc	2.572	1.236	0.618
48h ATc	2.364	0.337	0.169
96h ATc	3.257	2.840	1.420

rTgmS35

Exp	Treatment	WB band	Mean	Ratio Mature/Immature
Exp 1	No ATc	Immature	10200	5.088
		Mature	51900	
	24h ATc	Immature	13000	4.577
		Mature	59500	
	48h ATc	Immature	24900	2.257
		Mature	56200	
	96h ATc	Immature	31600	2.516
		Mature	79500	
Exp 2	No ATc	Mature	20100	3.204
		Immature	64400	
	24h ATc	Mature	19400	3.242
		Immature	62900	
	48h ATc	Mature	23400	2.953
		Immature	69100	
	96h ATc	Mature	35400	2.799
		Immature	99100	
Exp 3	No ATc	Immature	27.047	3.527
		Mature	7.668	
	24h ATc	Immature	24.722	2.647
		Mature	9.338	
	48h ATc	Immature	75.592	3.533
		Mature	21.399	
	96h ATc	Immature	49.737	2.343
		Mature	21.226	
Exp 4	No ATc	Immature	56.26	2.639
		Mature	21.316	
	24h ATc	Immature	64.506	3.063
		Mature	21.063	
	48h ATc	Immature	63.127	1.700
		Mature	37.125	
	96h ATc	Immature	31.98	2.299
		Mature	13.912	

Treatment	Ratio Average	STDEV	SEM
No ATc	3.615	1.049	0.524
24h ATc	3.382	0.834	0.417
48h ATc	2.611	0.800	0.400
96h ATc	2.489	0.227	0.113

rTGME49_240270

Exp	Treatment	WB band	Mean	Ratio Mature/Immature
Exp 1	No ATc	Immature	8840	5.226
		Mature	46200	
	24h ATc	Immature	49100	2.118
		Mature	104000	
	48h ATc	Immature	40900	2.836
		Mature	116000	
	96h ATc	Immature	18200	3.912
		Mature	71200	
Exp 2	No ATc	Mature	19.395	2.105
		Immature	40.835	
	24h ATc	Mature	19.1	2.497
		Immature	47.686	
	48h ATc	Mature	21.875	1.998
		Immature	43.713	
	96h ATc	Mature	23.659	1.894
		Immature	44.806	
Exp 3	No ATc	Immature	20.009	2.412
		Mature	8.297	
	24h ATc	Immature	12.809	2.489
		Mature	5.147	
	48h ATc	Immature	53.263	3.469
		Mature	15.352	
	96h ATc	Immature	13.419	2.905
		Mature	4.619	
Exp 4	No ATc	Immature	55.792	3.266
		Mature	17.084	
	24h ATc	Immature	49.019	3.782
		Mature	12.962	
	48h ATc	Immature	52.002	1.974
		Mature	26.339	
	96h ATc	Immature	49.425	3.756
		Mature	13.159	

Treatment	Ratio Average	STDEV	SEM
No ATc	3.252	1.405	0.702
24h ATc	2.721	0.729	0.364
48h ATc	2.570	0.721	0.361
96h ATc	3.117	0.928	0.464

Sheet 2 - Parental line One-way ANOVA

Anova: Single Factor

SUMMARY

Groups	Count	Sum	Average	Variance
No ATc	4	9.893129	2.473282	1.229076
24h ATc	4	10.2892	2.5723	1.528718
48h ATc	4	9.456919	2.36423	0.113703
96h ATc	4	13.02936	3.25734	8.064733

ANOVA

Source of Variation	SS	df	MS	F	P-value	F crit
Between Groups	1.946663	3	0.648888	0.237335	0.868631	3.490295
Within Groups	32.80869	12	2.734058			
Total	34.75535	15				

Sheet 3 - rTgmS35 One-way ANOVA

Anova: Single Factor

SUMMARY

Groups	Count	Sum	Average	Variance
No ATc	4	14.4588	3.614701	1.099662
24h ATc	4	13.52918	3.382295	0.696325
48h ATc	4	10.44291	2.610728	0.64021
96h ATc	4	9.957204	2.489301	0.051515

ANOVA

Source of Variation	SS	df	MS	F	P-value	F crit
Between Groups	3.735998	3	1.245333	2.002375	0.167479	3.490295
Within Groups	7.463134	12	0.621928			
Total	11.19913	15				

Sheet 4 - rTGME49_240270 One-way ANOVA

Anova: Single Factor

SUMMARY

Groups	Count	Sum	Average	Variance
No ATc	4	13.00902	3.252256	1.972904
24h ATc	4	10.88516	2.721289	0.530989
48h ATc	4	10.27828	2.56957	0.520504
96h ATc	4	12.46707	3.116768	0.860498

ANOVA

Source of Variation	SS	df	MS	F	P-value	F crit
Between Groups	1.245191	3	0.415064	0.427362	0.737043	3.490295
Within Groups	11.65469	12	0.971224			
Total	12.89988	15				

12.3. Appendix protocol

Lab protocol of the tRNA affinity pull down

Modified from Seidman *et al.*, (2012)

<u>Preparation of the beads:</u>

-Use 50µl of paramagnetic streptavidin resin (DYNAL Magnetic Beads, Invitrogen) containing 6.7×10^8 beads/ml per sample. Wash beads 3 times with 500µl SSC buffer (1X).

<u>Experiment:</u>

- Washed resin was resuspended in 500ul $0.5 \times$ SSC
- Synthetic 5'-biotinylated *T. gondii* tRNA^{Ile} (and tRNA^{Met} as negative control) was added to the resin to a final concentration of 2µM and incubated at 65°C for 10 min to form the tRNA-streptavidin affinity resin (10ul/sample of the 100uM stock).
- After incubation, the tRNA-bound resin was washed 3 times with 300 µl of $0.1 \times$ SSC
- Equilibrate the resin in 300 µl of fresh protein binding buffer (PB):
    PB prep: 5ml is enough for one IP (prepare fresh as sucrose and BSA makes it go bad and DTT and prot. inhibitor are not stable):
    - MOPS 167.4mg
    - Sucrose 350.5mg
    - MgCl$_2$ 31.25ul of the 1 M solution
    - KCl 400ul 1.6 ml of the 1.2 M solution
    - DTT 7mg
    - BSA 5mg
    - RNase inhibitor 1.67ul of the commercial stock (20U/ul)
    - MiliQ H2O 4.5ml
- Leave incubating 1 min.
- Each of the starting samples was adjusted to 6.0×10^9 cell equivalents, and volumes were adjusted to 300 µl with PB buffer containing 1% Triton X-100 (Add 4ul to 400ul of PB for 1 sample)
- PB buffer was removed from the beads and replaced by the samples in PB buffer-Triton X-100 1%
- Samples were incubated with the tRNA affinity resin for 30 min at RT under agitation
- Unbound protein was collected, and the tRNA affinity resin was washed 6 times in 500µl of PB buffer.
- tRNA-bound proteins were eluted in 50ul of elution buffers containing increasing ionic concentrations of NaCl (0.25, 0.5, 0.75, 1M NaCl; 20 mM MOPS, pH 7.2)
- Protein samples from each elution were precipitated by TCA method as followed:
    - Add 1 vol TCA to 4 vol protein (12.5 ul of TCA 100% + 50 ul elution), invert to mix
    - Incubate 10 min at 4C
    - Spin 14,000rpm 5 min 4C
    - Wash pellet with 200uL cold acetone (Pellet might only be in FT)
    - Spin 14,000rpm 5 min 4C
    - Pour off the supernatant into waste, and dab tube on towel to dry
    - Repeat acetone wash x1
    - Spin down quickly and remove liquid with a P10 to speed up drying
    - Dry pellet 10 min 95C
    - Resuspend in a V_{tot} = 20ul: 15ul H2O + 5ul of LDS-2mercaptoethanol 4X, and vortex
    - Freeze for later use or boil the samples 5 min 95C to proceed to the WB protocol
- Run samples on 8–18% SDS-PAGE

- Gel staining using SYPRO ORANGE Protein Gel Stain:
    - Pour 1X staining solution into a clean, detergent free glass or polypropylene staining dish. Use ~50 ml for one or two standard minigels, and up to 750 ml for larger gels.
    - Place gel in staining solution and cover with aluminum foil to protect from light during staining.

- Place on a platform shaker for gentle agitation for 10–60 minutes or until optimal staining is achieved. Extended staining times will not improve sensitivity, but can increase background fluorescence.
- Rinse gel in 7.5% acetic acid solution for 1 minute to remove excess dye from the gel.
- Place gel directly on the transilluminator for photographing. Do not use plastic wrap because it will autofluoresce more than normal in the presence of SYPRO Orange. If the gel has a plastic backing it should be removed if it autofluoresces. The backing may bind the dye resulting in high background.

- For LC-MS/MS analysis, bands of interest are cut out of the gel and sent to Polyomics.

Negative control: Mitochondrial proteins were also incubated with paramagnetic streptavidin resin without bound tRNA as a control to identify proteins that bound to the resin non-specifically.

Buffers:

- SSC: 1 × SSC; 150 mM NaCl, 15 mM trisodium citrate dihydrate, pH 7.2. Dilute form the 20X solution.
- Protein binding buffer: 160 mM MOPS (MW=209.26), 310 mM sucrose (MW=342.29), 6.25 mM MgCl$_2$, 100 mM KCl, 9 mM DTT (MW=154.25), 2 units/300 µl of RNAse inhibitor (10U/ul stock), 1 mg/ml BSA → Always make fresh!
- Elution buffer: 20 mM MOPS, 1 M NaCl (MW=58.44), pH 7.2.

13. Bibliography

Adl, S. M. *et al.* (2007) 'Diversity, nomenclature, and taxonomy of protists', *Systematic Biology*, pp. 684–689. doi: 10.1080/10635150701494127.

Agop-Nersesian, C. *et al.* (2009) 'Rab11A-Controlled Assembly of the Inner Membrane Complex Is Required for Completion of Apicomplexan Cytokinesis', *PLoS Pathogens*. Edited by L. D. Sibley, 5(1), p. e1000270. doi: 10.1371/journal.ppat.1000270.

Agop-Nersesian, C. *et al.* (2010) 'Biogenesis of the Inner Membrane Complex Is Dependent on Vesicular Transport by the Alveolate Specific GTPase Rab11B', *PLoS Pathogens*. Edited by L. D. Sibley, 6(7), p. e1001029. doi: 10.1371/journal.ppat.1001029.

Agrawal, S. *et al.* (2009) 'Genetic evidence that an endosymbiont-derived endoplasmic reticulum-associated protein degradation (ERAD) system functions in import of apicoplast proteins', *Journal of Biological Chemistry*. American Society for Biochemistry and Molecular Biology, 284(48), pp. 33683–33691. doi: 10.1074/jbc.M109.044024.

Agrawal, S. *et al.* (2013) 'An Apicoplast Localized Ubiquitylation System Is Required for the Import of Nuclear-encoded Plastid Proteins', *PLoS Pathogens*. Public Library of Science, 9(6). doi: 10.1371/journal.ppat.1003426.

Ajioka, W. and Boothroyd, J. C. (2009) 'NIH Public Access', *Microbiology*, 314(5806), pp. 1780–1783. doi: 10.1126/science.1133690.Polymorphic.

Akpunarlieva, S. *et al.* (2017) 'Integration of proteomics and metabolomics to elucidate metabolic adaptation in Leishmania', *Journal of Proteomics*. Elsevier B.V., 155, pp. 85–98. doi: 10.1016/j.jprot.2016.12.009.

Alexander, D. L. *et al.* (2005) 'Identification of the moving junction complex of Toxoplasma gondii: a collaboration between distinct secretory organelles.', *PLoS pathogens*. Public Library of Science, 1(2), p. e17. doi: 10.1371/journal.ppat.0010017.

Altschul, S. F. *et al.* (1990) 'Basic local alignment search tool', *Journal of Molecular Biology*. J Mol Biol, 215(3), pp. 403–410. doi: 10.1016/S0022-2836(05)80360-2.

Amunts, A. *et al.* (2014) 'Structure of the yeast mitochondrial large ribosomal subunit.', *Science (New York, N.Y.)*. Europe PMC Funders, 343(6178), pp. 1485–1489. doi: 10.1126/science.1249410.

Amunts, A. *et al.* (2015) 'Ribosome. The structure of the human mitochondrial ribosome.', *Science (New York, N.Y.)*, 348(6230), pp. 95–8. doi: 10.1126/science.aaa1193.

Andenmatten, N. *et al.* (2013) 'Conditional genome engineering in Toxoplasma gondii uncovers alternative invasion mechanisms', *Nature Methods*, 10(2), pp. 125–127. doi: 10.1038/nmeth.2301.

Andersson, S. G. E. *et al.* (2003) 'On the origin of mitochondria: A genomics perspective', in *Philosophical Transactions of the Royal Society B: Biological Sciences*. Royal Society, pp. 165–179. doi: 10.1098/rstb.2002.1193.

Anne, M. *et al.* (2000) *Selective importation of RNA into isolated mitochondria from Leishmania tarentolae*.

Aphasizhev, R., Karmarkar, U. and Simpson, L. (1998) 'Are tRNAs imported into the mitochondria of kinetoplastid protozoa as 5′-extended precursors?', *Molecular and Biochemical Parasitology*, 93(1), pp. 73–80. doi: 10.1016/S0166-6851(98)00022-X.

Aranda, P. S., Lajoie, D. M. and Jorcyk, C. L. (2012) 'Bleach gel: A simple agarose gel for analyzing RNA quality', *Electrophoresis*. Electrophoresis, 33(2), pp. 366–369. doi: 10.1002/elps.201100335.

Azad, A. K. *et al.* (2001) 'Role of Nuclear Pools of Aminoacyl-tRNA Synthetases in tRNA Nuclear Export', *Molecular Biology of the Cell*. Edited by P. A. Silver. American Society for Cell Biology, 12(5), pp. 1381–1392. doi: 10.1091/mbc.12.5.1381.

Baleva, M. *et al.* (2015) 'A moonlighting human protein is involved in mitochondrial import of tRNA', *International Journal of Molecular Sciences*, 16(5), pp. 9354–9367. doi: 10.3390/ijms16059354.

Balk, J. and Lobréaux, S. (2005) 'Biogenesis of iron-sulfur proteins in plants', *Trends in Plant Science*. Elsevier, pp. 324–331. doi: 10.1016/j.tplants.2005.05.002.

Ban, N. *et al.* (2014) 'A new system for naming ribosomal proteins', *Current Opinion in Structural Biology*. Elsevier Ltd, pp. 165–169. doi: 10.1016/j.sbi.2014.01.002.

Barrientos, A., Fontanesi, F. and Díaz, F. (2009) 'Evaluation of the mitochondrial respiratory Chain and oxidative phosphorylation system using polarography and spectrophotometric enzyme assays', *Current Protocols in Human Genetics*. Blackwell Publishing Inc., p. Unit19.3. doi: 10.1002/0471142905.hg1903s63.

Barylyuk, K. *et al.* (2020) 'A subcellular atlas of Toxoplasma reveals the functional context of the proteome', pp. 1–23.

BD, L. and L, S. (1996) 'Sequence-dependent in vivo importation of tRNAs into the mitochondrion of Leishmania tarentolae.', *RNA (New York, N.Y.)*, 2(5), pp. 429–440.

Behnke, M. S. *et al.* (2010) 'Coordinated progression through two subtranscriptomes underlies the tachyzoite cycle of toxoplasma gondii', *PLoS ONE*, 5(8). doi: 10.1371/journal.pone.0012354.

Behnke, M. S. *et al.* (2011) 'Virulence differences in Toxoplasma mediated by amplification of a family of polymorphic pseudokinases', *Proceedings of the National Academy of Sciences of the United States of America*, 108(23), pp. 9631–9636. doi: 10.1073/pnas.1015338108.

Behnke, M. S. *et al.* (2015) 'Rhoptry Proteins ROP5 and ROP18 Are Major Murine Virulence Factors in Genetically Divergent South American Strains of Toxoplasma gondii', *PLoS Genetics*. doi: 10.1371/journal.pgen.1005434.

Bhargava, K., Templeton, P. and Spremulli, L. L. (2004) 'Expression and characterization of isoform 1 of human mitochondrial elongation factor G', *Protein Expression and Purification*. Academic Press, 37(2), pp. 368–376. doi: 10.1016/j.pep.2004.06.030.

Bhattacharyya, S. N. *et al.* (2003) '"Ping-Pong" Interactions between Mitochondrial tRNA Import Receptors within a Multiprotein Complex', *Molecular and Cellular Biology*. American Society for Microbiology, 23(15), pp. 5217–5224. doi: 10.1128/mcb.23.15.5217-5224.2003.

Biagini, G. A. *et al.* (2006) 'Functional characterization and target validation of alternative complex I of Plasmodium falciparum mitochondria', *Antimicrobial Agents and Chemotherapy*. American Society for Microbiology Journals, 50(5), pp. 1841–1851. doi: 10.1128/AAC.50.5.1841-1851.2006.

Biddau, M. *et al.* (2018) 'Two essential Thioredoxins mediate apicoplast biogenesis, protein import, and gene expression in Toxoplasma gondii', *PLoS Pathogens*. Public Library of Science, 14(2). doi: 10.1371/journal.ppat.1006836.

Biology, O. *et al.* (2017) '| WORMBOOK Cell Biology of the Mitochondrion', *Genetics*, 207, pp. 843–871. doi: 10.1534/genetics.117.300262.

Black, M. *et al.* (1995) 'Restriction enzyme-mediated integration elevates transformation frequency and enables co-transfection of Toxoplasma gondii', *Molecular and Biochemical Parasitology*. Elsevier, 74(1), pp. 55–63. doi: 10.1016/0166-6851(95)02483-2.

Blader, I. *et al.* (2015) 'The lytic cycle of Toxoplasma gondii: 15 years later'. doi: 10.1146/annurev-micro-091014-104100.

Blank, M. L. *et al.* (2018) 'A Toxoplasma gondii locus required for the direct manipulation of host mitochondria has maintained multiple ancestral functions.', *Molecular microbiology*. NIH Public Access, 108(5), pp. 519–535. doi: 10.1111/mmi.13947.

Bohnert, M. *et al.* (2010) 'Cooperation of stop-transfer and conservative sorting

mechanisms in mitochondrial protein transport', *Current Biology*. Cell Press, 20(13), pp. 1227–1232. doi: 10.1016/j.cub.2010.05.058.

Boothroyd, J. C. and Dubremetz, J.-F. (2008) 'Kiss and spit: the dual roles of Toxoplasma rhoptries', *Nature Reviews Microbiology*, 6(1), pp. 79–88. doi: 10.1038/nrmicro1800.

Bougdour, A., Tardieux, I. and Hakimi, M.-A. (2014) '*T oxoplasma* exports dense granule proteins beyond the vacuole to the host cell nucleus and rewires the host genome expression', *Cellular Microbiology*, 16(3), pp. 334–343. doi: 10.1111/cmi.12255.

Bouzaidi-Tiali, N. *et al.* (2007) 'Elongation factor 1a mediates the specificity of mitochondrial tRNA import in T. brucei', *EMBO Journal*. European Molecular Biology Organization, 26(20), pp. 4302–4312. doi: 10.1038/sj.emboj.7601857.

Boxma, B. *et al.* (2004) 'The anaerobic chytridiomycete fungus Piromyces sp. E2 produces ethanol via pyruvate:formate lyase and an alcohol dehydrogenase E', *Molecular Microbiology*. John Wiley & Sons, Ltd, 51(5), pp. 1389–1399. doi: 10.1046/j.1365-2958.2003.03912.x.

Brown, A. *et al.* (2014) 'Structure of the large ribosomal subunit from human mitochondria.', *Science (New York, N.Y.)*. Europe PMC Funders, 346(6210), pp. 718–722. doi: 10.1126/science.1258026.

Brydges, S. D. and Carruthers, V. B. (2003) 'Mutation of an unusual mitochondrial targeting sequence of SODB2 produces multiple targeting fates in Toxoplasma gondii', *Journal of Cell Science*. The Company of Biologists Ltd, pp. 4675–4685. doi: 10.1242/jcs.00750.

Burki, F. (2016) 'Mitochondrial Evolution: Going, Going, Gone.', *Current biology : CB*. Elsevier, 26(10), pp. R410-2. doi: 10.1016/j.cub.2016.04.032.

Caldas, L. A., de Souza, W. and Attias, M. (2010) 'Microscopic analysis of calcium ionophore activated egress of Toxoplasma gondii from the host cell', *Veterinary Parasitology*, 167(1), pp. 8–18. doi: 10.1016/j.vetpar.2009.09.051.

Carey, K. L. *et al.* (2004) 'The Toxoplasma gondii rhoptry protein ROP4 is secreted into the parasitophorous vacuole and becomes phosphorylated in infected cells.', *Eukaryotic cell*. American Society for Microbiology (ASM), 3(5), pp. 1320–30. doi: 10.1128/EC.3.5.1320-1330.2004.

Del Carmen, M. G. *et al.* (2009) 'Induction and regulation of conoid extrusion in *Toxoplasma gondii*', *Cellular Microbiology*, 11(6), pp. 967–982. doi: 10.1111/j.1462-5822.2009.01304.x.

Carroll, A. J. (2017) 'Isolation of mitochondrial ribosomes', in *Methods in Molecular Biology*. Humana Press Inc., pp. 267–280. doi: 10.1007/978-1-4939-6533-5_21.

Carruthers, V. B. *et al.* (2000) 'Toxoplasma gondii uses sulfated proteoglycans for substrate and host cell attachment.', *Infection and immunity*. American Society for Microbiology (ASM), 68(7), pp. 4005–11. doi: 10.1128/iai.68.7.4005-4011.2000.

Carruthers, V. B. (2002) 'Host cell invasion by the opportunistic pathogen Toxoplasma gondii.', *Acta tropica*, 81(2), pp. 111–22. doi: 10.1016/s0001-706x(01)00201-7.

Carruthers, V. B., Giddings, O. K. and Sibley, L. D. (1999) 'Secretion of micronemal proteins is associated with toxoplasma invasion of host cells', *Cellular Microbiology*. John Wiley & Sons, Ltd (10.1111), 1(3), pp. 225–235. doi: 10.1046/j.1462-5822.1999.00023.x.

Carruthers, V. B. and Tomley, F. M. (2008) 'Microneme proteins in apicomplexans.', *Sub-cellular biochemistry*, 47, pp. 33–45. Available at: http://www.ncbi.nlm.nih.gov/pubmed/18512339 (Accessed: 30 September 2019).

Carruthers, V. and Boothroyd, J. C. (2007) 'Pulling together: an integrated model of Toxoplasma cell invasion', *Current Opinion in Microbiology*. Elsevier Current Trends, 10(1), pp. 83–89. doi: 10.1016/J.MIB.2006.06.017.

Chacinska, A. *et al.* (2004) 'Essential role of Mia40 in import and assembly of mitochondrial intermembrane space proteins', *EMBO Journal*. European Molecular Biology Organization, 23(19), pp. 3735–3746. doi: 10.1038/sj.emboj.7600389.

Chan, K. W. *et al.* (2005) 'A novel ADP/ATP transporter in the mitosome of the microaerophilic human parasite Entamoeba histolytica', *Current Biology*. Cell Press, 15(8), pp. 737–742. doi: 10.1016/j.cub.2005.02.068.

Charron, A. J. and Sibley, L. D. (2002) 'Host cells: Mobilizable lipid resources for the intracellular parasite Toxoplasma gondii', *Journal of Cell Science*, 115(15), pp. 3049–3059.

Chatterjee, K. *et al.* (2018) 'tRNA dynamics between the nucleus, cytoplasm and mitochondrial surface: Location, location, location', *Biochimica et Biophysica Acta - Gene Regulatory Mechanisms*. Elsevier B.V., pp. 373–386. doi: 10.1016/j.bbagrm.2017.11.007.

Checkley, W. *et al.* (2015) 'A review of the global burden, novel diagnostics, therapeutics, and vaccine targets for cryptosporidium.', *The Lancet. Infectious diseases*. NIH Public Access, 15(1), pp. 85–94. doi: 10.1016/S1473-3099(14)70772-8.

Chen, R. *et al.* (2016) 'Identification of a novel mitochondrial interacting protein of C1QBP using subcellular fractionation coupled with CoIP-MS', *Analytical and Bioanalytical Chemistry*, 408(6), pp. 1557–1564. doi: 10.1007/s00216-015-9228-7.

CHIBBER, R. and CASTLE, A. G. (1983) 'Subcellular fractionation of porcine neutrophils by nitrogen cavitation and sucrose-density-gradient centrifugation', *European Journal of Biochemistry*, 136(2), pp. 383–389. doi: 10.1111/j.1432-1033.1983.tb07753.x.

Christian, B. E. and Spremulli, L. L. (2012) 'Mechanism of protein biosynthesis in mammalian mitochondria', *Biochimica et Biophysica Acta - Gene Regulatory Mechanisms*. NIH Public Access, pp. 1035–1054. doi:

10.1016/j.bbagrm.2011.11.009.

Christoforou, A. *et al.* (2016) 'A draft map of the mouse pluripotent stem cell spatial proteome', *Nature Communications*. Nature Publishing Group, 7(1), pp. 1–12. doi: 10.1038/ncomms9992.

Cinar, H. N. *et al.* (2015) 'The complete mitochondrial genome of the foodborne parasitic pathogen Cyclospora cayetanensis', *PLoS ONE*. Public Library of Science, 10(6). doi: 10.1371/journal.pone.0128645.

Claros, M. G. and Vincens, P. (1996) 'Computational method to predict mitochondrially imported proteins and their targeting sequences', *European Journal of Biochemistry*. Blackwell Publishing Ltd, 241(3), pp. 779–786. doi: 10.1111/j.1432-1033.1996.00779.x.

Clough, B. and Frickel, E.-M. (2017) 'The Toxoplasma Parasitophorous Vacuole: An Evolving Host–Parasite Frontier', *Trends in Parasitology*. Elsevier Current Trends, 33(6), pp. 473–488. doi: 10.1016/J.PT.2017.02.007.

Courjol, F. *et al.* (2017) 'Characterization of a nuclear pore protein sheds light on the roles and composition of the Toxoplasma gondii nuclear pore complex', *Cellular and Molecular Life Sciences*. Birkhauser Verlag AG, 74(11), pp. 2107–2125. doi: 10.1007/s00018-017-2459-3.

Couvillion, M. T. *et al.* (2016) 'Article Synchronized mitochondrial and cytosolic translation programs', *Nature*. Nature Publishing Group, 533(7604), pp. 499–503. doi: 10.1038/nature18015.

Crausaz Esseiva, A. *et al.* (2004) 'The T-Stem Determines the Cytosolic or Mitochondrial Localization of Trypanosomal tRNAs Met', *Molecular Biology of the Cell*, 15, pp. 2750–2757. doi: 10.1091/mbc.E03-11-0821.

Critchlow, S. E. and Jackson, S. P. (1998) 'DNA end-joining: From yeast to man', *Trends in Biochemical Sciences*. Trends Biochem Sci, pp. 394–398. doi: 10.1016/S0968-0004(98)01284-5.

Curt-Varesano, A. *et al.* (2016) 'The aspartyl protease TgASP5 mediates the export of the Toxoplasma GRA16 and GRA24 effectors into host cells', *Cellular Microbiology*. Blackwell Publishing Ltd, 18(2), pp. 151–167. doi: 10.1111/cmi.12498.

Dagley, M. J. *et al.* (no date) 'The Protein Import Channel in the Outer Mitosomal Membrane of Giardia intestinalis'. doi: 10.1093/molbev/msp117.

Dahl, E. L. *et al.* (2006) 'Tetracyclines specifically target the apicoplast of the malaria parasite Plasmodium falciparum', *Antimicrobial Agents and Chemotherapy*. American Society for Microbiology (ASM), 50(9), pp. 3124-3131. doi: 10.1128/AAC.00394-06.

Daoud, R., Forget, L. and Lang, B. F. (no date) 'Yeast mitochondrial RNase P, RNase Z and the RNA degradosome are part of a stable supercomplex'. doi: 10.1093/nar/gkr941.

David, A. *et al.* (2012) 'Nuclear translation visualized by ribosome-bound nascent chain puromycylation', *Journal of Cell Biology*. The Rockefeller University Press, 197(1), pp. 45-57. doi: 10.1083/jcb.201112145.

Delage, L. *et al.* (2003) 'In Vitro Import of a Nuclearly Encoded tRNA into Mitochondria of Solanum tuberosum', *Molecular and Cellular Biology*. American Society for Microbiology, 23(11), pp. 4000-4012. doi: 10.1128/mcb.23.11.4000-4012.2003.

Dennerlein, S., Wang, C. and Rehling, P. (2017) 'Plasticity of Mitochondrial Translation', *Trends in Cell Biology*. Elsevier Ltd, 27(10), pp. 712-721. doi: 10.1016/j.tcb.2017.05.004.

DeRocher, A. *et al.* (2000) 'Analysis of targeting sequences demonstrates that trafficking to the Toxoplasma gondii plastid branches off the secretory system', *Journal of Cell Science*, 113(22), pp. 3969-3977.

Dietrich, A. *et al.* (1996) 'Editing and import: Strategies for providing plant mitochondria with a complete set of functional transfer RNAs', *Biochimie*.

Elsevier B.V., 78(6), pp. 518–529. doi: 10.1016/0300-9084(96)84758-4.

Donald, R. G. K. and Roos, D. S. (1993) 'Stable molecular transformation of Toxoplasma gondii: A selectable dihydrofolate reductase-thymidylate synthase marker based on drug-resistance mutations in malaria', *Proceedings of the National Academy of Sciences of the United States of America*. National Academy of Sciences, 90(24), pp. 11703–11707. doi: 10.1073/pnas.90.24.11703.

Van Dooren, G. G. *et al.* (2002) 'Processing of an apicoplast leader sequence in Plasmodium falciparum and the identification of a putative leader cleavage enzyme', *Journal of Biological Chemistry*. American Society for Biochemistry and Molecular Biology, 277(26), pp. 23612–23619. doi: 10.1074/jbc.M201748200.

Van Dooren, G. G. *et al.* (2008) 'Toxoplasma gondii Tic20 is essential for apicoplast protein import', *Proceedings of the National Academy of Sciences of the United States of America*. National Academy of Sciences, 105(36), pp. 13574–13579. doi: 10.1073/pnas.0803862105.

Van Dooren, G. G. *et al.* (2016) 'The import of proteins into the mitochondrion of toxoplasma gondii', *Journal of Biological Chemistry*, 291(37), pp. 19335–19350. doi: 10.1074/jbc.M116.725069.

Van Dooren, G. G., Stimmler, L. M. and McFadden, G. I. (2006) 'Metabolic maps and functions of the Plasmodium mitochondrion', *FEMS Microbiology Reviews*. Oxford Academic, pp. 596–630. doi: 10.1111/j.1574-6976.2006.00027.x.

DUBEY, J. P. and FRENKEL, J. K. (1972) 'Cyst-Induced Toxoplasmosis in Cats*', *The Journal of Protozoology*. John Wiley & Sons, Ltd (10.1111), 19(1), pp. 155–177. doi: 10.1111/j.1550-7408.1972.tb03431.x.

Dubey, J. P., Lindsay, D. S. and Speer, C. A. (1998) 'Structures of Toxoplasma gondii tachyzoites, bradyzoites, and sporozoites and biology and development of tissue cysts', *Clinical Microbiology Reviews*.

Dubey, J. P., Miller, N. L. and Frenkel, J. K. (1970a) 'Characterization of the new fecal form of Toxoplasma gondii.', *The Journal of parasitology*, 56(3), pp.

447–56. Available at: http://www.ncbi.nlm.nih.gov/pubmed/5467864 (Accessed: 30 September 2019).

Dubey, J. P., Miller, N. L. and Frenkel, J. K. (1970b) 'The Toxoplasma gondii oocyst from cat feces.', *The Journal of experimental medicine*. The Rockefeller University Press, 132(4), pp. 636–62. doi: 10.1084/jem.132.4.636.

Dubremetz, J. F. (2007) 'Rhoptries are major players in Toxoplasma gondii invasion and host cell interaction', *Cellular Microbiology*, 9(4), pp. 841–848. doi: 10.1111/j.1462-5822.2007.00909.x.

Dunn, D. *et al.* (1999) 'Mother-to-child transmission of toxoplasmosis: risk estimates for clinical counselling', *The Lancet*. Elsevier, 353(9167), pp. 1829–1833. doi: 10.1016/S0140-6736(98)08220-8.

Dyall, S. D., Brown, M. T. and Johnson, P. J. (2004) 'Ancient Invasions: From Endosymbionts to Organelles', *Science*. Science, pp. 253–257. doi: 10.1126/science.1094884.

Eckers, E. *et al.* (2013) 'Divergent molecular evolution of the mitochondrial sulfhydryl: Cytochrome c oxidoreductase Erv in opisthokonts and parasitic protists', *Journal of Biological Chemistry*. American Society for Biochemistry and Molecular Biology, 288(4), pp. 2676–2688. doi: 10.1074/jbc.M112.420745.

Egarter, S. *et al.* (2014) 'The toxoplasma acto-myoA motor complex is important but not essential for gliding motility and host cell invasion', *PLoS ONE*. Public Library of Science, 9(3), p. e91819. doi: 10.1371/journal.pone.0091819.

Elsheikha, H. M., Büsselberg, D. and Zhu, X. Q. (2016) 'The known and missing links between Toxoplasma gondii and schizophrenia', *Metabolic Brain Disease*, pp. 749–759. doi: 10.1007/s11011-016-9822-1.

Embley, T. M. *et al.* (2003) 'Hydrogenosomes, mitochondria and early eukaryotic evolution.', *IUBMB life*, 55(7), pp. 387–95. doi: 10.1080/15216540310001592834.

Embley, T. M. and Finlay, B. J. (1994) 'The use of small subunit rRNA sequences

to unravel the relationships between anaerobic ciliates and their methanogen endosymbionts', *Microbiology*. Microbiology Society, pp. 225–235. doi: 10.1099/13500872-140-2-225.

Entelis, N. *et al.* (2006) 'A glycolytic enzyme, enolase, is recruited as a cofactor of tRNA targeting toward mitochondria in Saccharomyces cerevisiae', *Genes and Development*. Cold Spring Harbor Laboratory Press, 20(12), pp. 1609–1620. doi: 10.1101/gad.385706.

Entelis, N. S. *et al.* (2001) 'RNA delivery into mitochondria', *Advanced Drug Delivery Reviews*. Elsevier, 49(1–2), pp. 199–215. doi: 10.1016/S0169-409X(01)00135-1.

Ernst, R. *et al.* (2011) 'Enzymatic blockade of the ubiquitin-proteasome pathway', *PLoS Biology*. Public Library of Science, 9(3). doi: 10.1371/journal.pbio.1000605.

Esseiva, A. C. *et al.* (2004) 'Mitochondrial tRNA import in Toxoplasma gondii', *Journal of Biological Chemistry*, 279(41), pp. 42363–42368. doi: 10.1074/jbc.M404519200.

Feagin, J. E. (1992) 'The 6-kb element of Plasmodium falciparum encodes mitochondrial cytochrome genes', *Molecular and Biochemical Parasitology*. Elsevier, 52(1), pp. 145–148. doi: 10.1016/0166-6851(92)90046-M.

Feagin, J. E. *et al.* (2012) 'The fragmented mitochondrial ribosomal RNAs of plasmodium falciparum', *PLoS ONE*. Public Library of Science, 7(6). doi: 10.1371/journal.pone.0038320.

Fellows, J. D. *et al.* (2017) 'A plastid protein that evolved from ubiquitin and is required for apicoplast protein import in Toxoplasma gondii', *mBio*. American Society for Microbiology, 8(3). doi: 10.1128/mBio.00950-17.

Fichera, M. E., Bhopale, M. K. and Roos, D. S. (1995) 'In vitro assays elucidate peculiar kinetics of clindamycin action against Toxoplasma gondii', *Antimicrobial Agents and Chemotherapy*. American Society for Microbiology,

39(7), pp. 1530–1537. doi: 10.1128/AAC.39.7.1530.

Fichera, M. E. and Roos, D. S. (1997) 'A plastid organelle as a drug target in apicomplexan parasites', *Nature*. Nature Publishing Group, 390(6658), pp. 407–409. doi: 10.1038/37132.

Finlay, B. J. and Fenchel, T. (1989) 'Hydrogenosomes in some anaerobic protozoa resemble mitochondria', *FEMS Microbiology Letters*. John Wiley & Sons, Ltd, 65(3), pp. 311–314. doi: 10.1111/j.1574-6968.1989.tb03679.x.

Flegr, J. *et al.* (2014) 'Toxoplasmosis - A global threat. Correlation of latent toxoplasmosis with specific disease burden in a set of 88 countries', *PLoS ONE*. doi: 10.1371/journal.pone.0090203.

Foury, F. *et al.* (1998) 'The complete sequence of the mitochondrial genome of *Saccharomyces cerevisiae*', *FEBS Letters*. Elsevier, 440(3), pp. 325–331. doi: 10.1016/S0014-5793(98)01467-7.

Fox, B. A. *et al.* (2009) 'Efficient gene replacements in Toxoplasma gondii strains deficient for nonhomologous end joining', *Eukaryotic Cell*. Eukaryot Cell, 8(4), pp. 520–529. doi: 10.1128/EC.00357-08.

Fox, Thomas D *et al.* (2012) 'Mitochondrial protein synthesis, import, and assembly.', *Genetics*. Genetics, 192(4), pp. 1203–34. doi: 10.1534/genetics.112.141267.

Franko, A. *et al.* (2013) 'Efficient Isolation of Pure and Functional Mitochondria from Mouse Tissues Using Automated Tissue Disruption and Enrichment with Anti-TOM22 Magnetic Beads', *PLoS ONE*. Edited by S. Strack. Public Library of Science, 8(12), p. e82392. doi: 10.1371/journal.pone.0082392.

Frénal, K. *et al.* (2010) 'Functional Dissection of the Apicomplexan Glideosome Molecular Architecture', *Cell Host & Microbe*. Cell Press, 8(4), pp. 343–357. doi: 10.1016/J.CHOM.2010.09.002.

Frénal, K., Dubremetz, J.-F., *et al.* (2017) 'Gliding motility powers invasion and

egress in Apicomplexa', *Nature Reviews Microbiology*. Nature Publishing Group, 15(11), pp. 645–660. doi: 10.1038/nrmicro.2017.86.

Frénal, K., Jacot, D., *et al.* (2017) 'Myosin-dependent cell-cell communication controls synchronicity of division in acute and chronic stages of Toxoplasma gondii', *Nature Communications*. Nature Publishing Group, 8(1), p. 15710. doi: 10.1038/ncomms15710.

Frenkel, J. K., Dubey, J. P. and Miller, N. L. (1970) 'Toxoplasma gondii in Cats: Fecal Stages Identified as Coccidian Oocysts', *Science*, 167(3919), pp. 893–896. doi: 10.1126/science.167.3919.893.

Gajria, B. *et al.* (2008) 'ToxoDB: an integrated Toxoplasma gondii database resource', *Nucleic Acids Research*, 36, pp. 553–556. doi: 10.1093/nar/gkm981.

Garbuz, T. and Arrizabalaga, G. (2017) 'Lack of mitochondrial MutS homolog 1 in Toxoplasma gondii disrupts maintenance and fidelity of mitochondrial DNA and reveals metabolic plasticity', *PLOS ONE*. Edited by I. J. Blader. Public Library of Science, 12(11), p. e0188040. doi: 10.1371/journal.pone.0188040.

Gardini, A. (2017) *Enhancer RNAs: Methods and Protocols*, *Methods in Molecular Biology*. doi: 10.1007/978-1-4939-4035-6.

Garweg, J. G., de Groot-Mijnes, J. D. F. and Montoya, J. G. (2011) 'Diagnostic approach to ocular toxoplasmosis.', *Ocular immunology and inflammation*. Taylor & Francis, 19(4), pp. 255–61. doi: 10.3109/09273948.2011.595872.

Gaur, R. *et al.* (2008) 'A Single Mammalian Mitochondrial Translation Initiation Factor Functionally Replaces Two Bacterial Factors', *Molecular Cell*. NIH Public Access, 29(2), pp. 180–190. doi: 10.1016/j.molcel.2007.11.021.

Geladaki, A. *et al.* (2019) 'Combining LOPIT with differential ultracentrifugation for high-resolution spatial proteomics', *Nature Communications*. Nature Publishing Group, 10(1), pp. 1–15. doi: 10.1038/s41467-018-08191-w.

Glaser, S. *et al.* (2012) 'Tic22 is an essential chaperone required for protein

import into the apicoplast', *Journal of Biological Chemistry*. American Society for Biochemistry and Molecular Biology, 287(47), pp. 39505–39512. doi: 10.1074/jbc.M112.405100.

Grasso, D. G. *et al.* (2007) 'Overexpression and Purification of Mammalian Mitochondrial Translational Initiation Factor 2 and Initiation Factor 3', in *Methods in Enzymology*. Academic Press Inc., pp. 59–78. doi: 10.1016/S0076-6879(07)30004-9.

Greber, B. J. *et al.* (2014) 'mammalian mitochondrial ribosome', *Nature*. Nature Publishing Group, 515(7526), pp. 283–286. doi: 10.1038/nature13895.

Greber, B. J. and Ban, N. (2016) 'Structure and Function of the Mitochondrial Ribosome', *Annual Review of Biochemistry*. Annual Reviews , 85(1), pp. 103–132. doi: 10.1146/annurev-biochem-060815-014343.

Grosjean, H. *et al.* (1995) *A novel enzymatic pathway leading to 1-methylinosine modification in Haloferax volcanai tRNA, Nucleic Acids Research*.

Grosshans, H., Hurt, E. and Simos, G. (2000) *An aminoacylation-dependent nuclear tRNA export pathway in yeast*. Available at: www.genesdev.org (Accessed: 18 May 2020).

Gupta, A. *et al.* (2014) 'Reduced ribosomes of the apicoplast and mitochondrion of Plasmodium spp. and predicted interactions with antibiotics', *Open Biology*, 4(MAY). doi: 10.1098/rsob.140045.

Hackstein, J. H. P. *et al.* (2001) 'Hydrogenosomes: Convergent adaptations of mitochondria to anaerobic environments', *Zoology*. Elsevier GmbH, pp. 290–302. doi: 10.1078/0944-2006-00035.

El Hajj, H. *et al.* (2007) 'Inverted topology of the Toxoplasma gondii ROP5 rhoptry protein provides new insights into the association of the ROP2 protein family with the parasitophorous vacuole membrane', *Cellular Microbiology*, 9(1), pp. 54–64. doi: 10.1111/j.1462-5822.2006.00767.x.

Håkansson, S. *et al.* (1999) 'Time-lapse video microscopy of gliding motility in Toxoplasma gondii reveals a novel, biphasic mechanism of cell locomotion.', *Molecular biology of the cell*. American Society for Cell Biology, 10(11), pp. 3539–47. doi: 10.1091/mbc.10.11.3539.

Hales, K. G. and Fuller, M. T. (1997) 'Developmentally regulated mitochondrial fusion mediated by a conserved, novel, predicted GTPase', *Cell*. Cell Press, 90(1), pp. 121–129. doi: 10.1016/S0092-8674(00)80319-0.

Hammarsund, M. *et al.* (2001) 'Identification and characterization of two novel human mitochondrial elongation factor genes, hEFG2 and hEFG1, phylogenetically conserved through evolution', *Human Genetics*. Springer, 109(5), pp. 542–550. doi: 10.1007/s00439-001-0610-5.

Hancock, K. *et al.* (1992) *Identification of Nuclear Encoded Precursor tRNAs within the Mitochondrion of Trypanosoma brucei"*.

Harding, C. R. *et al.* (2016) 'Gliding Associated Proteins Play Essential Roles during the Formation of the Inner Membrane Complex of Toxoplasma gondii.', *PLoS pathogens*. Public Library of Science, 12(2), p. e1005403. doi: 10.1371/journal.ppat.1005403.

Hassink, G. C. *et al.* (2006) 'Ubiquitination of MHC class I heavy chains is essential for dislocation by human cytomegalovirus-encoded US2 but not US11', *Journal of Biological Chemistry*. American Society for Biochemistry and Molecular Biology, 281(40), pp. 30063–30071. doi: 10.1074/jbc.M602248200.

Hata, M., Sato, S. and Kita, K. (2019) 'Method for the separation of mitochondria and apicoplast from the malaria parasite Plasmodium falciparum', *Parasitology International*. Elsevier Ireland Ltd, 69, pp. 99–102. doi: 10.1016/j.parint.2018.12.003.

Hauser, R. and Schneider1, A. (1995) *tRNAs are imported into mitochondria of Trypanosoma brucei independently of their genomic context and genetic origin*, *The EMBO Journal*.

He, C. Y. *et al.* (2001) 'A plastid segregation defect in the protozoan parasite Toxoplasma gondii', *EMBO Journal*, 20(3), pp. 330–339. doi: 10.1093/emboj/20.3.330.

Hikosaka, K., Kita, K. and Tanabe, K. (2013) 'Diversity of mitochondrial genome structure in the phylum Apicomplexa', *Molecular and Biochemical Parasitology*. doi: 10.1016/j.molbiopara.2013.02.006.

Hill, D. E., Chirukandoth, S. and Dubey, J. P. (2005) 'Biology and epidemiology of Toxoplasma gondii in man and animals', *Animal Health Research Reviews*, 6(1), pp. 41–61. doi: 10.1079/AHR2005100.

Hillebrand, A. *et al.* (2018) 'Identification of clustered organellar short (cos) RNAs and of a conserved family of organellar RNA-binding proteins, the heptatricopeptide repeat proteins, in the malaria parasite', *Nucleic acids research*, 46(19), pp. 10417–10431. doi: 10.1093/nar/gky710.

Van Den Hoff, M. J. B., Moorman, A. F. M. and Lamers, W. H. (2902) *Electroporation in 'intracellular' buffer increases cell survival*, *Nucleic Acids Research*.

Hohlfeld, P. *et al.* (1989) 'Fetal toxoplasmosis: Outcome of pregnancy and infant follow-up after in utero treatment', *The Journal of Pediatrics*. Mosby, 115(5), pp. 765–769. doi: 10.1016/S0022-3476(89)80660-2.

Hopper, A. K. (2013) 'Transfer RNA post-transcriptional processing, turnover, and subcellular dynamics in the yeast Saccharomyces cerevisiae', *Genetics*. Genetics, 194(1), pp. 43–67. doi: 10.1534/genetics.112.147470.

Hopper, A. K. and Nostramo, R. T. (2019) 'TRNA processing and subcellular trafficking proteins multitask in pathways for other RNAs', *Frontiers in Genetics*. Frontiers Media S.A., p. 96. doi: 10.3389/fgene.2019.00096.

Hornig-Do, H. T. *et al.* (2009) 'Isolation of functional pure mitochondria by superparamagnetic microbeads', *Analytical Biochemistry*. Academic Press Inc., 389(1), pp. 1–5. doi: 10.1016/j.ab.2009.02.040.

Hu, K. *et al.* (2002) 'Daughter cell assembly in the protozoan parasite Toxoplasma gondii.', *Molecular biology of the cell*. American Society for Cell Biology, 13(2), pp. 593–606. doi: 10.1091/mbc.01-06-0309.

Hu, K., Roos, D. S. and Murray, J. M. (2002) 'A novel polymer of tubulin forms the conoid of Toxoplasma gondii.', *The Journal of cell biology*. The Rockefeller University Press, 156(6), pp. 1039–50. doi: 10.1083/jcb.200112086.

Huet, D. *et al.* (2018) 'Identification of cryptic subunits from an apicomplexan ATP synthase', *eLife*. eLife Sciences Publications Ltd, 7. doi: 10.7554/eLife.38097.

Huynh, M.-H. *et al.* (2003) 'Rapid invasion of host cells by Toxoplasma requires secretion of the MIC2-M2AP adhesive protein complex.', *The EMBO journal*. European Molecular Biology Organization, 22(9), pp. 2082–90. doi: 10.1093/emboj/cdg217.

Huynh, M.-H. and Carruthers, V. B. (2016) 'A Toxoplasma gondii Ortholog of Plasmodium GAMA Contributes to Parasite Attachment and Cell Invasion crossmark Downloaded from'. doi: 10.1128/mSphere.00012-16.

Huynh, M. H. and Carruthers, V. B. (2009) 'Tagging of endogenous genes in a Toxoplasma gondii strain lacking Ku80', *Eukaryotic Cell*, 8(4), pp. 530–539. doi: 10.1128/EC.00358-08.

Jacot, D. *et al.* (2016) 'An Apicomplexan Actin-Binding Protein Serves as a Connector and Lipid Sensor to Coordinate Motility and Invasion', *Cell Host & Microbe*. Cell Press, 20(6), pp. 731–743. doi: 10.1016/J.CHOM.2016.10.020.

Janado, M. *et al.* (1986) 'Effect of salt on the inter- and intramolecular hydrophobic interactions of macromolecules', *Journal of Solution Chemistry*. Kluwer Academic Publishers-Plenum Publishers, 15(10), pp. 839–850. doi: 10.1007/BF00646091.

Jewett, T. J. and Sibley, L. D. (2003) 'Aldolase Forms a Bridge between Cell Surface Adhesins and the Actin Cytoskeleton in Apicomplexan Parasites',

Molecular Cell. Cell Press, 11(4), pp. 885–894. doi: 10.1016/S1097-2765(03)00113-8.

Jomaa, H. *et al.* (1999) 'Inhibitors of the nonmevalonate pathway of isoprenoid biosynthesis as antimalarial drugs', *Science*. American Association for the Advancement of Science, 285(5433), pp. 1573–1576. doi: 10.1126/science.285.5433.1573.

Jones, C. N. *et al.* (2008) 'Lack of secondary structure characterizes the 5′ ends of mammalian mitochondrial mRNAs', *RNA*. Cold Spring Harbor Laboratory Press, 14(5), pp. 862–871. doi: 10.1261/rna.909208.

Jones, T. C. and Hirsch, J. G. (1972) 'THE INTERACTION BETWEEN TOXOPLASMA GONDII AND MAMMALIAN CELLS: II. THE ABSENCE OF LYSOSOMAL FUSION WITH PHAGOCYTIC VACUOLES CONTAINING LIVING PARASITES', *Journal of Experimental Medicine*, 136(5), pp. 1173–1194. doi: 10.1084/jem.136.5.1173.

Kafsack, B. F. C. and Carruthers, V. B. (2010) 'Apicomplexan perforin-like proteins', *Communicative & Integrative Biology*. Taylor & Francis, 3(1), pp. 18–23. doi: 10.4161/cib.3.1.9794.

Kamerkar, S. and Davis, P. H. (2012) 'Toxoplasma on the brain: understanding host-pathogen interactions in chronic CNS infection.', *Journal of parasitology research*. Hindawi Limited, 2012, p. 589295. doi: 10.1155/2012/589295.

Kapushoc, S. T. *et al.* (2000) 'End processing precedes mitochondrial importation and editing of tRNAs in Leishmania tarentolae', *Journal of Biological Chemistry*. American Society for Biochemistry and Molecular Biology, 275(48), pp. 37907–37914. doi: 10.1074/jbc.M007838200.

Karnataki, A. *et al.* (2009) 'Sequential processing of the Toxoplasma apicoplast membrane protein FtsH1 in topologically distinct domains during intracellular trafficking', *Molecular and Biochemical Parasitology*. Elsevier, 166(2), pp. 126–133. doi: 10.1016/j.molbiopara.2009.03.004.

Karnkowska, A. *et al.* (2016) 'A eukaryote without a mitochondrial organelle',

Current Biology. Cell Press, 26(10), pp. 1274-1284. doi: 10.1016/j.cub.2016.03.053.

Katris, N. J. *et al.* (2014) 'The apical complex provides a regulated gateway for secretion of invasion factors in Toxoplasma.', *PLoS pathogens*. Public Library of Science, 10(4), p. e1004074. doi: 10.1371/journal.ppat.1004074.

Ke, H. *et al.* (2018) 'The mitochondrial ribosomal protein L13 is critical for the structural and functional integrity of the mitochondrion in Plasmodium falciparum', *Journal of Biological Chemistry*, 293(21), pp. 8128–8137. doi: 10.1074/jbc.RA118.002552.

Keithly, J. S., Marchewka, M. J. and Zhu, G. (2000) 'Cryptosporidium parvum appears to lack a plastid genome', *Microbiology*, 146(2), pp. 315–321. doi: 10.1099/00221287-146-2-315.

Kerscher, S. J. (2000) 'Diversity and origin of alternative NADH:ubiquinone oxidoreductases', *Biochimica et Biophysica Acta - Bioenergetics*. Elsevier, 1459(2–3), pp. 274–283. doi: 10.1016/S0005-2728(00)00162-6.

Kessler, H. *et al.* (2008) 'Microneme protein 8 - a new essential invasion factor in Toxoplasma gondii', *Journal of Cell Science*, 121(7), pp. 947–956. doi: 10.1242/jcs.022350.

Kibbe, W. A. (2007) 'OligoCalc: an online oligonucleotide properties calculator', *Nucleic Acids Research*, 35, pp. 43–46. doi: 10.1093/nar/gkm234.

Kim, K. and Boothroyd, J. C. (1995) 'Toxoplasma gondii: Stable Complementation of sag1 (p30) Mutants Using SAG1 Transfection and Fluorescence-Activated Cell Sorting', *Experimental Parasitology*. Academic Press, 80(1), pp. 46-53. doi: 10.1006/expr.1995.1006.

Kim, K., Soldati, D. and Boothroyd, J. C. (1993) 'Gene replacement in Toxoplasma gondii with chloramphenicol acetyltransferase as selectable marker', *Science*. Science, 262(5135), pp. 911–914. doi: 10.1126/science.8235614.

KLINGENBERG, M. and ROTTENBERG, H. (1977) 'Relation between the Gradient of the ATP/ADP Ratio and the Membrane Potential across the Mitochondrial Membrane', *European Journal of Biochemistry*. John Wiley & Sons, Ltd, 73(1), pp. 125–130. doi: 10.1111/j.1432-1033.1977.tb11298.x.

Kobayashi, T. *et al.* (2007) 'Mitochondria and apicoplast of Plasmodium falciparum: Behaviour on subcellular fractionation and the implication', *Mitochondrion*. Mitochondrion, 7(1–2), pp. 125–132. doi: 10.1016/j.mito.2006.11.021.

Kolesnikova, O. *et al.* (2010) 'Selection of RNA aptamers imported into yeast and human mitochondria', *RNA*. Cold Spring Harbor Laboratory Press, 16(5), pp. 926–941. doi: 10.1261/rna.1914110.

Kozjak-Pavlovic, V. *et al.* (2007) 'Conserved roles of Sam50 and metaxins in VDAC biogenesis', *EMBO reports*. John Wiley & Sons, Ltd, 8(6), pp. 576–582. doi: 10.1038/sj.embor.7400982.

Kozjak, V. *et al.* (2003) 'An essential role of Sam50 in the protein sorting and assembly machinery of the mitochondrial outer membrane', *Journal of Biological Chemistry*. American Society for Biochemistry and Molecular Biology, 278(49), pp. 48520–48523. doi: 10.1074/jbc.C300442200.

Kudryashev, M. *et al.* (2010) 'Positioning of large organelles by a membrane-associated cytoskeleton in *Plasmodium* sporozoites', *Cellular Microbiology*, 12(3), pp. 362–371. doi: 10.1111/j.1462-5822.2009.01399.x.

Kunji, E. R. S. (2004) 'The role and structure of mitochondrial carriers', in *FEBS Letters*. FEBS Lett, pp. 239–244. doi: 10.1016/S0014-5793(04)00242-X.

Kunzmann, A., Brennicke, A. and Marchfelder, A. (1998) '5′ end maturation and RNA editing have to precede tRNA 3′ processing in plant mitochondria', *Proceedings of the National Academy of Sciences of the United States of America*. National Academy of Sciences, 95(1), pp. 108–113. doi: 10.1073/pnas.95.1.108.

Kutik, S. *et al.* (2008) 'Dissecting Membrane Insertion of Mitochondrial β-Barrel Proteins', *Cell*. Cell Press, 132(6), pp. 1011–1024. doi: 10.1016/j.cell.2008.01.028.

Kuzmenko, A. *et al.* (2014) 'Mitochondrial translation initiation machinery: Conservation and diversification', *Biochimie*. Elsevier, pp. 132–140. doi: 10.1016/j.biochi.2013.07.024.

Kwasniak-Owczarek, M. and Janska, H. (2014) 'In organello Protein Synthesis', *BIO-PROTOCOL*. Bio-Protocol, LLC, 4(12). doi: 10.21769/bioprotoc.1157.

Lacombe, A. *et al.* (2019) 'Identification of the Toxoplasma gondii mitochondrial ribosome, and characterisation of a protein essential for mitochondrial translation', *Molecular Microbiology*. Blackwell Publishing Ltd, 112(4), pp. 1235–1252. doi: 10.1111/mmi.14357.

Lamarque, M. *et al.* (2011) 'The RON2-AMA1 Interaction is a Critical Step in Moving Junction-Dependent Invasion by Apicomplexan Parasites', *PLoS Pathogens*. Edited by D. Soldati-Favre, 7(2), p. e1001276. doi: 10.1371/journal.ppat.1001276.

Lamarque, M. H. *et al.* (2014) 'Plasticity and redundancy among AMA–RON pairs ensure host cell entry of Toxoplasma parasites', *Nature Communications*, 5(1), p. 4098. doi: 10.1038/ncomms5098.

Lang, B. F., Gray, M. W. and Burger, G. (1999) 'Mitochondrial Genome Evolution and the Origin of Eukaryotes', *Annual Review of Genetics*. Annual Reviews, 33(1), pp. 351–397. doi: 10.1146/annurev.genet.33.1.351.

LeBlanc, A. J., Yermovsky-Kammerer, A. E. and Hajduk, S. L. (1999) 'A nuclear encoded and mitochondrial imported dicistronic tRNA precursor in Trypanosoma brucei', *Journal of Biological Chemistry*. American Society for Biochemistry and Molecular Biology, 274(30), pp. 21071–21077. doi: 10.1074/jbc.274.30.21071.

Lee, P. Y. *et al.* (2012) 'Agarose gel electrophoresis for the separation of DNA fragments', *Journal of Visualized Experiments*. Journal of Visualized

Experiments, (62). doi: 10.3791/3923.

Lekutis, C. *et al*. (2001) 'Surface antigens of Toxoplasma gondii: Variations on a theme', *International Journal for Parasitology*. Pergamon, pp. 1285–1292. doi: 10.1016/S0020-7519(01)00261-2.

Leung, J. M. *et al*. (2014) 'Disruption of TgPHIL1 alters specific parameters of Toxoplasma gondii motility measured in a quantitative, three-dimensional live motility assay.', *PloS one*. Public Library of Science, 9(1), p. e85763. doi: 10.1371/journal.pone.0085763.

Levine, N. D. (1988) 'Progress in taxonomy of the Apicomplexan protozoa.', *The Journal of protozoology*, 35(4), pp. 518–20. doi: 10.1111/j.1550-7408.1988.tb04141.x.

Lewis, W. H. *et al*. (2020) 'Convergent Evolution of Hydrogenosomes from Mitochondria by Gene Transfer and Loss', *Molecular biology and evolution*. NLM (Medline), 37(2), pp. 524–539. doi: 10.1093/molbev/msz239.

Liao, P.-C. *et al*. (2018) 'Isolation of mitochondria from Saccharomyces cerevisiae using magnetic bead affinity purification', *PLOS ONE*. Edited by J. Santos. Public Library of Science, 13(4), p. e0196632. doi: 10.1371/journal.pone.0196632.

Lill, R. (2009) 'Function and biogenesis of iron-sulphur proteins', *Nature*. Nature Publishing Group, pp. 831–838. doi: 10.1038/nature08301.

Lill, R. *et al*. (2015) 'The role of mitochondria and the CIA machinery in the maturation of cytosolic and nuclear iron-sulfur proteins', *European Journal of Cell Biology*. Elsevier GmbH, pp. 280–291. doi: 10.1016/j.ejcb.2015.05.002.

Lill, R. and Mühlenhoff, U. (2008) 'Maturation of Iron-Sulfur Proteins in Eukaryotes: Mechanisms, Connected Processes, and Diseases', *Annual Review of Biochemistry*. Annual Reviews, 77(1), pp. 669–700. doi: 10.1146/annurev.biochem.76.052705.162653.

Lim, L. and McFadden, G. I. (2010) 'The evolution, metabolism and functions of the apicoplast.', *Philosophical transactions of the Royal Society of London. Series B, Biological sciences*. The Royal Society, 365(1541), pp. 749–63. doi: 10.1098/rstb.2009.0273.

Lin, S. S., Gross, U. and Bohne, W. (2011) 'Two internal type II NADH dehydrogenases of Toxoplasma gondii are both required for optimal tachyzoite growth', *Molecular Microbiology*. John Wiley & Sons, Ltd (10.1111), 82(1), pp. 209–221. doi: 10.1111/j.1365-2958.2011.07807.x.

Lin, T.-Y., Nagano, S. and Gardiner Heddle, J. (2015) 'Functional Analyses of the Toxoplasma gondii DNA Gyrase Holoenzyme: A Janus Topoisomerase with Supercoiling and Decatenation Abilities.', *Scientific reports*. Nature Publishing Group, 5, p. 14491. doi: 10.1038/srep14491.

Ling, Y. *et al.* (2007) 'The farnesyl-diphosphate/geranylgeranyl-diphosphate synthase of Toxoplasma gondii is a bifunctional enzyme and a molecular target of bisphosphonates', *Journal of Biological Chemistry*. J Biol Chem, 282(42), pp. 30804–30816. doi: 10.1074/jbc.M703178200.

Lithgow, T. and Schneider, A. (2010) 'Evolution of macromolecular import pathways in mitochondria, hydrogenosomes and mitosomes', *Philosophical Transactions of the Royal Society B: Biological Sciences*, 365(1541), pp. 799–817. doi: 10.1098/rstb.2009.0167.

Lorenz, C., Lünse, C. E. and Mörl, M. (2017) 'Trna modifications: Impact on structure and thermal adaptation', *Biomolecules*. MDPI AG. doi: 10.3390/biom7020035.

Lourido, S., Tang, K. and Sibley, L. D. (2012) 'Distinct signalling pathways control Toxoplasma egress and host-cell invasion.', *The EMBO journal*. European Molecular Biology Organization, 31(24), pp. 4524–34. doi: 10.1038/emboj.2012.299.

Lund, E. and Dahlberg, J. E. (1998) 'Proofreading and aminoacylation of tRNAs before export from the nucleus', *Science*. American Association for the

Advancement of Science, 282(5396), pp. 2082–2085. doi: 10.1126/science.282.5396.2082.

Maenz, M. *et al.* (2014) 'Ocular toxoplasmosis past, present and new aspects of an old disease', *Progress in Retinal and Eye Research*. Pergamon, 39, pp. 77–106. doi: 10.1016/J.PRETEYERES.2013.12.005.

Mallo, N. *et al.* (2018) 'Protein import into the endosymbiotic organelles of apicomplexan parasites', *Genes*. MDPI AG, p. 412. doi: 10.3390/genes9080412.

Mare, L., Salinas, T. and Duche, A. (2008) 'Recent advances in tRNA mitochondrial import', (May). doi: 10.1016/j.tibs.2008.04.010.

Marini, F. *et al.* (2020) 'Exploring the HeLa Dark Mitochondrial Proteome', *Frontiers in Cell and Developmental Biology*, 8(March), pp. 1–8. doi: 10.3389/fcell.2020.00137.

Markus, B. M. *et al.* (2019) ' Optimizing Systems for Cas9 Expression in Toxoplasma gondii ', *mSphere*. American Society for Microbiology, 4(3). doi: 10.1128/msphere.00386-19.

Martínez-Reyes, I. and Chandel, N. S. (2020) 'Mitochondrial TCA cycle metabolites control physiology and disease', *Nature Communications*. Nature Research, pp. 1–11. doi: 10.1038/s41467-019-13668-3.

Mather, M. W., Morrisey, J. M. and Vaidya, A. B. (2010) 'Hemozoin-free Plasmodium falciparum mitochondria for physiological and drug susceptibility studies', *Molecular and Biochemical Parasitology*. NIH Public Access, 174(2), pp. 150–153. doi: 10.1016/j.molbiopara.2010.07.006.

Mazumdar, J. *et al.* (2006) *Apicoplast fatty acid synthesis is essential for organelle biogenesis and parasite survival in Toxoplasma gondii*. Available at: www.pnas.orgcgidoi10.1073pnas.0603391103 (Accessed: 15 June 2020).

McCoy, J. M. *et al.* (2012) 'TgCDPK3 regulates calcium-dependent egress of Toxoplasma gondii from host cells.', *PLoS pathogens*. Public Library of Science,

8(12), p. e1003066. doi: 10.1371/journal.ppat.1003066.

McFadden, D. C. *et al.* (2000) 'Characterization of cytochrome b from Toxoplasma gondii and Q(o) domain mutations as a mechanism of atovaquone-resistance', *Molecular and Biochemical Parasitology*. Mol Biochem Parasitol, 108(1), pp. 1–12. doi: 10.1016/S0166-6851(00)00184-5.

McFadden, G. I. *et al.* (1996) 'Plastid in human parasites', *Nature*. Nature Publishing Group, 381(6582), pp. 482–482. doi: 10.1038/381482a0.

Meisinger, C. *et al.* (2004) 'The mitochondrial morphology protein Mdm10 functions in assembly of the preprotein translocase of the outer membrane', *Developmental Cell*. Elsevier, 7(1), pp. 61–71. doi: 10.1016/j.devcel.2004.06.003.

Meissner, M. *et al.* (2001) 'Modulation of myosin A expression by a newly established tetracycline repressor-based inducible system in Toxoplasma gondii.', *Nucleic acids research*. Oxford University Press, 29(22), p. E115. doi: 10.1093/nar/29.22.e115.

Meissner, M. *et al.* (2005) 'Tetracycline analogue-regulated transgene expression in Plasmodium falciparum blood stages using Toxoplasma gondii transactivators', *Proceedings of the National Academy of Sciences of the United States of America*. National Academy of Sciences, 102(8), pp. 2980–2985. doi: 10.1073/pnas.0500112102.

Melatti, C. *et al.* (2019) 'A unique dynamin-related protein is essential for mitochondrial fission in Toxoplasma gondii', *PLOS Pathogens*. Edited by K. Kim. Public Library of Science, 15(4), p. e1007512. doi: 10.1371/journal.ppat.1007512.

Mercier, C. *et al.* (2002) 'Biogenesis of nanotubular network in Toxoplasma parasitophorous vacuole induced by parasite proteins.', *Molecular biology of the cell*. American Society for Cell Biology, 13(7), pp. 2397–409. doi: 10.1091/mbc.e02-01-0021.

Mercier, C. *et al.* (2005) 'Dense granules: Are they key organelles to help understand the parasitophorous vacuole of all apicomplexa parasites?', *International Journal for Parasitology*, pp. 829–849. doi: 10.1016/j.ijpara.2005.03.011.

Meyer, B. *et al.* (2007) 'Identification of two proteins associated with mammalian ATP synthase.', *Molecular & cellular proteomics : MCP.* American Society for Biochemistry and Molecular Biology, 6(10), pp. 1690–9. doi: 10.1074/mcp.M700097-MCP200.

Mital, J. *et al.* (2005) 'Conditional Expression of *Toxoplasma gondii* Apical Membrane Antigen-1 (TgAMA1) Demonstrates That TgAMA1 Plays a Critical Role in Host Cell Invasion', *Molecular Biology of the Cell*. American Society for Cell Biology, 16(9), pp. 4341–4349. doi: 10.1091/mbc.e05-04-0281.

Mogi, T. and Kita, K. (2010) 'Diversity in mitochondrial metabolic pathways in parasitic protists Plasmodium and Cryptosporidium', *Parasitology International*. Elsevier, pp. 305–312. doi: 10.1016/j.parint.2010.04.005.

Mokranjac, D. and Neupert, W. (2009) 'Thirty years of protein translocation into mitochondria: Unexpectedly complex and still puzzling', *Biochimica et Biophysica Acta - Molecular Cell Research*. Biochim Biophys Acta, pp. 33–41. doi: 10.1016/j.bbamcr.2008.06.021.

Montoya, J. and Liesenfeld, O. (2004) 'Toxoplasmosis', *The Lancet*, 363(9425), pp. 1965–1976. doi: 10.1016/S0140-6736(04)16412-X.

Morrissette, N., Murray, J. M. and Roos, D. S. (1997) 'Subpellicular microtubules associate with an intramembranous particle lattice in the protozoan parasite Toxoplasma gondii', *Journal of Cell Science*, 110. Available at: https://www.researchgate.net/publication/14197453_Subpellicular_microtubules_associate_with_an_intramembranous_particle_lattice_in_the_protozoan_parasite_Toxoplasma_gondii (Accessed: 30 September 2019).

Morrissette, N. S. and Sibley, L. D. (2002) 'Cytoskeleton of Apicomplexan Parasites', *Microbiology and Molecular Biology Reviews*. American Society for

Microbiology (ASM), 66(1), p. 21. doi: 10.1128/MMBR.66.1.21-38.2002.

Mukherjee, S. *et al.* (2007) 'Necessary and sufficient factors for the import of transfer RNA into the kinetoplast mitochondrion.', *EMBO reports*. European Molecular Biology Organization, 8(6), pp. 589–95. doi: 10.1038/sj.embor.7400979.

Müller, J. M. *et al.* (2008) 'Precursor oxidation by Mia40 and Erv1 promotes vectorial transport of proteins into the mitochondrial intermembrane space', *Molecular Biology of the Cell*. The American Society for Cell Biology, 19(1), pp. 226–236. doi: 10.1091/mbc.E07-08-0814.

Muller, M. (1993) 'Review Article: The hydrogenosome', *Journal of General Microbiology*. Microbiology Society, 139(12), pp. 2879–2889. doi: 10.1099/00221287-139-12-2879.

Mulvey, C. M. *et al.* (2017) 'Using hyperLOPIT to perform high-resolution mapping of the spatial proteome', *Nature Protocols*. Nature Publishing Group, 12(6), pp. 1110–1135. doi: 10.1038/nprot.2017.026.

N., D. *et al.* (2017) 'The structure of the yeast mitochondrial ribosome', *Science*, 355(6324), pp. 528–531. doi: 10.1126/science.aal2415.

Nagao, A., Suzuki, Takeo and Suzuki, Tsutomu (2007) 'Aminoacyl-tRNA surveillance by EF-Tu in mammalian mitochondria.', *Nucleic Acids Symposium Series*. Oxford Academic, 51(1), pp. 41–42. doi: 10.1093/nass/nrm021.

Namasivayama, S. *et al.* (2020) 'A novel fragmented mitochondrial genome in the protist pathogen Toxoplasma 1 gondii and related tissue coccidia 2 3', *bioRxiv*. Cold Spring Harbor Laboratory, p. 2020.05.16.099366. doi: 10.1101/2020.05.16.099366.

Nassoury, N., Wang, Y. and Morse, D. (2005) 'Brefeldin A Inhibits Circadian Remodeling of Chloroplast Structure in the Dinoflagellate Gonyaulax', *Traffic*. John Wiley & Sons, Ltd, 6(7), pp. 548–561. doi: 10.1111/j.1600-0854.2005.00296.x.

Nathanson, L. and Deutscher, M. P. (2000) 'Active aminoacyl-tRNA synthetases are present in nuclei as a high molecular weight multienzyme complex', *Journal of Biological Chemistry*. American Society for Biochemistry and Molecular Biology Inc., 275(41), pp. 31559–31562. doi: 10.1074/jbc.C000385200.

Niehaus, M. *et al.* (2020) 'Rapid Affinity Purification of Tagged Plant Mitochondria (Mito-AP) for Metabolome and Proteome Analyses', *Plant physiology*, 182(3), pp. 1194–1210. doi: 10.1104/pp.19.00736.

Nightingale, D. J. H., Oliver, S. G. and Lilley, K. S. (2019) 'Mapping the Saccharomyces cerevisiae Spatial Proteome with High Resolution Using hyperLOPIT', in *Methods in Molecular Biology*. Humana Press Inc., pp. 165–190. doi: 10.1007/978-1-4939-9736-7_10.

Nishi, M. *et al.* (2008) 'Organellar dynamics during the cell cycle of Toxoplasma gondii', *Journal of Cell Science*. J Cell Sci, 121(9), pp. 1559–1568. doi: 10.1242/jcs.021089.

Nolan, S. J., Romano, J. D. and Coppens, I. (2017) 'Host lipid droplets: An important source of lipids salvaged by the intracellular parasite Toxoplasma gondii', *PLoS Pathogens*. Public Library of Science, 13(6). doi: 10.1371/journal.ppat.1006362.

Nozaki, Y. *et al.* (2008) 'HMRF1L is a human mitochondrial translation release factor involved in the decoding of the termination codons UAA and UAG', *Genes to Cells*. Genes Cells, 13(5), pp. 429–438. doi: 10.1111/j.1365-2443.2008.01181.x.

O'Brien, T. W. (1970) 'The General in Mammalian Occurrence of 55 S Ribosomes Liver Mitochondria', *Journal of Biological Chemistry*, 246(10), pp. 3409–3417.

Ogedengbe, M. E. *et al.* (2015) 'A linear mitochondrial genome of Cyclospora cayetanensis (Eimeriidae, Eucoccidiorida, Coccidiasina, Apicomplexa) suggests the ancestral start position within mitochondrial genomes of eimeriid coccidia', *International Journal for Parasitology*. Elsevier Ltd, 45(6), pp. 361–365. doi: 10.1016/j.ijpara.2015.02.006.

Ojala, D., Montoya, J. and Attardi, G. (1981) 'TRNA punctuation model of RNA processing in human mitochondria', *Nature*. Nature Publishing Group, 290(5806), pp. 470–474. doi: 10.1038/290470a0.

Ossorio, P. N., Sibley, L. D. and Boothroyd, J. C. (1991) 'Mitochondrial-like DNA sequences flanked by direct and inverted repeats in the nuclear genome of Toxoplasma gondii', *Journal of Molecular Biology*. Academic Press, 222(3), pp. 525–536. doi: 10.1016/0022-2836(91)90494-Q.

Ovciarikova, J. *et al.* (2017) 'Mitochondrial behaviour throughout the lytic cycle of Toxoplasma gondii', *Scientific Reports*. Nature Publishing Group, 7(February), pp. 1–13. doi: 10.1038/srep42746.

Painter, H. J. *et al.* (2007) 'Specific role of mitochondrial electron transport in blood-stage Plasmodium falciparum', *Nature*. Nature Publishing Group, 446(7131), pp. 88–91. doi: 10.1038/nature05572.

Panigrahi, A. K. *et al.* (2009) 'A comprehensive analysis of trypanosoma brucei mitochondrial proteome', *Proteomics*. Proteomics, 9(2), pp. 434–450. doi: 10.1002/pmic.200800477.

Pappas, G., Roussos, N. and Falagas, M. E. (2009) 'Toxoplasmosis snapshots: Global status of Toxoplasma gondii seroprevalence and implications for pregnancy and congenital toxoplasmosis', *International Journal for Parasitology*, 39(12), pp. 1385–1394. doi: 10.1016/j.ijpara.2009.04.003.

Pelletier, L. *et al.* (2002) 'Golgi biogenesis in Toxoplasma gondii', *Nature*, 418(6897), pp. 548–552. doi: 10.1038/nature00946.

Periz, J. *et al.* (2017) 'Toxoplasma gondii F-actin forms an extensive filamentous network required for material exchange and parasite maturation', *eLife*, 6. doi: 10.7554/eLife.24119.

Pernas, L. *et al.* (2014) 'Toxoplasma Effector MAF1 Mediates Recruitment of Host Mitochondria and Impacts the Host Response', *PLoS Biology*. Edited by B. Striepen. Public Library of Science, 12(4), p. e1001845. doi:

10.1371/journal.pbio.1001845.

Pino, P. *et al*. (2007) 'Dual Targeting of Antioxidant and Metabolic Enzymes to the Mitochondrion and the Apicoplast of Toxoplasma gondii', *PLoS Pathogens*. Edited by D. E. Goldberg. Public Library of Science, 3(8), p. e115. doi: 10.1371/journal.ppat.0030115.

Pino, P. *et al*. (2010) 'Mitochondrial translation in absence of local tRNA aminoacylation and methionyl tRNAMet formylation in Apicomplexa', *Molecular Microbiology*, 76(3), pp. 706–718. doi: 10.1111/j.1365-2958.2010.07128.x.

Pon, L. *et al*. (1989) 'Protein import into mitochondria: ATP-dependent protein translocation activity in a submitochondrial fraction enriched in membrane contact sites and specific proteins', *Journal of Cell Biology*. The Rockefeller University Press, 109(6 I), pp. 2603–2616. doi: 10.1083/jcb.109.6.2603.

Poria, D. and Ray, P. (2017) 'RNA-protein UV-crosslinking Assay', *BIO-PROTOCOL*. Bio-Protocol, LLC, 7(6). doi: 10.21769/bioprotoc.2193.

Prinz, W. A., Toulmay, A. and Balla, T. (2020) 'The functional universe of membrane contact sites', *Nature Reviews Molecular Cell Biology*. Nature Research, pp. 7–24. doi: 10.1038/s41580-019-0180-9.

Ralph, S. A. *et al*. (2004) 'Metabolic maps and functions of the Plasmodium falciparum apicoplast', *Nature Reviews Microbiology*. Nature Publishing Group, pp. 203–216. doi: 10.1038/nrmicro843.

Ramrath, D. J. F. *et al*. (2018) 'Evolutionary shift toward protein-based architecture in trypanosomal mitochondrial ribosomes', *Science*. American Association for the Advancement of Science, 362(6413), p. eaau7735. doi: 10.1126/SCIENCE.AAU7735.

Ramya, T. N. C. *et al*. (2007) 'Inhibitors of nonhousekeeping functions of the apicoplast defy delayed death in Plasmodium falciparum', *Antimicrobial Agents and Chemotherapy*. American Society for Microbiology Journals, 51(1), pp. 307–316. doi: 10.1128/AAC.00808-06.

Rehling, P. *et al.* (2003) 'Protein insertion into the mitochondrial inner membrane by a twin-pore translocase', *Science*. American Association for the Advancement of Science, 299(5613), pp. 1747–1751. doi: 10.1126/science.1080945.

Remington, J. S. (1974) 'Toxoplasmosis in the adult.', *Bulletin of the New York Academy of Medicine*. New York Academy of Medicine, 50(2), pp. 211–27. Available at: http://www.ncbi.nlm.nih.gov/pubmed/4592097 (Accessed: 24 August 2016).

Richman, T. R. *et al.* (2016) 'Loss of the RNA-binding protein TACO1 causes late-onset mitochondrial dysfunction in mice', *Nature Communications*. Nature Publishing Group, 7(1), p. 11884. doi: 10.1038/ncomms11884.

Richter, U. *et al.* (2015) 'Quality control of mitochondrial protein synthesis is required for membrane integrity and cell fitness', *Journal of Cell Biology*. Rockefeller University Press, 211(2), pp. 373–389. doi: 10.1083/jcb.201504062.

Rinehart, J. *et al.* (2005) 'Saccharomyces cerevisiae imports the cytosolic pathway for Gln-tRNA synthesis into the mitochondrion.', *Genes & development*. Cold Spring Harbor Laboratory Press, 19(5), pp. 583–92. doi: 10.1101/gad.1269305.

Riordan, C. E. *et al.* (2003) 'Cryptosporidium parvum Cpn60 targets a relict organelle', *Current Genetics*. Springer, 44(3), pp. 138–147. doi: 10.1007/s00294-003-0432-1.

Robert-Gangneux, F. and Dardé, M.-L. (2012) 'Epidemiology of and diagnostic strategies for toxoplasmosis.', *Clinical microbiology reviews*. American Society for Microbiology (ASM), 25(2), pp. 264–96. doi: 10.1128/CMR.05013-11.

Robles, P. and Quesada, V. (2017) 'Emerging roles of mitochondrial ribosomal proteins in plant development', *International Journal of Molecular Sciences*. MDPI AG. doi: 10.3390/ijms18122595.

Rorbach, J. *et al.* (2008) 'The human mitochondrial ribosome recycling factor is

essential for cell viability', *Nucleic Acids Research*, 36(18), pp. 5787–5799. doi: 10.1093/nar/gkn576.

Rossmanith, W. *et al.* (1995) 'Human mitochondrial tRNA processing', *Journal of Biological Chemistry*. American Society for Biochemistry and Molecular Biology, 270(21), pp. 12885–12891. doi: 10.1074/jbc.270.21.12885.

Rossmanith, W. (2012) 'Of P and Z: Mitochondrial tRNA processing enzymes', *Biochimica et Biophysica Acta - Gene Regulatory Mechanisms*. Elsevier, pp. 1017–1026. doi: 10.1016/j.bbagrm.2011.11.003.

Rötig, A. (2011) 'Human diseases with impaired mitochondrial protein synthesis', *Biochimica et Biophysica Acta - Bioenergetics*. Elsevier, pp. 1198–1205. doi: 10.1016/j.bbabio.2011.06.010.

Roux, K. J. *et al.* (no date) 'BioID: A Screen for Protein-Protein Interactions'. doi: 10.1002/cpps.51.

Rubio, M. A. T. *et al.* (2000) 'Selective importation of RNA into isolated mitochondria from Leishmania tarentolae', *RNA*. Cold Spring Harbor Laboratory Press, 6(7), pp. 988–1003. doi: 10.1017/S1355838200991519.

Rubio, M. A. T. and Hopper, A. K. (2011) 'Transfer RNA travels from the cytoplasm to organelles', *Wiley Interdisciplinary Reviews: RNA*, 2(6), pp. 802–817. doi: 10.1002/wrna.93.

Ruggiano, A., Foresti, O. and Carvalho, P. (2014) 'ER-associated degradation: Protein quality control and beyond', *Journal of Cell Biology*. Rockefeller University Press, pp. 869–879. doi: 10.1083/jcb.201312042.

Rusconi, C. P. and Cech, T. R. (1996) 'The anticodon is the signal sequence for mitochondrial import of glutamine tRNA in Tetrahymena', *Genes and Development*. Cold Spring Harbor Laboratory Press, 10(22), pp. 2870–2880. doi: 10.1101/gad.10.22.2870.

Sabar, M., Balk, J. and Leaver, C. J. (2005) 'Histochemical staining and

quantification of plant mitochondrial respiratory chain complexes using blue-native polyacrylamide gel electrophoresis', *The Plant Journal*. John Wiley & Sons, Ltd, 44(5), pp. 893–901. doi: 10.1111/j.1365-313X.2005.02577.x.

Saleh, A. *et al.* (2007) 'Growth inhibition of Toxoplasma gondii and Plasmodium falciparum by nanomolar concentrations of 1-hydroxy-2-dodecyl-4(1H)quinolone, a high-affinity inhibitor of alternative (type II) NADH dehydrogenases', *Antimicrobial Agents and Chemotherapy*. American Society for Microbiology Journals, 51(4), pp. 1217–1222. doi: 10.1128/AAC.00895-06.

Salinas-Giegé, T., Giegé, R. and Giegé, P. (2015) 'TRNA biology in mitochondria', *International Journal of Molecular Sciences*, 16(3), pp. 4518–4559. doi: 10.3390/ijms16034518.

Salinas, T. *et al.* (2005) 'Sequence dependence of tRNAGly import into tobacco mitochondria', in *Biochimie*. Biochimie, pp. 863–872. doi: 10.1016/j.biochi.2005.04.004.

Salinas, T. *et al.* (2006) 'The voltage-dependent anion channel, a major component of the tRNA import machinery in plant mitochondria', *Proceedings of the National Academy of Sciences of the United States of America*. National Academy of Sciences, 103(48), pp. 18362–18367. doi: 10.1073/pnas.0606449103.

Salunke, R. *et al.* (2018) 'Highly diverged novel subunit composition of apicomplexan F-type ATP synthase identified from Toxoplasma gondii', *PLOS Biology*. Edited by B. Striepen. Public Library of Science, 16(7), p. e2006128. doi: 10.1371/journal.pbio.2006128.

Salvato, F. *et al.* (2014) 'The potato tuber mitochondrial proteome', *Plant Physiology*. Plant Physiol, 164(2), pp. 637–653. doi: 10.1104/pp.113.229054.

Sbicego, S. *et al.* (1998) *In vivo import of unspliced tRNA Tyr containing synthetic introns of variable length into mitochondria of Leishmania tarentolae*, *Nucleic Acids Research*.

Schindelin, J. *et al.* (2012) 'Fiji: An open-source platform for biological-image

analysis', *Nature Methods*. Nature Publishing Group, pp. 676–682. doi: 10.1038/nmeth.2019.

Schindelin, J. *et al.* (2015) 'The ImageJ ecosystem: An open platform for biomedical image analysis', *Molecular Reproduction and Development*. John Wiley and Sons Inc., pp. 518–529. doi: 10.1002/mrd.22489.

Schneider, A. (2011) 'Mitochondrial tRNA Import and Its Consequences for Mitochondrial Translation', *Annual Review of Biochemistry*, 80(1), pp. 1033–1053. doi: 10.1146/annurev-biochem-060109-092838.

Seeber, F., Feagin, J. E. and Parsons, M. (2013) 'The Apicoplast and Mitochondrion of Toxoplasma gondii', in *Toxoplasma Gondii: The Model Apicomplexan - Perspectives and Methods: Second Edition*. Elsevier Ltd., pp. 297–350. doi: 10.1016/B978-0-12-396481-6.00009-X.

Seeber, F. and Soldati-Favre, D. (2010) 'Metabolic pathways in the apicoplast of apicomplexa', *International Review of Cell and Molecular Biology*. Elsevier Inc., 281(C), pp. 161–228. doi: 10.1016/S1937-6448(10)81005-6.

Seidi, A., Muellner-Wong, Linden S., *et al.* (2018) 'Elucidating the mitochondrial proteome of toxoplasma gondii reveals the presence of a divergent cytochrome c oxidase', *eLife*. eLife Sciences Publications Ltd, 7. doi: 10.7554/eLife.38131.

Seidi, A., Muellner-Wong, Linden S, *et al.* (2018) 'Elucidating the mitochondrial proteome of Toxoplasma gondii reveals the presence of a divergent cytochrome c oxidase', *eLife*, 7. doi: 10.7554/eLife.38131.

Seidman, D. *et al.* (2012) 'Mitochondrial membrane complex that contains proteins necessary for tRNA import in Trypanosoma brucei', *Journal of Biological Chemistry*. American Society for Biochemistry and Molecular Biology, 287(12), pp. 8892–8903. doi: 10.1074/jbc.M111.300186.

Seligman, A. M. *et al.* (1968) 'Nondroplet ultrastructural demonstration of cytochrome oxidase activity with a polymerizing osmiophilic reagent, diaminobenzidine (DAB).', *The Journal of cell biology*. The Rockefeller

University Press, 38(1), pp. 1–14. doi: 10.1083/jcb.38.1.1.

Serpeloni, M. *et al.* (2016) 'UAP56 is a conserved crucial component of a divergent mRNA export pathway in *Toxoplasma gondii*', *Molecular Microbiology*. Blackwell Publishing Ltd, 102(4), pp. 672–689. doi: 10.1111/mmi.13485.

Sharma, Arvind and Sharma, Amit (2014) ' Plasmodium falciparum mitochondria import tRNAs along with an active phenylalanyl-tRNA synthetase ', *Biochemical Journal*, 465(3), pp. 459–469. doi: 10.1042/bj20140998.

Sharma, M. R. *et al.* (2003) 'Structure of the mammalian mitochondrial ribosome reveals an expanded functional role for its component proteins', *Cell*. Cell Press, 115(1), pp. 97–108. doi: 10.1016/S0092-8674(03)00762-1.

Sharma, P. and Chitnis, C. E. (2013) 'Key molecular events during host cell invasion by Apicomplexan pathogens', *Current Opinion in Microbiology*. Elsevier Current Trends, 16(4), pp. 432–437. doi: 10.1016/J.MIB.2013.07.004.

Shaw, K. *et al.* (no date) 'Microtubules, but not actin filaments, drive daughter cell budding and cell division in Toxoplasma gondii'. Available at: https://www.researchgate.net/publication/12612089_Microtubules_but_not_actin_filaments_drive_daughter_cell_budding_and_cell_division_in_Toxoplasma_gondii (Accessed: 30 September 2019).

Shaw, M. K. and Tilney, L. G. (1999) 'Induction of an acrosomal process in Toxoplasma gondii: visualization of actin filaments in a protozoan parasite.', *Proceedings of the National Academy of Sciences of the United States of America*. National Academy of Sciences, 96(16), pp. 9095–9. doi: 10.1073/pnas.96.16.9095.

Sheiner, L. *et al.* (2011) 'A systematic screen to discover and analyze apicoplast proteins identifies a conserved and essential protein import factor', *PLoS Pathogens*, 7(12). doi: 10.1371/journal.ppat.1002392.

Sheiner, L. *et al.* (2015) '*Toxoplasma gondii* Toc75 Functions in Import of Stromal but not Peripheral Apicoplast Proteins', *Traffic*. Blackwell Munksgaard,

16(12), pp. 1254–1269. doi: 10.1111/tra.12333.

Shen, B. and Sibley, L. D. (2014) 'Toxoplasma aldolase is required for metabolism but dispensable for host-cell invasion.', *Proceedings of the National Academy of Sciences of the United States of America*. National Academy of Sciences, 111(9), pp. 3567–72. doi: 10.1073/pnas.1315156111.

Sibley, L. D. *et al.* (1995) 'Regulated secretion of multi-lamellar vesicles leads to formation of a tubulo-vesicular network in host-cell vacuoles occupied by Toxoplasma gondii', *Journal of Cell Science*, 108(4). Available at: https://jcs.biologists.org/content/108/4/1669 (Accessed: 30 September 2019).

Sibley, L. D. *et al.* (2009) 'Genetic diversity of Toxoplasma gondii in animals and humans.', *Philosophical transactions of the Royal Society of London. Series B, Biological sciences*, 364(1530), pp. 2749–2761. doi: 10.1098/rstb.2009.0087.

Sidik, S. M. *et al.* (2014) 'Efficient Genome Engineering of Toxoplasma gondii Using CRISPR/Cas9', *PLoS ONE*. Edited by I. J. Blader. Public Library of Science, 9(6), p. e100450. doi: 10.1371/journal.pone.0100450.

Sidik, S. M. *et al.* (2016) 'A Genome-Wide CRISPR Screen in Toxoplasma Identifies Essential Apicomplexan Genes HHS Public Access', *Cell*, 166(6), pp. 1423–1435. doi: 10.1016/j.cell.2016.08.019.

De Silva, D. *et al.* (2015) 'Mitochondrial ribosome assembly in health and disease', *Cell Cycle*. Taylor and Francis Inc., pp. 2226–2250. doi: 10.1080/15384101.2015.1053672.

Siregar, J. E. *et al.* (2008) 'Mutation underlying resistance of Plasmodium berghei to atovaquone in the quinone binding domain 2 (Qo2) of the cytochrome b gene', *Parasitology International*. Parasitol Int, 57(2), pp. 229-232. doi: 10.1016/j.parint.2007.12.002.

Soleimanpour-Lichaei, H. R. *et al.* (2007) 'mtRF1a Is a Human Mitochondrial Translation Release Factor Decoding the Major Termination Codons UAA and UAG', *Molecular Cell*. Cell Press, 27(5), pp. 745-757. doi:

10.1016/j.molcel.2007.06.031.

Sommer, M. S. *et al.* (2007) 'Der1-mediated Preprotein Import into the Periplastid Compartment of Chromalveolates?', *Molecular Biology and Evolution*. Narnia, 24(4), pp. 918–928. doi: 10.1093/molbev/msm008.

Soto, I. C. *et al.* (2012) 'Biogenesis and assembly of eukaryotic cytochrome c oxidase catalytic core', *Biochimica et Biophysica Acta (BBA) - Bioenergetics*. Elsevier, 1817(6), pp. 883–897. doi: 10.1016/J.BBABIO.2011.09.005.

Speer, C. A. and Dubey, J. P. (2005) 'Ultrastructural differentiation of Toxoplasma gondii schizonts (types B to E) and gamonts in the intestines of cats fed bradyzoites', *International Journal for Parasitology*, 35(2), pp. 193–206. doi: 10.1016/j.ijpara.2004.11.005.

Steiner-Mosonyi, M. and Mangroo, D. (2004) *The nuclear tRNA aminoacylation-dependent pathway may be the principal route used to export tRNA from the nucleus in Saccharomyces cerevisiae*, *Biochem. J.*

Stilger, K. L. and Sullivan, W. J. (2013) 'Elongator protein 3 (Elp3) lysine acetyltransferase is a tail-anchored mitochondrial protein in toxoplasma gondii', *Journal of Biological Chemistry*. American Society for Biochemistry and Molecular Biology, 288(35), pp. 25318–25329. doi: 10.1074/jbc.M113.491373.

Stortz, J. F. (2020) *A conditional CRISPR / Cas9 system gives novel insights into actin dynamics in Toxoplasma gondii*. Available at: http://theses.gla.ac.uk/77880/ (Accessed: 18 March 2020).

Strub, A., Röttgers, K. and Voos, W. (2002) 'The Hsp70 peptide-binding domain determines the interaction of the ATPase domain with Tim44 in mitochondria', *EMBO Journal*, 21(11), pp. 2626–2635. doi: 10.1093/emboj/21.11.2626.

Su, C. *et al.* (2003) 'Recent expansion of Toxoplasma through enhanced oral transmission', *Science*. American Association for the Advancement of Science, 299(5605), pp. 414–416. doi: 10.1126/science.1078035.

Suhm, T. *et al.* (2018) 'A novel system to monitor mitochondrial translation in yeast', *Microbial Cell*. Shared Science Publishers OG, 5(3), pp. 158–164. doi: 10.15698/mic2018.03.621.

Suplick, K. *et al.* (1988) 'Molecular cloning and partial sequence of a 5.8 kilobase pair repetitive DNA from Plasmodium falciparum', *Molecular and Biochemical Parasitology*. Mol Biochem Parasitol, 30(3), pp. 289–290. doi: 10.1016/0166-6851(88)90098-9.

Suss-Toby, E., Zimmerberg, J. and Ward, G. E. (1996) 'Toxoplasma invasion: the parasitophorous vacuole is formed from host cell plasma membrane and pinches off via a fission pore.', *Proceedings of the National Academy of Sciences*, 93(16), pp. 8413–8418. doi: 10.1073/pnas.93.16.8413.

Sweetlove, L. J., Taylor, N. L. and Leaver, C. J. (2007) 'Isolation of intact, functional mitochondria from the model plant Arabidopsis thaliana.', *Methods in molecular biology (Clifton, N.J.)*. Methods Mol Biol, 372, pp. 125–136. doi: 10.1007/978-1-59745-365-3_9.

Tan, T. H. P. *et al.* (2002) 'tRNAs in Trypanosoma brucei: Genomic Organization, Expression, and Mitochondrial Import', *Molecular and Cellular Biology*. American Society for Microbiology (ASM), 22(11), p. 3707. doi: 10.1128/MCB.22.11.3707-3716.2002.

Tarassov, I. *et al.* (2007) 'Import of nuclear DNA-encoded RNAs into mitochondria and mitochondrial translation', *Cell Cycle*. Taylor and Francis Inc., pp. 2473–2477. doi: 10.4161/cc.6.20.4783.

Tarassov, Ivan, Entelis, N. and Martin, R. P. (1995) 'An intact protein translocating machinery is required for mitochondrial import of a yeast cytoplasmic tRNA', *Journal of Molecular Biology*. Academic Press, pp. 315–323. doi: 10.1006/jmbi.1994.0026.

Tarassov, I., Entelis, N. and Martin, R. P. (1995) 'Mitochondrial import of a cytoplasmic lysine-tRNA in yeast is mediated by cooperation of cytoplasmic and mitochondrial lysyl-tRNA synthetases.', *The EMBO Journal*. John Wiley & Sons,

Ltd, 14(14), pp. 3461–3471. doi: 10.1002/j.1460-2075.1995.tb07352.x.

Tardieux, I. and Baum, J. (2016) 'Reassessing the mechanics of parasite motility and host-cell invasion.', *The Journal of cell biology*. Rockefeller University Press, 214(5), pp. 507–15. doi: 10.1083/jcb.201605100.

Temperley, R. J. *et al.* (2010) 'Human mitochondrial mRNAs-like members of all families, similar but different', *Biochimica et Biophysica Acta - Bioenergetics*. Elsevier, pp. 1081–1085. doi: 10.1016/j.bbabio.2010.02.036.

Tjhin, E. T. *et al.* (2020) 'Characterization of the apicoplast-localized enzyme TgUroD in Toxoplasma gondii reveals a key role of the apicoplast in heme biosynthesis', *Journal of Biological Chemistry*. American Society for Biochemistry and Molecular Biology Inc., 295(6), pp. 1539–1550. doi: 10.1074/jbc.RA119.011605.

Tomal, A., Kwasniak-Owczarek, M. and Janska, H. (2019) 'An Update on Mitochondrial Ribosome Biology: The Plant Mitoribosome in the Spotlight', *Cells*. MDPI AG, 8(12), p. 1562. doi: 10.3390/cells8121562.

Toursel, C. *et al.* (2000) 'Molecular cloning, organellar targeting and developmental expression of mitochondrial chaperone HSP60 in Toxoplasma gondii', *Molecular and Biochemical Parasitology*. Elsevier, 111(2), pp. 319–332. doi: 10.1016/S0166-6851(00)00324-8.

Tovar, J., Cox, S. S. E. and Giezen, M. van der (2007) 'A Mitosome Purification Protocol Based on Percoll Density Gradients and Its Use in Validating the Mitosomal Nature of Entamoeba histolytica Mitochondrial Hsp70', in *Protein Targeting Protocols*. Humana Press, pp. 167–177. doi: 10.1007/978-1-59745-466-7_11.

Tovar, J., Fischer, A. and Clark, C. G. (1999) 'The mitosome, a novel organelle related to mitochondria in the amitochondrial parasite Entamoeba histolytica', *Molecular Microbiology*. Mol Microbiol, 32(5), pp. 1013–1021. doi: 10.1046/j.1365-2958.1999.01414.x.

Tsaousis, A. D. *et al.* (2008) 'A novel route for ATP acquisition by the remnant mitochondria of Encephalitozoon cuniculi', *Nature*. Nature Publishing Group, 453(7194), pp. 553–556. doi: 10.1038/nature06903.

Tschopp, F., Charrière, F. and Schneider, A. (2011) 'In vivo study in Trypanosoma brucei links mitochondrial transfer RNA import to mitochondrial protein import.', *EMBO reports*. European Molecular Biology Organization, 12(8), pp. 825–32. doi: 10.1038/embor.2011.111.

Uddin, T., McFadden, G. I. and Goodman, C. D. (2018) 'Validation of putative apicoplast-targeting drugs using a chemical supplementation assay in cultured human malaria parasites', *Antimicrobial Agents and Chemotherapy*. American Society for Microbiology. doi: 10.1128/AAC.01161-17.

Vaidya, A. B., Akella, R. and Suplick, K. (1989) 'Sequences similar to genes for two mitochondrial proteins and portions of ribosomal RNA in tandemly arrayed 6-kilobase-pair DNA of a malarial parasite', *Molecular and Biochemical Parasitology*. Elsevier, 35(2), pp. 97–107. doi: 10.1016/0166-6851(89)90112-6.

Vaidya, A. B. and Mather, M. W. (2009) 'Mitochondrial Evolution and Functions in Malaria Parasites', *Annual Review of Microbiology*, 63(1), pp. 249–267. doi: 10.1146/annurev.micro.091208.073424.

Velours, J. and Arselin, G. (2000) 'TheSaccharomyces cerevisiaeATP Synthase', *Journal of Bioenergetics and Biomembranes*. Kluwer Academic Publishers-Plenum Publishers, 32(4), pp. 383–390. doi: 10.1023/A:1005580020547.

Vögtle, F. N. *et al.* (2009) 'Global Analysis of the Mitochondrial N-Proteome Identifies a Processing Peptidase Critical for Protein Stability', *Cell*. Elsevier, 139(2), pp. 428–439. doi: 10.1016/j.cell.2009.07.045.

Waller, R. F. and McFadden, G. I. (2005) 'The apicoplast: A review of the derived plastid of apicomplexan parasites', *Current Issues in Molecular Biology*, pp. 57–80. Available at: https://www.researchgate.net/publication/8146672_The_Apicoplast_a_review_ of_the_derived_plastid_of_Apicomplexan_parasites (Accessed: 30 September

2019).

Wang, Z. and Wu, M. (2015) 'An integrated phylogenomic approach toward pinpointing the origin of mitochondria', *Scientific Reports*. Nature Publishing Group, 5(1), pp. 1–12. doi: 10.1038/srep07949.

Weiss, L. M. and Dubey, J. P. (2009) 'Toxoplasmosis: A history of clinical observations.', *International journal for parasitology*. NIH Public Access, 39(8), pp. 895–901. doi: 10.1016/j.ijpara.2009.02.004.

Whitelaw, J. A. *et al.* (2017) 'Surface attachment, promoted by the actomyosin system of Toxoplasma gondii is important for efficient gliding motility and invasion.', *BMC biology*. BioMed Central, 15(1), p. 1. doi: 10.1186/s12915-016-0343-5.

WHO (2016) *World Malaria Report 2016. Switzerland, World Health Organization*. doi: 10.1071/EC12504.

Wideman, J. G. and Muñoz-Gómez, S. A. (2016) 'The evolution of ERMIONE in mitochondrial biogenesis and lipid homeostasis: An evolutionary view from comparative cell biology', *Biochimica et Biophysica Acta - Molecular and Cell Biology of Lipids*. Elsevier B.V., 1861(8), pp. 900–912. doi: 10.1016/j.bbalip.2016.01.015.

Wiedemann, N. and Pfanner, N. (2017a) 'Mitochondrial Machineries for Protein Import and Assembly'.

Wiedemann, N. and Pfanner, N. (2017b) 'Mitochondrial Machineries for Protein Import and Assembly', *Annual Review of Biochemistry*. Annual Reviews , 86(1), pp. 685–714. doi: 10.1146/annurev-biochem-060815-014352.

Williams, B. A. P. *et al.* (2002) 'A mitochondrial remnant in the microsporidian Trachipleistophora hominis', *Nature*, 418(6900), pp. 865–869. doi: 10.1038/nature00949.

Williams, E. G. *et al.* (2018) 'Quantifying and localizing the mitochondrial

proteome across five tissues in a mouse population', *Molecular and Cellular Proteomics*. American Society for Biochemistry and Molecular Biology Inc., 17(9), pp. 1766–1777. doi: 10.1074/mcp.RA118.000554.

Wilson, R. J. M. (Iain. *et al.* (1996) 'Complete gene map of the plastid-like DNA of the malaria parasite Plasmodium falciparum', *Journal of Molecular Biology*. Academic Press, 261(2), pp. 155–172. doi: 10.1006/jmbi.1996.0449.

Wittig, I., Karas, M. and Scha, H. (2007) 'for In-gel Functional Assays and Fluorescence Studies of Membrane Protein Complexes *', pp. 1215–1225. doi: 10.1074/mcp.M700076-MCP200.

Woo, Y. H. *et al.* (2015) 'Chromerid genomes reveal the evolutionary path from photosynthetic algae to obligate intracellular parasites', *eLife*. eLife Sciences Publications Ltd, 4(JULY 2015), pp. 1–41. doi: 10.7554/eLife.06974.

Xin, H. *et al.* (1995) 'Cloning and expression of mitochondrial translational elongation factor Ts from bovine and human liver', *Journal of Biological Chemistry*. J Biol Chem, 270(29), pp. 17243–17249. doi: 10.1074/jbc.270.29.17243.

Yamamoto, M. *et al.* (2011) 'ATF6beta is a host cellular target of the Toxoplasma gondii virulence factor ROP18.', *The Journal of experimental medicine*. The Rockefeller University Press, 208(7), pp. 1533–46. doi: 10.1084/jem.20101660.

Yang, N. *et al.* (2013) 'Genetic basis for phenotypic differences between different Toxoplasma gondii type I strains.', *BMC genomics*. BMC Genomics, 14(1), p. 467. doi: 10.1186/1471-2164-14-467.

Yeh, E. and DeRisi, J. L. (2011) 'Chemical rescue of malaria parasites lacking an apicoplast defines organelle function in blood-stage plasmodium falciparum', *PLoS Biology*. Public Library of Science, 9(8). doi: 10.1371/journal.pbio.1001138.

Yermovsky-Kammerer, A. E. and Hajduk, S. L. (1999) 'In vitro import of a nuclearly encoded tRNA into the mitochondrion of Trypanosoma brucei.',

Molecular and cellular biology. American Society for Microbiology Journals, 19(9), pp. 6253–9. doi: 10.1128/mcb.19.9.6253.

Youle, R. J. and Van Der Bliek, A. M. (2012) 'Mitochondrial fission, fusion, and stress', *Science*. American Association for the Advancement of Science, pp. 1062–1065. doi: 10.1126/science.1219855.

Yung, S., Unnasch, T. R. and Lang-Unnasch, N. (2001) 'Analysis of apicoplast targeting and transit peptide processing in Toxoplasma gondii by deletional and insertional mutagenesis', *Molecular and Biochemical Parasitology*. Elsevier, 118(1), pp. 11–21. doi: 10.1016/S0166-6851(01)00359-0.

Zeng, R., Smith, E. and Barrientos, A. (2018) 'Yeast Mitoribosome Large Subunit Assembly Proceeds by Hierarchical Incorporation of Protein Clusters and Modules on the Inner Membrane', *Cell Metabolism*. Cell Press, 27(3), pp. 645-656.e7. doi: 10.1016/j.cmet.2018.01.012.

Zhou, M. and Philips, M. R. (2017) 'Nitrogen Cavitation and Differential Centrifugation Allows for Monitoring the Distribution of Peripheral Membrane Proteins in Cultured Cells.', *Journal of visualized experiments : JoVE*. MyJoVE Corporation, (126). doi: 10.3791/56037.

Zhu, G., Marchewka, M. J. and Keithly, J. S. (2000) 'Cryptosporidium parvum appears to lack a plastid genome', *Microbiology*. Society for General Microbiology, 146(2), pp. 315–321. doi: 10.1099/00221287-146-2-315.